ZooKeys 1113: 1–110 (2022)
doi: 10.3897/zookeys.1113.82172
https://zookeys.pensoft.net

CATALOGUE

A peer-reviewed open-access journal
ZooKeys
Launched to accelerate biodiversity research

Benthic megafauna of the western Clarion-Clipperton Zone, Pacific Ocean

Guadalupe Bribiesca-Contreras[1], Thomas G. Dahlgren[2,3], Diva J. Amon[4], Stephen Cairns[5], Regan Drennan[1], Jennifer M. Durden[6], Marc P. Eléaume[7], Andrew M. Hosie[8], Antonina Kremenetskaia[9], Kirsty McQuaid[10], Timothy D. O'Hara[11], Muriel Rabone[1], Erik Simon-Lledó[6], Craig R. Smith[12], Les Watling[13], Helena Wiklund[2], Adrian G. Glover[1]

1 *Life Sciences Department, Natural History Museum, London, UK* **2** *Department of Marine Sciences, University of Gothenburg, Gothenburg, Sweden* **3** *Norwegian Research Centre, NORCE, Bergen, Norway* **4** *SpeSeas, D'Abadie, Trinidad and Tobago* **5** *Department of Invertebrate Zoology, National Museum of Natural History, Smithsonian Institution, Washington, D.C., USA* **6** *National Oceanography Centre, Southampton, UK* **7** *UMR ISYEB, Départment Origines et Évolution, Muséum national d'Histoire Naturelle, Paris, France* **8** *Collections & Research, Western Australia Museum, Perth, Australia* **9** *Shirshov Institute of Oceanology, Russian Academy of Sciences, Moscow, Russia* **10** *School of Biological and Marine Sciences, University of Plymouth, Plymouth, UK* **11** *Museums Victoria, Melbourne, Australia* **12** *Department of Oceanography, University of Hawai'i at Mānoa, Honolulu, USA* **13** *School of Life Sciences, University of Hawai'i at Mānoa, Honolulu, USA*

Corresponding author: Guadalupe Bribiesca-Contreras (l.bribiesca-contreras@nhm.ac.uk)

Academic editor: Pavel Stoev | Received 12 February 2022 | Accepted 5 May 2022 | Published 18 July 2022

http://zoobank.org/F503CB11-01EF-40D8-998C-135E8E8E44CE

Citation: Bribiesca-Contreras G, Dahlgren TG, Amon DJ, Cairns S, Drennan R, Durden JM, Eléaume MP, Hosie AM, Kremenetskaia A, McQuaid K, O'Hara TD, Rabone M, Simon-Lledó E, Smith CR, Watling L, Wiklund H, Glover AG (2022) Benthic megafauna of the western Clarion-Clipperton Zone, Pacific Ocean. ZooKeys 1113: 1–110. https://doi.org/10.3897/zookeys.1113.82172

Abstract

There is a growing interest in the exploitation of deep-sea mineral deposits, particularly on the abyssal seafloor of the central Pacific Clarion-Clipperton Zone (CCZ), which is rich in polymetallic nodules. In order to effectively manage potential exploitation activities, a thorough understanding of the biodiversity, community structure, species ranges, connectivity, and ecosystem functions across a range of scales is needed. The benthic megafauna plays an important role in the functioning of deep-sea ecosystems and represents an important component of the biodiversity. While megafaunal surveys using video and still images have provided insight into CCZ biodiversity, the collection of faunal samples is needed to confirm species identifications to accurately estimate species richness and species ranges, but faunal collections are very rarely carried out. Using a Remotely Operated Vehicle, 55 specimens of benthic megafauna were

collected from seamounts and abyssal plains in three Areas of Particular Environmental Interest (APEI 1, APEI 4, and APEI 7) at 3100–5100 m depth in the western CCZ. Using both morphological and molecular evidence, 48 different morphotypes belonging to five phyla were found, only nine referrable to known species, and 39 species potentially new to science. This work highlights the need for detailed taxonomic studies incorporating genetic data, not only within the CCZ, but in other bathyal, abyssal, and hadal regions, as representative genetic reference libraries that could facilitate the generation of species inventories.

Keywords
Biogeography, deep-sea mining, DNA barcoding, DNA taxonomy, megafauna, polymetallic nodules

Table of contents

Introduction

The Clarion-Clipperton Zone (CCZ) in the central abyssal Pacific has become of great interest for deep-sea mineral extraction. This large area of abyssal seafloor, approximately 6 million km^2 (Wedding et al. 2013), has the largest concentrations of high-grade polymetallic nodules, representing a vast source of commercially valuable metals such as nickel, copper, and cobalt, many of which are currently used in high-tech and green industries (Hein et al. 2020). Although new technological advances are taking deep-sea mining closer to reality, the impacts of mining activities on deep-sea ecosystems remain of concern and are still poorly understood (Jones et al. 2017). To date, the International Seabed Authority (ISA), which governs seabed mining in this area, has granted 17 exploration contracts to permit baseline surveys and resource assessment (but not commercial mining) in the CCZ, and has adopted an environmental management plan establishing 13 areas where exploitation is currently prohibited (called Areas of Particular Environmental Interest, or APEIs) (Smith et al. 2021). Four of these were recently implemented, but the representativity of the APEI network still needs to be assessed.

During the last few decades, there has been a dramatic increase in the scientific exploration of the CCZ, but our knowledge of the faunal communities associated with nodule fields is still limited, and taxonomic records for the area are scarce (Glover et al. 2018). Although the CCZ was first explored in 1875 by the H.M.S. Challenger (Thomson and Murray 1885), relatively little taxonomic work has been carried out in this vast area and hence very little biogeographic information is available (Simon-Lledó et al. 2020). This is particularly problematic as such information is critical to characterise the biodiversity, biogeographic ranges, and connectivity patterns across the entire CCZ in order to make better predictions about the potential impacts of deep-sea mining. In addition, the APEIs designated to preserve regional biodiversity are severely understudied (Glover et al. 2016a; International Seabed Authority 2020; Jones et al. 2021).

The CCZ abyssal seafloor is rich in topographic features such as hills, troughs, fracture zones, and seamounts (Kaiser et al. 2017). It encompasses many habitats with a range of different environmental conditions such as depth, nodule coverage, sediment composition, bathymetric relief, flow intensification on seamounts, and particulate organic carbon (POC) flux (Wedding et al. 2013; International Seabed Authority 2020; McQuaid et al. 2020; Washburn et al. 2021b). Benthic assemblages have been found to change across the CCZ (Wilson 2017; Bonifácio et al. 2020; Simon-Lledó et al. 2020), with POC flux influencing regional megafaunal community patterns, and local environmental factors (i.e., nodule coverage) and bathymetric features having an effect at local scales (Amon et al. 2016; Simon-Lledó et al. 2019c). Seamounts are abundant in the CCZ, most commonly in the eastern and western ends of the area, with elevations of > 1000 m above the plain, and are a major source of hard-substrate habitat (Wedding et al. 2013). Even though seamounts were hypothesised to provide a potential refugia and to be larval sources of nodule-associated fauna that could aid

in recolonising nodule fields, of similar depths, disturbed by mining activities, a recent study suggested that the seamounts sampled in the CCZ appear inadequate as refuge areas (Cuvelier et al. 2020). Nonetheless, the biodiversity of the CCZ seamounts remains largely unknown, with only few having been explored on the eastern (Cuvelier et al. 2020; Jones et al. 2021) and western (Durden et al. 2021) margins.

Large benthic organisms (benthic megafauna) have been prioritised for monitoring deep-sea ecosystems because they can be studied from seabed imagery (Danovaro et al. 2020), provide inferences on trophic interactions, ecosystem functioning (Rex and Etter 2010), and processes of disturbances (Jones et al. 2017) and recovery (Simon-Lledó et al. 2019a). In the CCZ, megafaunal benthic assemblages have been studied almost exclusively from video and still images (e.g., Amon et al. 2016; Simon-Lledó et al. 2019c, 2020; Cuvelier et al. 2020; Durden et al. 2021). While these studies have vastly increased our understanding of biodiversity and community structure, uncertainty remains as to the identity of operational taxonomic units (unique identifiers for different morphospecies) recognised in imaged-based survey, and whether they are conspecific with other known species from elsewhere in the deep sea. It is thus critical to complement spatial/temporal analyses with detailed morphological and DNA-sequence analyses of collected specimens (Amon et al. 2016, 2017b).

The DeepCCZ project was conceived to increase our understanding of faunal assemblages and biodiversity in the western CCZ, targeting both unexplored seamounts and APEIs. Here, we provide the first taxonomic synthesis of western CCZ megafauna, which is also the largest megafaunal faunistic study from anywhere in the CCZ based on collected specimens. We provide morphological descriptions, genetic data, and high-resolution imagery for all megafauna specimens collected, including specimens from both the abyssal plains and seamount habitats. It complements similar studies of the high diversity of megafaunal xenophyophores (Gooday et al. 2020a, b), and imagery-based community analysis of the megafauna in this area (Durden et al. 2021).

Materials and methods

The DeepCCZ expedition, aboard the RV *Kilo Moana*, from 14 May to 16 June 2018, surveyed seamounts and abyssal plains in three Areas of Particular Environmental Interest (**APEIs** 1, 4, and 7) located in the western Clarion-Clipperton Zone (**CCZ**; Fig. 1). All material presented here was collected during this expedition using the Remotely Operated Vehicle (**ROV**) Lu'ukai, and specimens were processed following the DNA taxonomy pipeline described in Glover et al. (2015).

Data resources

Sequences generated for this study have been deposited on GenBank: ON400681–ON400730 (COI), ON406602–ON406622 (16S), ON406623–ON406643 (18S), ON406596–ON406601 (28S), and ON411254–ON411256 (ALG11).

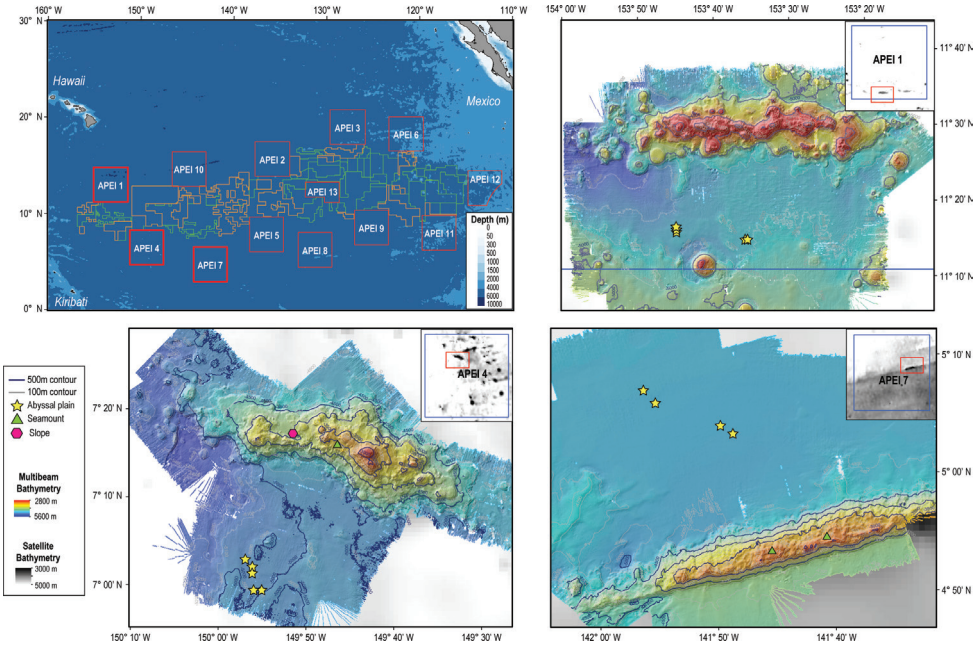

Figure 1. Map of the Clarion-Clipperton Zone (top left) indicating the nine Areas of Particular Environmental Interest (APEIs) in red, exploration areas in green, and reserved areas in orange. Shapefiles were sourced from https://www.naturalearthdata.com/downloads/10m-physical-vectors/10m-bathymetry/, and https://www.isa.org.jm/minerals/maps. Detailed maps of the study areas: APEIs 1 (top right), 4 (bottom left), and 7 (bottom right) show bathymetry from satellite values for the entire APEI, and multibeam values obtained during the DeepCCZ expedition. Sites, and specific geoform, where megafauna samples were collected are indicated as yellow stars in abyssal plains, green triangles in seamounts, and pink hexagons in seamount slopes.

Sampling

Specimens were selected from across as many taxonomic groups as possible, with duplicates of similar morphotypes avoided; thus, the aim was to increase our understanding of megafaunal diversity. A total of 55 specimens were collected during different dives in three APEIs and three different geoforms (abyssal plain, seamount, and seamount slope), 14 specimens were collected from abyssal seafloor in APEI 1; 13 from abyssal seafloor, two from the seamount slope and six from a seamount in APEI 4; and nine from abyssal seafloor and 11 from a seamount in APEI 7 (Fig. 1). In situ photographs and/or video frame grabs of each specimen were captured, with parallel lasers for scale at 15 cm spacing. Megafaunal specimens were collected with the manipulator ('Orion'), suction sampler, or push cores, depending on the characteristics of each specimen in order to best preserve morphological characters. Specimens collected with the manipulator were placed into the biobox receptacle, while those collected with the suction sampler were stored in a suction box. Collection data were recorded at the time

of capture (e.g., date and time, ROV latitude/longitude, seabed water depth, ROV waypoint name).

After ROV recovery, specimens were transferred and maintained in cold (2–4 °C), filtered seawater until processed. Following Glover et al. (2015), all specimens were photographed, given a preliminary identification and assigned a unique voucher code (e.g., CCZ_020). A tissue sample was taken from each specimen for downstream molecular analyses, and stored in 95% non-denatured ethanol at -20 °C. Specimens were fixed in 10% borax-buffered formalin and transferred to 70% non-denatured ethanol after 48 h, except for sponges, which were kept frozen at -80 °C. After the expedition, specimens and tissue sub-samples were sent to the University of Hawai'i Manoa. Specimens were archived at the Natural History Museum, London (**NHMUK**), and the Western Australian Museum (**WAM**), following taxonomic inspection.

DNA extraction, amplification, and sequencing

DNA extraction was performed using the DNeasy Blood and Tissue Kit (Qiagen). The barcode gene cytochrome oxidase I (COI) was the main target because this gene has been used in previous studies on megafauna in the CCZ (e.g., Dahlgren et al. 2016; Glover et al. 2016b). Additional markers for specific taxa (16S, 18S, 28S, and ALG11) were amplified when either COI amplification was unsuccessful or to improve identification or phylogenetic inference. The PCR mix for each reaction contained 10.5 µl of Red Taq DNA Polymerase 1.1X MasterMix (VWR), 0.5 µl of each primer (10 µM), and 1 µl of DNA template. PCR protocols and primers used for COI, 16S, and 18S were following Glover et al. (2016b) and Dahlgren et al. (2016), and Hestetun et al. (2016) for ALG11 and 28S. The PCR products were purified and sequenced at the NHM Sequencing Facilities using a Millipore Multiscreen 96-well PCR Purification System and ABI 3730XL DNA Analyser (Applied Biosystems), respectively. Sequencing primers used were the same as those for the PCR reactions, with the addition of internal primers for 18S and only using primers from the second PCR for the ALG11 gene. DNA sequences were analysed using Geneious 7.0.6 (https://www.geneious.com), with contigs assembled from both forward and reverse sequences and ambiguous base calls corrected manually. DNA sequences generated in this study were submitted to GenBank, with accession numbers ON400681–ON400730 for COI, ON406602–ON406622 for 16S, ON406623–ON406643 for 18S, ON406596–ON406601 for 28S, and ON411254–ON411256 for ALG11.

Phylogenetic assignments

Phylogenetic relationships of the western CCZ megafauna were explored by estimating phylogenetic trees for all taxa at different taxonomic levels: phylum Annelida: family Aphroditidae; phylum Arthropoda: order Scalpellomorpha; phylum Cnidaria: order Actiniaria, subclass Ceriantharia, subclass Octocorallia, and class Scyphozoa; phylum Echinodermata: class Asteroidea, class Crinoidea, class Echinoidea, class

Holothuroidea, and class Ophiuroidea; and phylum Porifera. Different sets of genes were used depending on published phylogenies and publicly available sequences for each taxon, considering both nuclear and mitochondrial genes if available. For each taxon, sequences were obtained from GenBank (Suppl. material 1: Table S1), except for Porifera as a published alignment was used (Dohrmann 2018). Protein-coding genes (COI, cytochrome oxidase III: COX3, mtMutS homolog: msh1, NADH-dehydrogenase subunit 2 gene: ND2) were aligned using MUSCLE in MEGA-X. Non-protein-coding genes (12S, 16S, 18S, 28S) were aligned using MAFFT v. 7 (Katoh et al. 2019) using the auto strategy, and unalignable regions filtered in GBLOCKS (Castresana 2000), allowing gap positions within final blocks and less strict flanking positions. Individual gene-alignments were concatenated in Geneious, and the best substitution model for each partition was determined using PartitionFinder 2 (Lanfear et al. 2017). For Porifera, we manually aligned our sequences for the 18S, 28S, 16S, and COI genes with the alignment provided in Dohrmann (2018).

Phylogenetic trees were estimated using partitioned maximum-likelihood (RAxML v8.2.10; Stamatakis 2006) and Bayesian inference (BEAST v. 2.4.7; Bouckaert et al. 2014), with the best inferred substitution model for each partition. In RAxML, the most common substitution model for each taxon was selected. RNA secondary structure, as in Dohrmann (2018), was also considered for Porifera, using the S16+G substitution model to paired sites of 18S and 28S. BEAST analyses were performed with trees and clock models linked, a Yule tree model, and relaxed clock log normal. Two independent runs of a maximum 100 M steps were combined after discarding 20% as burn-in. Runs were checked for convergence and a median consensus tree was estimated from the combined post-burn-in samples.

Taxonomic assignments

Taxonomic assignments considered information drawn from both molecular and morphological analyses. For the latter, the collected specimens were sent to expert taxonomists for morphological assignments. We assigned every specimen to the lowest Operational Taxonomic Unit (**OTU**), each representing a species. However, we took a precautionary approach when assigning species names (Dahlgren et al. 2016; Glover et al. 2016b; Horton et al. 2021), therefore recording species as 'cf.' when uncertain about their identity based on (i) differences in morphological characters, (ii) missing type locality DNA data, or (iii) when type localities are at significantly different depths or vast distances from the western CCZ. Also, those species that could not be identified as a described species were given a unique identifier using the lowest taxonomic level confidently identified and the voucher code (assigned at sea; i.e., CCZ_060). In cases where more than one specimen represented a species with a unique identifier, this only included the voucher code of the best-preserved voucher specimen of that species. Additionally, open taxonomic nomenclature signs were used to indicate that the specimen was not identified any further ('stet'; e.g., '*Laetmonice* stet. CCZ_060'), or when the identification is still uncertain ('inc'; e.g., Bathymetrinae inc. CCZ_176), and 'sp.' was only used for potentially new species (e.g., *Psychronaetes* sp. CCZ_101) after Glover et al. (2016b).

Current records available on OBIS, at a minimum depth of 3000 m, were recovered for each taxon on January 12, 2022 (robis::occurrence; Provoost and Bosch 2020). Records within a box defined by 13°N, 158°W; 18°N, 118°W; 10°N, 112°W; 2°N, 155°W were considered as occurring within the CCZ (Glover et al. 2015).

Comparison with seabed-imagery database

To gain preliminary insight into connectivity and distributions, morphology of specimens was compared to and, where possible, aligned with a standardised megafauna morphotype catalogue developed from in situ seabed imagery from across the north Pacific abyss, mostly eastern CCZ (Simon-Lledó et al., pers. obs.). The catalogue aligns invertebrate morphotypes, only for specimens larger than 1 cm, encountered in quantitative megafaunal assessments. At the time of writing, the survey areas so far encompassed in the standardised megafauna catalogue are, from east to west: UK-1 (Amon et al. 2016); BGR, GSR, and APEI 3 (Cuvelier et al. 2020); APEI 6 (Simon-Lledó et al. 2019b); TOML areas B, C, and D (Simon-Lledó et al. 2020); APEIs 1, 4, and 7 (this study; Durden et al. 2021); and the EEZ of Kiribati (Simon-Lledó et al. 2019d). The catalogue assigns each documented taxon a 7-character, unique morphotype code (e.g., POR_001) that differs from unique identifiers used for the species in this study. The level of taxonomic precision achieved in each catalogued taxon is indicated using the open taxonomic nomenclature signs recommended for image-based identifications by Horton et al. (2021). A suffix is added to each morphotype identification specifying the taxonomic rank (e.g., "fam.", "family"; "gen.", "genus" or "sp.", "species") and the signs "indet."or "inc.". The "indet." (*indeterminabilis*) indicates that further identification was not possible as diagnostic features are not typically visible in images, while the "inc." (*incerta*) indicates that despite diagnostic features being visible in images, the identification still has some uncertainty, needing further comparable material for validation.

Results

A total of 55 specimens was collected in the western CCZ (Table 1). Based on molecular data these represent 48 species of invertebrate megafauna (43 singletons, four doubletons, and a single species with four representatives) belonging to ten classes in five phyla. However, for three of the doubletons, each specimen was collected in a different APEI, but all were consistently found in the same geoform (i.e., abyssal plain, seamount, or seamount slope). Most of the taxa were collected on the abyssal seafloor (36 specimens from 33 species) > 4800 m deep, followed by seamounts (17 specimens from 13 species) between 3095–3562 m deep, and only two specimens from two species collected on a seamount slope at 4125 m deep. Out of the 48 taxa, only nine were assigned to previously described species, all from adjacent regions such as the Kuril-Kamchatka, Mariana, and Izu-Bonin Trenches, the South China Sea, and other areas of the Northwest and Southwest Pacific.

Table 1. Megafauna specimens collected during the DeepCCZ expedition, including details of their collection such as collection site and geoform (S, seamount; AP, abyssal plain; Sl, seamount slope), substrate or attachment (S, on sediment; E, epibiont, N, nodule; C, crust, Sa, anchored to sediment; B, attached to bone), depth, decimal latitude and longitude, scientific collection and accession number, voucher number, and GenBank accession number.

Classification	Species	Site	Substrate / Attachment	Depth (m)	Coordinates (Latitude, Longitude)	Collection	Accession no.	Voucher	GenBank accession no.
Annelida Polychaeta Phyllodocida Aphroditidae	*Laetmonice* stet. CCZ_060	APEI 7 (S)	S	3096	4.8897, -141.7500	NHMUK	2022.760	CCZ_060	ON400687 (COI)
Arthropoda Thecostraca Scalpellomorpha Scalpellidae	*Trianguloscalpellum gigas*	APEI 7 (AP)	E	4875	5.0442, -141.8165	WAM	C74110	CCZ_074	ON400698 (COI), ON406624 (18S)
	Catherinum cf. *albatrossianum*	APEI 7 (AP)	E	4875	5.0442, -141.8165	WAM	C74109	CCZ_073	ON400697 (COI), ON406623 (18S)
	Catherinum cf. *novaezelandiae*	APEI 1 (AP)	E	5241	11.2751, -153.7444	WAM	C74111	CCZ_185	ON400722 (COI), ON406625 (18S)
Cnidaria Anthozoa Actiniaria	Metridioidea stet. CCZ_072	APEI 1 (AP)	E	4875	5.0442, -141.8165	NHMUK	2021.19	CCZ_072	ON400696 (COI)
	Metridioidea stet. CCZ_154	APEI 4 (AP)	N	5009	6.9702, -149.9426	NHMUK	2021.27	CCZ_154	ON400715 (COI)
	Metridioidea stet. CCZ_164	APEI 7 (AP)	E	5001	6.9880, -149.9326	NHMUK	2021.5	CCZ_164	ON400717 (COI)
Actinostolidae	Actinostolidae stet. CCZ_183	APEI 1 (AP)	N	5241	11.2751, -153.7444	NHMUK	2021.28	CCZ_183	ON406626 (18S)
	Actinostolidae stet. CCZ_202	APEI 4 (AP)	N	5206	11.2518, -153.6059	NHMUK	2021.22	CCZ_202	ON406627 (18S)
Scleractinia Caryophyllidae	*Fungiacyathus (Fungiacyathus)* cf. *fragilis*	APEI 4 (S)	S	3562	7.2647, -149.7740	NHMUK	2021.26	CCZ_107	NA
Alcyonacea Chrysogorgiidae	*Chrysogorgia* sp. CCZ_112	APEI 4 (Sl)	C	4125	7.2874, -149.8578	NHMUK*		CCZ_112	ON400711 (COI), ON406602 (16S)
Mopseidae	Mopseidae sp. CCZ_088	APEI 4 (AP)	N	5018	7.0089, -149.9109	NHMUK*		CCZ_088	ON400705 (COI), ON406603 (16S)
Primnoidae	*Calyptrophora distolos*	APEI 4 (Sl)	C	4125	7.2874, -149.8578	USNM	1550968	CCZ_113	ON400712 (COI), ON406604 (16S)
Pennatulacea Protoptilidae	*Protoptilum* stet. CCZ_068	APEI 7 (S)	Sa	3096	4.8897, -141.7500	NHMUK	2021.24	CCZ_068	ON400694 (COI), ON406605 (16S)
Spirularia	Spirularia stet. CCZ_067	APEI 7 (S)	Sa	3132	4.8875, -141.7572	NHMUK	2021.23	CCZ_067	ON400693 (COI), ON406606 (16S)
Scyphozoa Somaeostomeae Ulmaridae	Ulmaridae stet. CCZ_069	APEI 7 (S)	S	3133	4.8876, -141.7572	NHMUK	2021.25	CCZ_069	ON400695 (COI)

Classification	Species	Site	Substrate / Attachment	Depth (m)	Coordinates (Latitude, Longitude)	Collection	Accession no.	Voucher	GenBank accession no.
Echinodermata	*Freyastera* cf. *tuberculata*	APEI 4 (AP)	S	5000	6.9879, -149.9123	NHMUK	2022.79	CCZ_087	ON400704 (COI)
Asteroidea		APEI 4 (AP)	S	5000	6.9873, -149.9331	NHMUK	2022.80	CCZ_157	ON400716 (COI)
Brisingida Freyellidae	*Freyastera* stet. CCZ_201	APEI 1 (AP)	S	5204	11.2518, -153.6059	NHMUK	2022.81	CCZ_201	ON400730 (COI)
Forcipulatida Zoroasteridae	*Zoroaster* stet. CCZ_065	APEI 7 (S)	S	3132	4.8877, -141.7569	NHMUK	2022.78	CCZ_065	ON400691 (COI), ON406607 (16S)
Crinoidea **Comatulida** Phrynocrinidae	cf. *Porphyrocrinus* sp. CCZ_165	APEI 4 (AP)	N	5002	6.9879, -149.9327	NHMUK	2022.76	CCZ_165	ON400718 (COI), ON406616 (16S)
Antedonidae	Bathymetrinae incert. CCZ_176	APEI 4 (AP)	E	5009	6.9879, -149.9326	NHMUK	2022.77	CCZ_176	ON400719 (COI), ON406617 (16S);
		APEI 1 (AP)	E	5241	11.2751, -153.7444	NHMUK	2022.60	CCZ_186	ON400723 (COI), ON406618 (16S)
Echinoidea **Aspidodiadematoida** Aspidodiadematidae	*Plesiodiadema* cf. *globulosum*	APEI 1 (AP)	S	5204	11.2527, -153.5848	CASIZ	229305	CCZ_196	ON400726 (COI), ON406628 (18S)
Echinothurioida Kamptosomatidae	*Kamptosoma abyssale*	APEI 4 (AP)	S	5040	7.0360, -149.9395	CASIZ	229306	CCZ_082	ON400701 (COI)
Holothuroidea	*Molpadiodemas* stet. CCZ_102	APEI 4 (S)	S	3552	7.2701, -149.7827	NHMUK	2022.66	CCZ_102	ON400708 (COI)
Persiculida Molpadiodemidae	*Molpadiodemas* stet. CCZ_194	APEI 1 (AP)	S	5205	11.2517, -153.6055	NHMUK	2022.71	CCZ_194	ON400725 (COI)
Synallactida Synallactidae	*Synallactes* stet. CCZ_153	APEI 4 (AP)	S	5009	6.9704, -149.9426	NHMUK	2022.69	CCZ_153	ON400714 (COI)
	Synallactidae stet. CCZ_061	APEI 7 (S)	S	3132	4.8877, -141.7569	NHMUK	2022.75	CCZ_061	ON400688 (COI), ON406640 (18S)
	Synallactidae stet. CCZ_066	APEI 7 (S)	S	3095	4.8896, -141.7500	NHMUK	2022.63	CCZ_066	ON400692 (COI), ON406642 (18S)
Deimatidae	*Oneirophanta* stet. CCZ_100	APEI 4 (S)	S	3550	7.2647, -149.7740	NHMUK	2022.84	CCZ_100	ON400706 (COI), ON406643 (16S), ON406620 (18S)
	Oneirophanta cf. *mutabilis*	APEI 1 (AP)	S	5203	11.2520, -153.5847	NHMUK	2021.20	CCZ_193	ON400724 (COI), ON406629 (16S), ON406619 (18S)
Elasipodida Psychropotidae	*Psychropotes verrucicaudatus*	APEI 4 (AP)	S	4999	6.9878, -149.9119	NHMUK	2021.19	CCZ_086	ON400703 (COI)
	Psychropotes dyscrita	APEI 4 (AP)	S	5040	7.0212, -149.9355	NHMUK	2022.83	CCZ_083	ON400702 (COI)
	Benthodytes cf. *sanguinolenta*	APEI 1 (AP)	S	5245	11.2953, -153.7420	NHMUK	2022.70	CCZ_178	ON400720 (COI)

Classification	Species	Site	Substrate / Attachment	Depth (m)	Coordinates (Latitude, Longitude)	Collection	Accession no.	Voucher	GenBank accession no.
Elasipodida Psychropotidae	*Benthodytes marianensis*	APEI 7 (AP)	S	4861	5.1043, -141.8865	NHMUK	2022.82	CCZ_019	ON400682 (COI)
Elpidiidae	*Peniagone leander*	APEI 7 (AP)	S	4860	5.1042, -141.8861	NHMUK	2022.61	CCZ_018	ON400681 (COI), ON406621 (16S)
	Peniagone vitrea	APEI 7 (AP)	S	4875	5.0442, -141.8164	NHMUK	2022.64	CCZ_077	ON400699 (COI), ON406622 (16S)
Laetmogonidae	*Psychronaetes* sp. CCZ_101	APEI 4 (S)	S	3562	7.2647, -149.7741	NHMUK	2022.65	CCZ_101	ON400707 (COI), ON406631 (18S)
		APEI 4 (S)	S	3562	7.2647, -149.7741	NHMUK	2022.68	CCZ_104	ON400710 (COI), ON406632 (18S)
		APEI 7 (S)	S	3132	4.8877, -141.7570	NHMUK	2022.62	CCZ_063	ON400690 (COI), ON406630 (18S)
		APEI 4 (S)	S	3562	7.2647, -149.7741	NHMUK	2022.67	CCZ_103	ON400709 (COI), ON406639 (18S)
	Laetmogone cf. *wyvillethomsoni*	APEI 7 (S)	S	3132	4.8877, -141.7569	NHMUK	2021.18	CCZ_062	ON400689 (COI), ON406641 (18S)
Ophiuroidea Ophioscolecida Ophioscolecidae	*Ophiocymbium tanyae*	APEI 1 (AP)	S	5204	11.2523, -153.5848	NHMUK	2022.74	CCZ_206	ON406633 (18S), ON406596 (28S)
	Ophiocymbium cf. *rarispinum*	APEI 1 (AP)	S	5206	11.2518, -153.6059	NHMUK	2022.73	CCZ_197	ON400727 (COI)
Ophiurida Ophiopyrgidae	*Ophiuroglypha* cf. *irrorata*	APEI 7 (S)	S	3239	4.9081, -141.6813	NHMUK	2021.21	CCZ_058	ON400685 (COI)
		APEI 7 (S)	S	3096	4.8897, -141.7500	NHMUK	2022.72	CCZ_059	ON400686 (COI)
Porifera Hexactinellida Amphidiscosida Hyalonematidae	*Hyalonema* stet. CCZ_020	APEI 7 (AP)	Sa	4856	5.1149, -141.8967	NHMUK		CCZ_020	ON400683 (COI), ON406634 (18S), ON406608 (16S), ON406597 (28S), ON411254 (ALG11)
		APEI 1 (AP)	Sa	5245	11.2954, -153.7422	NHMUK	2022.8	CCZ_179	ON400721 (COI), ON406609 (16S)
	Hyalonema stet. CCZ_081	APEI 4 (AP)	Sa	5031	7.0360, -149.9395	NHMUK	2022.9	CCZ_081	ON406610 (16S)
Lyssacinosida Euplectellidae	Euplectellinae stet. CCZ_199	APEI 1 (AP)	Sa	5202	11.2518, -153.5853	NHMUK		CCZ_199	ON400729 (COI), ON406611 (16S)
	Docosaccus sp. CCZ_021	APEI 7 (AP)	Sa	4860	5.1043, -141.8867	NHMUK	2022.6	CCZ_021	ON400684 (COI), ON406635 (18S), ON406612 (16S), ON406598 (28S), ON411255 (ALG11)

Classification	Species	Site	Substrate / Attachment	Depth (m)	Coordinates (Latitude, Longitude)	Collection	Accession no.	Voucher	GenBank accession no.
Lyssacinosida Euplectellidae	*Holascus* stet. CCZ_078	APEI 7 (AP)	Sa	4874	5.0443, -141.8162	NHMUK	2022.7	CCZ_078	ON400700 (COI), ON406636 (18S), ON406613 (16S), ON406599 (28S), ON411256 (ALG11)
	Bolosominae stet. CCZ_198	APEI 1 (AP)	Sa	5205	11.2518, -153.6053	NHMUK	2022.10	CCZ_198	ON400728 (COI), ON406637 (18S), ON406614 (16S), ON406600 (28S)
Sceptrulophora Euretidae	*Bathyxiphus* sp. CCZ_151	APEI 4 (AP)	B	5001	6.9881, -149.9321	NHMUK		CCZ_151	ON400713 (COI), ON406638 (18S), ON406615 (16S), ON406601 (28S)

* Temporarily stored at University of Hawai'i at Mānoa, Honolulu, USA.

Only two of these nine species had been previously found in the CCZ. Juveniles of the brittle star *Ophiocymbium tanyae* Martynov, 2010 were collected in the eastern IFREMER contract area and in APEI 3, but due to their early life stage, they lacked taxonomically informative characters and were only assigned to family level using DNA barcoding data (Christodoulou et al. 2020). In this study, genetic data confirmed the taxonomic identity of these specimens. The other species previously known from the CCZ is the sea cucumber *Peniagone leander* Pawson & Foell, 1986, which also occurs in the Mariana Trench (Gong et al. 2020). Additionally, ten species were assigned as 'cf.' based on morphological differences from similar described species, or because prior collections were in other ocean basins or different bathymetric ranges. These, and the remaining 30 taxa, likely represent undescribed species. Based on morphological and genetic evidence, two of these undescribed taxa have also been previously reported for the eastern CCZ (*Freyastera* cf. *benthophila* and Crinoidea sp. NHM_055 from Glover et al. (2016b) and (Amon et al. 2017b), referred to herein as *Freyastera* cf. *tuberculata* and cf. *Porphyrocrinus* sp. CCZ_165, respectively).

The in situ images taken for 53 specimens were classified into a total of 45 morphotypes using the standardised megafauna imagery catalogue (Simon-Lledó et al., pers. obs.). From these, 11 (24%) were new additions to the existing catalogue, thus representing morphotypes exclusively (to-date) encountered in the western CCZ (i.e., APEIs 1, 4 and 7), while 27 (60%) had already been encountered in other areas. More specifically, nine (20%) of the 45 morphotypes encountered in the western CCZ have also previously been found both in abyssal areas of the Kiribati EEZ (west of the areas studied) and in the eastern CCZ. Two (4%) of the morphotypes encountered in the western CCZ have been found in Kiribati (but not in eastern CCZ locations), whereas 16 (36%) of the western CCZ morphotypes have been encountered in the eastern CCZ, but not in Kiribati.

Descriptions

Phylum Annelida Lamarck, 1809
Class Polychaeta Grube, 1850
Subclass Errantia Audouin & H Milne Edwards, 1832
Order Phyllodocida Dales, 1962
Suborder Aphroditiformia Levinsen, 1883
Family Aphroditidae Malmgren, 1867
Genus *Laetmonice* Kinberg, 1856

Currently, there are no records from ≥ 3000 m depth for the genus *Laetmonice* Kinberg, 1856, in the Clarion-Clipperton Zone (OBIS 2022). A single polychaete specimen was collected, for which the genetic sequence of the COI gene was generated and used to estimate a COI-only phylogenetic tree (Fig. 2).

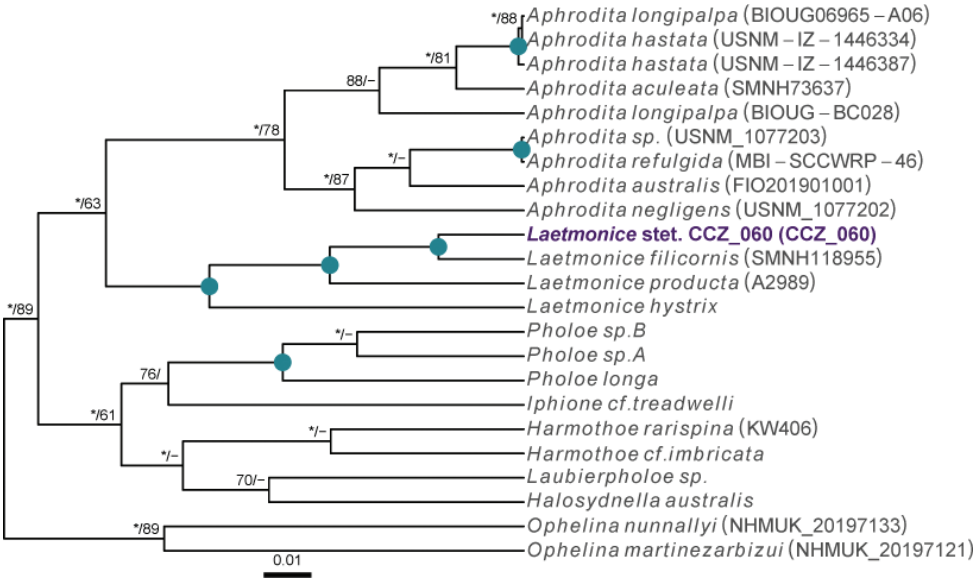

Figure 2. Rooted Bayesian phylogeny for the family Aphroditidae. COI-only BEAST median consensus tree with posterior probability (PP) and bootstrap (BS) values indicated for each node. Only values of PP > 0.70 and BS > 50 are shown, with values of PP > 0.95 and BS > 90 indicated with a circle. Nodes not recovered on the RAxML tree are indicated with a hyphen. Sequences generated in this study are highlighted in violet.

Laetmonice stet. CCZ_060

Fig. 3

Material. Clarion-Clipperton Zone • 1 specimen; APEI 7; 4.8897°N, 141.75°W; 3096 m deep; 27 May. 2018; Smith & Durden leg.; GenBank: ON400687 (COI); NHMUK 2022.76; Voucher code: CCZ_060.

Description. Single specimen (Fig. 3A). Body short, ovoid, flattened ventrally and somewhat arched dorsally. Specimen ~ 1 cm at widest point and 2 cm long, with 31 chaetigers. Dorsal felt not present. Specimen caked dorsally in dense layer of pale sediment (Fig. 3B, E), easily removed from dorsum but adhering to prostomium, parapodia, chaetae, and pygidium, obscuring respective features. Elytra 15 pairs, semi-translucent, smooth, and overlapping to cover dorsum (Fig. 3C). Dorsal cirri long, fine and tapering, extending beyond parapodia. Ventrum smooth. Ventral cirri, short, mostly broken off, not extending to base of neurochaetae. Parapodia biramous. Notochaetae include long, dark, brassy spines (Fig. 3E) with simple, tapered tips or with harpoon-shaped tips bearing four or five recurved fangs (Fig. 3D); both types of notochaetae with tuberculated shafts (Fig. 3G); neurochaetae include finer, shorter, paler chaetae with subdistal lateral spur and distal fringe of filamentous hairs (Fig. 3F), tips frequently broken off or covered in sediment.

Remarks. The presence of harpoon-shaped notochaetae supports the placement of this specimen within the genus *Laetmonice* (Fauchald 1977). Forms a monophyletic clade with other species of the genus *Laetmonice* based on COI sequences. Genetically distinct from *Laetmonice* stet. CCZ_060, the closest match is with *Laetmonice filicornis* Kinberg, 1856 (90.8% similarity). *Laetmonice filicornis* is described from shelf depths near Sweden in the North Atlantic.

Ecology. This specimen was observed crawling on the sedimented seafloor on the seamount of APEI 7 at 3096 m depth.

Comparison with image-based catalogue. No exactly identical Aphroditiformia morphotypes have been so far catalogued from seabed imagery collected in the eastern CCZ or in abyssal areas of the Kiribati EEZ. Consequently, the in situ image of *Laetmonice* stet. CCZ_060 was added as a new morphotype (i.e., *Laetmonice* sp. indet., ANN_019) in the megafauna imagery catalogue. Only one other Aphroditiformia morphotype (i.e., Aphroditidae gen. indet., ANN_022; with much larger spines and no sediment coating), was catalogued from seabed imagery in the eastern CCZ, also found on a seamount. In vertically-facing seabed images, Aphroditiformia

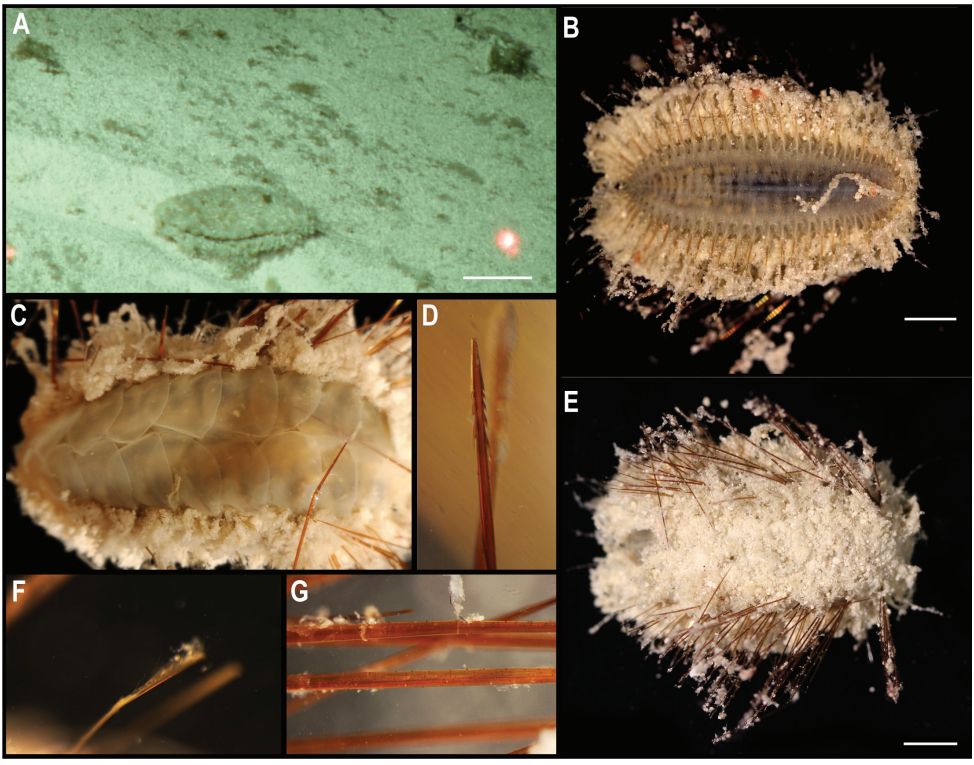

Figure 3. *Laetmonice* stet. CCZ_060 **A** in situ image **B** ventral surface **C** elytra on dorsal surface **D** harpoon-shaped chaeta **E** dorsal surface **F** neurochaeta with fringed tips **G** notochaetal spine shafts. Scale bars: 2cm (**A**); 0.5 cm (**B, E**). Image attribution: Durden and Smith (**A**), Wiklund, Durden, Drennan, and McQuaid (**B, E**), Drennan (**C, D, F, G**).

morphotypes could potentially be confused with plate-shaped Xenophyophore tests (e.g., Psamminidae), particularly a dense layer of sediment is found coating specimens, as observed in *Laetmonice* stet. CCZ_060 (Fig. 3A).

Phylum Arthropoda von Siebold, 1848
Subphylum Crustacea Brünnich, 1772
Superclass Multicrustacea Regier, Shultz, Zwick, Hussey, Ball, Wetzer, Martin & Cunningham, 2010
Class Thecostraca Gruvel, 1905
Subclass Cirripedia Burmeister, 1834
Infraclass Thoracica Darwin, 1854
Superorder Thoracicalcarea Gale, 2015
Order Scalpellomorpha Buckeridge & Newman, 2006
Family Scalpellidae Pilsbry, 1907

To date, there is a single record at > 3,000 m depth for the order Scalpellomorpha in the CCZ (OBIS 2022), but no collected material. Three specimens were collected during the DeepCCZ expedition; these belong to three different species from which only one was confidently assigned to a previously described species. Sequences for the COI and 18S genes were generated for the three specimens and included in a phylogenetic tree estimated from 18S and COI sequences (Fig. 4).

Scalpellomorpha have been commonly found in image-based megafauna surveys across the north Pacific abyss, usually attached to sponge stalks or nodules. However, their classification beyond family level (e.g., Scalpellidae) from seabed imagery is constrained by their generally small size; only large specimens (> 3 cm) which are rarely encountered can sometimes be classified to genus level from in situ images. Consequently, scalpellid specimens usually are collated into a single, generic morphotype (i.e., Scalpellidae gen. indet., ART_010) in image-based quantitative analyses.

Genus *Trianguloscalpellum* Zevina, 1978

***Trianguloscalpellum gigas* (Hoek, 1883)**
Fig. 5

Material. Clarion-Clipperton Zone • 1 specimen; APEI 7; 5.0442°N, 141.8165°W; 4874 m deep; 28 May. 2018; Smith & Durden leg.; GenBank: ON400698 (COI), ON406624 (18S); WAM C74110; Voucher code: CCZ_074.

Description. Single specimen, found attached to a glass sponge stalk (Fig. 5A). Capitulum elongated, longer than wide (L = 8 mm, W = 5 mm), white, with short peduncle (2 mm) covered by large scales (Fig. 5B, C). Capitulum is formed by 14 capitular plates, and growth lines are not visible. Carina is simply bowed, narrowing distally but being approx. the same breath proximally. The tergum is somewhat oval-shaped, long, ~ 2× as long as wide, with pointed basal angle, carinal margin arched,

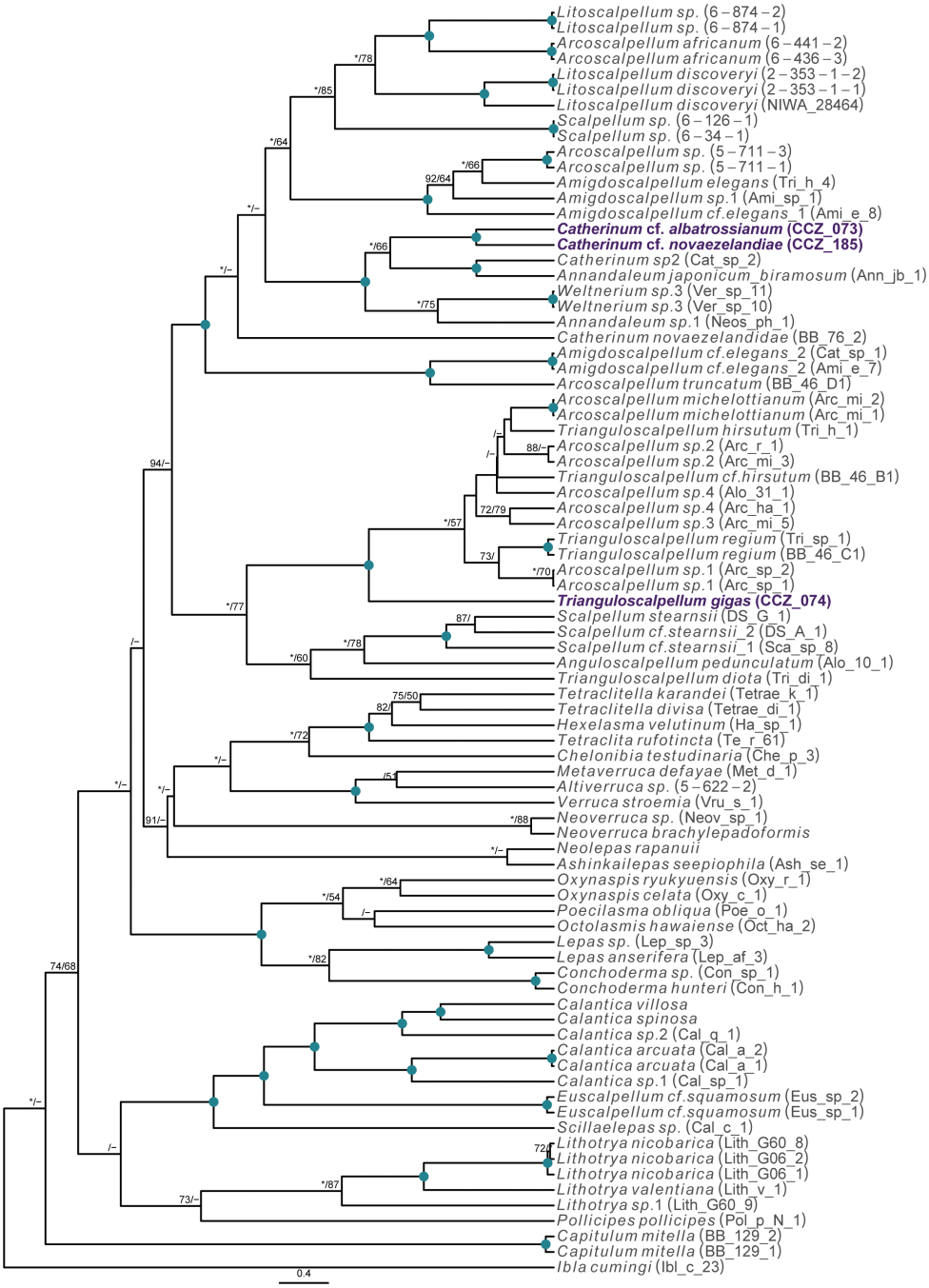

Figure 4. Rooted Bayesian phylogeny of Scalpellomorpha. Concatenated (18S, and COI) BEAST median consensus tree with posterior probability (PP) and bootstrap (BS) values indicated. Only values of PP > 0.70 and BS > 50 are shown, with values of PP > 0.95 and BS > 90 indicated with a circle. Nodes not recovered on the RAxML tree are indicated with a hyphen. Sequences generated in this study are highlighted in violet.

and occludent margin straight. Scutum is somewhat quadrangular, broad, 1.5× as long as wide, with occludent margin much longer than the lateral margin. Inframedian latus is triangular, reaching upper latus. Carinolatus triangular, umbo apical, higher than rostrolatus.

Remarks. The specimen appears to be a juvenile of the species *T. gigas* based on the plate arrangement, although diagnostic characters are not fully developed. There are no sequences available on public databases for *T. gigas*, but the 18S gene sequence is very similar (> 99%) to other species within the family Scalpellidae, mostly within the subfamily Arcoscalpellinae. However, the COI sequence is highly divergent (> 15% nucleotide divergence and > 3% amino-acid divergence) from published sequences of other species within the subfamily. The phylogenetic tree from concatenated data for COI and 18S recovered a well-supported clade of species of *Anguloscalpellum* and *Trianguloscalpellum*, but did not recover the genera as monophyletic. The type material for *T. gigas* was collected during the H.M.S. Challenger expedition in the middle of the North Pacific (Station 246: 36.1667°N, 178.0°E) at 3749 m depth (Hoek 1883). The species has been recorded from the Northwest and Southwest Pacific, and the Indian Ocean, from 3310 to 4820 m depth (Shalaeva and Boxshall 2014).

Ecology. The specimen was collected in the sedimented abyssal plain of APEI 7, at 4874 m depth. It was attached to a glass sponge stalk, along with another barnacle (*Catherinum* cf. *albatrossianum*; specimen CCZ_073), and an anemone (Metridioidea stet. CCZ_072; specimen CCZ_072).

Comparison with image-based catalogue. No exactly similar Scalpellidae morphotypes have been so far catalogued from seabed imagery collected in the eastern

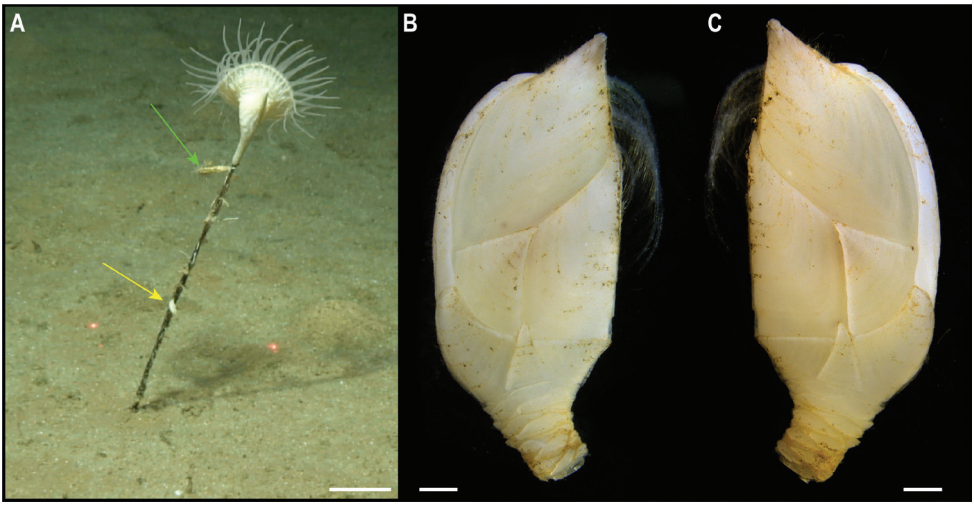

Figure 5. *Trianguloscalpellum gigas* (Hoek, 1883). Specimen CCZ_074: **A** in situ photograph, attached to a glass sponge stalk **B** left **C** and right lateral views. Scale bars: 5 cm (**A**); 1 mm (**B, C**). Image attribution: Durden and Smith (**A**), Hosie (**B, C**). Arrows indicate position of *T. gigas* (specimen CCZ_074; lower, yellow) and *Catherinum* cf. *albatrossianum* (specimen CCZ_073; upper, green).

CCZ or in abyssal areas of the Kiribati EEZ. Consequently, the in situ image of *Trianguloscalpellum gigas* was catalogued as a new morphotype (i.e., *Trianguloscalpellum gigas* sp. inc., ART_033). However, given the small size of specimen CCZ_074, this morphotype could have easily been i.e., undetected in seabed image surveys conducted in other areas of the CCZ.

Genus *Catherinum* Zevina, 1978

Catherinum cf. *albatrossianum* (Pilsbry, 1907)

Fig. 6

Material. Clarion-Clipperton Zone • 1 specimen; APEI 7; 5.0442°N, 141.8165°W; 4875 m deep; 28 May. 2018; Smith & Durden leg.; GenBank: ON400697 (COI), ON406623 (18S); WAM C74109; Voucher code: CCZ_073.

Description. Single specimen 21 mm long, attached to glass sponge stalk (Fig. 5A; upper, green arrow). Capitulum elongated, white, ~ 2× as long as wide (L = 16 mm, W = 8 mm); widest in the middle, tapering towards summit and base; short peduncle (4 mm) with small scales (Fig. 6A, B). Fourteen capitular plates fully calcified, showing growth lines, and separated by very narrow chitinous spaces. Carina is strongly arched in the distal half, tapering proximally, with flat roof and apical umbo. Tergum is almost a right triangle, longer than wide, with slightly convex occludent margin. Scutum is more than twice as wide as long, with arcuate occludent margin, with a distal indent on the lateral margin for the reception of the apex of the upper latus; baso-lateral margin rounded and next to the infra-median latus. Upper latus is pentagonal; with apical umbo projecting into notch on the scutum; scutal margin in concave; very short basal margin and carinolateral margin longer than carinal margin. Rostrolatus has an umbo projecting from the rostral margin. Rostrum minute. Large carinolatus, ~ 2× as long as wide, umbo sub-basal, abutting base of carina, apex slightly extending approximately one fifth of the carina. Inframedian latus is > 2× as long as the widest section, widest distally and with rostral and carinal margins concave, with umbo sub-basal.

Remarks. Morphological characters are in accordance with the description of *C. albatrossianum*. The 18S sequence matches three genera within the subfamily Arcoscalpellinae Zevina, 1978, while the closest match (85% similarity) for the COI sequence is to another species of *Catherinum*. Like, *C.* cf. *novaezelandiae* it differs morphologically from *C. tortilum*, reported from the CCZ by Poltarukha and Mel'Nik (2012), in the form of the inframedian latus. The type locality of *C. albatrossianum* is off Cape Hatteras, in the northwest Atlantic, at ~ 3740 m depth, but it has been reported for the North Atlantic, Gulf of Mexico, and Indian Ocean between 760 and 4180 m depth (Zevina and Poltarukha 2014). The original description states that the species lacks a rostrum, however, a minute rostrum is present in the specimen examined herein. This in addition to the documented range of this species is the reason for the use of cf. in the identification.

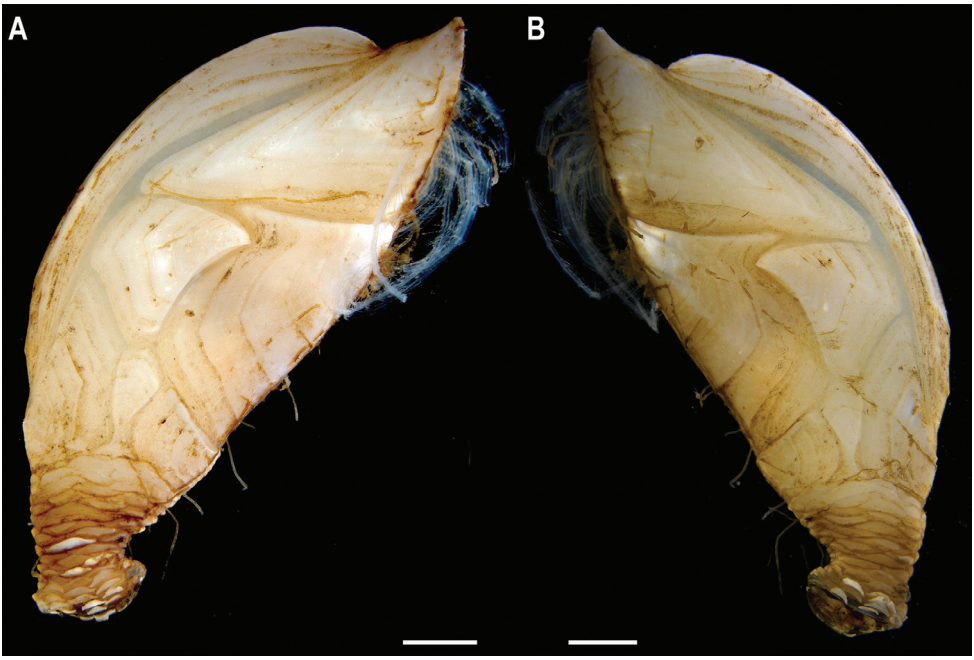

Figure 6. *Catherinum* cf. *albatrossianum* (Pilsbry, 1907). Specimen CCZ_073: **A** left **B** right lateral views. Scale bars: 2 mm. Image attribution: Hosie (**A, B**).

Ecology. Specimen was collected in a muddy abyssal area of APEI 7, at 4874 m depth. It was attached to a glass sponge stalk (Fig. 5A; upper, green arrow), along with another barnacle (*Trianguloscalpellum gigas*, specimen CCZ_074; lower, yellow arrow), and an anemone (Metridioidea stet. CCZ_072; specimen CCZ_072). It had hydrozoans and two serpulid polychaetes attached to it.

Comparison with image-based catalogue. A very similar morphotype (*Catherinum* sp. indet., ART_032) has been encountered (e.g., large specimens > 3 cm in length) in seabed image surveys conducted across the eastern CCZ and in abyssal areas of the Kiribati EEZ.

Catherinum cf. *novaezelandiae* (Hoek, 1883)

Fig. 7

Material. Clarion-Clipperton Zone • 1 specimen; APEI 1; 11.2751°N, 153.7444°W; 5241 m deep; 09 Jun. 2018; Smith & Durden leg.; GenBank: ON400722 (COI), ON406625 (18S); WAM C74111; Voucher code: CCZ_185.

Description. Single specimen 14 mm long; with elongated, white capitulum, > 2× as long as wide (L = 12 mm, W = 5 mm), and short peduncle (2 mm) with small scales (Fig. 7). Capitulum consists of 14 fully calcified capitular plates with

growth lines, separated from each other by narrow chitinous sutures. Carina is simply bowed, with flat roof. Tergum is triangular, shorter on the occludent margin, with apical umbo; apical angle is similar to angle between the carinal and scutal margins. Upper latus somewhat pentagonal, with lower edge truncated, and apical edge reaching over the scutum; with apical umbo. Rostrolatus with umbo apical on the rostral margin, and arched lateral margin. Inframedian latus irregular in shape, narrow, almost 3× as long as the widest part, with umbo sub-medial; rostral and carinal margins concave. Carinolatus is large, ~ 2× as long as wide, with umbo sub-carinal, above basal angle.

Remarks. Morphological characters of the capitulum conform to the description of the genus *Catherinum*. The sequence for the 18S gene is similar to sequences from other species within the same family. Another species within the genus, *C. tortilum* (Zevina, 1973), originally described from the Indian Ocean at 2760 m depth has also been recorded for the CCZ at similar depths (4872–4877 m depth; Poltarukha and Mel'Nik 2012). In *C. tortilum*, the inframedian latus' umbo is conspicuously displaced laterally away from the midline. The species *C. novaezelandiae* is distributed in the Western and Eastern Indian Ocean, Western Central and Southwest Pacific, from depths 455–4800 m (Shalaeva and Boxshall 2014), but was originally described from East Cape, New Zealand (Southwest Pacific), at 1280 m.

Ecology. The specimen was collected in the sedimented abyssal plain of APEI 1 at 5241 m depth. It was attached to a glass sponge stalk, along with a crinoid (Bathymetrinae inc. CCZ_176; specimen CCZ_186), a polychaete, and anemones, that was anchored in the mud.

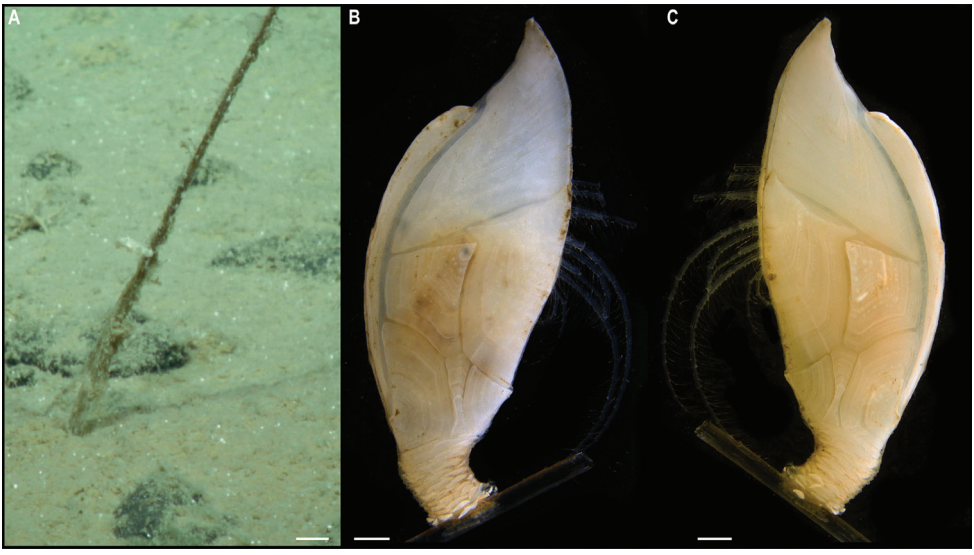

Figure 7. *Catherinum* cf. *novaezelandiae* (Hoek, 1883). Specimen CCZ_185: **A** in situ photograph **B** right **C** left lateral views. Scale bars: 1 cm (**A**); 1 mm (**B, C**). Image attribution: Durden and Smith (**A**), Hosie (**B, C**).

Comparison with image-based catalogue. Relatively large abundances of a very similar morphotype (*Catherinum* sp. indet., ART_031) were observed in seabed imagery collected within abyssal areas of the Kiribati EEZ, but not in eastern CCZ surveys.

Phylum Cnidaria Hatschek, 1888

A total of 12 cnidarians w collected, belonging to six orders in two classes (Anthozoa and Scyphozoa).

Class Anthozoa Ehrenberg, 1834
Subclass Hexacorallia Haeckel, 1896
Order Actiniaria Hertwig, 1882

To date, there are 33 records of Actiniaria found at > 3000 m depth in the CCZ (OBIS 2022), but only two of these represent collected specimens. We collected five specimens, all belonging to different species, and for which genetic sequences of the COI or 18S genes were generated and included in a phylogenetic tree built from a concatenated alignment of 12S, 16S, 18S, 28S, COI, and COX3 (Fig. 8).

Suborder Enthemonae Rodríguez & Daly in Rodríguez et al. 2014
Superfamily Metridioidea Carlgren, 1893

Metridioidea stet. CCZ_072
Fig. 9

Material. Clarion-Clipperton Zone • 1 specimen; APEI 1; 5.0442°N, 141.8165°W; 4875 m deep; 28 May. 2018; Smith & Durden leg.; GenBank: ON400696 (COI); NHMUK 2021.19; Voucher code: CCZ_072.

Description. Single specimen, white (Figs 5, 9). Body subcylindrical, pedal disc modified and attached to a glass sponge stalk, oral disc is > 2× column width; with at least two cycles of slender, tapered, long, white tentacles, almost as long as the oral disc diameter (Fig. 5A). Tubercles are evident on the top half of the column when preserved, but tentacles completely retracted (Fig. 9 A, B).

Remarks. COI sequence is similar (97.3%) to other species within the subfamily Metridioidea but based on COI we were unable to delimit species because interspecific divergence is very low. Additionally, only a few studies have included sequences for COI, therefore hindering comparisons based solely on this gene. The COI divergence between Metridiodea stet. CCZ_164 and Metridiodea stet. CCZ_072 (1.95% K2P distance) was higher than the genetic distance between other species in the family Metridiodea (Rodriguez et al. 2014), suggesting these to belong to separate species. The phylogenetic tree recovered both CCZ specimens within the subfamily Metridioidea (Fig. 8), in a clade belonging to Cuticulata. Clades within Cuticulata were not well resolved in the phylogeny, but this group includes the Graspina clade (families

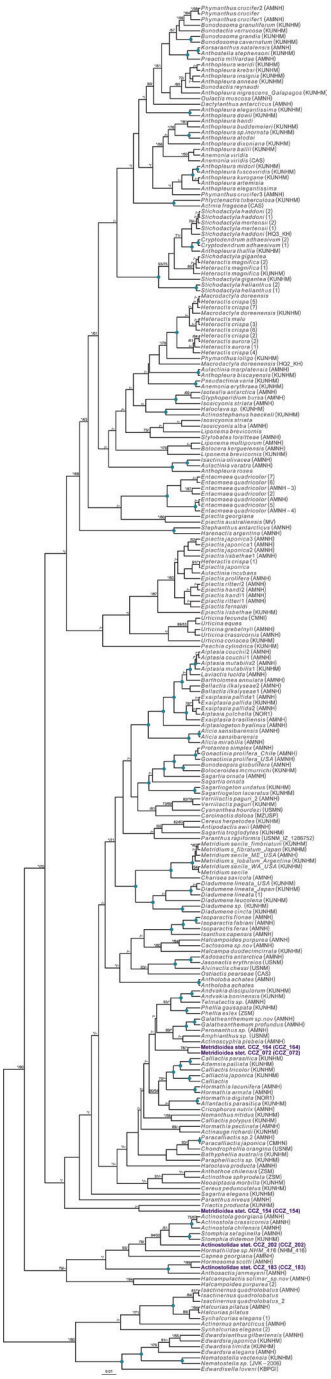

Figure 8. Rooted Bayesian phylogeny of Actiniaria. Concatenated (12S, 16S, 18S, 28S, COI, and COX3) BEAST median consensus tree with posterior probability (PP) and bootstrap (BS) values indicated. Only values of PP > 0.70 and BS > 50 are shown, with values of PP > 0.95 and BS > 90 indicated with a circle. Nodes not recovered on the RAxML tree are indicated with a hyphen. Sequences generated in this study are highlighted in violet.

Amphiantidae, Galantheanthenidae, and Actinoscyphiidae) that is characterised by a modified pedal disc that enables them to attach to other substrates, such as sponge stalks (Rodriguez et al. 2014), and is advantageous in deep-sea ecosystems. Based on this modified pedal disc, the specimen very likely belongs to a family within the Graspina clade.

Ecology. The specimen was collected in a muddy abyssal plain in APEI 7, at 4874 m depth. It was attached to a glass sponge stalk (Fig. 5A; top of stalk), along with two barnacles (*Catherinum* cf. *albatrossianum*, specimen CCZ_073; and *Triangulloscalpellum gigas*, specimen CCZ_074).

Comparison with image-based catalogue. A very similar Actiniaria morphotype (Metridioidea fam. indet., ACT_042) mostly attached to sponge stalks, has been commonly encountered in seabed image surveys conducted across the eastern CCZ but not in abyssal areas of the Kiribati EEZ.

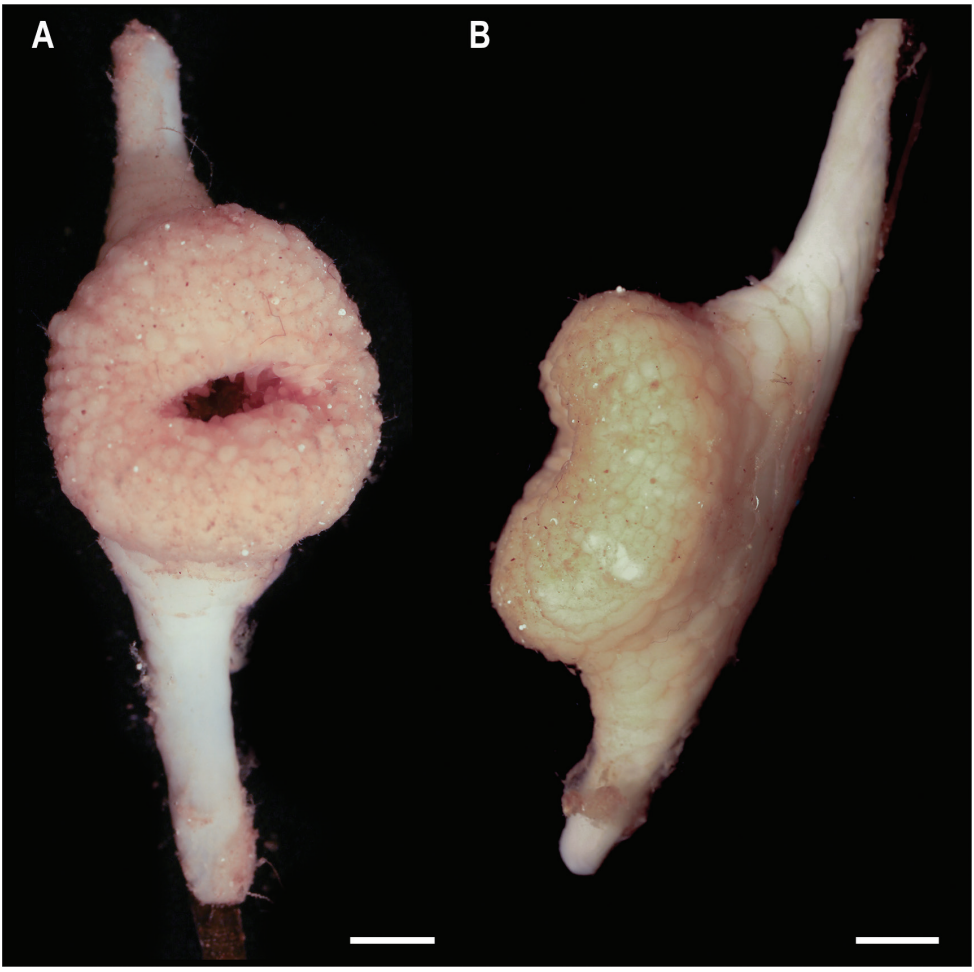

Figure 9. Metridioidea stet. CCZ_072 **A** oral **B** lateral views. Scale bars: 5 mm (**A, B**). Image attribution: Wiklund, Durden, Drennan, and McQuaid (**A, B**).

Metridioidea stet. CCZ_154
Fig. 10

Material. Clarion-Clipperton Zone • 1 specimen; APEI 4; 6.9702°N, 149.9426°W; 5009 m deep; 06 Jun. 2018; Smith & Durden leg.; GenBank: ON400715 (COI); NHMUK 2021.27; Voucher code: CCZ_154.

Description. Single specimen, completely white when alive (Fig. 10). Body of live specimen is more or less cylindrical, wider proximally and distally, 29 mm long. Pedal disc is the widest, 35 mm in diameter, attached to a manganese nodule, and oral disc 24 mm in diameter (Fig. 10B). Large and small conical, tapered tentacles alternating on the margin of the oral disc in two cycles: ~ 20 + 20, with the larger ones being approx. half the oral disc diameter and located above the smaller tentacles (Fig. 10A). Tentacles are only visible in in situ images (Fig. 10A), as they are fully retracted in the preserved specimen.

Ecology. This specimen was attached to a nodule in abyssal sediments in APEI 4 at 5009 m depth.

Remarks. The COI sequence is similar to sequences of species within different families, but in the phylogenetic tree it is recovered within the superfamily Metridioidea (Fig. 8).

Comparison with image-based catalogue. No similar Actiniaria morphotypes had been catalogued so far from seabed imagery in the eastern CCZ or in abyssal areas of the Kiribati EEZ. The in situ image of Metridiodea stet. CCZ_154 was hence catalogued as a new morphotype (i.e., Metridioidea fam. indet., ACT_044).

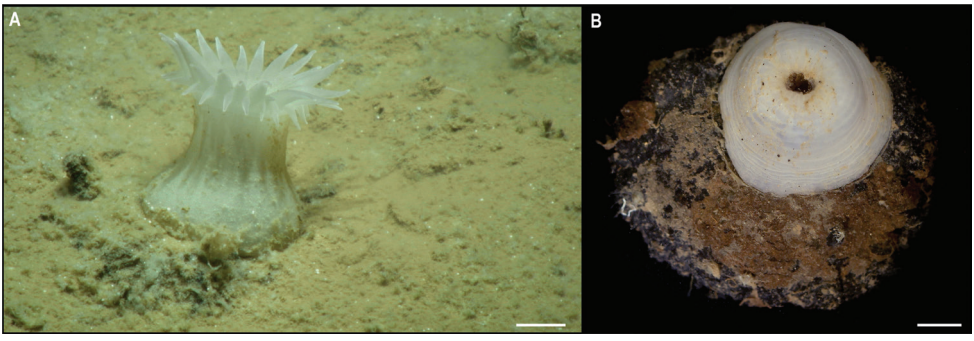

Figure 10. Metridioidea stet. CCZ_154 **A** in situ image **B** specimen before preservation. Scale bars: **A, B** 1 cm. Image attribution: Durden and Smith (**A**), Wiklund, Durden, Drennan, and McQuaid (**B**).

Metridioidea stet. CCZ_164
Fig. 11

Material. Clarion-Clipperton Zone • 1 specimen; APEI 7; 6.988°N, 149.9326°W; 5001 m deep; 06 Jun. 2018; Smith & Durden leg.; GenBank: ON400717 (COI); NHMUK 2021.5; Voucher code: CCZ_164

Description. Single specimen, white (Fig. 11A). Specimen with a short, subcylindrical column, with pedal and oral discs almost the same diameter (Fig. 11A). Long, slender, tapered, white tentacles arranged in at least two cycles (Fig. 11A). When preserved, column is more cylindrical, almost as long as wide (H = 18 mm, oral disc diameter = 21 mm), and tubercles are evident on the top half of the column; tentacles completely retracted (Fig. 11B, C).

Remarks. COI sequence is very similar to Metridiodea sp. CCZ_072 and they are recovered as sister species, in the multi-gene phylogeny, within the Cuticulata in the superfamily Metridioidea (Fig. 8). This species very likely belongs to a family within the Graspina clade (Amphiantidae, Galantheanthenidae and Actinoscyphiidae) based on the modified pedal disc that allows them to attach to substrates other than rocks (Rodriguez et al. 2014).

Ecology. This specimen was collected in muddy abyssal sediments in APEI 4 at 5001 m depth, attached to a glass sponge stalk.

Comparison with image-based catalogue. As with specimen from Metridiodea stet. CCZ_072, a very similar morphotype has been commonly found in seabed image surveys conducted across the eastern CCZ (i.e., Metridioidea fam. indet., ACT_042), but it does not seem possible to differentiate between the species Metridiodea stet. CCZ_072 and Metridiodea stet. CCZ_164 from in situ imagery. Morphotype ACT_042 is hence likely to encompass, at least, these two species in image-based analyses conducted across the CCZ.

Superfamily Actinostoloidea Carlgren, 1932
Family Actinostolidae Carlgren, 1932

Actinostolidae stet. CCZ_183
Fig. 12

Material. Clarion-Clipperton Zone • 1 specimen; APEI 1; 11.2751°N, 153.7444°W; 5241 m deep; 09 Jun. 2018; Smith & Durden leg.; GenBank: ON406626 (18S); NHMUK 2021.28; Voucher code: CCZ_183.

Description. Single specimen, white, attached to a nodule (Fig. 12A). Column is very short (3 mm), cylindrical (6 mm diameter), pedal disc much wider and completely attached to the nodule. Small tubercles scatter on the column (Fig. 12B).

Remarks. Closest matches for the 18S sequence are sequences from other members of the family Actinostolidae (> 99.3%). In the phylogenetic tree, it is also recovered in a well-supported clade with species of the family Actinostolidae (Fig. 8). However, this clade also includes *Capnea*, which has been recovered within the same clade in previous studies (Rodriguez et al. 2014), and a specimen collected in the eastern CCZ identified as a member of the family Hormathiidae (Hormathiidae sp. NHM_416, Dahlgren et al, 2016). No in situ photos are available.

Ecology. This specimen was collected in abyssal sediment in APEI 1 at 5241 m depth, attached to a polymetallic nodule.

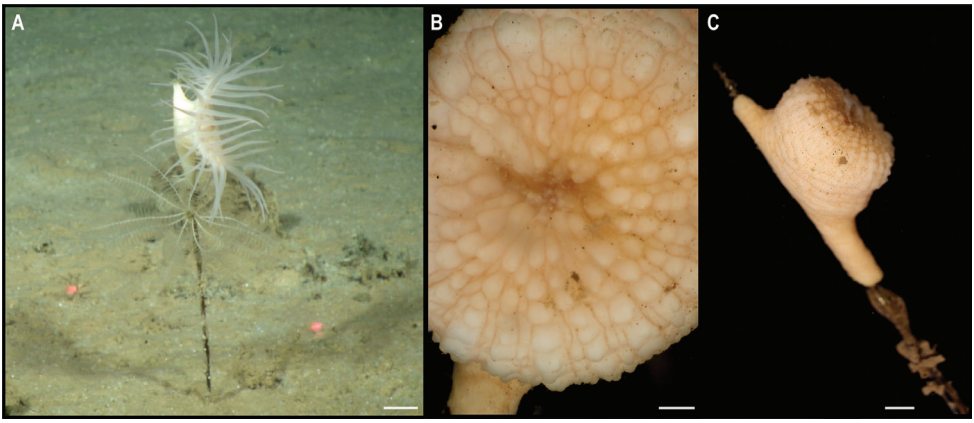

Figure 11. Metridioidea stet. CCZ_164 **A** in situ image of specimen CCZ_164 **B** detail of oral disc **C** lateral view of specimen. Scale bars: 2 cm (**A**); 2 mm (**B**); 5 mm (**C**). Image attribution: Durden and Smith (**A**), Wiklund, Durden, Drennan, and McQuaid (**B, C**).

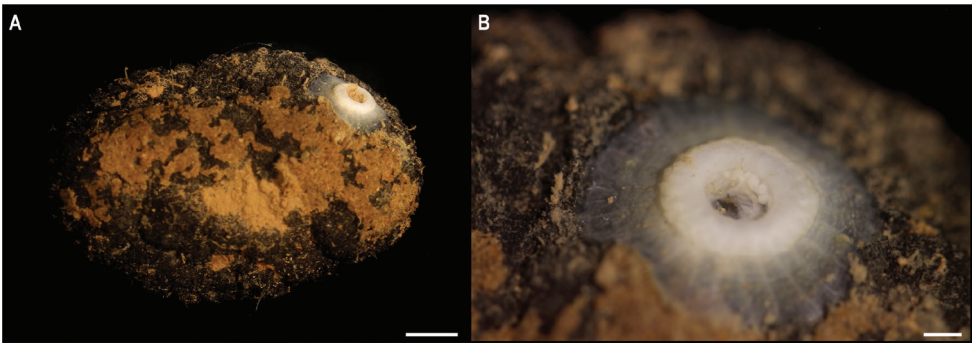

Figure 12. Actinostolidae stet. CCZ_183 **A** specimen attached to nodule **B** close-up of specimen. Scale bars: 1 cm (**A**), 2 mm (**B**). Image attribution: Wiklund, Durden, Drennan, and McQuaid (**A, B**).

Actinostolidae stet. CCZ_202
Fig. 13

Material. Clarion-Clipperton Zone • 1 specimen; APEI 4; 11.2518°N, 153.6059°W; 5206 m deep; 10 Jun. 2018; Smith & Durden leg.; GenBank: ON406627 (18S); NHMUK 2021.22; Voucher code: CCZ_202.

Description. Single, white specimen (Fig. 13A). Specimen with short column (4 mm), pedal and oral disc approx. the same diameter (8 mm). Between 8–10 white, long tentacles, approx. as long as the oral disc diameter (Fig. 13A). Column with scale-like pattern in preserved specimen (Fig. 13B), with tentacles fully retracted.

Remarks. The closest matches to the 18S sequence are species in different suborders within the Actiniaria (98.3% sequence similarity), including Hormathiidae sp. NHM_416 from the CCZ (Dahlgren et al. 2016). However, in the phylogenetic tree it is confidently recovered within the Actinostolidae (Fig. 8), along with the specimen Hormathiidae sp. NHM_416.

Ecology. This specimen was attached to a polymetallic nodule collected in abyssal sediments of APEI 1 at 5206 m depth.

Comparison with image-based catalogue. No similar Actiniaria morphotypes have been so far catalogued from seabed imagery in the eastern CCZ or in abyssal areas of the Kiribati EEZ. The in situ image of Actinostolidae stet. CCZ_202 was hence catalogued as a new morphotype (i.e., Actinostolidae gen. indet., ACT_080). However, small actiniarians (e.g., oral disc < 2 cm) are usually difficult to classify from seabed imagery as basic morphological features (e.g., number of tentacles) are often not clearly visible. Consequently, ACT_080 could be potentially confused with similarly small actinian morphotypes commonly encountered in the eastern CCZ (i.e., Hormathiidae gen. inc., ACT_022, also with a short pedal approx. the same diameter as the oral disc, but with 16–18 long thin tentacles).

Order Scleractinia Bourne, 1900

For Scleractinia, there are only two records at > 3000 m depth in the CCZ (OBIS 2022), with no specimens collected. A single scleractinian was collected, for which DNA amplification was unsuccessful.

Family Fungiacyathidae Chevalier & Beauvais, 1987
Genus *Fungiacyathus* Sars, 1872

Fungiacyathus (Fungiacyathus) cf. *fragilis* Sars, 1872
Fig. 14

Material. Clarion-Clipperton Zone • 1 specimen; APEI 4; 7.2647°N, 149.774°W; 3562 m deep; 03 Jun. 2018; Smith & Durden leg.; NHMUK 2021.26; Voucher code: CCZ_107

Description. Single specimen, solitary, and unattached, ~ 27 mm in transverse diameter. Live specimen with tapered, transparent tentacles, longer than half the corallum diameter and arranged in two or three cycles (Fig. 14A). Corallum is light brown distally and darker proximally on live specimen (Fig. 14B, C). The base is flat and the lower cycle septa are strongly arched upward; septa are arranged in five cycles, those of the fifth are rudimentary.

Remarks. No genetic sequences were obtained from this specimen. Morphological characters match the genus *Fungiacyathus*.

Ecology. This free-living specimen was found on a sedimented area on a seamount in APEI 4, at 3561 m depth.

Comparison with image-based catalogue. A very similar scleractinian morphotype (i.e., *Fungiacyathus* sp. indet., SCL_003) has been encountered in seabed image surveys conducted across the eastern CCZ but not in abyssal areas of the Kiribati EEZ, usually on sediment. As with other solitary scleractinians, this taxon could be confused with an anemone in seabed imagery (e.g., SCL_003 was originally catalogued as an

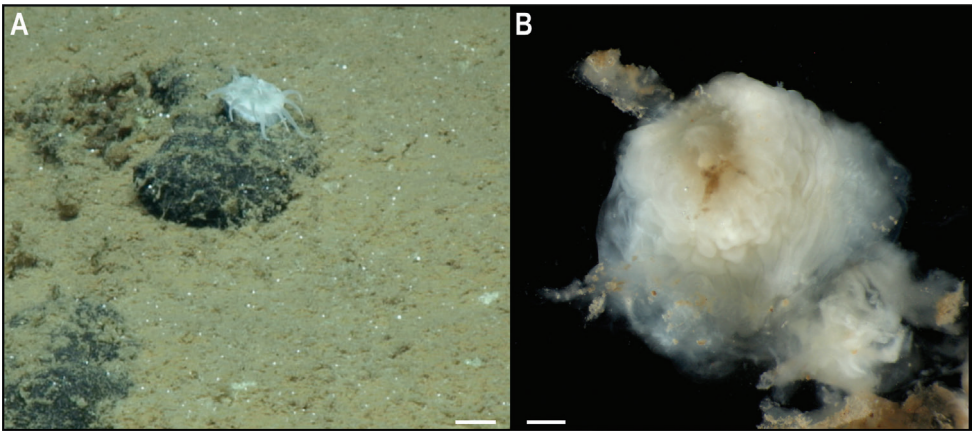

Figure 13. Actinostolidae stet. CCZ_202 **A** in situ image **B** detail of specimen. Scale bars: 1 cm (**A**); 1 mm (**B**). Image attributions: Durden and Smith (**A**), Wiklund, Durden, Drennan, and McQuaid (**B**).

Actiniaria from in situ images, which was addressed following the collection and analysis of the specimen collected in this study).

Subclass Octocorallia Haeckel, 1866
Order Alcyonacea Lamouroux, 1812

There are 131 records of Alcyonacea at > 3000 m depth in the CCZ, only eight of those representing preserved specimens (OBIS 2022). We collected three specimens belonging to three different species, only one assigned to a previously described species. Genetic sequences for both 16S and COI genes were amplified for each specimen, and included in a concatenated alignment (16S, COI, mtMutS, NADH2) used to generate a phylogenetic tree of Octocorallia (Fig. 15). Classification of Alcyonacea specimens from seabed imagery is often constrained by the lack of visibility of polyp morphology, particularly when these are small (e.g., family Primnoidae). Therefore, classification from in situ images is mostly based on broader features like the branching pattern, the length of the main stem, and/or the number, size, and positioning of polyps on branch nodes.

Suborder Calcaxonia Grasshoff, 1999
Family Chrysogorgiidae Verrill, 1883
Genus *Chrysogorgia* Duchassaing & Michelotti, 1864

***Chrysogorgia* sp. CCZ_112**
Fig. 16

Material. Clarion-Clipperton Zone • 1 specimen; APEI 4; 7.2874°N, 149.8578°W; 4125 m deep; 04 Jun. 2018; Smith & Durden leg.; GenBank: ON400711 (COI), ON406602 (16S); NHMUK; Voucher code: CCZ_112.

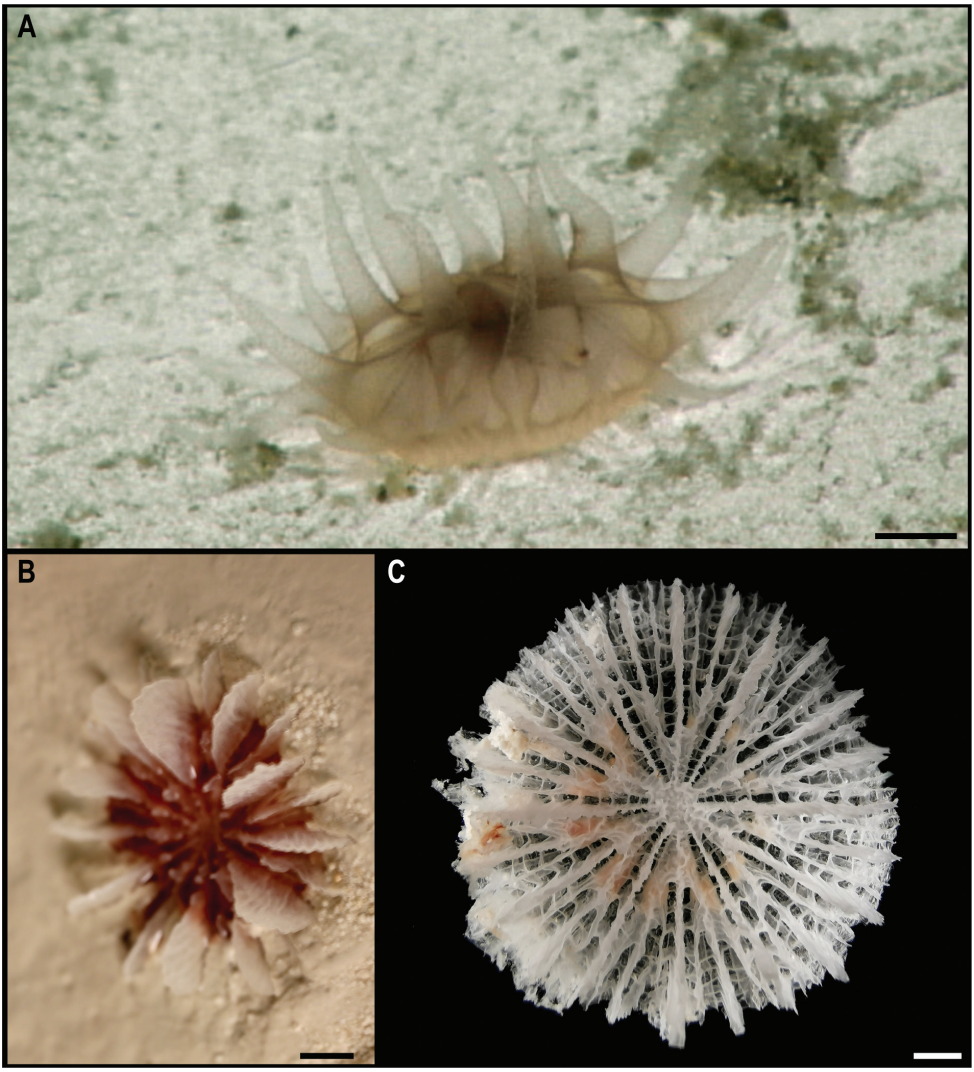

Figure 14. *Fungiacyathus (Fungiacyathus)* cf. *fragilis* Sars, 1872. Specimen CCZ_107: **A** in situ image **B** dorsal view of live specimen **C** bleached skeleton. Scale bars: 1 cm (**A**); 3 mm (**B, C**). Image attribution: Durden and Smith (**A**); Wiklund, Durden, Drennan, and McQuaid (**B**); Bribiesca-Contreras (**C**).

Description. Wide, long, sparsely branched colony, ~ 30 cm tall from the base (Fig. 16A, B). Polyps constricted basally on the neck (Fig. 16C–E), placed on internodes and absent from the main stem (Fig. 16A, B). Polyps are light orange when alive (Fig. 16C, D) and white after preservation (Fig. 16E). Sclerites near the polyp base are scale-like, but throughout the body and along the tentacle rachis are all elongate flat rods; sclerites are absent from the tentacle pinnules.

Remarks. The sequence for the COI gene is 0% divergent from a sequence of a specimen of *Chrysogorgia abludo* Pante & Watling, 2011 (specimen NAS102-3, GenBank accession number GQ180138) collected at Nashville Seamount, New England

Figure 15. Rooted Bayesian phylogeny of Octocorallia. Concatenated (16S, COI, mtMutS, NADH2) median consensus BEAST tree with posterior probability (PP) and bootstrap (BS) values indicated. Only values of PP > 0.70 and BS > 50 are shown, with values of PP > 0.95 and BS > 90 indicated with a circle. Nodes not recovered on the RAxML tree are indicated with a hyphen. Sequences generated in this study are highlighted in violet.

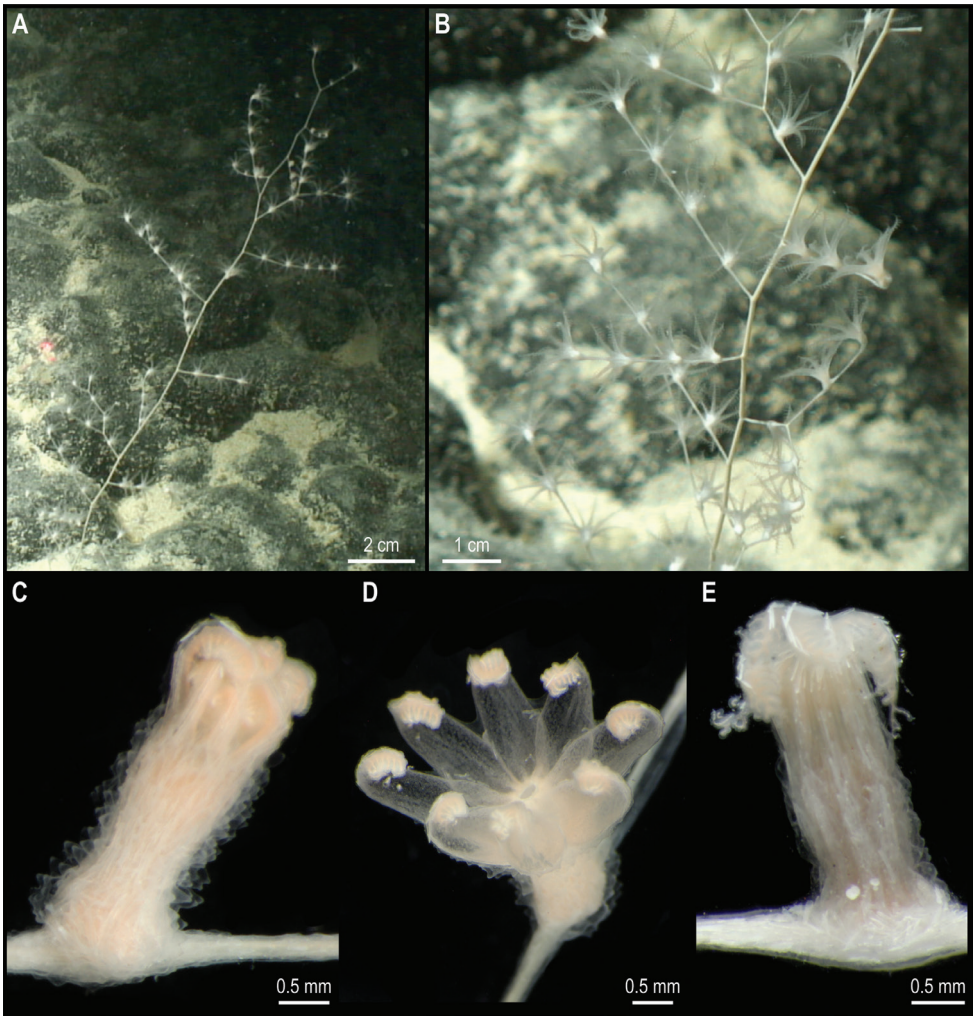

Figure 16. *Chrysogorgia* sp. CCZ_112 **A, B** in situ images of colony **C** closed polyp on live specimen **D** opened polyp on live specimen showing light orange colouration **E** closed polyp of preserved specimen. Scale bars: 2 cm (**A**); 0.5 mm (**C–E**). Image attribution: Durden and Smith (**A, B**); Wiklund, Durden, Drennan, and McQuaid (**C, D**); Bribiesca-Contreras (**E**).

Seamounts at 2246 m depth (Station 102; 34.5828°N, 56.8433°W) included as comparative material during the species description (Pante and Watling 2011). In octocorals, it has been found that COI evolves very slowly and therefore it is not suitable for species discrimination, with different species having the same haplotype (McFadden et al. 2011). *Chrysogorgia abludo* is distributed in the Atlantic Ocean, and morphological characters of the specimen collected in this study differ from the original description of *C. abludo*, as well as other species within the genus and hence considered a potentially new species In the phylogenetic tree (Fig. 15) the specimen was also recovered along with another specimen of *Chrysogorgia*, supporting its placement within the genus.

Comparison with image-based catalogue. No similar Alcyonacea morphotypes have been catalogued so far from seabed imagery in the eastern CCZ or in abyssal areas of the Kiribati EEZ. Consequently, the in situ image of *Chrysogorgia* sp. CCZ_112 was catalogued as a new morphotype (i.e., *Chrysogorgia* sp. indet., ALC_017).

Ecology. The specimen was attached to polymetallic crust on the slope of a seamount in the APEI 4, at 4124 m depth.

Family Mopseidae Gray, 1870

Mopseidae sp. CCZ_088
Fig. 17

Material. Clarion-Clipperton Zone • 1 specimen; APEI 4; 7.0089°N, 149.9109°W; 5018 m deep; 02 Jun. 2018; Smith & Durden leg.; GenBank: ON400705 (COI), ON406603 (16S); NHMUK XXX; Voucher code: CCZ_088.

Description. Single specimen, with white axis and polyps; polyps standing perpendicular to the axis when alive (Fig. 17A). Colony is long, ~ 45 cm tall, and unbranched (Fig. 17A, B). Polyps are tall, ~ 2 mm, clavate, and standing parallel to the branch (Fig. 17C).

Remarks. Both 16S (0.3% K2P) and COI (0.6% K2) sequences are very similar to Mopseinae sp. NHM_330 (Dahlgren et al. 2016), which morphologically resembles the genus *Primnoisis*. The specimen from the western CCZ likely belongs to the same genus but based on genetic and morphological differences represents a different species from that of the eastern CCZ.

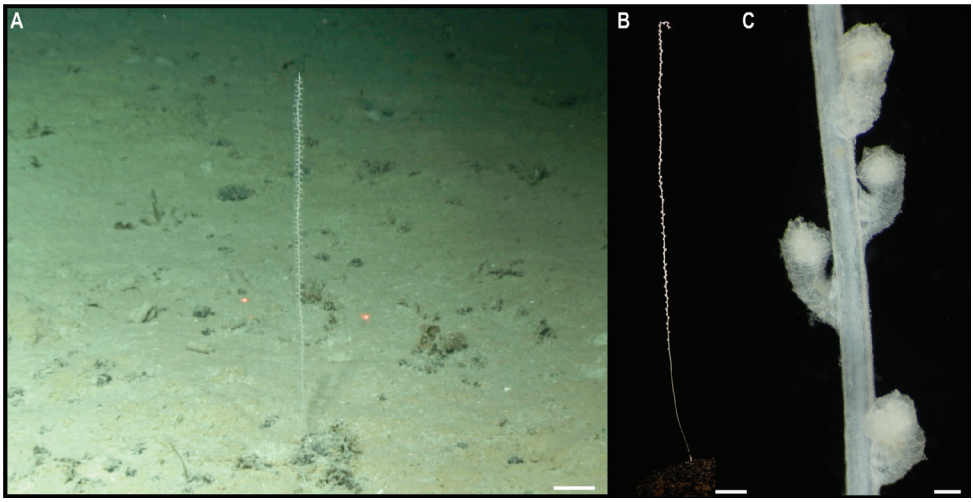

Figure 17. Mopseidae sp. CCZ_088 **A** in situ image **B** whole colony attached to a nodule **C** detail of polyps before preservation. Scale bars: 5 cm (**A**); 2 cm (**B**); 5 mm (**C**). Image attribution: Durden and Smith (**A**); Wiklund, Durden, Drennan, and McQuaid (**B, C**).

Ecology. The specimen was found attached to a nodule in abyssal sediments of APEI 4 at 5018 m depth.

Comparison with image-based catalogue. No similar Alcyonacea morphotypes had been catalogued so far from seabed imagery in the eastern CCZ or in abyssal areas of the Kiribati EEZ. Consequently, the in situ image of CCZ_088 was catalogued as a new morphotype (i.e., Mopseidae gen. indet., ALC_018). However, it is often not possible to determine whether such small and abundant polyps are arranged in pairs or not, or the actual orientation of these with regards to the axis from seabed images.

Family Primnoidae Milne Edwards, 1857
Genus *Calyptrophora* Gray, 1866

***Calyptrophora distolos* Cairns, 2018**
Fig. 18

Material. Clarion-Clipperton Zone • 1 specimen; APEI 4; 7.2874°N, 149.8578°W; 4125 m deep; 04 Jun. 2018; Smith & Durden leg.; GenBank: ON400712 (COI), ON406604 (16S); USNM 1550968; Voucher: CCZ_131.

Description. Branching uniplanar, colony ~ 20.8 cm tall, with polyps perpendicular to the stem in in situ images (Fig. 18A). Downward-oriented polyps, arranged parallel to the branch, mostly paired, but a few whorls with three to four polyps are present; polyps are ~ 2.7 mm tall and with an operculum longer than either of the body wall scales (Fig. 18B, C).

Remarks. Morphological characters are concordant with the description of *Calyptrophora distolos* (Cairns 2018). In addition to the paired polyps mentioned in the species description, this specimen also presents a few whorls with three or four polyps (Fig. 18C). Polyps are downward-oriented, therefore belonging to the *wyvillei* complex (Cairns 2018). The species is most similar to *C. persephone* Cairns, 2015, which has been described for the UK-1 and BGR areas in the CCZ (Cairns 2015). However, *C. persephone* is characterised as having polyps oriented upwards, therefore belonging to the *japonica* complex, and that are consistently arranged in whorls of three or four, with each basal scale bearing two prominent distal spines. *Calyptrophora distolos* was described from the Enigma Seamount, south of Guam, at 3737 m depth, and has also been recorded for American Samoa at 2994 m depth (Cairns 2018). There are no genetic sequences available for other specimens of *C. distolos*, but the sequences generated here cluster with other species of the genus (Fig. 15). However, the genus was not recovered as monophyletic.

Ecology. The specimen was found attached to a polymetallic crust on the slope of a seamount on APEI 4, at 4124 m depth.

Comparison with image-based catalogue. A similar primnoid morphotype (i.e., *Calyptrophora distolos* sp. inc., ALC_016) was catalogued from seabed imagery (also collected on a seamount) in the eastern CCZ (e.g., Cuvelier et al. 2020), but not in abyssal areas of the Kiribati EEZ.

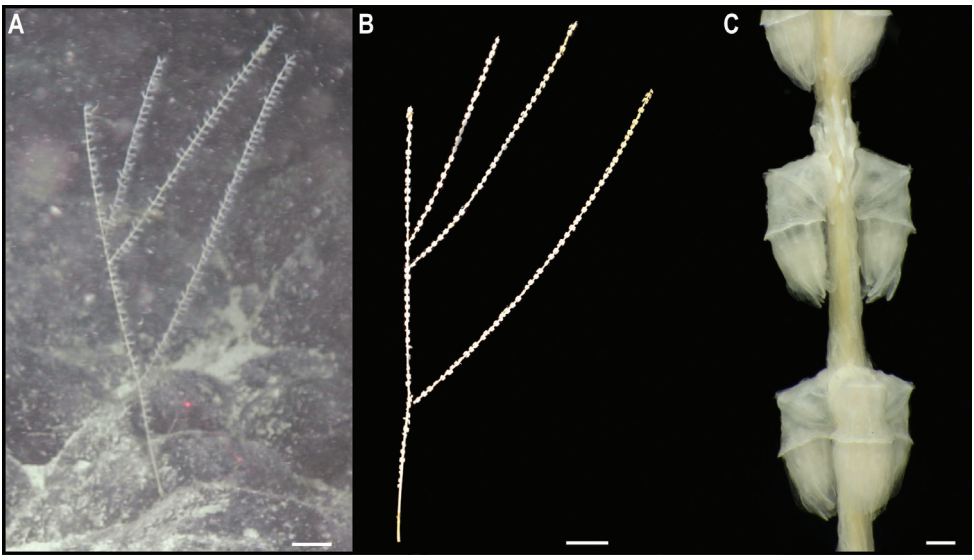

Figure 18. *Calyptrophora distolos* Cairns, 2018. Specimen CCZ_132: **A** in situ image **B** whole colony **C** detail of polyps before preservation. Scale bars: 2 cm (**A, B**); 5 mm (**C**). Image attribution: Durden and Smith (**A**); Wiklund, Durden, Drennan, and McQuaid (**B, C**).

Order Pennatulacea Verrill, 1865

A total of 79 records of Pennatulacea occurring at > 3000 m depth in the CCZ have been recorded in OBIS, but none represent preserved specimens (OBIS 2022). We recovered a single specimen, for which sequences of both 16S and COI genes were obtained, and which were included in the phylogenetic analysis of the Octocorallia (Fig. 15).

Suborder Sessiliflorae Kükenthal, 1915
Family Protoptilidae Kölliker, 1872
Genus *Protoptilum* Kölliker, 1872

Protoptilum stet. CCZ_068
Fig. 19

Material. Clarion-Clipperton Zone • 1 specimen; APEI 7; 4.8897°N, 141.75°W; 3096 m deep; 27 May. 2018; Smith & Durden leg.; GenBank: ON400694 (COI), ON406605 (16S); NHMUK 2021.24; Voucher: CCZ_068

Description. Single specimen, ~ 12 cm tall, narrow sea pen; in situ colouration orange with whitish polyps (Fig. 19A). Two rows, opposite to each other, of elongated polyp calyces along the rachis (Fig. 19B, C).

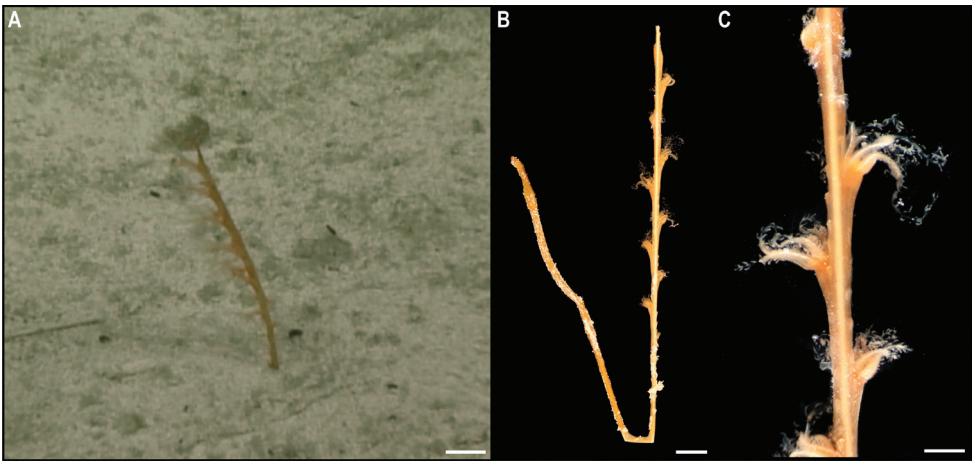

Figure 19. *Protoptilum* stet. CCZ_068 **A** in situ image **B** whole colony **C** detail of polyps before preservation. Scale bars: 1 cm (**A**); 5 mm (**B**); 2 mm (**C**). Image attribution: Durden and Smith (**A**); Wiklund, Durden, Drennan, and McQuaid (**B, C**).

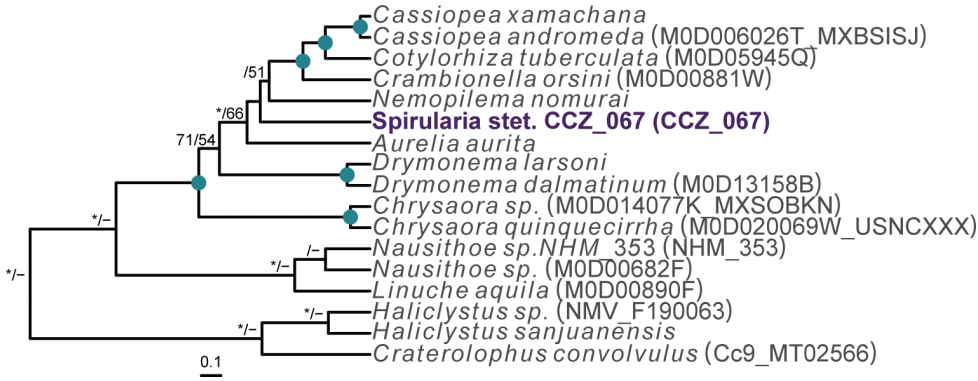

Figure 20. Rooted Bayesian phylogeny of Ceriantharia. Concatenated (12S, 16S, 18S, 28S, and COI) median consensus BEAST tree with posterior probability (PP) and bootstrap (BS) values indicated. Only values of PP > 0.70 and BS > 50 are shown, with values of PP > 0.95 and BS > 90 indicated with a circle. Nodes not recovered on the RAxML tree are indicated with a hyphen. Sequences generated in this study are highlighted in violet.

Remarks. The COI sequence forms a clade with sequences from *Protoptilum* (< 1% genetic divergence), a genus within the family Protoptilidae, while the 16S sequence is very similar to sequences of *Protoptilum* and *Distichoptilum*, both genera within the same family. In the phylogenetic tree, the family Protoptilidae was not recovered as monophyletic, but the CCZ specimen was recovered (with 1.00 posterior probability) as sister to *Protoptilum carpenterii* Kölliker, 1872.

Ecology. The specimen was found anchored to soft sediment on a seamount of APEI 7, at 3096 m depth.

Comparison with image-based catalogue. No similar Pennatulacea morphotypes have been catalogued so far from seabed imagery in the eastern CCZ or in abyssal areas of the Kiribati EEZ. Consequently, the in situ image of *Protoptilum* stet. CCZ_068 was catalogued as a new morphotype (i.e., *Protoptilum* sp. indet., PEN_024). In seabed images, PEN_024 can resemble other single-branched sea pens or even soft corals.

Subclass Ceriantharia Perrier, 1893
Order Spirularia den Hartog, 1977

To date, there are no records from a minimum of 3000 m depth in the CCZ for the order Spirularia (OBIS 2022). We recovered a single specimen, for which the COI and 16S genes were successfully amplified and included in a concatenated matrix (12S, 16S, 18S, 28S, and COI) to estimate a phylogenetic tree of the Ceriantharia (Fig. 20).

Spirularia stet. CCZ_067

Fig. 21

Material. Clarion-Clipperton Zone • 1 specimen; APEI 7; 4.8875°N, 141.7572°W; 3132 m deep; 27 May. 2018; Smith & Durden leg.; GenBank: ON400693 (COI), ON406606 (16S); NHMUK 2021.23; Voucher: CCZ_067.

Description. Single specimen, unattached, tube-dweller with tentacles extended above the sediment in situ (Fig. 21A). Very long, conical, tapering, reddish brown tentacles; capitulum whitish when alive (Fig. 21A). Column is 12 mm in height and 5 mm in width excluding tentacles (Fig. 21B). Tube consisting of soft sediment.

Remarks. The closest matches to the COI and 16S sequences were sequences from other members of the family Cerianthidae: *Pachycenrianthus*, *Cerianthus*, *Ceriantheromorphe*. However, in the concatenated phylogeny, it forms a clade with *Boctrunidifer* sp. 1 and *Ceriantheopsis americanus*, belonging to the families Botrucnidiferidae and Cerianthidae, respectively (Fig. 20). As Forero-Mejia et al. (2019) recovered both families as non-monophyletic and a revision of these is suggested, we were unable to assign it to a family.

Ecology. The specimen was found buried in the sediment on a seamount in APEI 7, at 3132 m depth.

Comparison with image-based catalogue. A very similar Ceriantharia morphotype (i.e., *Spirularia* sp. indet., CER_001) has been commonly encountered in seabed image surveys conducted across the eastern CCZ, always found semi-buried with the tentacles extending above the sediment surface.

Class Scyphozoa Goette, 1887

For the class Scyphozoa, there are currently 128 records from > 3000 m depth in the CCZ, but none represent preserved specimens (OBIS 2022). We collected a single specimen, for which the sequence for the COI gene was successfully amplified and included in a multi-gene phylogeny (16S, 18S, 28S, and COI) of the Scyphozoa (Fig. 22).

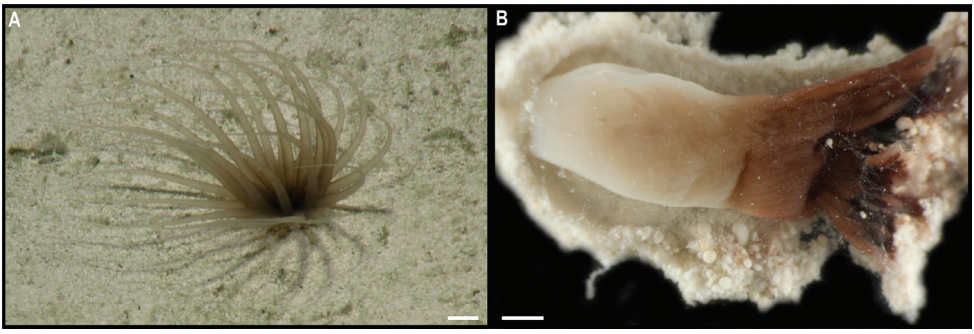

Figure 21. Spirularia stet. CCZ_067 **A** in situ image **B** specimen before preservation. Scale bars: 1 cm (**A**); 2 mm (**B**). Image attribution: Durden and Smith (**A**); Wiklund, Durden, Drennan, and McQuaid (**B**).

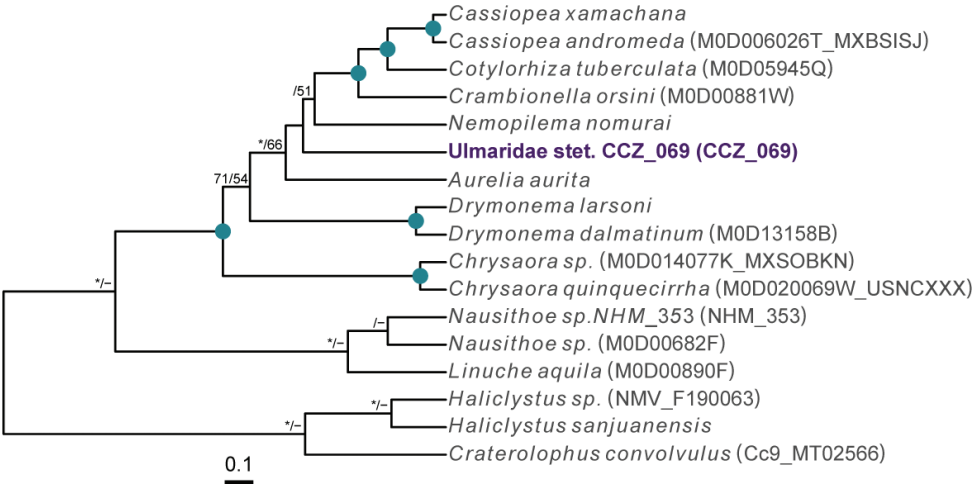

Figure 22. Rooted Bayesian phylogeny of Scyphozoa. Concatenated (16S, 18S, 28S, and COI) median consensus BEAST tree with posterior probability (PP) and bootstrap (BS) values indicated. Only values of PP > 0.70 and BS > 50 are shown, with values of PP > 0.95 and BS > 90 indicated with a circle. Nodes not recovered on the RAxML tree are indicated with a hyphen. Sequences generated in this study are highlighted in violet.

Subclass Discomedusae Haeckel, 1880
Order Somaeostomeae Agassiz, 1862
Family Ulmaridae Haeckel, 1880

Ulmaridae stet. CCZ_069
Fig. 23

Material. Clarion-Clipperton Zone • 1 specimen; APEI 7; 4.8876°N, 141.7572°W; 3133 m deep; 27 May. 2018; Smith & Durden leg.; GenBank: ON400695 (COI); NHMUK 2021.25; Voucher: CCZ_069.

Description. Single specimen, ~ 4.5 cm in diameter; with transparent bell and light brown tentacles in situ (Fig. 23A). Rhopalia are evident around the bell (Fig. 23B, C).

Remarks. Only the sequence for the COI gene was successfully amplified, but none of the matches on public databases were informative. In the phylogenetic tree (Fig. 22), the CCZ specimen was recovered in a clade with other members of the class Discomedusae. As both the Rhizostomeae and Semaeostomeae were not well supported, the specimen was not confidently assigned to any of both orders based on COI only. However, the specimen morphologically resembles an undescribed ulmariid scyphozoan (Somaeostomeae) that was observed in the New Britain Trench (Gallo et al. 2015).

Ecology. The specimen was found on the sediment of a seamount in APEI 7 at 3095–3132 m depth. A similar species of ulmariid from the New Britain Trench was found to skim the seafloor to feed on particulates on the sediment (Gallo et al. 2015).

Comparison with image-based catalogue. No similar Ulmaridae morphotypes have been catalogued so far from seabed imagery in the eastern CCZ or in abyssal areas of the Kiribati EEZ. Consequently, the in situ image of Ulmaridae stet. CCZ_069 was catalogued as a new morphotype (i.e., Ulmaridae gen. indet., SCY_010). A similarly shaped Ulmaridae morphotype (e.g., Ulmaridae gen. indet., SCY_009; opaque reddish bell, dark brown tentacles encircled with a white ring, and dark rhopalia around the bell), also eventually found crawling on the seabed surface, was previously catalogued from seabed imagery in nodule field areas of the eastern CCZ. When photographed lying on the seabed (as opposed to swimming in the water column), SCY_019 and SCY_010 may resemble an anemone, particularly in images collected at high altitude above the seabed (e.g., > 5 m).

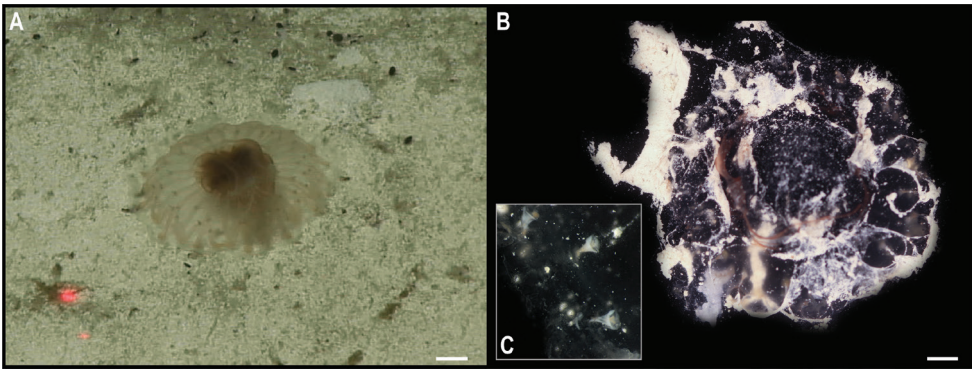

Figure 23. Ulmaridae stet. CCZ_069 **A** in situ image **B** specimen before preservation **C** rhopalia. Scale bars: 1 cm (**A**); 5 mm (**B**). Image attribution: Durden and Smith (**A**); Wiklund, Durden, Drennan, and McQuaid (**B, C**).

Phylum Echinodermata
Class Asteroidea de Blainville, 1830

There are currently 245 records of sea stars occurring at a minimum of 3000 m depth in the CCZ, with only five of those representing preserved specimens (OBIS 2022). Four specimens were collected on the western CCZ, and sequences of the barcoding gene COI were generated for all of them, and 16S for a single specimen. These were included in a concatenated alignment of 12S, 16S, 18S, COI, and H3 used to estimate a phylogenetic tree (Fig. 24).

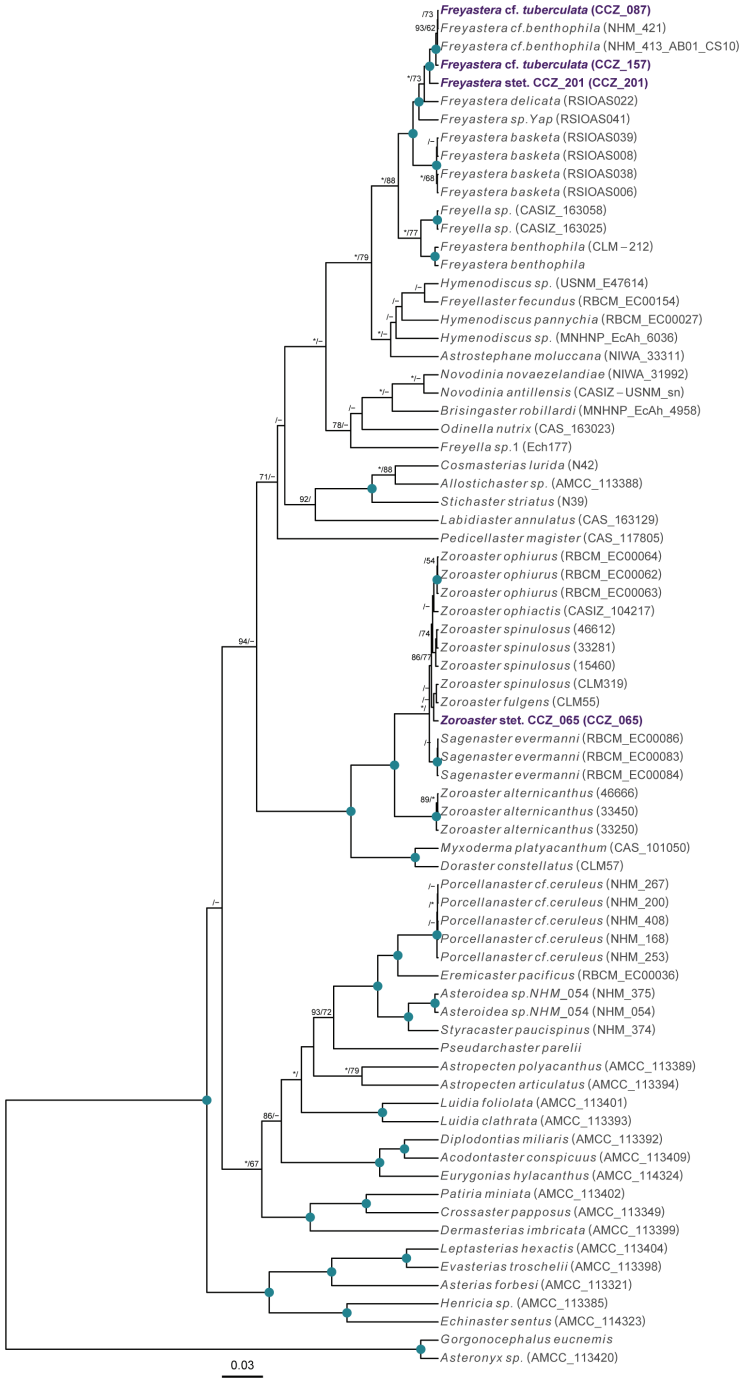

Figure 24. Rooted Bayesian phylogeny of Asteroidea. Concatenated (12S, 16S, 18S, COI, and H3) median consensus BEAST tree with posterior probability (PP) and bootstrap (BS) values indicated. Only values of PP > 0.70 and BS > 50 are shown, with values of PP > 0.95 and BS > 90 indicated with a circle. Nodes not recovered on the RAxML tree are indicated with a hyphen. Sequences generated in this study are highlighted in violet.

Superorder Forcipulatacea Blake, 1987
Order Brisingida Fisher, 1928
Family Freyellidae Downey, 1986
Genus *Freyastera* Downey, 1986

***Freyastera* cf. *tuberculata* (Sladen, 1889)**
Fig. 25

Material. Clarion-Clipperton Zone • 1 specimen; APEI 4; 6.9879°N, 149.9123°W; 5000 m deep; 02 Jun. 2018; Smith & Durden leg.; GenBank: ON400716 (COI); NHMUK 2022.80; Voucher code: CCZ_157 • 1 specimen; APEI 4; 6.9873°N, 149.9331°W; 5000 m deep; 06 Jun. 2018; Smith & Durden leg.; GenBank: ON400704 (COI); NHMUK 2022.79; Voucher code: CCZ_087.

Comparative material. Pacific Ocean • 1 specimen, holotype of *Freyella benthophila* Sladen, 1889; mid-South Pacific; 39.6833°S, 131.3833°W; 4663 m deep; Challenger Expedition, Stn. 289; NHMUK 1890.5.7.1078. Atlantic Ocean • 1 specimen, syntype of *Freyella tuberculata* Sladen, 1889; between west coast of Africa and Ascencion Islands; 22.3°N, 22.0333°W; 4389 m deep; Challenger Expedition, Stn. 346; NHMUK 1890.5.7.1077. • 1 specimen, syntype of *Freyella tuberculata*; between Canary Islands and Cape Verde Islands; 2.7° S, 14.6833°W; 4298 m deep; Challenger Expedition, Stn. 89; NHMUK 1890.5.7.1076.

Description. Two specimens (R = 106 mm, r = 3 mm; R = 164 mm, r = 6 mm); live specimens whitish on both actinal and abactinal surfaces, tube feet transparent with bright orange flattened discs (Fig. 25A, B). Disc is small, somewhat rounded, slightly orange on actinal and abactinal surfaces (Fig. 25E, F); with six long, slender arms (Fig. 25A–C); lacking furrow spines (Fig. 25D). Each abactinal plate on the genital area bears a single spinelet (Fig. 25E), covered with a membrane with pedicellariae. Each mouth plate has two oral spines covered by a clear membrane bearing pedicellariae (Fig. 25F); one located on the adoral margin of the mouth plate and the suboral spine located above the centre of the mouth plate.

Remarks. The COI sequences were very similar to sequences of *Freyastera* cf. *benthophila* (Sladen, 1889) collected in the UK-1 contract area from the CCZ (Glover et al. 2016a), and which were recovered in a single clade (Fig. 24). Only arm segments were recovered from the UK-1 specimens, and although they were found to resemble *F. benthophila*, the whole specimens collected in the western CCZ differ from the original description for the species. Only five species are known for having six rays: *F. sexradiata* (Perrier, 1885), *F. benthophila*, *F. tuberculata* (Sladen, 1889), *F. basketa* Zhang et al., 2019, and *F. delicata* Zhang et al., 2019. However, *F. benthophila* is easily distinguished from the other two species by its abactinal armament; each abactinal plate bearing two or three spinelets covered with a simple membrane with no pedicellariae (Sladen 1889). The specimens from the CCZ have abactinal spinelets covered by a membrane that bears pedicellariae (Fig. 25E). They also differ from *F. benthophila* in having the spines on the adoral margin of the mouth-plates covered by a clear

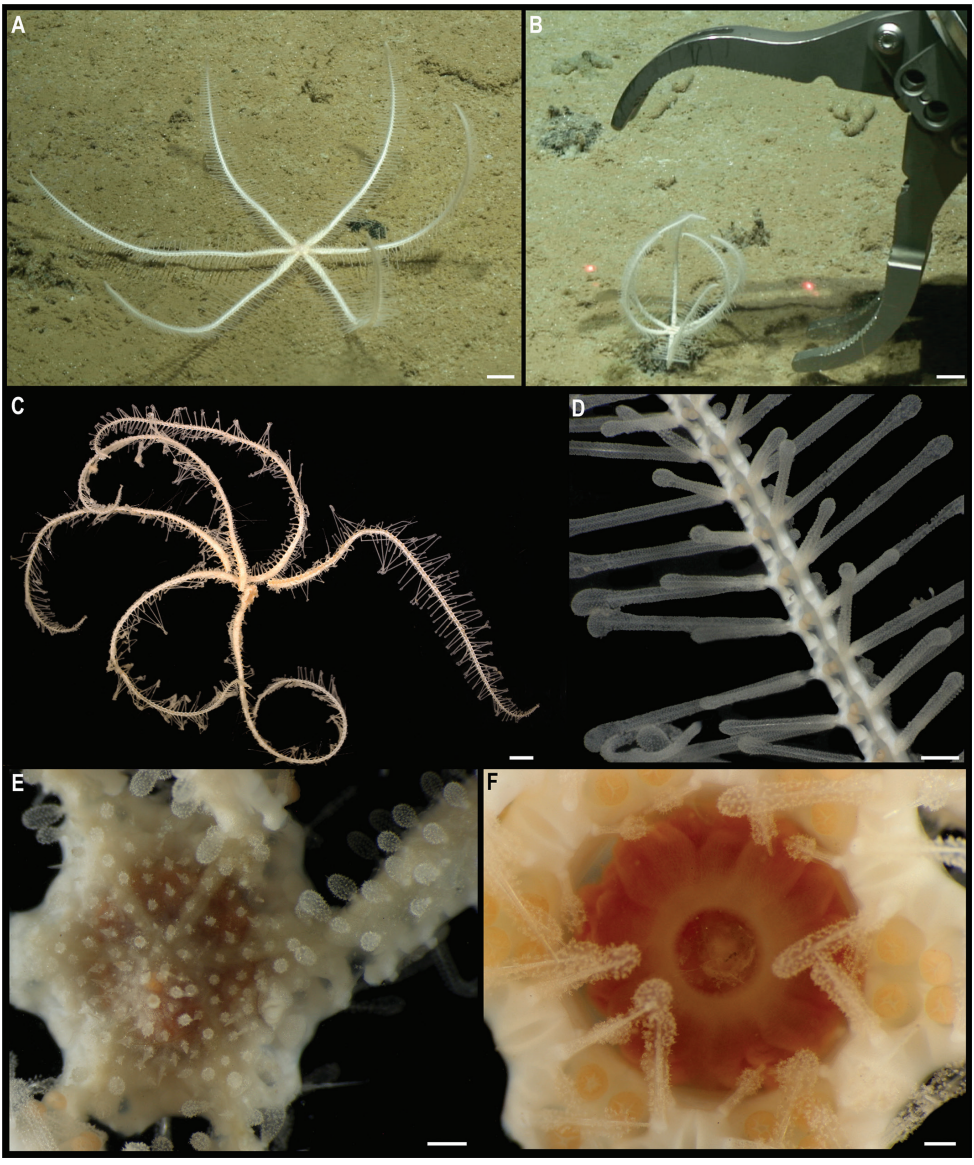

Figure 25. *Freyastera* cf. *tuberculata* (Sladen, 1889). Specimen CCZ_175: **A** in situ image **C** whole specimen **D** ventral surface of the arms before preservation. Specimen CCZ_087: **B** in situ image **E** details of dorsal disc **F** ventral disc surface before preservation. Scale bars: 2 cm (**A, B**); 1 cm (**C**); 2 mm (**D**); 1 mm (**E**); 0.5 mm (**F**). Image attribution: Durden and Smith (**A, B**); Wiklund, Durden, Drennan, and McQuaid (**C–F**).

membrane bearing pedicellariae instead of an opaque membrane with no pedicellariae (Downey 1986). In addition, the suboral spines are located above the centre of the mouth plate (Fig. 25F), as in *F. tuberculata*, and not below the centre of the mouth plate as described for *F. benthophila* (Downey 1986). Syntypes from *F. tuberculata*

are from the Atlantic Ocean (Sladen 1889), but it has been reported for the Eastern Tropical Pacific (0.05°N, 117.25°W) at 4243 m depth (Downey 1986). Unfortunately, there are no genetic sequences available for this species, but COI sequences from CCZ specimens are highly divergent from the sequence of *F. benthophila* collected in the Mariana Trench (K2P distance: 13–14%). In the phylogenetic tree they are also recovered in different clades, very close to another species reported herein, and to *F. delicata* and *Freyastera* sp. Yap (in Zhang et al. 2019) (Fig. 24). The specimen collected here represents the same species as found in the eastern CCZ, *Freyastera* cf. *benthophila* (Glover et al. 2016b).

Ecology. One specimen was observed on the sedimented seafloor (CCZ_157), while another was sitting on a nodule with the actinal surface against the muddy seafloor and lifting the tip of the arms like a basket (CCZ_087). Both seastars were collected on abyssal sediments of APEI 4 at 5000 m depth. During morphological examination of these samples, the exoskeleton of a large (> 6 mm long), digested copepod was found in the stomach of specimen CCZ_157.

Freyastera stet. CCZ_201

Fig. 26

Material. Clarion-Clipperton Zone • 1 specimen; APEI 1; 11.2518°N, 153.6059°W; 5204 m deep; 10 Jun. 2018; Smith & Durden leg.; GenBank: ON400730 (COI); NHMUK 2022.81; Voucher code: CCZ_201.

Comparative material. Pacific Ocean • 1 specimen, holotype of *Freyella benthophila* Sladen, 1889; mid-South Pacific; 39.6833°S, 131.3833°W; 4663 m deep; Challenger Expedition, Stn. 289; NHMUK 1890.5.7.1078. Atlantic Ocean • 1 specimen, syntype of *Freyella tuberculata* Sladen, 1889; between west coast of Africa and Ascencion Islands; 22.3°N, 22.0333°W; 4389 m deep; Challenger Expedition, Stn. 346; NHMUK 1890.5.7.1077. • 1 specimen, syntype of *Freyella tuberculata*; between Canary Islands and Cape Verde Islands; 2.7°S, 14.6833°W; 4298 m deep; Challenger Expedition, Stn. 89; NHMUK 1890.5.7.1076.

Description. Single specimen, with very small disc and six long, slender, tapered arms (R = 190 mm, r = 5 mm; Fig. 26A). Specimen before preservation has a slightly orange adoral disc surface, white arms, and bright orange tube feet discs (Fig. 26A–D). Disc is somewhat rounded, covered with short, scattered spines covered by a membrane bearing pedicellariae (Fig. 26B). Arms with long, slender lateral spines, also covered with a membrane bearing pedicellariae (Fig. 26C). Each abactinal plate on the genital area bears a one to few spinelets, completely covered with a membrane with pedicellariae. Each mouth plate has two oral spines covered by a clear membrane bearing pedicellariae; one located on the adoral margin of the mouth plate and the suboral spine located above the centre of the mouth plate.

Remarks. The COI sequence is 4% divergent from the two specimens of *Freyastera* cf. *tuberculata* reported herein, and hence considered a separate species. It is also divergent (> 4% K2P distance) to sequences of other species of *Freyastera*, but forms a

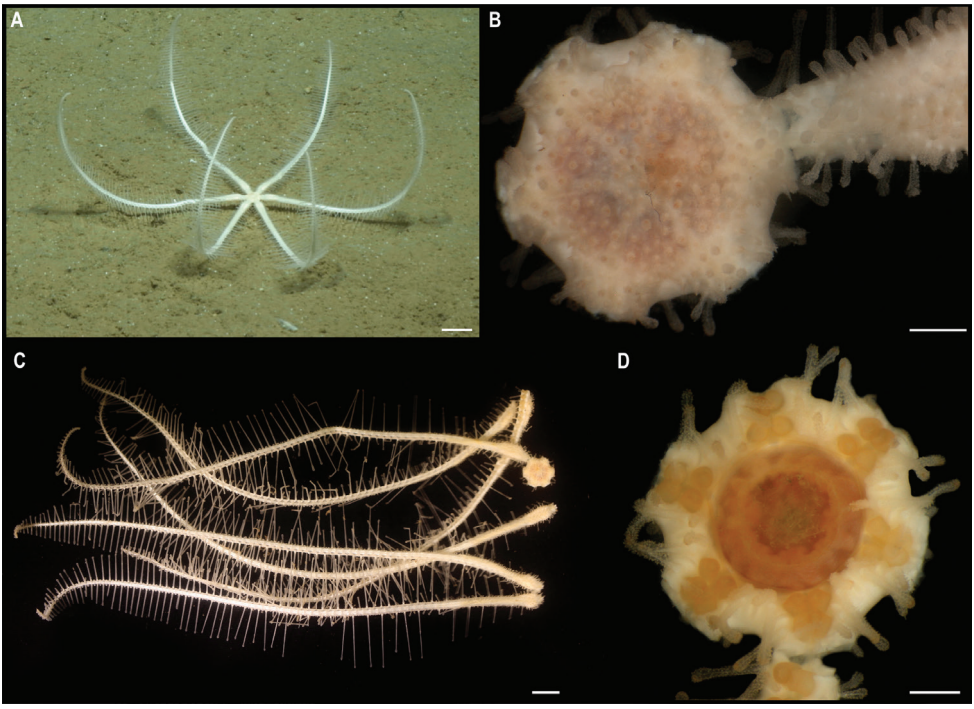

Figure 26. *Freyastera* stet. CCZ_201 **A** in situ image **B** whole specimen **C** dorsal disc surface **D** ventral disc surface. Scale bars: 2 cm (**A**); 2 mm (**B**); 1 cm (**C**); 2 mm (**D**). Image attribution: Durden and Smith (**A**); Wiklund, Durden, Drennan, and McQuaid (**B–D**).

monophyletic clade with those, confirming its placement within the genus (Fig. 24). Morphologically it resembles *Freyastera* cf. *tuberculata*, but differ in having slightly shorter and more scattered spinelets on the abactinal surface of the disc. Also, the spinelets on the abactinal plates on the genital area are more numerous, and completely covered by a membrane bearing pedicellariae, instead of having a membrane that does not cover the spine all the way down to the base as in *F.* cf. *tuberculata*. In addition, the genetic distance with specimens of that species corresponds to the genetic distance between morphologically distinct species and hence considered a separate species.

Ecology. The specimen was collected on the sedimented abyssal plain of APEI 1 at 5204 m depth, with arms curled up like a basket (Fig. 26A).

Comparison with image-based catalogue. *Freyastera* spp. are commonly found in image-based megafauna assessments across the CCZ (e.g., Amon et al. 2016; Amon et al. 2017b), abyssal areas of the Kiribati EEZ, and other areas of the Pacific abyss (e.g., Peru Basin: Simon-Lledó et al. 2019a), both in nodule fields and in seamount areas. The relatively large size of adult specimens facilitates the detection of these brisingids even upon imagery collected at high altitudes (> 5 m) above the seabed. However, only one *Freyastera* sp. morphotype (e.g., *Freyastera* sp. indet., AST_002) has been catalogued so far, as differences in structure of the abactinal armament and/or the suboral spines are not visible from seabed images.

Order Forcipulatida Perrier, 1884
Family Zoroasteridae Sladen, 1889
Genus *Zoroaster* Wyville Thomson, 1873

***Zoroaster* stet. CCZ_065**
Fig. 27

Material. Clarion-Clipperton Zone • 1 specimen; APEI 7; 4.8877°N, 141.7569°W; 3132 m deep; 27 May. 2018; Smith & Durden leg.; GenBank: ON400691 (COI), ON406607 (16S); NHMUK 2022.78; Voucher code: CCZ_065.

Description. Single specimen (R = 16.6 cm, r = 1.3 cm). Actinal and abactinal surfaces are bright orange when alive, with ambulacrum slightly darker orange (Fig. 27A–D). Small disc; with five long, slender arms, gradually tapering distally (Fig. 27B). Carinal plates bear conical primary spines, forming a single longitudinal row that runs along the arm (Fig. 27A, C).

Remarks. Morphological characters are concordant with the description of the genus *Zoroaster*. The phylogenetic analyses also recovered the specimen in a well-supported clade with other species of the genus (Fig. 24). However, COI divergence between species in the genus is very low (K2P distance ≈ 1–2%) and species-level clades were not recovered in the phylogeny, preventing us from assigning it to any species based on COI sequences. The closest match to the COI sequence of the CCZ specimen is a sequence from the long-armed morphotype (K2P distance 0.6%, GenBank accession number AY225785.1) identified for *Z. fulgens* Wyville Thomson, 1873 in the Porcupine Seabight, Atlantic Ocean (50.1987°N, 14.6593°W; 4001 m depth; Howell et al. 2004). Although this value is concordant with intraspecific divergence in the genus, the 16S sequences divergence between the CCZ specimen and the long-armed morphotype (K2P 1.1%) is larger than between the long-armed morphotype and *Z. spinulosus* Fisher, 1906 (K2P 0.0%) and between *Z. spinulosus* and *Z. ophiactis* Fisher, 1916 (K2P 0.3%).

Ecology. The specimen was found partially buried in the sediment on the seamount on APEI 7 at 3133 m depth.

Comparison with image-based catalogue. No similar Zoroasteridae morphotypes have been catalogued so far from seabed imagery in the eastern CCZ nor in abyssal areas of the Kiribati EEZ. Consequently, the in situ image of Zoroaster stet. CCZ_065 was catalogued as a new morphotype (i.e., *Zoroaster* sp. indet., AST_025).

Class Crinoidea

To date, there are 66 records of crinoids occurring deeper than 3000 m in the CCZ, with only seven of these representing preserved specimens (OBIS 2022). Three specimens, belonging to two species, were collected in the western CCZ. The barcoding gene COI was amplified for all specimens, and sequences were included in a concatenated alignment (16S, 18S, 28S, COI, and CytB) used to estimate a phylogenetic tree for the class (Fig. 28).

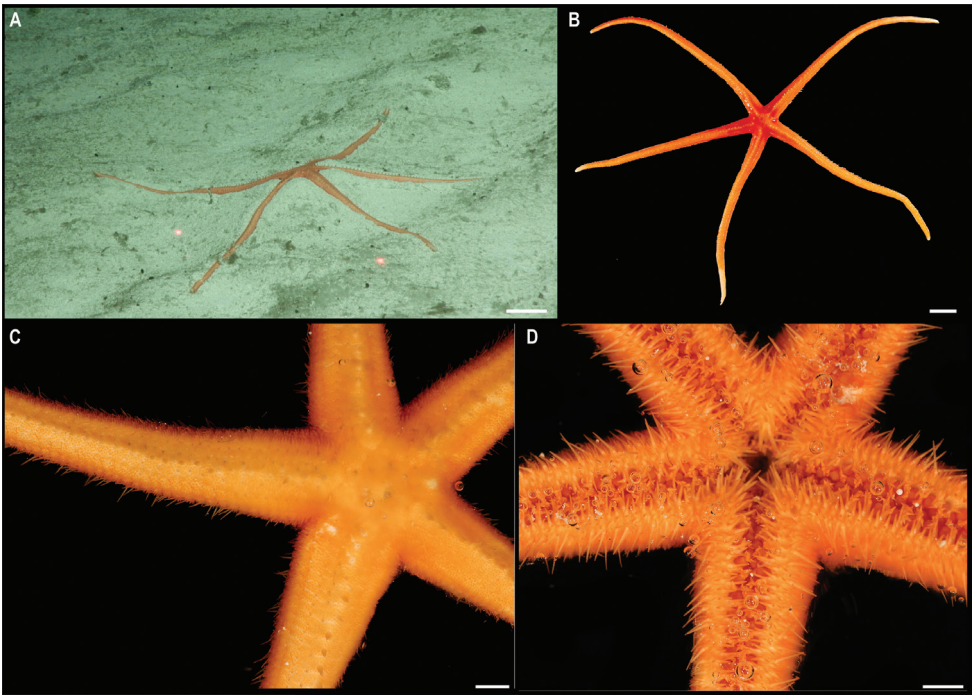

Figure 27. *Zoroaster* stet. CCZ_065 **A** in situ image **B** abactinal view of whole specimen **C** detail of abactinal surface **D** detail of actinal surface before preservation. Scale bars: 3 cm (**A**); 2 cm (**B**); 5 mm (**C, D**). Image attribution: Durden and Smith (**A**); Wiklund, Durden, Drennan, and McQuaid (**B–D**).

Subclass Articulata Zittel, 1879
Order Comatulida
Suborder Bourgueticrinina Sieverts-Doreck, 1953
Family Phrynocrinidae AH Clark, 1907
Subfamily Porphyrocrininae AM Clark, 1973
Genus *Porphyrocrinus* Gislén, 1925

cf. *Porphyrocrinus* sp. CCZ_165
Fig. 29

Material. Clarion-Clipperton Zone • 1 specimen; APEI 4; 6.9879°N, 149.9327°W; 5002 m deep; 06 Jun. 2018; Smith & Durden leg.; GenBank: ON400718 (COI), ON406616 (16S); NHMUK 2022.76; Voucher code: CCZ_165.

Description. Single specimen, attached to a nodule by a xenomorphic stalk (Fig. 29A). Crown (Fig. 29C) detached from stalk (Fig, 29B); L = 32 mm, composed of a crown and short proximal part of stalk. Proximal stalk composed of 5 very thin discoidal columnals up to 0.54 mm in diameter. Basal circlet truncated conical with distal diameter 0.54 mm and adoral diameter 0.78 mm; basals five, pentagonal

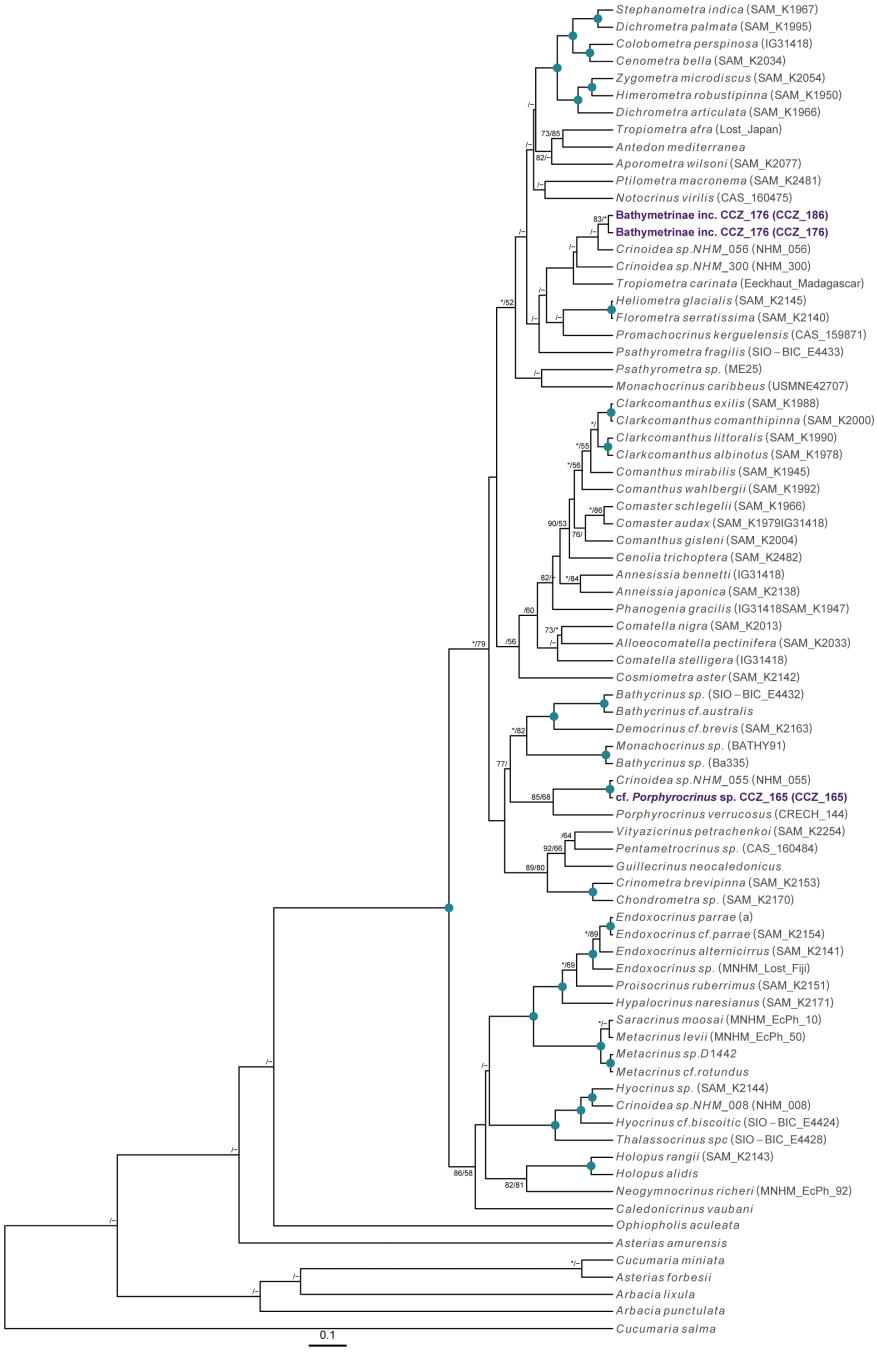

Figure 28. Rooted Bayesian phylogeny of Crinoidea. Concatenated (16S, 18S, 28S, COI, and CytB) median consensus BEAST tree with posterior probability (PP) and bootstrap (BS) values indicated. Only values of PP > 0.70 and BS > 50 are shown, with values of PP > 0.95 and BS > 90 indicated with a circle. Nodes not recovered on the RAxML tree are indicated with a hyphen. Sequences generated in this study are highlighted in violet.

in shape, with sunken lateral edges. Marked angle (~ 120°) between basals and radials. Radials five, pentagonal in shape; distal diameter 1.48 mm. Crown has five undivided arms. IBr1 are in close apposition with thin lateral flanges. Brachial formula 1+2 3+4 5+6 7+8 8+9 etc. First pinnule at IBr6; following pinnules every second ossicle; P1 has eight segments 4.04 mm in length; P2 is similar with eight pinnulars and 4.9 mm in length; P1 and P2 display lateral discoidal plates along ambulacral groove.

Remarks. Morphological characters are concordant with those of the family Phrynocrinidae and the genus *Porphyrocrinus* as understood by Messing (2016). This is the first record of the genus in the Eastern Pacific. Only two specimens have been previously recorded from similar depths but collected from the Eastern Atlantic and attributed to *Porphyrocrinus* cf. *incrassatus* (Eléaume et al. 2012). In the phylogenetic tree the specimen is recovered in a monophyletic clade with other sequences from members of the family (Fig. 28) and represents a new species. Based on genetic divergence of the COI gene (0.5% K2P), the specimen found in the eastern CCZ (Crinoidea sp. NHM_055; Glover et al. 2016b) belongs to the same species. However, the specimen in Glover et al. (2016b) was not identified to family level or lower taxonomic level due to its early developmental stage, lacking key diagnostic morphological features.

Ecology. The specimen was found attached to a nodule in the abyssal sediments of APEI 4 at 5001 m depth.

Comparison with image-based catalogue. No similar Comatulida morphotypes have been catalogued so far from seabed imagery in the eastern CCZ or in abyssal areas of the Kiribati EEZ. Consequently, the in situ image of CCZ_065 was catalogued as a new morphotype (i.e., *Porphyrocrinus* sp. indet., CRI_008). Note however, that the in situ image of CCZ_065 was collected from an oblique angle and zoomed-in camera, generating a detailed view of a specimen that, owing to its small size, would be otherwise difficult to identify in quantitative assessments, e.g., where images are usually collected vertically-facing, fully zoomed out, and at a higher altitude above the seabed.

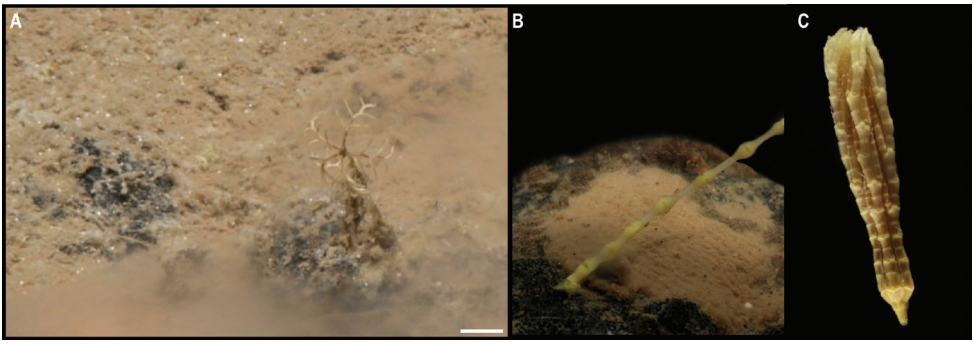

Figure 29. cf. *Porphyrocrinus* sp. CCZ_165 **A** in situ image **B** xenomorph stalk attached to a polymetallic nodule **C** detached crown before preservation. Scale bars:1 cm (**A**). Image attribution: Durden and Smith (**A**); Wiklund, Durden, Drennan, and McQuaid (**B, C**).

Superfamily Antedonoidea Norman, 1865
Family Antedonidae Norman, 1865
Subfamily Bathymetrinae AH Clark, 1909

Bathymetrinae inc. CCZ_176
Fig. 30

Material. Clarion-Clipperton Zone • 1 adult specimen; APEI 4; 6.9879°N, 149.9326°W; 5009 m deep; 06 Jun. 2018; Smith & Durden leg.; GenBank: ON400719 (COI), ON406617 (16S); NHMUK 2022.77; Voucher code: CCZ_176. • 1 specimen pentacrinoid stage; APEI 1; 11.2751°N, 153.7444°W; 5241 m deep; 09 Jun. 2018; Smith & Durden leg.; GenBank: ON400723 (COI), ON406618 (16S); NHMUK 2022.60; Voucher code: CCZ_186.

Description. Two specimens, one adult (CCZ_176; Fig. 30A, B) and one pentacrinoid stage (CCZ_186; Fig. 30C, D), both whitish when alive and attached to a glass sponge stalk. Adult with 10 arms; centrodorsal low conical. Cirri ~ 17, length 7.5 mm; c1 W > L; c2 W = L; c3 longest L = 0.95 mm, W at centre of ossicle = 0,25, W distal = 0,45; following cirrals decreasing in length to c8 or c9; c3 to c17 with everted distal edge; c8 to c14 with a spine on distal edge; c17 slightly longer than wide; claw same length as c17; opposing spine small. No basal visible. Radial 5, visible, extending beyond the rim of centrodorsal. First brachitaxis of two ossicles well separated laterally. Ibr1 rectangular slightly incised by Ibr2; Ibr2 axillery, losangic. Subsequent brachials very long; syzygies at 3+4, 9+10. First pinnule P1 on br2, 14 segments very thin and slender, composed of very long segments starting at p3 with L < 6× W. In pentacrinoid stage, five arms are visible, with orals, and stalk.

Remarks. Morphological characters are concordant with those of the subfamily Bathymetrinae in the family Antedonidae. The closest match (2.7% K2P) to the COI sequences is a sequence of *Psathyrometra fragilis* (AH Clark, 1907) from Rodriguez Seamount (1887 m; SIO-BIC E4433), within the family Zenometridae. However, in the phylogenetic analysis the specimens were recovered in a different clade from *Psathyrometra* spp. (Fig. 28), but in a well-supported clade with two species (Crinoidea sp. NHM_056, Crinoidea sp. NHM_300) from the eastern CCZ (Glover et al. 2016b). The two species previously recorded in the eastern CCZ were delimited only from genetic sequences, as they seem to be early pentacrinoid stages and thus lack morphological characters for identification. However, based on the genetic divergence values with the species Bathymetrinae inc. CCZ_176 (~ 10% K2P), the two eastern CCZ species are most likely members of the subfamily Bathymetrinae.

Ecology. The adult specimen was found attached to a glass sponge stalk (Fig. 11A), along with an anemone, in abyssal sediments of APEI 4 at 5001 m depth. After careful examination of the material in the laboratory, a pentacrinoid stage was found attached to a sponge stalk (Figs 6A, 30B), along with the cirriped *Catherinum* cf. *novaezelandiae* (specimen CCZ_185) and the anemone Metridioidea stet. CCZ_164, in abyssal sediments of APEI 1 at 5241 m depth.

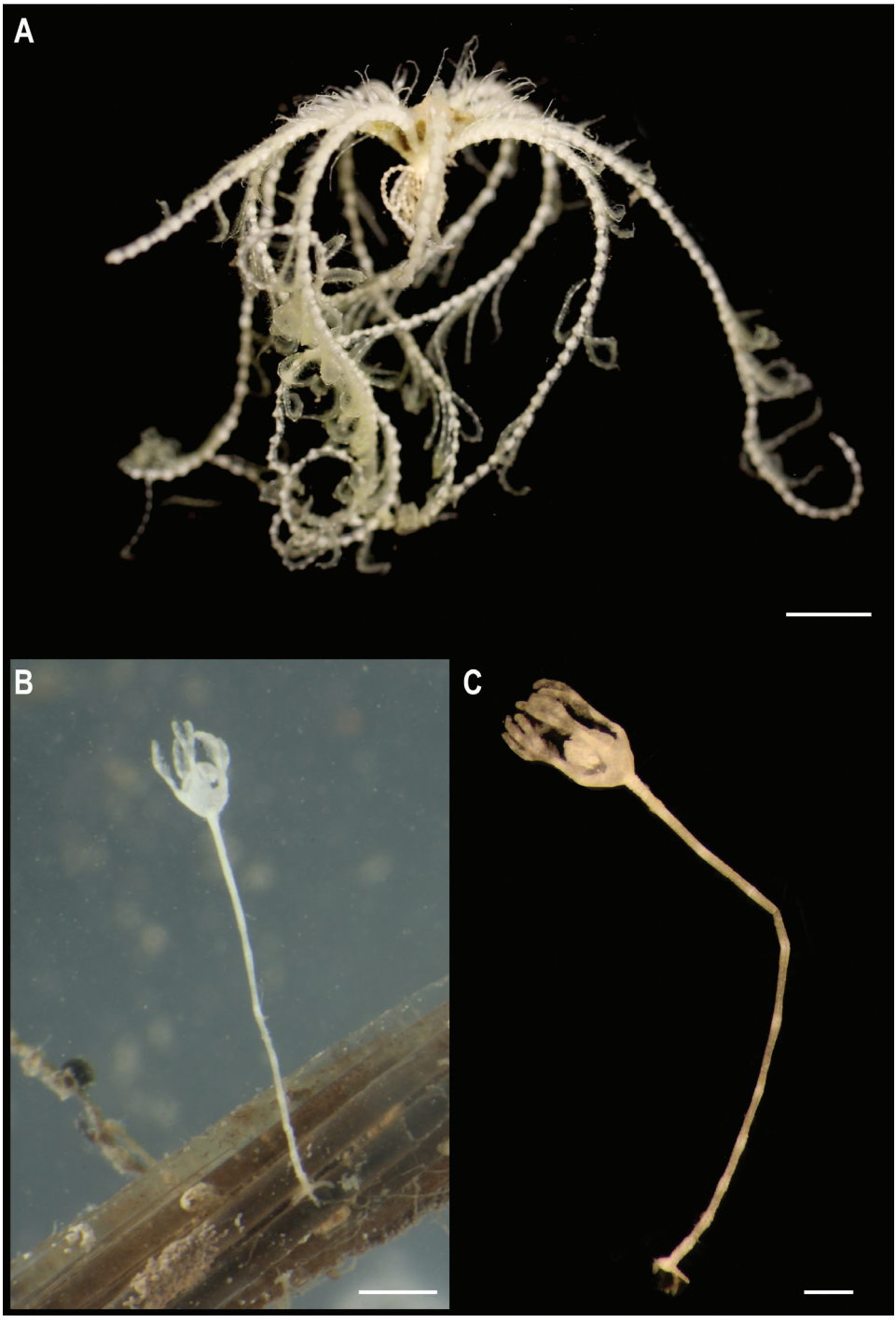

Figure 30. Bathymetrinae inc. CCZ_176 **A** side view of adult specimen. Specimen CCZ_186 **B** pentacrinoid stage attached to a glass sponge stalk **C** pentacrinoid stage. Scale bars: 5 mm (**A**); 1 mm (**B**); 0.5 mm (**C**). Image attribution: Wiklund, Durden, Drennan, and McQuaid (**A, B**); Bribiesca-Contreras 2019 (**C**).

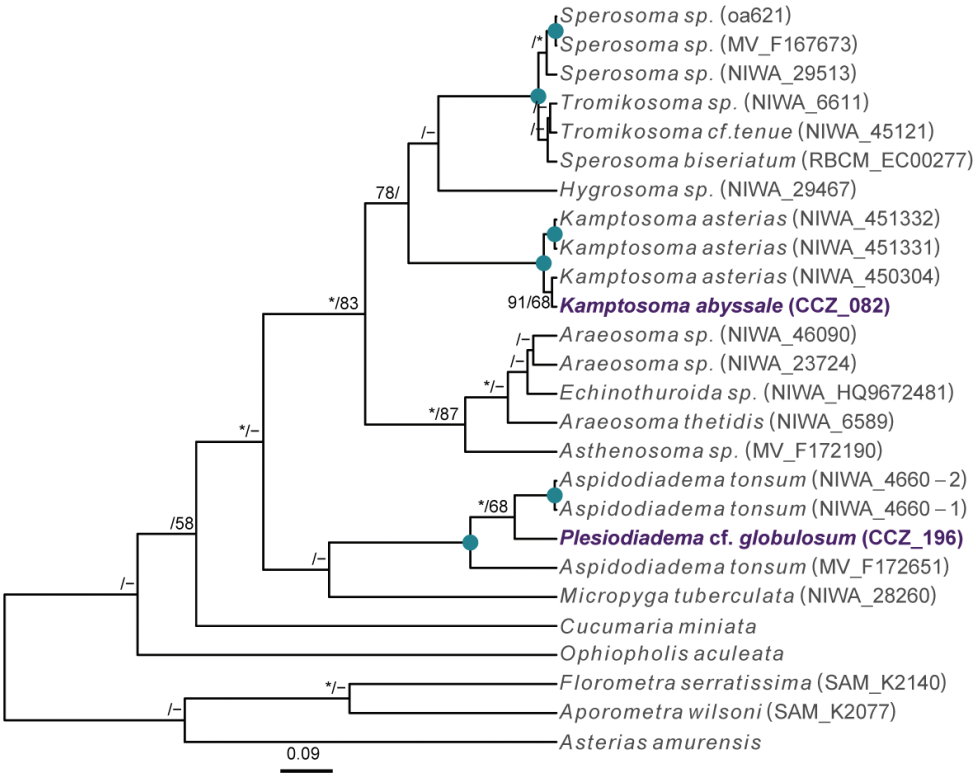

Figure 31. Phylogenetic tree of Echinoidea. COI-only median consensus BEAST tree with posterior probability (PP) and bootstrap (BS) values indicated. Only values of PP > 0.70 and BS > 50 are shown, with values of PP > 0.95 and BS > 90 indicated with a circle. Nodes not recovered on the RAxML tree are indicated with a hyphen. Sequences generated in this study are highlighted in violet.

Comparison with image-based catalogue. A very similar Comatulida morphotype (i.e., Bathymetrinae gen. indet., CRI_001) has been commonly encountered in seabed image surveys conducted across the eastern CCZ, both in nodule fields and in seamount areas (Amon et al. 2017b). In contrast, CRI_001 was not encountered in image surveys conducted within abyssal areas of the Kiribati EEZ, where the presence of Crinoids was substantially lower than at the eastern CCZ (e.g., only nine specimens representing three morphotypes encountered in ~ 15,000 m^2 of seabed surveyed; Simon-Lledó et al. 2019d).

Class Echinoidea

To date, there are 1455 records of echinoids occurring deeper than 3000 m in the CCZ, 11 of these representing preserved specimens (OBIS 2022). Two specimens belonging to different species were collected. Sequences for the barcoding gene COI were successfully amplified for both specimens and included in a COI-only phylogenetic tree.

Subclass Euechinoidea Bronn, 1860
Infraclass Audolonta Jackson, 1912
Superoder Echinothuriacea Jensen, 1982
Order Aspidodiadematoida Kroh & Smith, 2010
Family Aspidodiadematidae Duncan, 1889
Genus *Plesiodiadema* Pomel, 1883

***Plesiodiadema* cf. *globulosum* (A. Agassiz, 1898)**
Fig. 32

Material. Clarion-Clipperton Zone • 1 specimen; APEI 1; 11.2527°N, 153.5848°W; 5204 m deep; 10 Jun. 2018; Smith & Durden leg.; GenBank: ON400726 (COI), ON406628 (18S); CASIZ 229305; Voucher code: CCZ_196.

Description. Single specimen, with a somewhat spherical, slightly flattened test (d = 2 cm, H = 1.5 cm). In situ colouration is purple, but the inflated anal cone is greyish blue (Fig. 32A). Primary spines are also purple, very long (up to 17 cm), thin, flexible, and strongly verticillate (Fig. 32B, C). Pedicellariae are tridentate (Fig. 32C).

Remarks. In 1980, the RV *Governor Ray* collected several Aspidodiadematidae specimens in the CCZ at ~ 4,800 m, and were assigned to the species *P. globulosum*. The type localities of *P. globulosum* are the north of Malpelo Island, and from off Galera Point, Ecuador in the Pacific Ocean, from 2877 to 3241 m depth (Agassiz 1898). There are no genetic sequences available on public databases for the genus, but both COI and 18S closest matches are to species of the genus *Aspidodiadema* A. Agassiz, 1879, within the same family (18S: 99.4% similar to *A. jacobyi* A. Agassiz, 1880). The COI-only tree recovered a monophyletic clade including three specimens of *A. tonsum* (Fig. 31), but the genetic divergence is within interspecific values for COI (6.5–11.7%). Despite morphological characters being in accordance with the diagnostic characters for *P. globulosum*, the specimen is listed as cf. as the collection site is much deeper than the type locality.

Ecology. The specimen was collected on the sedimented abyssal plain of APEI 1, at 5203 m depth.

Comparison with image-based catalogue. A very similar *Plesiodiadema* sp. morphotype (i.e., *Plesiodiadema globulosum* sp. inc., URC_003) has been commonly found in image-based megafauna assessments conducted in the eastern CCZ (e.g., Amon et al. 2017b) and other areas of the eastern Pacific abyss (e.g., Yuzhmorgeologiya exploration area; Kamenskaya et al. 2013; Peru Basin; Simon-Lledó et al. 2019a), both in nodule fields and in seamount areas. URC_003 is usually the most abundant echinoid encountered in image-based megafauna surveys conducted at the eastern CCZ. In contrast, URC_003 was not encountered in surveys conducted in abyssal areas of the Kiribati EEZ, where kamptosomatids (e.g., see below) appeared to dominate the echinoid community (Simon-Lledó et al. 2019d).

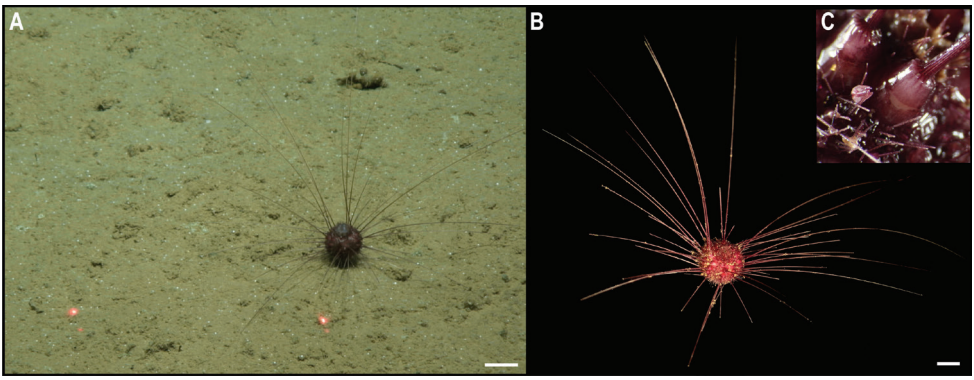

Figure 32. *Plesiodiadema* cf. *globulosum* (A. Agassiz, 1898). Specimen CCZ_196: **A** in situ image **B** specimen after recovery **C** detail of pedicellaria of specimen CCZ_196. Scale bars: 2 cm (**A**); 1 cm (**B**). Image attribution: Durden and Smith (**A**); Wiklund, Durden, Drennan, and McQuaid (**B, C**).

Order Echinothurioida Claus, 1880
Family Kamptosomatidae Mortensen, 1934
Genus *Kamptosoma* Mortensen, 1903

Kamptosoma abyssale Mironov, 1971

Fig. 33

Material. Clarion-Clipperton Zone • 1 specimen; APEI 4; 7.036°N, 149.9395°W; 5040 m deep; 01 Jun. 2018; Smith & Durden leg.; GenBank: ON400701 (COI); CASIZ 229306; Voucher code: CCZ_082.

Other material. Pacific Ocean • 1 specimen, holotype of *Kamptosoma asterias* (A. Agassiz); off the coast of Chile; 33.5167°S, 74.7167°W; 3950 m deep; Challenger Expedition, Stn. 299; NHMUK 1881.11.22.114. • 2 specimens, *Kamptosoma abyssale* Mironov, 1971; Tasman Sea; 0°N, 0°E; 4850–4800 m deep; Galathea Expedition, Stn. 574; NHMUK 1984.1.25.86-87.

Description. Single specimen (d = 3.4 cm, H = 1.6 cm). In situ, the body is reddish brown, rounded and flattened (Fig. 33A, B). Spines are the same reddish brown colour of the body; oral primary spines are encased by a fleshy, clear sac, swollen and brighter at the tip. The test and covering skin are very thin and gonads are visible through; primary spines are projected upwards and tube feet extending downwards from the lower half of the body. Whole abactinal surface (ambulacral and interambulacral) covered by primaries arranged in irregular lines along the median lines of the plates, with few secondaries or militaries near ambitus (Fig. 33C). Claviform (globiferous) pedicellariae carries two saccules and two valves. Before preservation, colouration was bright orange.

Remarks. Only two species of *Kamptosoma* have been described to date. *Kamptosoma asterias* (Agassiz, 1881) was first described from off the coast of Chile

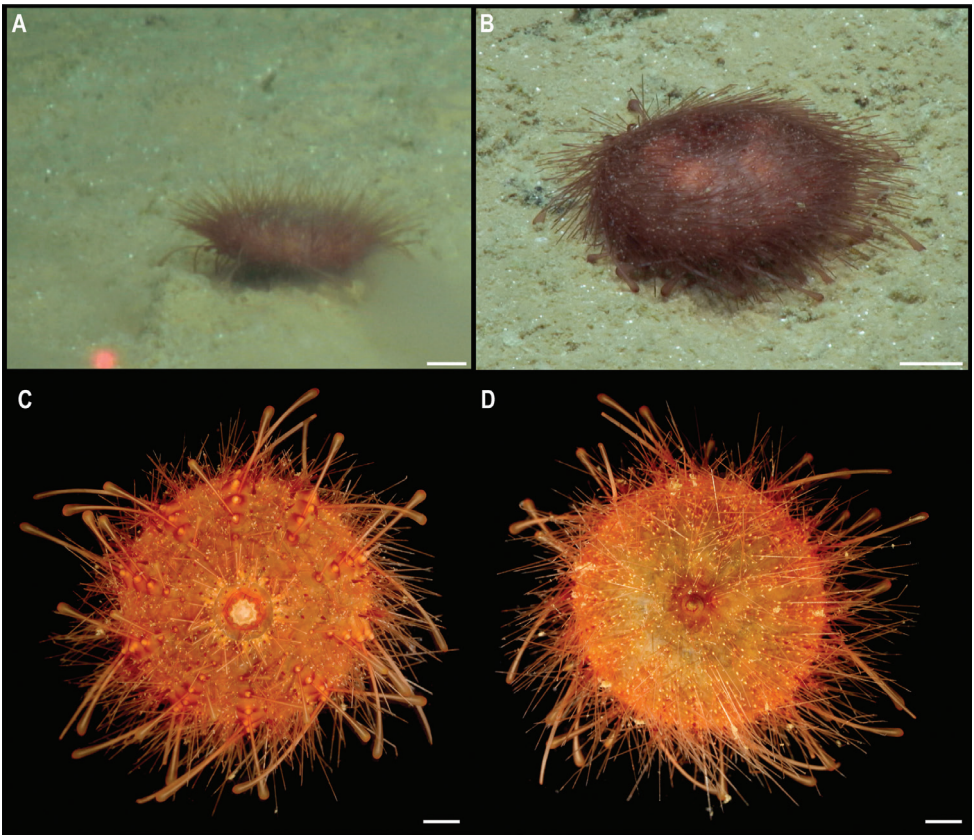

Figure 33. *Kamptosoma abyssale* Mironov, 1971. Specimen CCZ_082: **A, B** in situ images **C** oral view **D** aboral view of specimen before preservation. Scale bars: 1 cm (**A, B**); 5 mm (**C, D**). Image attribution: Durden and Smith (**A, B**); Wiklund, Durden, Drennan, and McQuaid (**C, D**).

at 3950 m depth (type locality: H.M.S *Challenger* St. 299), and from the east of Malden Island, Central Pacific, at 4750 m depth (type locality for *K. indistinctum* synonymous with *K. asterias*: H.M.S. Challenger St. 272) (Agassiz 1881; 1904). It has also been reported for the central Pacific Ocean, the Tasman Sea, Chile, Antarctica, and the southern Indian Ocean from 3890–4950 m depth (Anderson 2016). *Kamptosoma abyssale* type locality is the Kuril-Kamchatka Trench, from 6090–6235 m (Mironov 1971), and occurs in the Northwest Pacific, from Aleutian Islands to Kermadec Trench, and from Madagascar to east of Hawaii between 4374–6235 m depth (Mooi et al. 2004). These two species are only differentiated by the shape of the claviform pedicellaria (previously referred to as globiferous pedicellaria, but Mironov et al. (2015) suggested these to belong to the claviform group as their rudimentary valves are not functional), with two valves in *K. abyssale*, and three valves in *K. asterias*. The specimen from the CCZ has pedicellariae

with two saccules and two valves, as described for *K. abyssale*. However, the COI sequence is very similar (0.47–1.4% K2P distance) to sequences of *K. asterias* collected in the Tasman Sea from 4570–4744 m depth, and are recovered in a well-supported clade (Fig. 31). These values of genetic divergence are within the intraspecific divergence that has been reported for echinoids (Chow et al. 2016), and therefore might belong to the same species. Nonetheless these specimens identified as *K. asterias* were reported to have claviform pedicellariae with two valves as described for *K. abyssale* (Anderson 2016). It has been suggested that *K. abyssale* is a synonym of *K. asterias*, and the former species will only be validated once material from both type localities is examined in detail (Anderson 2016; Mironov et al. 2015; Mooi et al. 2004). *Kamptosoma asterias* from the Central Pacific (St. 272) has been re-examined and was reported to have pedicellariae with three valves (Mironov et al. 2015). The holotype from St. 299 was examined in this study. Unfortunately, most pedicellariae have been lost and only a single claviform pedicellariae was found, this with two valves.

Ecology. The specimen was found crawling rapidly across abyssal sediment in APEI 4, at 5040 m depth. This morphotype has an unusually high crawling speed.

Comparison with image-based catalogue. A very similar *Kamptosoma* sp. morphotype (i.e., *Kamptosoma abyssale* sp. inc., URC_010) has been encountered in seabed image surveys conducted in abyssal areas of Kiribati's EEZ, but not in the eastern CCZ. URC_010 was the most abundant echinoid morphotype encountered in the abyssal areas explored within Kiribati's EEZ (Simon-Lledó et al. 2019d).

Class Holothuroidea

Holothurians are important components of the benthic deep-sea megafauna, and currently there are 367 records at a minimum depth of 3000 m in the CCZ, with 141 representing preserved specimens (OBIS 2022). Holothurians are amongst the most diverse invertebrate megafaunal taxa in the CCZ seafloor; a total of 106 different holothurian morphotypes has been so far catalogued in the image-based assessments consulted for this study, across the CCZ and nearby locations. We collected 18 specimens belonging to 15 different species, for which the COI gene was successfully amplified for all but one specimen. The gene 18S was successfully amplified for that specimen, as well as for other three. These were included in a concatenated alignment (12S, 16S, 18S, 28S, COI, and H3) used to estimate a phylogenetic tree (Fig. 34).

Subclass Actinopoda Ludwig, 1891
Order Persiculida Miller, Kerr, Paulay, Reich, Wilson, Carvajal & Rouse, 2017
Family Molpadiodemidae Miller, Kerr, Paulay, Reich, Wilson, Carvajal & Rouse, 2017
Genus *Molpadiodemas* Heding, 1935

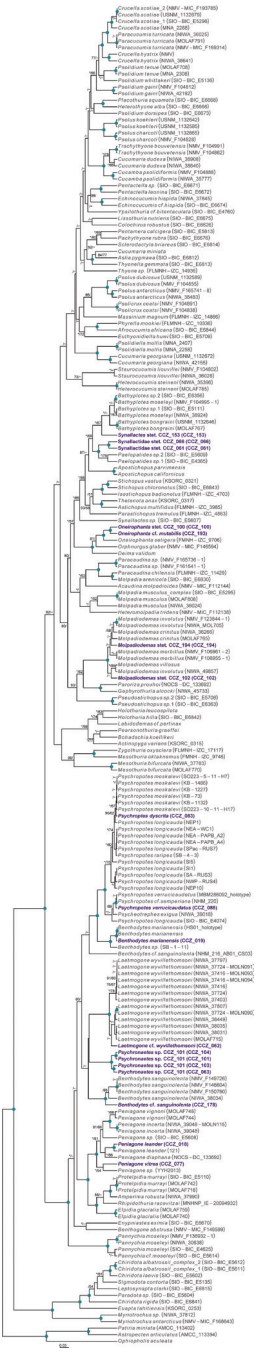

Figure 34. Phylogenetic tree of the class Holothuroidea. Concatenated (12S, 16S, 18S, 28S, COI, and H3) median consensus BEAST tree with posterior probability (PP) and bootstrap (BS) values indicated. Only values of PP > 0.70 and BS > 50 are shown, with values of PP > 0.95 and BS > 90 indicated with a circle. Nodes not recovered on the RAxML tree are indicated with a hyphen. Sequences generated in this study are highlighted in violet.

***Molpadiodemas* stet. CCZ_102**
Fig. 35

Material. Clarion-Clipperton Zone • 1 specimen; APEI 4; 7.2701°N, 149.7827°W; 3552 m deep; 03 Jun. 2018; Smith & Durden leg.; GenBank: ON400708 (COI); NHMUK 2022.66; Voucher code: CCZ_102.

Description. Single specimen, ~ 32 cm long (Fig. 35A). Body subcylindrical when alive, dorso-ventrally flattened in preserved specimen (L = 22 cm, W = 9 cm; Fig. 35E, F), tapering distally; body wall is completely covered in sediment and globigerinas, firm, wrinkly, with transverse folds and ridges giving a partly serrated appearance to the margin; brim present; anus and mouth ventral (Fig. 35D, E). Tube feet only visible on the ventral surface, cylindrical, and orange (Fig. 35C). Dorsal surface is whitish and ventral is yellowish in preserved specimen, but heavily covered by sediment. Ossicles in tentacles; unbranched rods and branched rods, with branches intertwining at the ends creating irregular perforated mesh (Fig. 35B).

Remarks. COI sequence forms a clade with other species of *Molpadiodemas* including *M. villosus* (Théel, 1886), *M. morbillus* O'Loughlin & Ahearn, 2005, *M. crinitus* O'Loughlin & Ahearn, 2005 and *M. involutus* (Sluiter, 1901). Closest is to *M. morbilus* (K2P 3.7–3.9%), and in the phylogenetic tree it is recovered in a well-supported clade with other species within the genus (Fig. 34), but species were not separated within the genus. Three species within the genus *Molpadiodemas* have been previously reported in the CCZ: *M. altanticus* (R. Perrier, 1898), *M. villosus* and *M. helios* O'Loughlin &

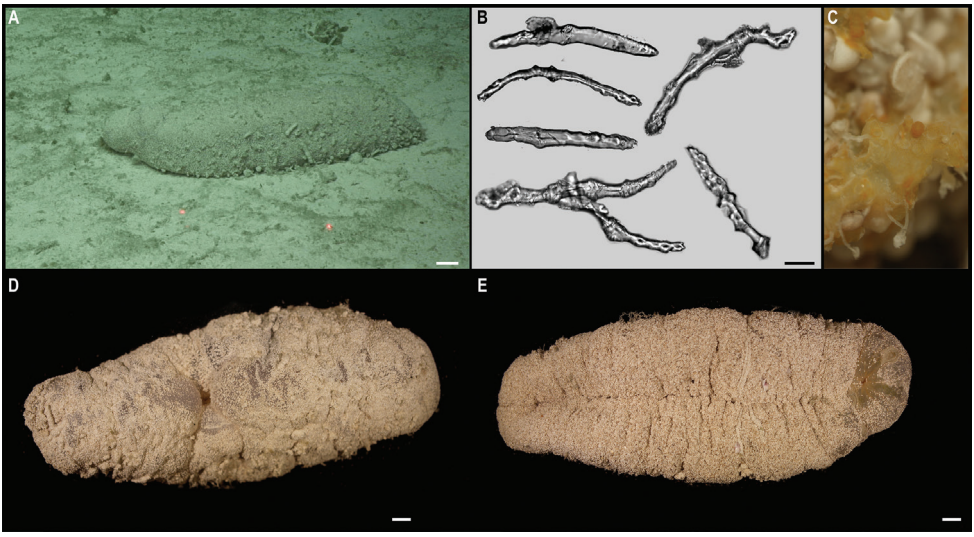

Figure 35. *Molpadiodemas* stet. CCZ_102 **A** in situ image **B** tentacle ossicles **C** tube feet **D** dorsal surface **E** ventral surface of specimen before preservation. Scale bars: 2 cm (**A**); 20 µm (**B**); 1 cm (**D, E**). Image attribution: Durden and Smith (**A**); Bribiesca-Contreras (**B, C**); Wiklund, Durden, Drennan, and McQuaid (**D, E**).

Ahearn, 2005, with the latter species being recently described from the CCZ and so far not reported elsewhere (O'Loughlin and Ahearn 2005). However, morphological characters of *Molpadiodemas* stet. CCZ_102 are not in accordance with the description of any of those three described species.

Ecology. This specimen was collected on the sediment seafloor of a seamount in APEI 4 at 3552 m depth.

Comparison with image-based catalogue. A very similar Molpadiodemidae morphotype (i.e., *Molpadiodemas* sp. indet., HOL_103) has been commonly encountered in seabed image surveys conducted across the eastern CCZ (e.g., Amon et al. 2017b) and in abyssal areas of the Kiribati EEZ, mostly in nodule field areas.

Molpadiodemas stet. CCZ_194

Fig. 36

Material. Clarion-Clipperton Zone • 1 specimen; APEI 1; 11.2517°N, 153.6055°W; 5205 m deep; 10 Jun. 2018; Smith & Durden leg.; GenBank: ON400725 (COI); NHMUK 2022.71; Voucher code: CCZ_194.

Description. Single specimen (Fig. 36A). Colouration of live specimen is whitish yellow, with skin somewhat translucent (Fig. 36A, E). Body subcylindrical in live specimen, but dorso-ventrally flattened when preserved, tapering anteriorly, ~ 4× as long as wide (L = 25 cm, W = 8.2 cm); semi-translucent body wall, longitudinal muscles visible through it; colouration of preserved specimen is yellowish (Fig. 36E), darker on the ventral side (Fig. 36F). Ventral surface with small, black, unidentified epibionts embedded in the skin (Fig. 36C, D). Specimen barely covered by sediment. Ossicles in tentacles; unbranched rods with thick central swelling; and branched rods, often with branches intertwining at the ends creating an irregular perforated mesh (Fig. 36B).

Remarks. The COI sequence of *Molpadiodemas* stet. CCZ_194 is similar to sequences of other species of *Molpadiodemas*, including *M. villosus*, *M. morbillus*, *M. crinitus*, *M. involutus*, and *Molpadiodemas* stet. CCZ_102. COI genetic divergence between both specimens collected in the CCZ is 6%, in accordance with values of genetic interspecific divergence for the genus. The specimen is recovered in a well-supported clade along with other members of the genus (Fig. 34), but species are not well delimited. As mentioned above, three species of *Molpadiodemas* have been previously reported in the CCZ (O'Loughlin and Ahearn 2005). The tentacle ossicles from specimen CCZ_194 are very similar to those of *M. helios*, but this latter species is distinguished by the prominent tube feet that are barely visible in our specimen.

Ecology. This specimen was found on the sedimented seafloor of an abyssal plain on APEI 1 at 5205 m depth.

Comparison with image-based catalogue. A very similar *Molpadiodemas* sp. morphotype (i.e., *Molpadiodemas* sp. indet., HOL_004) has been commonly encountered in seabed image surveys conducted across nodule fields areas of the eastern CCZ (e.g., Amon et al. 2017b), but not in abyssal areas surveyed within the Kiribati EEZ.

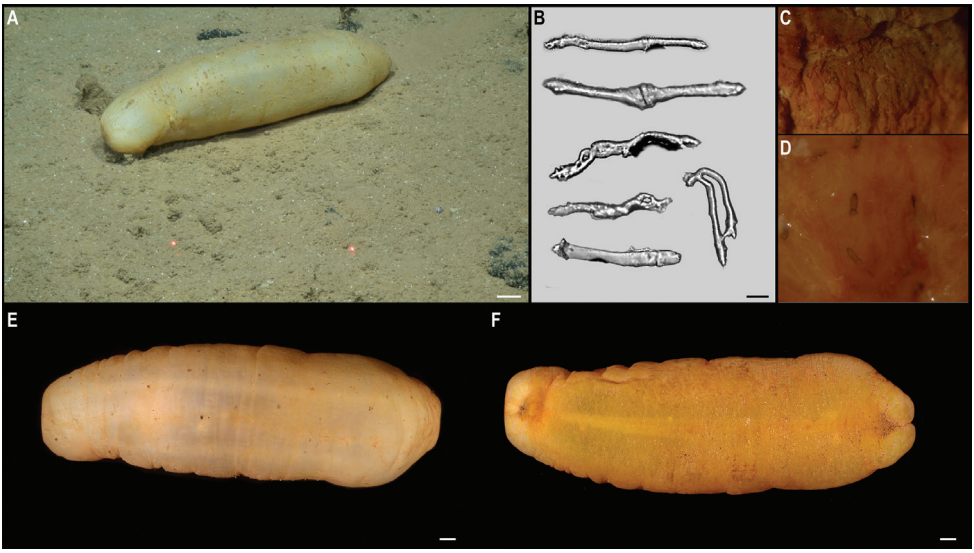

Figure 36. *Molpadiodemas* stet. CCZ_194 **A** in situ image **B** tentacle ossicles **C** epibionts on ventral surface **D** detail of epibionts **E** dorsal surface **F** ventral view of specimen before preservation. Scale bars: 2 cm (**A**); 25 μm (**B**); 1 cm (**E, F**). Image attribution: Durden and Smith (**A**); Bribiesca-Contreras (**B–D**); Wiklund, Durden, Drennan, and McQuaid (**E, F**).

Order Synallactida Miller, Kerr, Paulay, Reich, Wilson, Carvajal & Rouse, 2017
Family Synallactidae Ludwig, 1894

Synallactidae stet. CCZ_061

Fig. 37

Material. Clarion-Clipperton Zone • 1 specimen; APEI 7; 4.8877°N, 141.7569°W; 3132 m deep; 27 May. 2018; Smith & Durden leg.; GenBank: ON400688 (COI), ON406640 (18S); NHMUK 2022.75; Voucher code: CCZ_061.

Description. Single specimen; description of external morphological features only from in situ image as the specimen was damaged during collection (Fig. 37A). Body semi-circular, with ventral surface flattened, tapering distally; very wide, widest part of body ~ 7 cm; anus posterodorsal; mouth anteroventral. Tegument seems thick. Ossicles present in tentacles, slightly curved rods, < 250 μm (Fig. 37B).

Remarks. There are no close matches to the COI sequence of Synallactidae stet. CCZ_061 in public databases. The closest match is to Synallactidae stet. CCZ_066 (14% K2P). Both specimens are recovered in a well-supported clade representing the family Synallactidae (Fig. 34). They are recovered very close to *Paelopatides* Théel, 1886, but COI divergence suggest they belong to different genera.

Comparison with image-based catalogue. No similar Synallactidae morphotypes have been so far catalogued from seabed imagery collected in the eastern CCZ or in

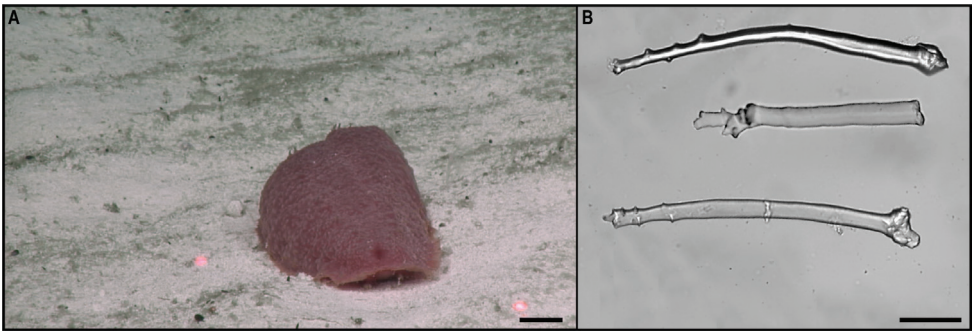

Figure 37. Synallactidae stet. CCZ_061 **A** in situ image **B** tentacle ossicles. Scale bars: 2 cm (**A**); 50 μm (**B**). Image attribution: Durden and Smith (**A**); Bribiesca-Contreras (**B**).

abyssal areas of the Kiribati EEZ. Consequently, the in situ image of Synallactidae stet. CCZ_061 was catalogued as a new morphotype (i.e., Synallactidae gen. indet., HOL_120).

Ecology. This specimen was collected on the sedimented seafloor of a seamount in APEI 7 at 3132 m depth.

Synallactidae stet. CCZ_066
Fig. 38

Material. Clarion-Clipperton Zone • 1 specimen; APEI 7; 4.8896°N, 141.75°W; 3095 m deep; 27 May. 2018; Smith & Durden leg.; GenBank: ON400692 (COI), ON406642 (18S); NHMUK 2022.63; Voucher code: CCZ_066.

Description. Single specimen, body semi-circular with ventral surface flattened; ~ 3× longer than wide (L = 21 cm, W = 6 cm; Fig. 38A). Mouth anteroventral, anus posterodorsal. Colouration in live specimen is bright red (Fig. 38D, E). Specimen severely damaged during collection, guts separated from skin. Tegument is thick and leathery, with wart-like protrusions on the dorsal surface, more evident on live specimen (Fig. 38A), and with a small, very short, triangular dorsal appendage. Brim evident on ventral surface. Small tube feet arranged in two irregular rows, one on each side of ventrum, running longitudinally. Tentacles 18. Ossicles present in dorsal skin (Fig. 38B) and tentacles (Fig. 38C).

Remarks. There are no close matches to the COI sequence of Synallactidae stet. CCZ_066 in public databases. The closest match is to specimen Synallactidae stet. CCZ_061 (14% K2P). Both specimens are recovered in a well-supported clade representing the family Synallactidae (Fig. 34). They are recovered very close to *Paelopatides* Théel, 1886, but COI divergence suggest they belong to different genera.

Ecology. This specimen was collected on the sedimented seafloor of a seamount on APEI 7 at 3095 m depth.

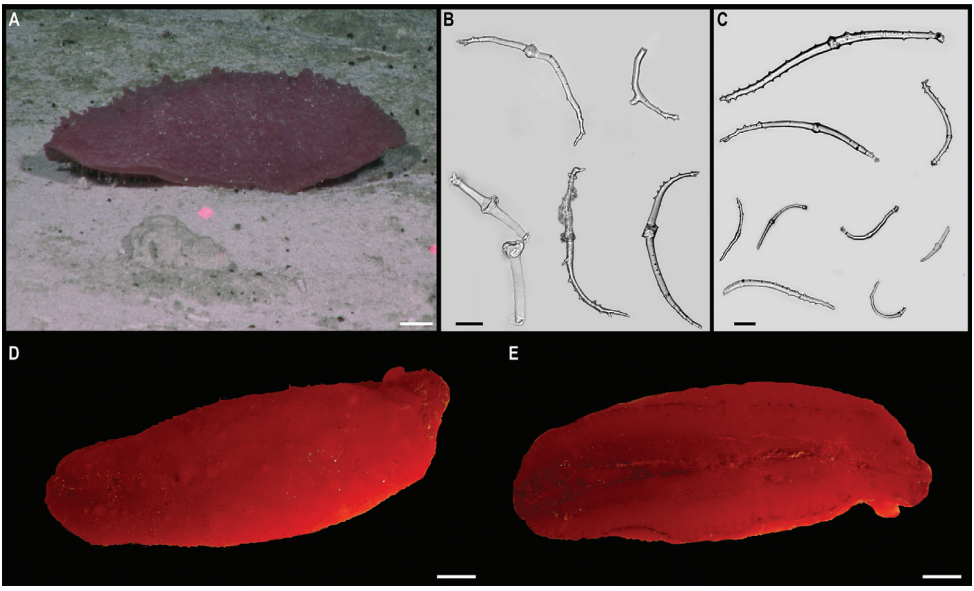

Figure 38. Synallactidae stet. CCZ_066 **A** in situ image **B** ossicles on dorsal skin **C** tentacle ossicles **D** dorsal surface **E** ventral surface of specimen before preservation. Scale bars: 2 cm (**A, D, E**); 50 µm (**B, C**). Image attribution: Durden and Smith (**A**); Bribiesca-Contreras (**B, C**); Wiklund, Durden, Drennan, and McQuaid (**D, E**).

Comparison with image-based catalogue. No similar Synallactidae morphotypes have been so far catalogued from seabed imagery collected in the eastern CCZ nor in abyssal areas of the Kiribati EEZ. Consequently, the in situ image of CCZ_066 was catalogued as a new morphotype (i.e., Synallactidae gen. indet., HOL_121). The dorsal protrusions that differentiate HOL_121 from HOL_120 may not be clearly visible in vertically-facing seabed imagery, and hence these two taxa might only be classifiable into a single, generic morphotype (i.e., HOL_120) in quantitative analyses.

Genus *Synallactes* Ludwig, 1894

Synallactes stet. CCZ_153

Fig. 39

Material. Clarion-Clipperton Zone • 1 specimen; APEI 4; 6.9704°N, 149.9426°W; 5009 m deep; 06 Jun. 2018; Smith & Durden leg.; GenBank: ON400714 (COI); NHMUK 2022.69; Voucher code: CCZ_153.

Description. Single specimen (Fig. 39A). Body cylindrical, white, ~ 4× as long as wide (L = 10 cm, W = 2.7 cm), flattened proximally and rounded distally; flattened ventral surface. Two rows, upper and lower, of lateral, small, conical, thin processes, similar to those around the proximal edge (Fig. 39D). There is a row of yellowish, very

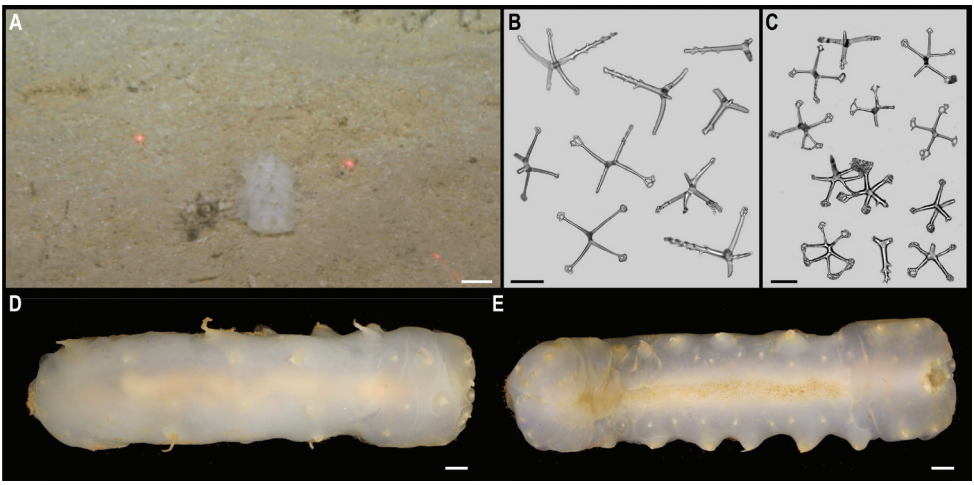

Figure 39. *Synallactes* stet. CCZ_153 **A** in situ image **B** ossicles from dorsal skin **C** ossicles from ventral skin **D** dorsal view of specimen before preservation, **E** ventral view. Scale bars: 2 cm (**A**); 50 µm (**B, C**); 5 mm (**D, E**). Image attribution: Durden and Smith (**A**); Bribiesca-Contreras (**B, C**); Wiklund, Durden, Drennan, and McQuaid (**D, E**).

small, tube feet in the mid-ventral surface, along the odd ambulacrum (Fig. 39E). Skin firm but translucent. Colour on live and preserved specimen is white. Ossicles abundant on dorsal body wall, spatulated crosses only with a long spinous apophysis, end of arms spatulated with holes (Fig. 39B). Ventral ossicles also spatulated crosses with a long spinous apophysis, smaller, sometimes with more than four arms, also spatulated ends of arms with holes (Fig. 39C).

Remarks. The closest matches for the barcoding gene COI sequence are published sequences from the genus *Bathyplotes* (89.9% similarity), also within the family Synallactidae. The sequence is distinct from the only sequence of *Synallactes* sp. (GenBank accession number: KX874365.1) included in the phylogeny (Fig. 34), and they were not recovered as a monophyletic group. The DeepCCZ specimen was recovered sister to species of *Bathyplotes*, with *Synallactes* sp. recovered separately from the other genera in the family Synallactidae, concordant with previous results (Miller et al. 2017). Despite this, the specimen was assigned to the genus *Synallactes* based on external morphological characters that are concordant with those described from the genus. Species of *Synallactes* have previously been reported in the CCZ: *Synallactes profundus* (Koehler & Vaney, 1905) and *Synallactes aenigma* Ludwig, 1894; the latter being associated with manganese substrates. External morphology does not resemble to *S. profundus.*

Ecology. This specimen was found on the sedimented seafloor of an abyssal plain on APEI 4 at 5008 m depth.

Comparison with image-based catalogue. A very similar Synallactidae morphotype (i.e., *Synallactes* sp. indet., HOL_007) has been commonly encountered in seabed

image surveys conducted across nodule field areas of the eastern CCZ (e.g., Amon et al. 2017b), but not in abyssal areas of the Kiribati EEZ, where synallactid specimens were very rarely encountered.

Family Deimatidae Théel, 1882
Genus *Oneirophanta* Théel, 1879

***Oneirophanta* stet. CCZ_100**
Fig. 40

Material. Clarion-Clipperton Zone • 1 specimen; APEI 4; 7.2647°N, 149.774°W; 3550 m deep; 03 Jun. 2018; Smith & Durden leg.; GenBank: ON400706 (COI), ON406643 (18S), ON406620 (16S); NHMUK 2022.84; Voucher code: CCZ_100.

Description. Single specimen; colouration of live specimen is beige, spotted with light brown and yellow on dorsal surface (Fig. 40A, C, D), and lighter on ventral surface, with suckers on tube feet and tentacles being dark brown (Fig. 40D). Body cylindrical, ~ 33 cm long and 8.8 cm wide; mouth anteroventral, anus posteroventral. Tentacles partly retracted. Papillae arranged in one or two rows along the dorsal radii, and in a single row along the ventrolateral radii above the tube feet. Tube feet ~ 50 pairs, arranged in two or three rows on each ventrolateral ambulacrum; few tube feet located along mid-ventral ambulacrum, among them two tube feet, one placed approx. half the body length and the other approx. three quarter of the body length; and few smaller feet close to anus. Dorsal ossicles spatulated crosses, crosses with open ramifications, and small irregular perforated plates; ventral ossicles crosses with open ramifications of different stage of development.

Remarks. Closest match for COI and 16S sequences is to *Oneirophanta setigera* (Ludwig, 1893) (86.7% and 96.3%, respectively). In the phylogenetic tree, it is recovered in a well-supported clade representing the family Deimatidae, including *Oneirophanta* (Fig. 34). According to the external morphology *Oneirophanta* sp. CCZ_100 differs from *Oneirophanta mutabilis mutabilis* Théel, 1879, *O. mutabilis affinis* Ludwig, 1893 and *O. conservata* Koehler & Vaney, 1905 in high number of tube feet arranged in two or three rows and by absence of large, perforated plates on dorsum. It differs from *O. setigera* in high number of tube feet arranged in two or three rows and by presence of small, perforated plates and bigger perforations on spatulated crosses.

Ecology. The specimen was found on the sediment seafloor of a seamount on APEI 4 at 3550 m depth.

Comparison with image-based catalogue. No exactly similar Deimatidae morphotypes have been so far catalogued from seabed imagery collected in the eastern CCZ nor in abyssal areas of the Kiribati EEZ. Consequently, the in situ image of CCZ_100 was catalogued as a new morphotype (i.e., *Oneirophanta* sp. indet., HOL_063). However, HOL_063 could be potentially confused with a similar shaped

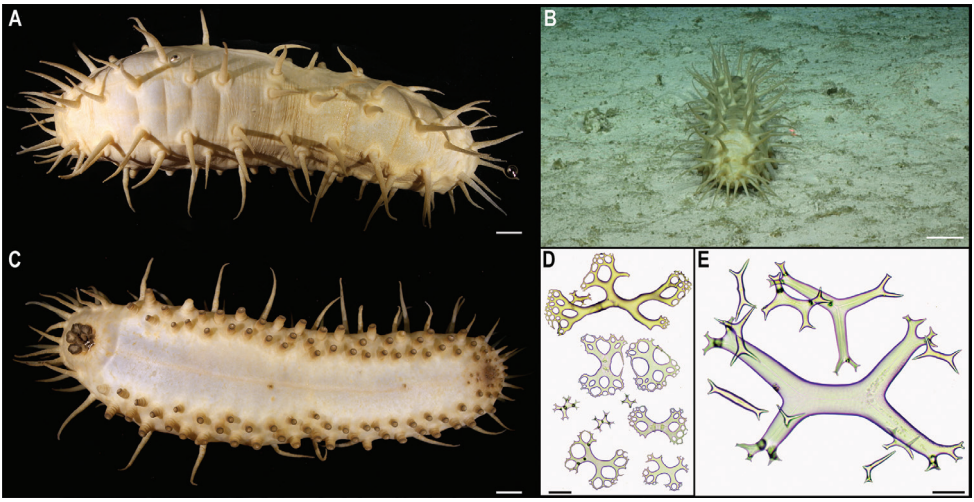

Figure 40. *Oneirophanta* stet. CCZ_100 **A** dorsal view of specimen before preservation **B** in situ image **C** ventral view **D** dorsal ossicles **E** ventral ossicles. Scale bars: 2 cm (**A, C**); 5 cm (**B**); 200 μm (**D**); 100 μm (**E**). Image attribution: Wiklund, Durden, Drennan, and McQuaid (**A, C**); Durden and Smith (**B**); Kremenetskaia (**D, E**).

Deimatidae morphotype (e.g., Deimatidae gen. indet., HOL_062; also beige, cylindrical, with conspicuous projections on the dorsal surface arranged in four rows) found in the eastern CCZ (e.g., Amon et al. 2017b), with more abundant -though slightly thinner- projections, that may be difficult to distinguish in vertically facing images.

Oneirophanta cf. *mutabilis* Théel, 1879

Fig. 41

Material. Clarion-Clipperton Zone • 1 specimen; APEI 1; 11.252°N, 153.5847°W; 5203 m deep; 10 Jun. 2018; Smith & Durden leg.; GenBank: ON400724 (COI), ON406629 (18S), ON406619 (16S); NHMUK 2021.20; Voucher code: CCZ_193.

Other material. Indian Ocean • 3 specimens, syntypes of *Oneirophanta mutabilis* Théel, 1879; Eastern Indian, Antarctic Basin; 53.9167° S, 108.5833° E; 3566 m deep; Challenger Expedition, Stn. 157; NHMUK 1883.6.18.33.

Description. Single specimen, body uniformly white (Fig. 41A). Body almost cylindrical, > 2× as long as wide (L = 16 cm; W = 6.9 cm), being of almost equal breadth throughout the whole length and tapering posteriorly; mouth anteroventral and anus posteroventral. Tentacles 20, small, with a lightly brown tip, each with a terminal part with 6–8 unbranched processes. Long, pointed processes, or different lengths, arranged in four distinct rows, two rows running along the dorsal ambulacra with eight processes on each row, and the longest being approx. half of the body

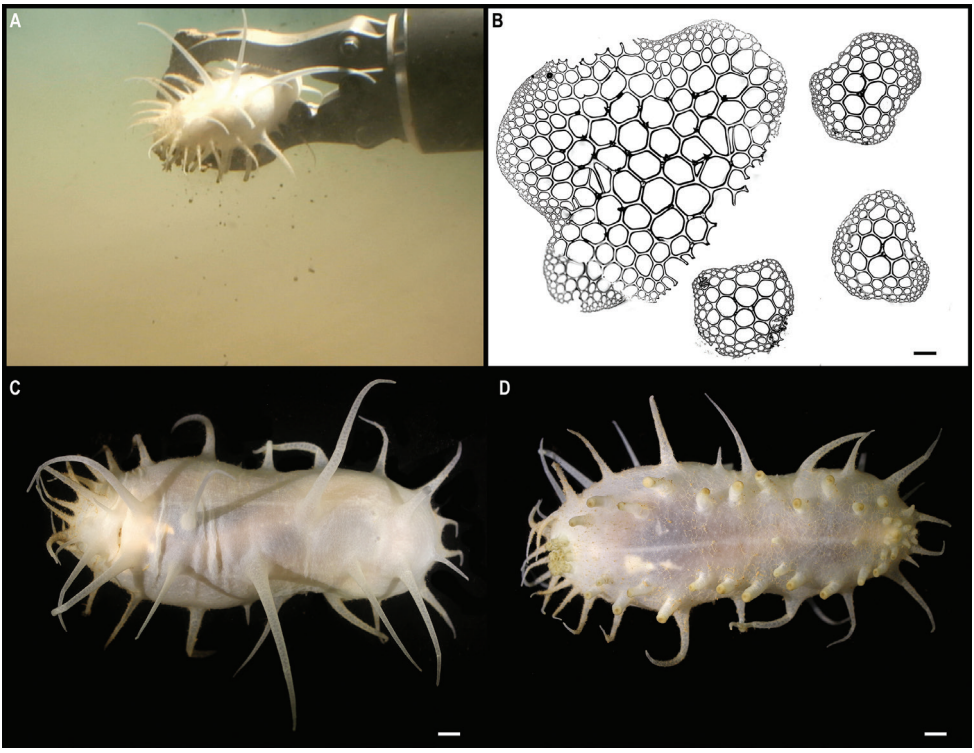

Figure 41. *Oneirophanta* cf. *mutabilis* Théel, 1879. Specimen CCZ_193 **A** in situ image **B** dorsal ossicles **C** dorsal view before preservation **D** ventral view. Scale bars: 200 μm (**B**); 1 cm (**C, D**). Image attribution: Durden and Smith (**A**); Bribiesca-Contreras (**B**); Wiklund, Durden, Drennan, and McQuaid (**C, D**).

length (Fig. 41C); the other two rows placed on the sides of the body, slightly above the ventral lateral ambulacra. Ventral ambulacra with 11 and 13 tube feet, arranged in two irregular rows; odd ambulacrum naked, except for two tube feet arranged in the posterior half of the body, and ten surrounding the anus; processes crowded anteriorly (Fig. 41D). Thin skin, translucent, but hard and brittle, with numerous small and large perforated plates, with the small ones bearing two or three spines near the centre, and the large ones ~ 30 spines; ossicles imbricated, almost forming a skeleton (Fig. 41B).

Remarks. Sequences for the 18S, 16S, and COI genes were most similar to sequences from *Oneirophanta setigera* (99.07%, 95.6%, 88.51% similarity, respectively), followed by other species within the family Deimatidae (i.e., *Orphnurgus glaber* Walsh, 1891 and *Deima validum* Théel, 1879). The specimen was recovered in a well-supported clade including all members of Deimatidae (Fig. 34), closest to *Oneirophanta* sp. CCZ_100 (K2P distance: 11%). Calcareous ossicles are concordant with those in *Oneirophanta mutabilis.* This species was originally described west of the Crozet Islands (H.M.S. Challenger station 146: 46.7667°S, 45.5167°E) at 2514 m depth (Théel

1879) but has been further divided in two sub-species, *O. mutabilis mutabilis* and *O. mutabilis affinis*. The former has been reported to be cosmopolitan, while the later has been recorded from the tropical eastern Pacific. Further analyses will be required to determine the validity of the subspecies and if the CCZ specimen belongs to any of those. It differs from the original description of *O. mutabilis* (Théel, 1879) in having an irregular number of pedicels around the ventral surface, the pedicels around the anus arranged triangularly instead of a transversal row, as well as the arrangement of the processes on bivium and trivium. However, Théel (1879) mentioned that several of the specimens examined differed from the specimen described in the number of pedicels and the arrangement of processes, and further studies should clarify if these are indeed subspecies.

Ecology. The specimen was found on the sediment surface of an abyssal plain on APEI 1 at 5203 m depth.

Comparison with image-based catalogue. A very similar *Oneirophanta* sp. morphotype (i.e., *Oneirophanta* sp. indet., HOL_058) has been encountered in seabed image surveys conducted across nodule fields areas of the eastern CCZ (e.g., Amon et al. 2017b), but not in the abyssal areas surveyed at the Kiribati EEZ.

Order Elasipodida Théel, 1882
Family Psychropotidae Théel, 1882
Genus *Psychropotes* Théel, 1882

***Psychropotes verrucicaudatus* Xiao, Gong, Kou, Li, 2019**
Fig. 42

Material. Clarion-Clipperton Zone • 1 specimen; APEI 4; 6.9878°N, 149.9119°W; 4999 m deep; 02 Jun. 2018; Smith & Durden leg.; GenBank: ON400703 (COI); NHMUK 2021.19; Voucher code: CCZ_086.

Description. Single specimen, colouration in situ is violet (Fig. 42A, B). Body elongated and anteriorly depressed (L = 34.7 cm, W = 10.2 mm); with a broad brim. Short (approx. one twelfth of body length), conical, single-pointed, dorsal unpaired appendage, placed 2/5 of the body length from the posterior end (Fig. 42A–C). Dorsal skin, including the dorsal appendage, covered in warts (Fig. 42C, F). Each wart has an ossicle in the centre, a giant cross with a central apophysis and strongly curved arms, all visible through the skin (Fig. 42E, F). Dorsal skin also contains smaller crosses with spiny arms (Fig. 42E, F). Approximately 30 pairs of mid-ventral tube feet arranged in two rows along the mid-ventral ambulacrum, arranged very close together on the anterior two thirds of the body, and scattered after posteriorly, with the last pairs being very close together again. Colouration of preserved specimen is also purple, with slightly lighter ventrum.

Remarks. COI sequence is very similar (K2P distance = 0.77%) to the holotype of *P. verrucicaudatus*, and they were recovered together in the phylogenetic tree (Fig. 34).

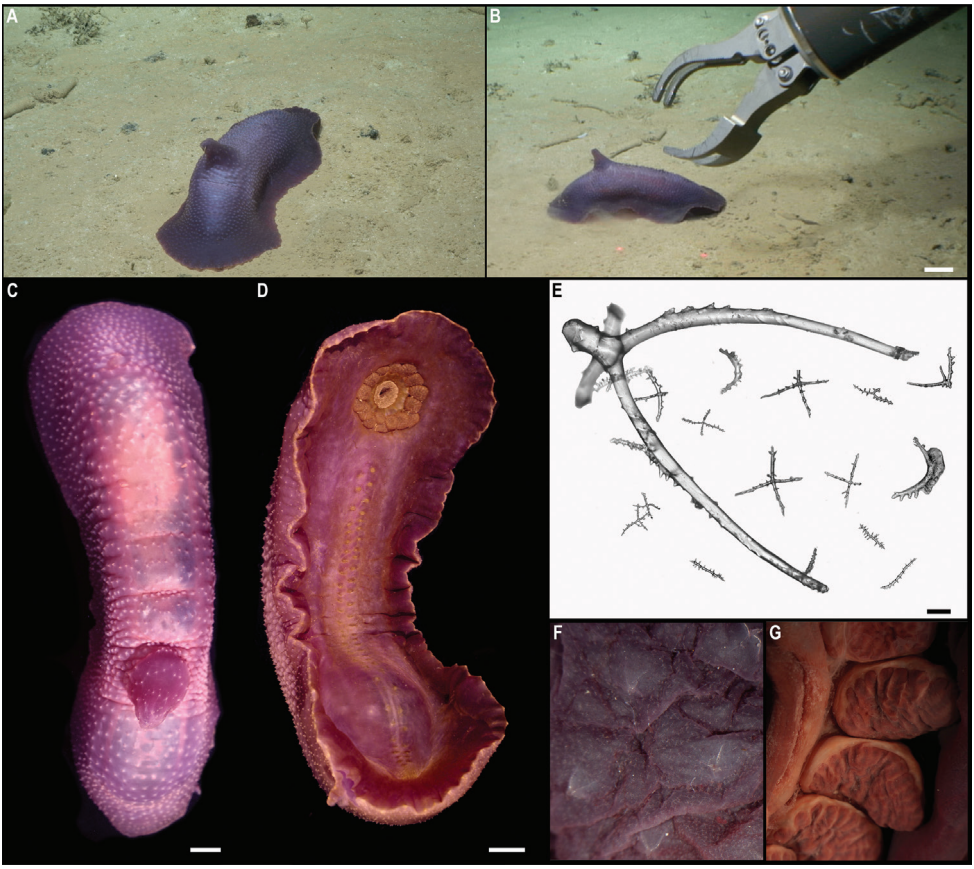

Figure 42. *Psychropotes verrucicaudatus* Xiao, Gong, Kou, Li, 2019. Specimen CCZ_086: **A, B** in situ images **C** dorsal view of specimen before preservation **D** ventral view **E** dorsal ossicles **F** detail of warts and ossicles on dorsal body wall **G** mouth tentacles. Scale bars: 5 cm (**B**); 2 cm (**C, D**); 100 µm (**E**). Image attribution: Durden and Smith (**A, B**); Wiklund, Durden, Drennan, and McQuaid (**C, D**); Bribiesca-Contreras (**E–G**).

This species was described from the Jiaolong seamount, in the South China Sea, western Pacific Ocean at 3615 m deep (Xiao et al. 2019). External morphological characters are in accordance with the original description.

Ecology. The specimen was found on the sedimented abyssal plain in APEI 4 at 4999 m depth.

Comparison with image-based catalogue. A very similar *Psychropotes* sp. morphotype (i.e., *Psychropotes verrucicaudatus* sp. inc., HOL_045) has been commonly encountered in seabed image surveys conducted across nodule fields areas of the eastern CCZ (e.g., Amon et al. 2017b), but not in the abyssal areas surveyed within the Kiribati EEZ.

***Psychropotes dyscrita* (Clark, 1920)**
Fig. 43

Material. Clarion-Clipperton Zone • 1 specimen; APEI 4; 7.0212°N, 149.9355°W; 5040 m deep; 02 Jun. 2018; Smith & Durden leg.; GenBank: ON400702 (COI); NHMUK 2022.83; Voucher code: CCZ_083.

Description. Single specimen, ~ 30 cm long (Fig. 43A). Colouration of live specimen is yellow (Fig. 43A, B), with reddish-light purple on ventral surface (Fig. 43C). Tentacles 18, also reddish-light purple. Long, dorsal appendage with round end, slightly longer than the total body length, and developed very close to the posterior end of the body.

Remarks. Gebruk et al. (2020) morphologically examined the specimen collected during the DeepCCZ and re-established the species *Psychropotes dyscrita* based on this specimen. The holotype was collected in Peru, at 5206 m depth, and the species is known from the Central Pacific Ocean at depths of 5040–5206 m (Gebruk et al. 2020). *Psychropotes dyscrita* and *P. moskalevi* Gebruk & Kremenetskaia, 2020 are the two only known yellow species for this genus and were recovered as sister species (Fig. 34). The COI sequence for the DeepCCZ specimen is 1.1 ± 0.4% divergent (K2P distance) from specimens of *P. moskalevi*. Although this value seems low, the COI gene seems to be more conserved in the genus *Psychropotes* (1.1–13.4%, mean = 6.5%), with < 2%

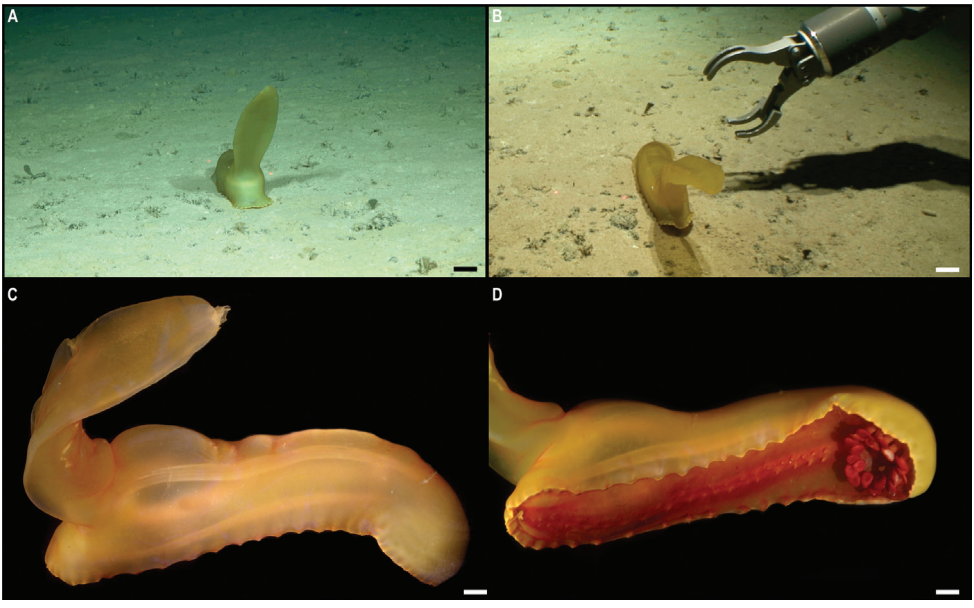

Figure 43. *Psychropotes dyscrita* (Clark, 1920). Specimen CCZ_083: **A, B** in situ images **C** lateral view **D** ventral view. Scale bars: 5 cm (**A, B**); 2 cm (**C, D**). Image attribution: Durden and Smith (**A, B**); Wiklund, Durden, Drennan, and McQuaid (**C, D**).

interspecific divergence between some species pairs (*P. dyscrita-P. moskalevi*, *P. moskalevi-P. raripes* Ludwig, 1893).

Ecology. The specimen was found on the sediment seafloor of an abyssal plain in APEI 4 at 5040 m depth.

Comparison with image-based catalogue. A very similar *Psychropotes* sp. morphotype (i.e., *Psychropotes* sp. indet., HOL_047) has been encountered in seabed image surveys conducted across nodule fields areas of the eastern CCZ (e.g., Tilot 2006), and in the Kiribati EEZ, where this taxon was the most abundant holothurian encountered (Simon-Lledó et al. 2019d). In pioneer seabed image surveys conducted at the CCZ, prior to the re-establishment of the species (Gebruk et al. 2020), this morphotype was typically classified as *P. longicauda.* Based on seabed imagery (e.g., without analysis of ossicles), it is not possible to determine whether HOL_047 specimens are *P. dyscrita* or *P. moskalevi.*

Genus *Benthodytes* Théel, 1882

Benthodytes cf. *sanguinolenta* Théel, 1882

Fig. 44

Material. Clarion-Clipperton Zone • 1 specimen; APEI 1; 11.2953°N, 153.742°W; 5245 m deep; 09 Jun. 2018; Smith & Durden leg.; GenBank: ON400720 (COI); NHMUK 2022.70; Voucher code: CCZ_178.

Description. Single specimen (Fig. 44A). Colouration of live specimen is light pink dorsally (Fig. 44B), darker ventrally (Fig. 44C). Tentacles 18, yellow, digitiform. Numerous dorsal papillae scattered on dorsal. Brim wide. Tube feet in double rows along the mid-ventral ambulacrum, ~ 30 pairs, yellowish. Ossicles not found.

Remarks. The closest match for the COI sequence is a sequence from *B. sanguinolenta* (GenBank: HM196505.1; 93.54% similarity) from the Ross Sea, Antarctica. A genetic study revealed two separate clades within *B. sanguinolenta* (O'Loughlin et al. 2011): (1) specimens from northwest Australia, and (2) Ross Sea. None of the samples included in O'Loughlin et al. (2011) are from the type locality (34.1167° S 73.9399°'W, off Chile, Pacific Ocean; 4000 m), but they identified at least two separate genetic species. The COI sequence of the specimen collected in the CCZ forms a third clade within the *B. sanguinolenta* species complex (Fig. 34). Genetic divergence (K2P distance) between the CCZ specimens and both NW Australia and Ross Sea clades is 10.1% and 7.3%, respectively, corresponding to values of intraspecific divergence in the group. In original description, Théel (1882) describes the body to be 6–7× longer than wide, whereas the preserved specimen collected in the CCZ is only ~ 3× longer than wide, but might be due to preservation as in in situ images it appears longer. However, the number of digitiform tentacles and appearance of small processes are concordant with the description of *B. sanguinolenta*. The sequence of *Benthodytes* cf. *sanguinolenta* from Glover et al. (2016b) does not form a clade with the CCZ specimen, with COI genetic distance being large (K2P 23%).

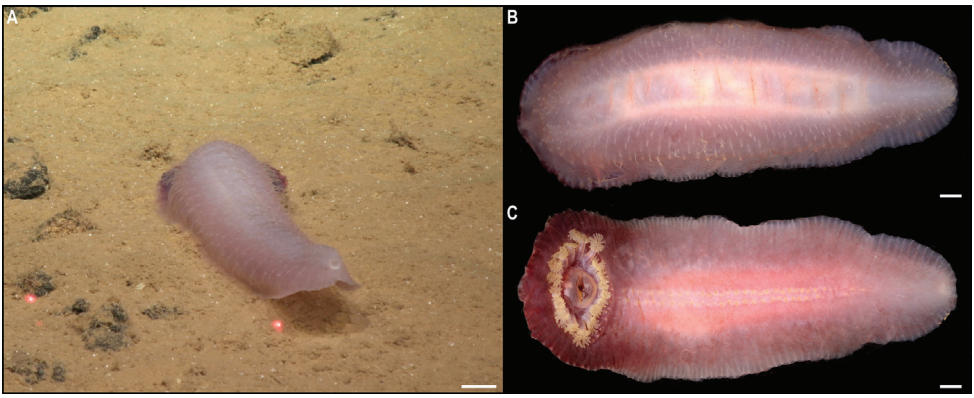

Figure 44. *Benthodytes* cf. *sanguinolenta* Théel, 1882. Specimen CCZ_178: **A** in situ image **B** dorsal view of specimen before preservation **C** ventral view. Scale bars: 2 cm (**A**); 1 cm (**B, C**). Image attribution: Durden and Smith (**A**); Wiklund, Durden, Drennan, and McQuaid (**B, C**).

Ecology. The specimen was found on the sedimented seafloor of an abyssal plain in APEI 1 at 5249 m depth.

Comparison with image-based catalogue. No exactly similar *Benthodytes* sp. morphotypes have been so far catalogued from seabed imagery collected in the eastern CCZ or in abyssal areas of the Kiribati EEZ. Consequently, the in situ image of specimen CCZ_178 was catalogued as a new morphotype (i.e., *Benthodytes sanguinolenta* sp. inc., HOL_124).

Benthodytes marianensis Li, Xiao, Zhang & Zhang, 2018

Fig. 45

Material. Clarion-Clipperton Zone • 1 specimen; APEI 7; 5.1043°N, 141.8865°W; 4861 m deep; 25 May. 2018; Smith & Durden leg.; GenBank: ON400682 (COI); NHMUK 2022.82; Voucher code: CCZ_019.

Description. Single specimen (Fig. 45). Body is elongated, ~ 49.4 cm, dorso-ventrally flattened with flat ventral surface and inflated dorsal surface; anteriorly depressed and tapering posteriorly; colouration in live specimen is dark violet. Two irregular rows of large conical papillae running along the paired dorsal ambulacra.

Remarks. The COI sequence is identical to the holotype of *B. marianensis* (K2P genetic distance = 0%) collected in the Mariana Trench at 5567 m depth (Li et al. 2018). These two sequences are also recovered together in the phylogenetic tree (Fig. 34). The species is only known from this location. Morphological characters are also concordant with the original description, including an uncommon, very peculiar, cross-shaped, dorsal ossicle (Fig. 45B).

Ecology. The specimen was found on the sedimented seafloor of an abyssal plain in APEI 7 at 4860 m depth.

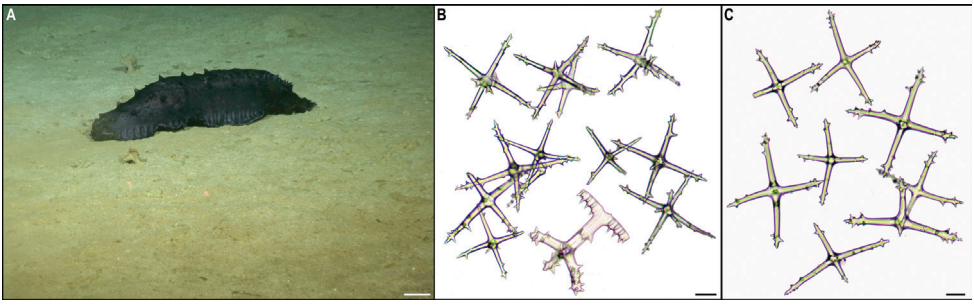

Figure 45. *Benthodytes marianensis* Li, Xiao, Zhang & Zhang, 2018. CCZ_019: **A** in situ image **B** dorsal ossicles including peculiar cross-shaped ossicle **C** ventral ossicles. Scale bar: 5 cm (**A**); 100 μm (**B, C**). Image attribution: Durden and Smith (**A**), Kremenetskaia (**B, C**).

Comparison with image-based catalogue. CCZ_019 resembles a *Benthodytes* sp. morphotype (i.e., *Benthodytes* sp. indet., HOL_111) encountered in seabed image surveys conducted across nodule fields areas of the eastern CCZ (Amon et al. 2017b) and the Kiribati EEZ. However, the vivid dark/violet colouration of HOL_011 (contrasting with background bright sediment) can constrain the visibility of papillae features in in situ photographed specimens, potentially making these hard to differentiate from other *Benthodythes* sp. morphotypes in vertically-facing seabed imagery.

Family Elpidiidae Théel, 1882
Genus *Peniagone* Théel, 1882

***Peniagone leander* Pawson & Foell, 1986**
Fig. 46

Material. Clarion-Clipperton Zone • 1 specimen; APEI 7; 5.1042°N, 141.8861°W; 4860 m deep; 25 May. 2018; Smith & Durden leg.; GenBank: ON400681 (COI), ON406621 (16S); NHMUK 2022.61; Voucher code: CCZ_018.

Description. Single specimen observed swimming (Fig. 46A). Specimen was severely damaged during collection, with only a few tentacles recovered, and hence description of morphological characters is based on in situ images. Body ovoid, slightly > 2× as long as it is wide. Velum composed of two pairs of fully fused papillae. Tube feet four pairs; three posteriormost pairs fused together forming a posterior swimming lobe; tube feet from the anteriormost pair very short.

Remarks. The specimen collected during the DeepCCZ expedition was recovered in bits, so no morphological features can be distinguished. Only four reddish orange tentacles were recovered, which are embedded in a transparent skin where ossicles are evident. However, *P. leander* is one of the few species that can be identified from images. The external morphological characters evident in in situ images from the CCZ specimen are in accordance with the species description. The species was

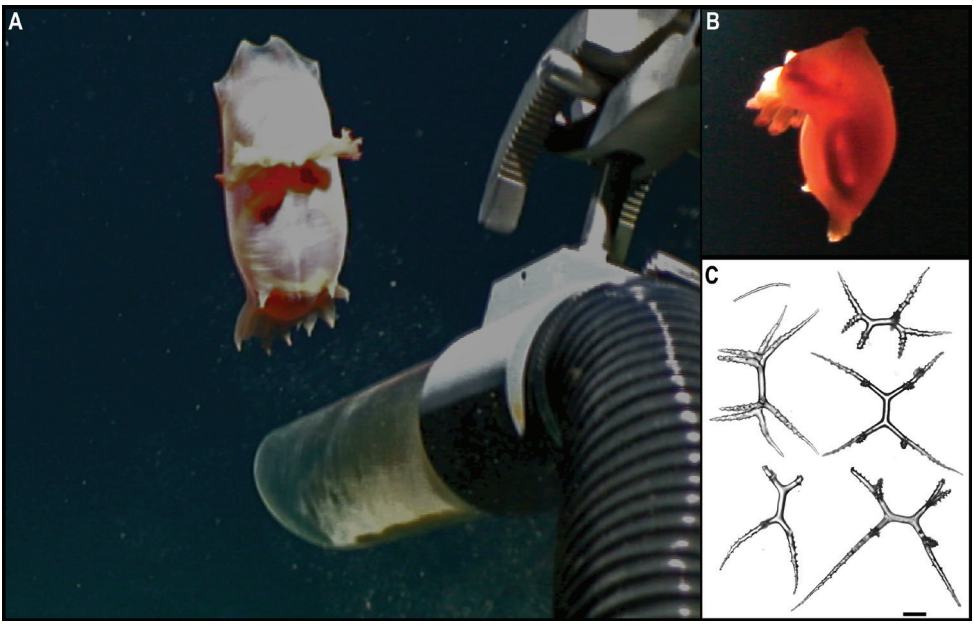

Figure 46. *Peniagone leander* Pawson & Foell, 1986. Specimen CCZ_018: **A, B** in situ images **C** tentacle ossicles. Scale bars: 100 µm (**C**). Image attribution: Durden and Smith (**A, B**); Bribiesca-Contreras (**C**).

originally described from in situ images and video footage collected across the eastern CCZ (Pawson and Foell 1986) and subsequently observed in the area (e.g., Amon et al. 2017b).

In the phylogenetic tree, the CCZ specimen was recovered in a well-supported clade with other species of *Peniagone* (Fig. 34). It was recovered together with a sequence of *P. leander*, which was recently rediscovered and collected for the first time in the Mariana Trench (Gong et al. 2020), both close to *P. diaphana* as reported by Gong et al. (2020). The 16S sequence of the CCZ specimen is similar (K2P distance = 2%) to the only available sequence from *P. leander*, but no COI sequence was made available. Our COI sequence is > 12% divergent (K2P distance) from other species within the genus. The COI gene seems to be highly divergent between species in this genus. Using the data provided in Kremenetskaia et al. (2021) and including the CCZ sequence of *P. leander*, COI mean interspecific divergence in the genus is 15.9% (min = 2.5% and max = 22.7%), with our sequence of *P. leander* being 14.5%–21.2% divergent from other species within the genus. Intraspecific divergence for species in the genus was estimated between 0.9%–3.0%.

Ecology. The specimen was found swimming near the sediment surface on an abyssal plain in APEI 7 at 4860 m depth.

Comparison with image-based catalogue. *Peniagone leander* (HOL_028) has been commonly encountered in seabed image surveys conducted across the eastern CCZ (e.g., Amon et al. 2017b) and in abyssal areas of the Kiribati EEZ, usually swim-

ming above the seabed but sometimes creeping on it. Body colour appears to be variable; bright red, semi-transparent, purplish, and whitish HOL_028 specimens have been encountered in seabed image surveys across the CCZ.

Peniagone vitrea Théel, 1882

Fig. 47

Material. Clarion-Clipperton Zone • 1 specimen; APEI 7; 5.0442°N, 141.8164°W; 4875 m deep; 28 May. 2018; Smith & Durden leg.; GenBank: ON400699 (COI), ON406622 (16S); NHMUK 2022.64; Voucher code: CCZ_077.

Other material. Pacific Ocean • 1 specimen, syntype of *Peniagone vitrea* var. *setosa* Ludwig; South Pacific; 0.6°S, 86.7667°W; 2418 m deep; Albatross Expedition; NHMUK 1895.11.12.7. • 3 specimens, syntypes of *Peniagone vitrea* Théel, 1882; East of St. Paul, Indian-Antarctic Ridge; 42.7167°S, 82.1833°W; 2652 m deep; Challenger Expedition, Stn. 302; NHMUK 1883.6.18.82.

Description. Single specimen. Body long, ~ 3× as long as wide (Fig. 47C, D). Mouth anterior, downwards; foremost neck-like part bent forwards in acute angle

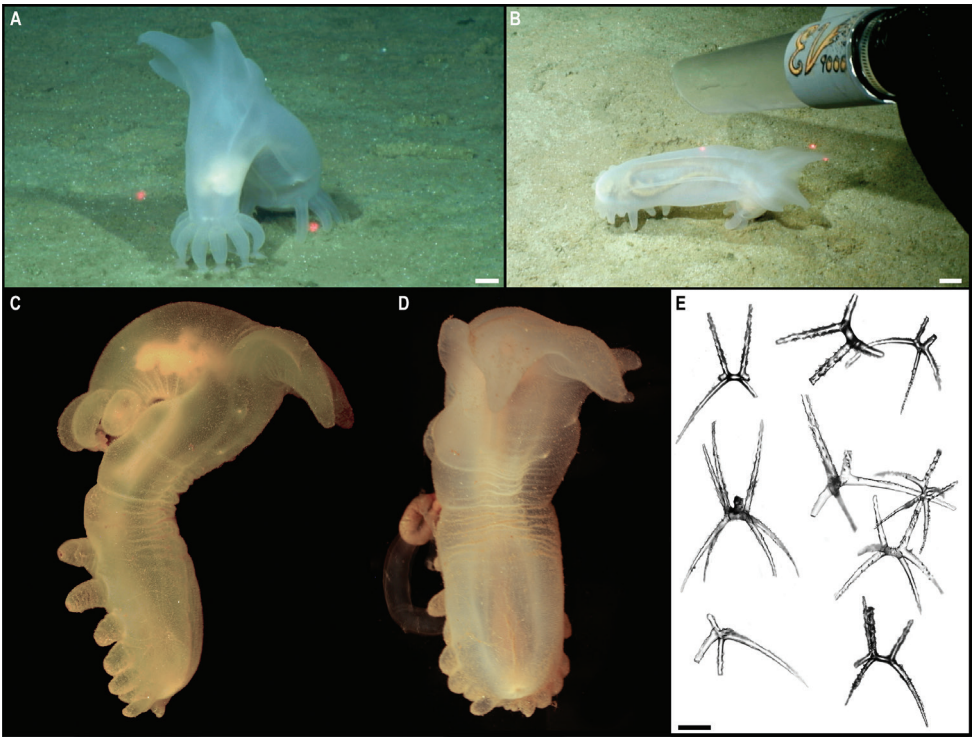

Figure 47. *Peniagone vitrea* Théel, 1882. Specimen CCZ_077: **A, B** in situ images **C** lateral view before preservation **D** dorsal view **E** dorsal ossicles. Scale bars:2 cm (**A**); 3 cm (**B**); 200 μm (**E**). Image attribution: Durden and Smith (**A, B**); Wiklund, Durden, Drennan, and McQuaid (**C, D**); Bribiesca-Contreras (**E**)

with ventral surface (Fig. 47C); with ten tentacles of similar sizes; anus terminal. Velum consists of two pairs processes, fully fused by a membrane forming a lobe, with only the tips free; the two middle processes are much larger (Fig. 47A, B, D). Eight pairs of tube feet surrounding the posterior third of ventral surface, decreasing in size distally. Skin translucent in live specimen (Fig. 47A, B), but white, hard, and brittle after preservation, with numerous calcareous deposits (Fig. 47C, D). Dorsal ossicles with four spinose arms, slightly arched, with mostly two long spinose processes (Fig. 47E).

Remarks. Morphological external characters and ossicle morphology are in accordance with the original description of *Peniagone vitrea*. Unfortunately, no genetic sequences of *P. vitrea* are available in public databases. This species was described from off Patagonia at 2652 m depth. Using data from Kremenetskaia et al. (2021), the COI sequence of *P. vitrea* is 16.5%–18.8% divergent (K2P) from other species of *Peniagone*, and 17.9% divergent from the COI sequence of *P. leander* generated in this study. In the phylogenetic tree, it is recovered in a well-supported clade with other species of *Peniagone* (Fig. 34).

Ecology. The specimen was found feeding on the sedimented seafloor of an abyssal plain in APEI 7 at 4874 m.

Comparison with image-based catalogue. A very similar *Peniagone* sp. morphotype (i.e., *Peniagone vitrea* sp. inc., HOL_059) has been commonly encountered in seabed image surveys conducted across nodule fields areas of the eastern CCZ (e.g., Amon et al. 2017b), but not in the abyssal areas surveyed within the Kiribati EEZ.

Family Laetmogonidae Ekman, 1926
Genus *Psychronaetes* Pawson, 1983

***Psychronaetes* sp. CCZ_101**
Fig. 48

Material. Clarion-Clipperton Zone • 1 specimen; APEI 7; 4.8877°N, 141.757°W; 3132 m deep; 27 May. 2018; Smith & Durden leg.; GenBank: ON400690 (COI), ON406630 (18S); NHMUK 2022.62; Voucher code: CCZ_063. • 1 specimen; APEI 4; 7.2647°N, 149.7741°W; 3562 m deep; 03 Jun. 2018; Smith & Durden leg.; GenBank: ON400707 (COI), ON406631 (18S); NHMUK 2022.65; Voucher code: CCZ_101. • 1 specimen; APEI 4; 7.2647°N, 149.7741°W; 3562 m deep; 03 Jun. 2018; Smith & Durden leg.; GenBank: ON400709 (COI), ON406639 (18S); NHMUK 2022.67; Voucher code: CCZ_103. • 1 specimen; APEI 4; 7.2647°N, 149.7741°W; 3562 m deep; 03 Jun. 2018; Smith & Durden leg.; GenBank: ON400710 (COI), ON406632 (18S); NHMUK 2022.68; Voucher code: CCZ_104.

Description. Four specimens (Fig. 48A–D). Body dorso-ventrally flattened (L = 15.9 cm, W = 3.4 cm), tapering at both ends; pronounced "neck" anteriorly; mouth anteroventral, anus posterodorsal. Tentacles 18, with long stems and large

elongate oval discs (Fig. 48G). Body wall firm and leathery, dark violet in preserved specimen, with evident, numerous calcareous wheel-like ossicles that make the skin sparkle under light. Mid-ventral ambulacrum is naked; one irregular row of ≥ 40 tube feet running along each ventrolateral ambulacra (Fig. 48G), very conspicu-

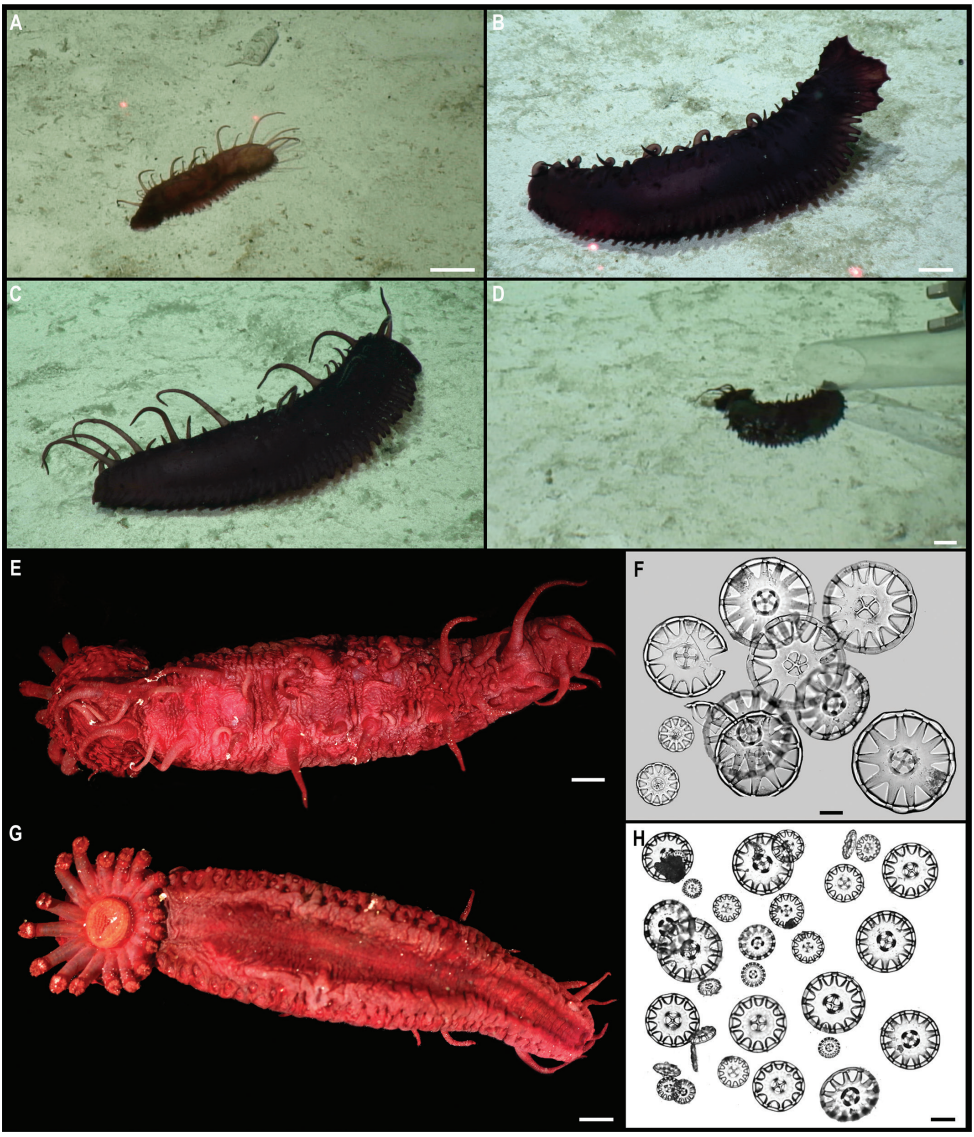

Figure 48. *Psychronaetes* sp. CCZ_101. Specimen CCZ_063 **A** in situ image. Specimen CCZ_101 **B** in situ image **F** dorsal ossicles. Specimen CCZ_103 **C** in situ image **H** dorsal ossicles. Specimen CCZ_104 **D** in situ image **E** dorsal view of specimen before preservation **G** ventral view. Scale bars: 5 cm (**A, D**); 2 cm (**B**); 1 cm (**E, G**); 75 μm (**F**); 100 μm (**H**). Image attribution: Durden and Smith (**A–D**); Wiklund, Durden, Drennan, and McQuaid (**E, G**); Bribiesca-Contreras (**F, H**).

ous on live specimens (Fig. 48A–D), but fully retracted on preserved specimens. Paired dorsal ambulacra with ~ 20 papillae each; ~ 7 long thick papillae distributed along each ambulacrum, interspersed with smaller ones (Fig. 48A–E). There are ~ 18 large conical papillae surrounding the anterior margin dorsally, fully fused forming a fringe (Fig. 48B, D). Dorsal ossicles numerous, wheel-like, of different sizes (ranging from 77–340 μm in diameter) but mostly large; strongly concave; central primary cross with 4–6 struts, mostly four; smooth rim; with 10–16, mostly 12, short spokes (Fig. 48F, H).

Remarks. Based on ossicle morphology, the four specimens were considered to belong to the same species. Sequence of the 18S were found to be identical between specimens CCZ_063, CCZ_101, and CCZ_104 (0.0% K2P distance) but 1.3% divergent from CCZ_103. The COI gene was amplified for the four specimens and genetic divergence ranges between 0.8% to 7.4%. The two specimens collected in APEI 4 are less genetically divergent (CCZ_101-CCZ_104 = 0.8% K2P). The specimen collected in APEI 7 (CCZ_063) is 2.3–2.9% divergent from the other three. The specimen CCZ_103 is 7.4% divergent to CCZ_101 and CCZ_104, but only 2.9% divergent from CCZ_063. While the former values are within the range of interspecific genetic divergence, we considered the specimen to belong to the same species as both the ossicle and external morphological characters are similar to the other three specimens. In addition, the trace files for both 18S and COI for this specimen are messy and the high genetic divergence could be an artifact of miss-called nucleotides. Unfortunately, there are no sequences available for *Psychronaetes*, but we included sequences of other genera within the family (*Pannychia*, *Laetmogone*, and *Benthogone*) for which COI genetic divergence ranged from 23–31%. In the phylogenetic tree, the four specimens were recovered in a well-supported clade (Fig. 34), close to other Laetmogonidae (poorly supported). This species has an anterior brim, which is characteristic of the monotypic genus *Psychronaetes. Psychronaetes hanseni* Pawson, 1983 differs from the four specimens in having smaller dorsal wheel ossicles (d = 50–80 μm) with 9–12 spokes, only 15 tube feet on each of paired ventral ambulacrum, 15 mouth tentacles instead of 18, and in the number of papillae on the dorsal paired ambulacra. The species and genus were described from two specimens collected in the CCZ (Pawson 1983).

Ecology. The four specimens were found on the sedimented seafloor of seamounts in APEIs 4 and 7 between 3132–3562 m depth.

Comparison with image-based catalogue. No exactly similar *Psychronaetes* sp. morphotypes have been encountered in seabed image surveys conducted in the eastern CCZ or in abyssal areas of the Kiribati EEZ. Consequently, the in situ images of these specimens were catalogued as a new morphotype (i.e., *Psychronaetes* sp. indet., HOL_110). However, HOL_110 can resemble at least two other Laetmogonidae morphotypes catalogued from seabed imagery; Laetmogonidae gen. indet., HOL_030 (e.g., dark violet, but with 8+ long papillae) which is commonly found in the eastern CCZ (but not in the Kiribati EEZ); and *Psychronaetes* sp. indet., HOL_122 (e.g., violet, but only with six or seven long papillae and with fewer (< 20) and larger, thick tube feet) which was also only found in the western CCZ.

Genus *Laetmogone* Théel, 1879

Laetmogone cf. *wyvillethomsoni* Théel, 1979

Fig. 49

Material. Clarion-Clipperton Zone • 1 specimen; APEI 7; 4.8877°N, 141.7569°W; 3132 m deep; 27 May. 2018; Smith & Durden leg.; GenBank: ON400689 (COI), ON406641 (18S); NHMUK 2021.18; Voucher code: CCZ_062.

Other material. Pacific Ocean • 1 specimen, holotype of *Laetmogone spongiosa* Théel, 1879; south of Japan; 34.1167°N, 138°E; 1033 m deep; Challenger Expedition, Stn. 235; NHMUK 1883.6.18.47.

Description. Single specimen (Fig. 49A). Body cylindrical, ~ 3× as long as wide (L = 15.6 cm, W = 5.2 cm), with convex dorsal surface and somewhat flattened ventral surface, tapering posteriorly; mouth anterior, subventral, terminal; anus posterior, terminal, slightly dorsal; violet colouration in live and preserved specimen, with darker ventral surface (Fig. 49A–C). Tentacles 15, of almost equal size, and very dark at the tips. Odd ambulacrum is naked; 27 or 28 tube feet arranged in a single row on each of the paired ventral ambulacra, forming a continuous line on the anterior ⅔ of the body and scattered posteriorly, also decreasing in size (Fig. 49C). Each paired dorsal ambulacrum with a single row of long processes, 12 on the left and 13 on the right; longest processes longer than ⅓ of the body length. Twenty pedicels along each side of the ventral surface, posterior pairs smaller than the others. Fourteen processes of the bivium along the left ambulacra and thirteen along the right. Tegument is thick, completely covered by calcareous ossicles. Dorsal ossicles are wheel-like of various sizes (40–226 μm in diameter), with four or five studs, mostly five, on primary central crosses, and with 8–17 spokes, mostly eight on large wheels; ossicle is convex, rim smooth, interspoke areas small, and large central area on large wheels (Fig. 49D).

Remarks. Closest match on public databases for the COI gene sequence was other sequences of *Laetmogone wyvillethomsoni* Théel, 1879 (4.0–5.8% K2P genetic distance) from the Ross Sea and Marie Byrd Seamounts (O'Loughlin et al. 2011). The specimen from the CCZ and specimens from *L. wyvillethomsoni* from Antarctica were recovered in our phylogeny (Fig. 34) in a well-supported clade (Fig. 34), which is subdivided in three clades including the two Antarctic clades stratified by depth reported in O'Loughlin et al. (2011), and the specimen from the CCZ. Type material for *L. wyvillethomsoni* was collected during the H.M.S. Challenger expedition at stations 300 (off the coast of South America; 33.7° S, 78.3°W; 2514 m depth) and 147 (west of the Crozet Islands; 46.2667° S, 48.45° E; 2926 m), and high morphological variability was reported (Théel 1879). The CCZ specimen morphologically resembles *L. wyvillethomsoni*, but no rod-shaped ossicles were found in the dorsal skin, differing from the original description.

Ecology. The specimen was found on the sedimented seafloor of a seamount in APEI 7 at 3132 m depth.

Comparison with image-based catalogue. No similar laetmogonid morphotypes have been encountered in seabed image surveys conducted in the eastern CCZ

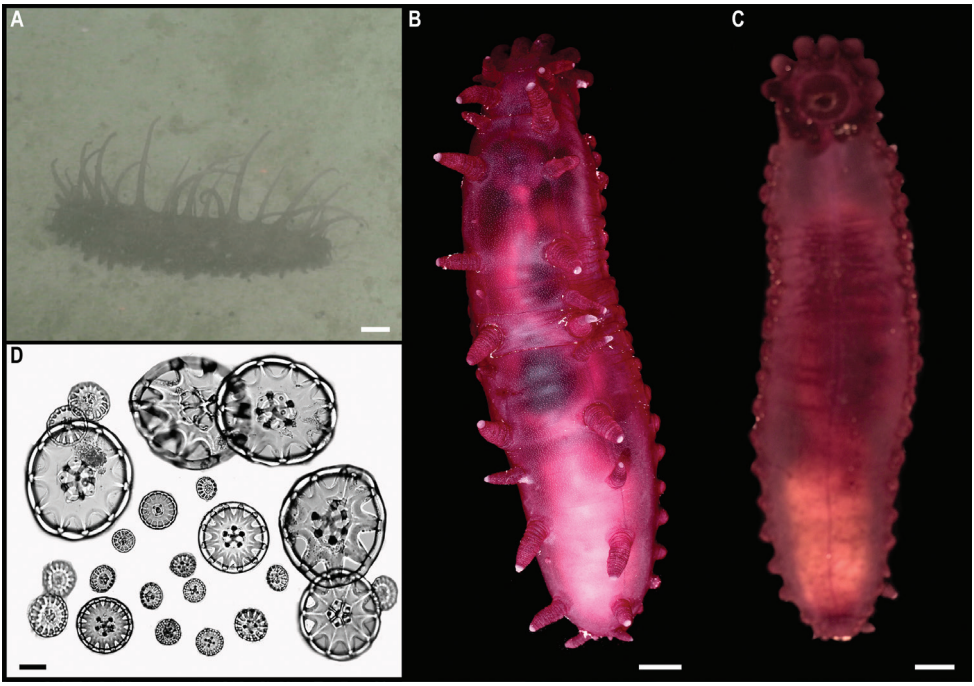

Figure 49. *Laetmogone* cf. *wyvillethomsoni* Théel, 1979. Specimen CCZ_062 **A** in situ image; **B** dorsal view of specimen before preservation **C** ventral view **D** dorsal calcareous ossicles. Scale bars: 2 cm (**A**); 1 cm (**B, C**); 50 µm (**D**). Image attribution: Durden and Smith (**A**); Wiklund, Durden, Drennan, and McQuaid (**B, C**); Bribiesca-Contreras (**D**).

or in abyssal areas of the Kiribati EEZ. Consequently, the in situ image of specimen CCZ_062 was catalogued as a new morphotype (i.e., *Laetmogone* sp. indet., HOL_123).

Class Ophiuroidea

To date, there are 1201 records of ophiuroids occurring at > 3000 m depth in the CCZ, with 117 representing preserved specimens (OBIS 2022). Four specimens belonging to three different species were collected and the barcoding gene COI was amplified for all but one, for which both 18S and 28S were amplified. These sequences, excluding 18S, were included in a concatenated alignment (28S, and COI) and used to estimate a phylogenetic tree (Fig. 50). Ophiuroidea is amongst the most challenging groups to identify and classify based on seabed image data only; key morphological features are too small to be appropriately visualised (e.g., plates and scales) and/or are found on the ventral disc (not visible in images). As a result, the taxonomic resolution of ophiuroid morphotypes catalogued from seabed imagery is usually much lower than that in other echinoderm groups. Consequently, connectivity and distribution patterns of ophiuroids derived from seabed image data should be interpreted cautiously.

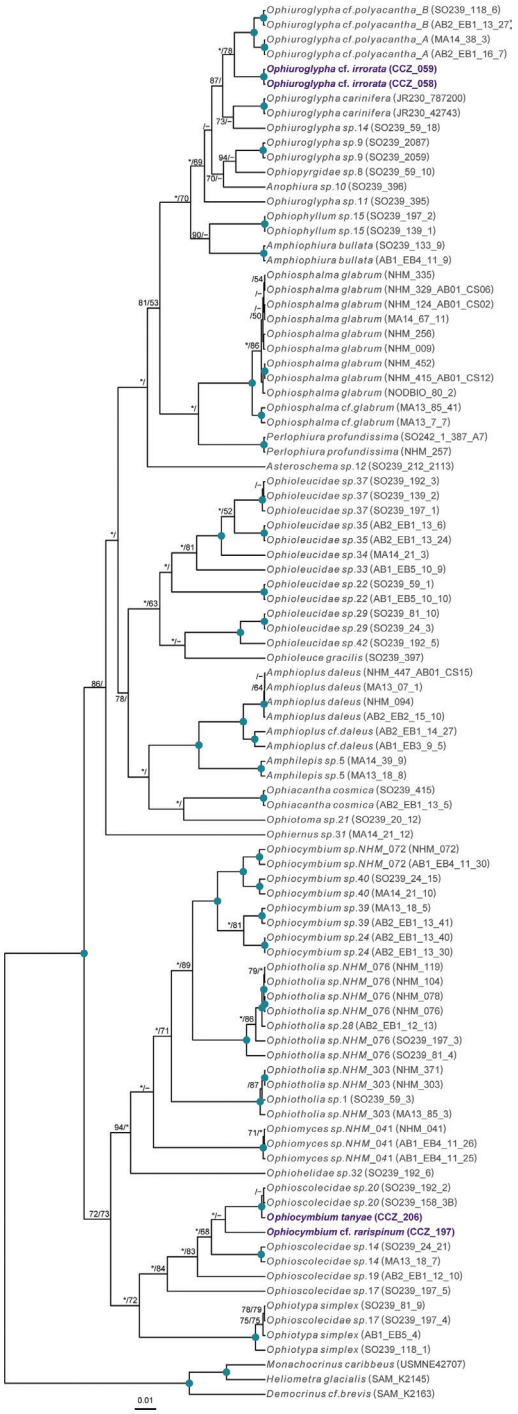

Figure 50. Phylogenetic tree of Ophiuroidea. Concatenated (28S, and COI) median consensus BEAST tree with posterior probability (PP) and bootstrap (BS) values indicated. Only values of PP > 0.70 and BS > 50 are shown, with values of PP > 0.95 and BS > 90 indicated with a circle. Nodes not recovered on the RAxML tree are indicated with a hyphen. Sequences generated in this study are highlighted in violet.

Subclass Myophiuroidea Matsumoto, 1915
Infraclass Metophiurida Matsumoto, 1913
Superorder Ophintegrida O'Hara, Hugall, Thuy, Stöhr & Martynov, 2017
Order Ophioscolecida O'Hara, Hugall, Thuy, Stöhr & Martynov, 2017
Family Ophioscolecidae Lütken, 1869
Genus *Ophiocymbium* Lyman, 1880

***Ophiocymbium tanyae* Martynov, 2010**
Fig. 51

Material. Clarion-Clipperton Zone • 1 specimen; APEI 1; 11.2523°N, 153.5848°W; 5204 m deep; 10 Jun. 2018; Smith & Durden leg.; GenBank: ON406633 (18S), ON406596 (28S); NHMUK 2022.74; Voucher code: CCZ_206.

Description. Single specimen (disc diameter = 9 mm, maximum arm length = 25 mm). Disc subpentagonal, flattened (Fig. 51A, B). Dorsal disc surface covered with numerous, imbricated, delicate disc scales, which are irregular in shape, decrease in size distally and extend dorsally onto the first arm segments (Fig. 51C). Radial shields and genital plates apparently absent. Disc covered by thin skin, not obscuring the scales. Ventral surface of the disc covered by scales similar to the dorsal disc scales (Fig. 51D). Oral shield somewhat triangular, approx. as long as wide, with convex distal edge; separated from first lateral arm plate by the adoral shields. Adoral shields are wing-shaped, narrowing proximally. Each jaw bears a large, spiniform, apical papillae and a smaller adjacent one on each side; additionally, there are two to three modified papillae placed distally on each side of the jaws, block-shaped, the distalmost being wing-shaped. Genital slit is not conspicuous. Arms are thin, longer than twice the disc diameter (Fig. 51A, B). Dorsal arm plates are triangular, wider than long, with pointed proximal and straight distal edges; separated by lateral arm plates and therefore not overlapping with preceding dorsal arm plate (Fig. 51C). Arm spines are conical, tapering distally but with rounded tips; two arm spines on first three arm segments, three arm spines on next three segments and four on the rest; middle arm spine is the longest, but all are approx. the same length, approx. half the length of one arm segment. First ventral arm plate is triangular, while the rest are pole-axe shaped, approx. as long as wide, separated from the preceding plate by the lateral arm plates except for the first two ventral arm plates (Fig. 51D). Tentacle pores are large and evident throughout the entire length of the arm. Three flattened, rounded, large adoral shield papillae. First four arms segments with two large papilliform tentacle scales attached to the lateral arm plate; subsequent arm segment with a single tentacle scale; tentacle scales absent on the remaining arm segments.

Remarks. Morphological characters of the specimen are in accordance with the description of *O. tanyae*, which was collected in the Izu-Bonin Trench at 6740–6850 m depth. It differs from the original description in having arms ≥ 2× as long as the disc diameter (dd), instead of being approx. the same. It also dif-

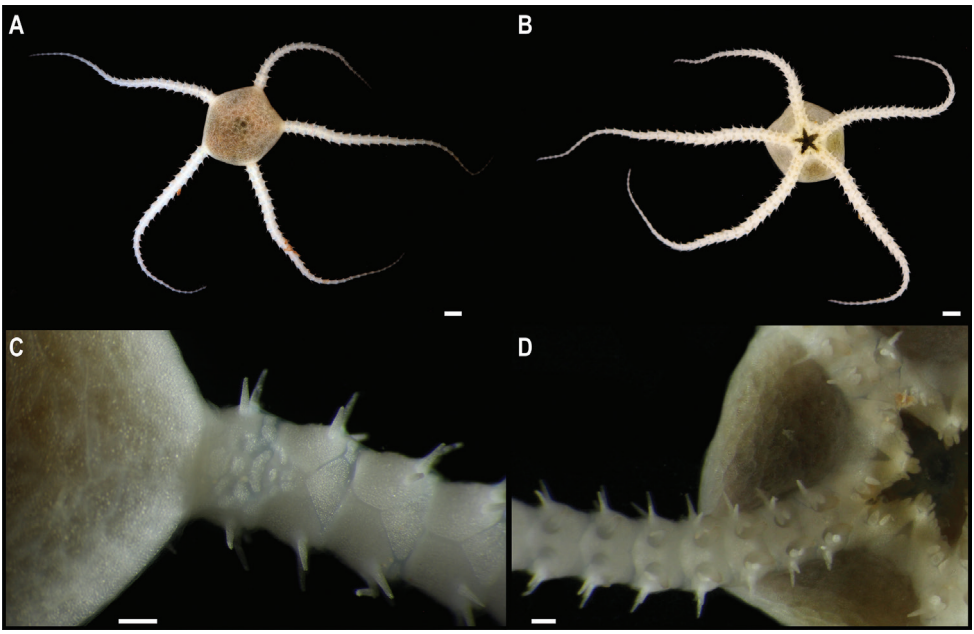

Figure 51. *Ophiocymbium tanyae* Martynov, 2010 **A** dorsal view of specimen CCZ_206 before preservation **B** ventral view **C** detail of dorsal disc surface and dorsal arm plates **D** detail of jaws, ventral disc surface and ventral arm plates. Scale bars: 2 cm (**A, B**); 5 mm (**C, D**). Image attribution: Wiklund, Durden, Drennan, and McQuaid (**A–D**).

fers on the tentacle scales, which extend to the fifth segment, instead of just the third, having two tentacle scales in the first four segments instead of just one, and in the number of arm spines of the first arm segments. The number of arm spines is discussed to vary amongst the paratypes (Martynov 2010), and it is very likely that tentacle scales are easily lost and therefore the number could differ between specimens. Only 18S and 28S were amplified for this specimen. The 28S sequence of the CCZ specimen is identical (K2P = 0%) to the sequence of the species Ophioscolecidae sp. 20 recently reported for the CCZ (Christodoulou et al. 2020). Both specimens are recovered within the same clade, that includes other species of the order Ophioscolescida (Fig. 50). Ophioscolescida sp. 20, *Ophiocymbium tanyae*, and *O. rarispinum* Martynov, 2010 are recovered as a clade possibly representing the genus *Ophiocymbium*. The species from Christodoulou et al. (2020) was identified from DNA sequences only, as the four specimens collected (eastern IFREMER and APEI 3) are tiny juveniles with no distinctive morphological characters. The species is therefore distributed in the Izu-Bonin Trench and the Clarion-Clipperton Zone.

Ecology. The specimen was found on the sedimented seafloor of an abyssal plain on APEI 1 at 5204 m depth.

***Ophiocymbium* cf. *rarispinum* Martynov, 2010**
Fig. 52

Material. Clarion-Clipperton Zone • 1 specimen; APEI 1; 11.2518°N, 153.6059°W; 5206 m deep; 10 Jun. 2018; Smith & Durden leg.; GenBank: ON400727 (COI); NHMUK 2022.73; Voucher code: CCZ_197.

Description. Single specimen, with white arms and greyish blue disc in situ (Fig. 52A). Disc is flattened and somewhat pentagonal; brownish when alive and white after preservation (Fig. 52B, D). Dorsal disc surface is covered by minute, thin, imbricated scales covered by a thin skin, not obscuring the scale margins; few granuliform spinelets scattered on the dorsal surface (Fig. 52B). Small, oval, radial shields, approx. as long as wide, arranged diagonally and touching proximally; distal margin extends beyond the disc margin (Fig. 52D). Ventral surface of the disc covered by scales similar to the ones on the dorsal surface, but lacking spinelets; gonads are visible through the thin scales (Fig. 52C). Each jaw bears two or three apical papillae, and three oral papillae on each side; two distalmost are block-shaped while the third distalmost is spiniform. Oral shield is triangular, longer than wide, rounded proximally; separated from the first lateral arm plate by the wing-shaped adoral shield. Supplementary oral shield, wider than long, located on the distal margin of the oral shield. Two adoral shield papillae, with one placed in the middle of each shield, resembling arm spines in shape and size. Arms are slender, ≥ 3× as long as the disc diameter. Dorsal arm plates triangular, with rounded distal margin and slightly convex distal edge, separated from preceding plates by lateral arm plates; first two dorsal arm plates absent but arm segments covered by thick skin with smaller plates embedded (Fig. 52D). Adjacent lateral arm plates are slightly separated by soft tissue; each lateral arm plate bears four long arm spines, similar in size; only two arm spines present in the first three arm segments and three on subsequent two arm segments. First ventral arm plate is small, broad and triangular, with the rest being pole-axe shaped and separated from the preceding plate except for the first two segments. Tentacle pores are large throughout the entire length of the arm, with no tentacle scales except for the first arm segment, where there is one attached to the lateral arm plate and resembles a small arm spine.

Remarks. In the phylogenetic tree, the specimen from the western CCZ is recovered as closely related to *Ophiocymbium tanyae* (Fig. 50). *Ophiocymbium rarispinum* was described from the Izu-Bonin Trench, between 6740 and 6850 m depth (ZMMU D-798), and no genetic sequences have been published. Morphological characters are concordant with the description of *O. rarispinum*, but differs in the length of the arms, the number of oral papillae and the number of arm spines.

Ecology. The specimen was found crawling on the abyssal sediments of APEI 1 at 5206 m depth.

Comparison with image-based catalogue. A similar Ophiuroidea morphotype (i.e., *Ophiocymbium* sp. indet., OPH_013) has been encountered in seabed image surveys conducted across nodule fields areas of the eastern CCZ, but not in the abyssal areas surveyed within the Kiribati EEZ.

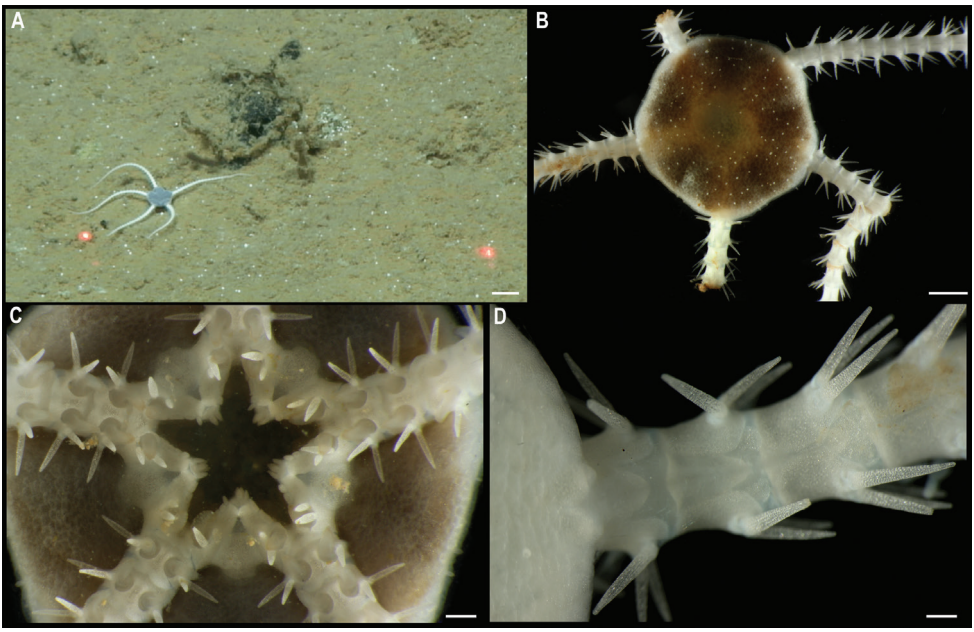

Figure 52. *Ophiocymbium* cf. *rarispinum* Martynov, 2010. Specimen CCZ_197 **A** in situ image **B** dorsal surface before preservation **C** detail of ventral surface, jaws and ventral arm plates **D** detail of dorsal arm plates. Scale bars: 1 cm (**A, B**); 5 mm (**C**); 2.5 mm (**D**). Image attribution: Durden and Smith (**A**); Wiklund, Durden, Drennan, and McQuaid (**B–D**).

Superorder Euryophiurida O'Hara, Hugall, Thuy, Stöhr & Martynov, 2017
Order Ophiurida Müller & Troschel, 1840 sensu O'Hara et al. 2017
Suborder Ophiurina Müller & Troschel, 1840 sensu O'Hara et al. 2017
Family Ophiopyrgidae Perrier, 1893
Genus *Ophiuroglypha* Hertz, 1927

***Ophiuroglypha* cf. *irrorata* (Lyman, 1878)**
Fig. 53

Material. Clarion-Clipperton Zone • 1 specimen; APEI 7; 4.9081°N, 141.6813°W; 3239 m deep; 26 May. 2018; Smith & Durden leg.; GenBank: ON400685 (COI); NHMUK 2021.21; Voucher code CCZ_058. • 1 specimen; APEI 7; 4.8897°N, 141.75°W; 3096 m deep; 27 May. 2018; Smith & Durden leg.; GenBank: ON400686 (COI); NHMUK 2022.72; Voucher code: CCZ_059.

Description. Two specimens, with greyish disc and pale arms in situ (Fig. 53A, B). Disc rounded to pentagonal, flattened, with slender, long arms, at least disc diameter (disc diameter = 2.6 cm, arm length = 13.1 cm; Fig. 53C, D). Dorsal disc surface covered by irregular, larger disc scales surrounded by small, imbricated disc scales that also vary in size and shape. Radial shields are small, subtriangular,

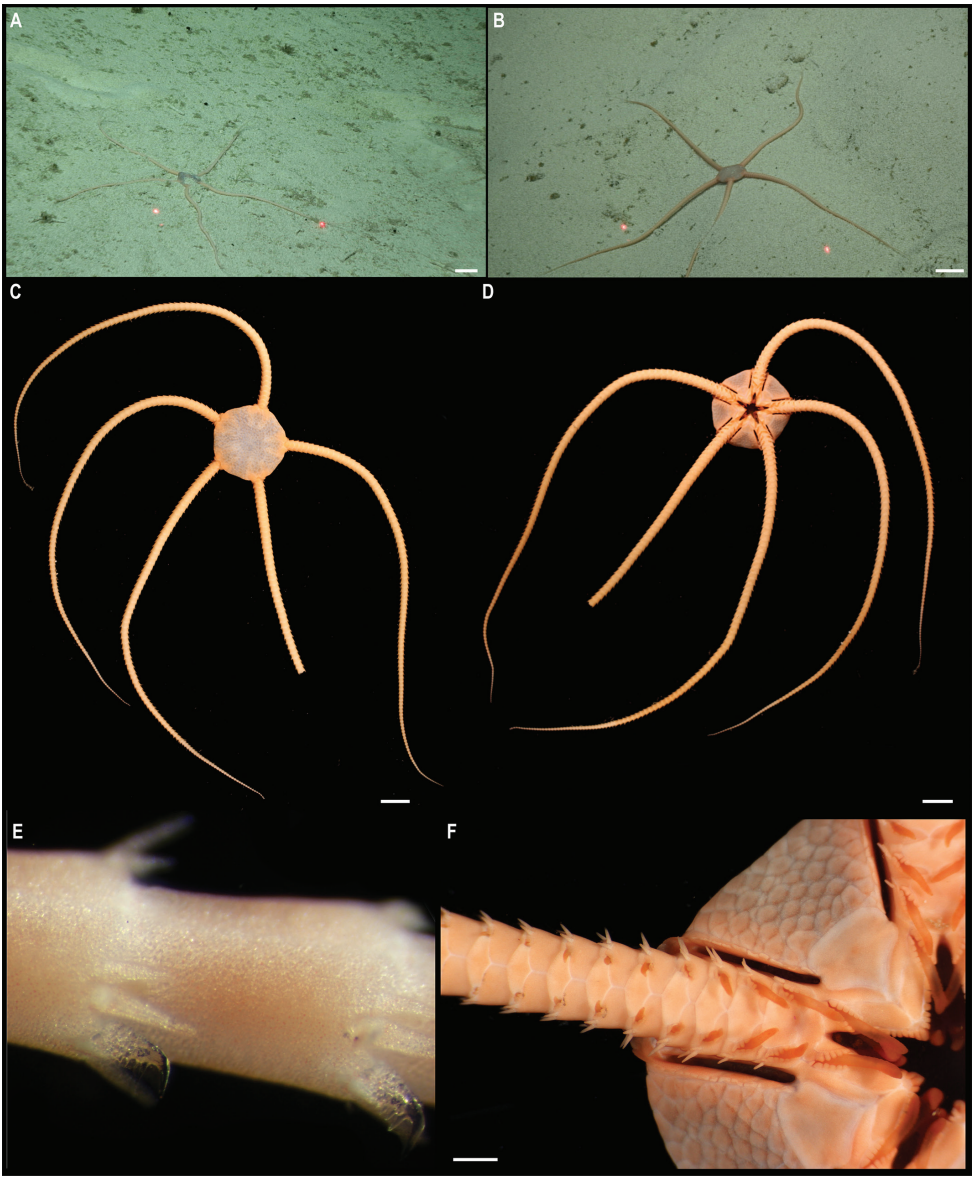

Figure 53. *Ophiuroglypha* cf. *irrorata* (Lyman, 1878). Specimen CCZ_059 **A** in situ image. Specimen CCZ_058 **B** in situ image **C** dorsal view of specimen before preservation **D** ventral view **E** arm hooklets **F** detail of ventral disc surface and ventral arm plates. Scale bars: 2 cm (**A, B**); 1 cm (**C, D**); 2 mm (**F**). Image attribution: Durden and Smith (**A, B**); Wiklund, Durden, Drennan, and McQuaid (**C–F**).

almost as wide as long. Arm combs visible under the radial shields; with five short block-like arm-comb spinelets, not continuous on dorsal midline. Ventral surface of the disc is covered by large, imbricated scales, increasing in size towards the margin of the disc (Fig. 53F). Oral plates with 6–8 oral papillae, proximalmost

are pointed, becoming block-like towards the distal side of the oral plate. Oral shield approx. as long as wide, subpentagonal, with somewhat concave proximal margins, a convex distal margin, and with lateral margins slightly constricted in the middle, where the genital slit begins. Adoral shields touching proximally, with a similar width all along, and separating the oral shield from the first lateral arm plates. Genital slits run from the middle of the oral shield to the disc margin, bordered by a continuous row of block-like genital papillae that continues dorsally as an arm-comb.

Dorsal arm plates fan-shaped, contiguous. Lateral arm plates bear three short (less than a third of the length of the arm segment) arm spines from the third arm segment; two are located ventrally, very close together, and one located dorsally, approx. halfway through the lateral arm plate; first arm segment bears two arm spines, the second two or three spines. Ventral arm plate trapezoidal, wider than long, only touching the preceding plate only on first three arm segments, after which they are separated by the lateral arm plates and become fan-shaped to rhomboidal, more than twice as wide as long, with pointed proximal edge and rounded distal margin. Towards the distal end of the arms, the second lowest spine is modified into a hyaline hooklet (Fig. 53E). Tentacle pores only on most proximal segments (8–11), with six ventral and six lateral tentacle scales on first arm segment and decreasing in number until there is a single, very small, spiniform, tentacle scale remaining for most of the arm length.

Remarks. Both specimens collected are only 0.4% divergent (K2P distance) in COI sequences between them. Closest genetic match is *Ophiuroglypha* sp. (8% K2P distance) collected in the CCZ (Christodoulou et al. 2020), and in the phylogenetic tree they were recovered in a well-supported clade along with other species of *Ophiuroglypha* (Fig. 50). Both specimens have an upturned hook in the second lowest arm spine, which is characteristic of species of the genus *Ophiuroglypha* (previously a subgenus but raised to genus by O'Hara et al. (2018)). Morphologically, the species resembles to *Ophiuroglypha irrorata concreta* (Koehler, 1901) based on the arm spine arrangement, dorsalmost spine separated from the two ventral spines. However, the DeepCCZ specimens are listed as *O.* cf. *irrorata*, as a recent study suggested that the arm spine arrangement might not be species specific, hence questioning the validity of *O. irrorata irrorata* (Lyman, 1878) and *O. irrorata concreta* (Stöhr and O'Hara 2021). Additionally, molecular data has suggested that *O. irrorata* represents an unresolved complex of species (Christodoulou et al. 2019).

Ecology. Both specimens were found on the sedimented seafloor of a seamount in APEI 7, at 3096 (specimen CCZ_059) and 3239 m (specimen CCZ_058) depth.

Comparison with image-based catalogue. No similar Ophiuroidea morphotypes have been encountered in seabed image surveys conducted in the eastern CCZ nor in abyssal areas of the Kiribati EEZ. Consequently, the in situ images of CCZ_058 and CCZ_059 were catalogued as a new morphotype (i.e., *Ophiuroglypha* sp. indet., OPH_012).

Phylum Porifera Grant, 1836

A total of eight sponges was collected in the western CCZ. All these belong to the class Hexactinellida and represent seven different species, but none was confidently assigned to any known species. To date, there are 255 records of hexactinellid sponges occurring at > 3000 m depth in the CCZ, with only eight representing preserved specimens (OBIS 2022). Several genes were targeted for amplification, but only 16S was successfully amplified for all of them. Other genes amplified were COI (7 specimens), 18S (5), 28S (5), and ALG11 (3). Sequences of these genes were combined with the concatenated alignment from Dohrmann (2018), and the phylogenetic tree was estimated using the same parameters (Fig. 54).

Class Hexactinellidae Schmidt, 1870
Subclass Amphidiscophora Schulze, 1886
Order Amphidiscosida Schrammen, 1924
Family Hyalonematidae Gray, 1857
Genus *Hyalonema* Gray, 1832

***Hyalonema* stet. CCZ_020**
Fig. 55

Material. Clarion-Clipperton Zone • 1 specimen; APEI 7; 5.1149°N, 141.8967°W; 4856 m deep; 25 May. 2018; Smith & Durden leg.; GenBank: ON400683 (COI), ON406634 (18S), ON406608 (16S), ON406597 (28S), ON411254 (ALG11); NHMUK; Voucher code: CCZ_020. • 1 specimen; APEI 1; 11.2954°N, 153.7422°W; 5245 m deep; 09 Jun. 2018; Smith & Durden leg.; GenBank: ON400721 (COI), ON406609 (16S); NHMUK 2022.8; Voucher code: CCZ_179.

Description. Two specimens. Lophophytous sponges (Fig. 55A–C). Body is white, ovoid, almost as wide as long (CCZ_020 W = 4.7 cm, L = 5 cm; CCZ_179 W = 8 cm, L = 8 cm); with an osculum (CCZ_020 d = 1 cm; CCZ_179 d = 4 cm) surrounded by a thin margin; separated atrial cavity. Attached to the sediment by a thin tuft of basalia that extends from the central lower body (CCZ_020 L > 7 cm; CCZ_179 L > 20 cm).

Remarks. Genetic sequences between specimens CCZ_020 and CCZ_179 are 1% and 0.8% divergent (K2P distance) for COI and 16S, respectively. COI and 16S closest matches are sequences from *Tabachnickia* sp. within the Hyalonematidae. The sequence for the 18S is > 95% similar to other species of *Hyalonema*. In the phylogenetic tree, both specimens were recovered together, in a well-supported clade with other members from different subgenera within the genus *Hyalonema* and including *Tabachnickia* sp. (Fig. 54).

Ecology. The specimens were collected attached to abyssal sediments of APEI 7 and APEI 1 at 4856 and 5245 m depth, respectively.

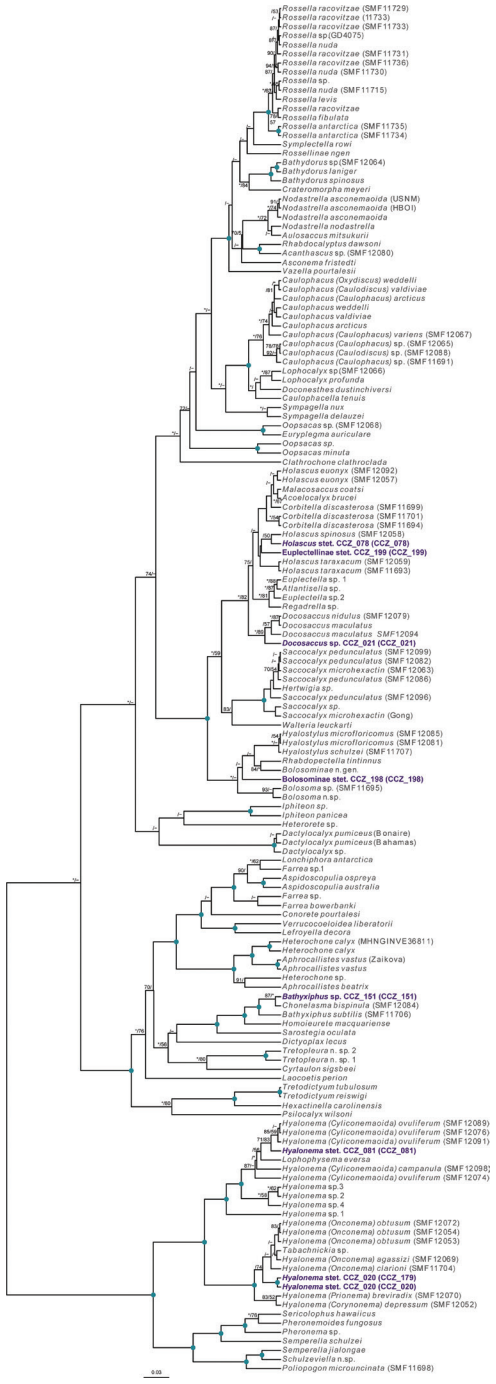

Figure 54. Phylogenetic tree of Hexactinellida. Concatenated (16S, 18S, 28S, and COI) median consensus BEAST tree with posterior probability (PP) and bootstrap (BS) values indicated. Only values of PP > 0.70 and BS > 50 are shown, with values of PP > 0.95 and BS > 90 indicated with a circle. Nodes not recovered on the RAxML tree are indicated with a hyphen. Sequences generated in this study are highlighted in violet.

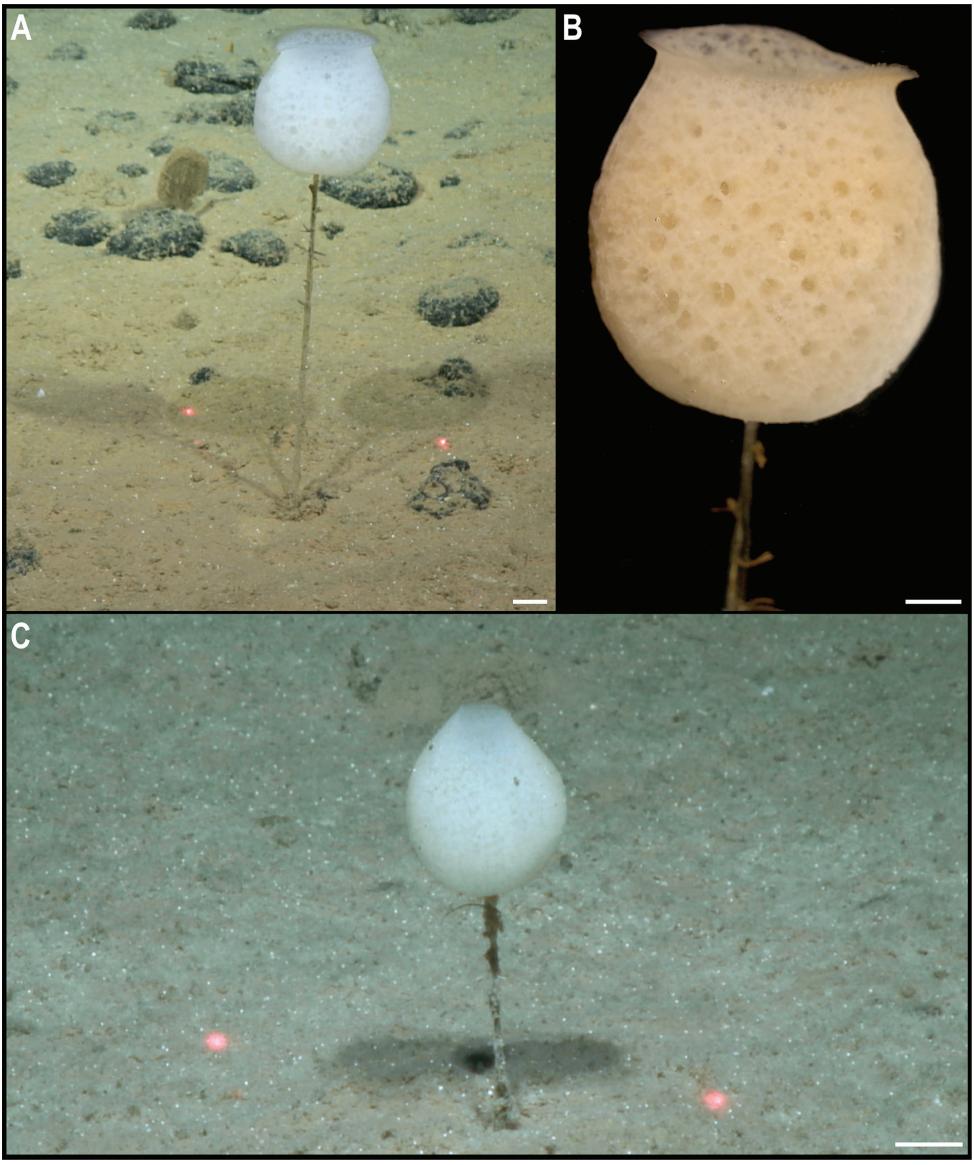

Figure 55. *Hyalonema* stet. CCZ_020. Specimen CCZ_179 **A** in situ image **B** specimen before preservation. Specimen CCZ_020 **C** in situ image. Scale bars: 2 cm (**A, C**); 1 cm (**B**). Image attribution: Durden and Smith (**A, C**); Wiklund, Durden, Drennan, and McQuaid (**B**).

Comparison with image-based catalogue. A very similar hyalonematid morphotype (i.e., *Hyalonema* sp. indet., HEX_002) has been commonly encountered in seabed image surveys conducted across the eastern CCZ and in abyssal areas of the Kiribati EEZ, mostly in nodule field areas. In situ images of HEX_002 (Fig. 55A, C) show that the aperture width of the central osculum is an unreliable character to distinguish different *Hyalonema* sp. morphotypes (nor these from other genera) in seabed imagery, as this contracts and expands episodically (e.g., Kahn et al. 2020).

***Hyalonema* stet. CCZ_081**
Fig. 56

Material. Clarion-Clipperton Zone • 1 specimen; APEI 4; 7.036°N, 149.9395°W; 5031 m deep; 01 Jun. 2018; Smith & Durden leg.; GenBank: ON406610 (16S); NHMUK 2022.9; Voucher code: CCZ_081.

Description. Single specimen (Fig. 56). Lophophytous sponge; body white, somewhat bowl-shaped, longer than wide (L = 3.9 cm, W = 2.8 cm); with a wide osculum (d = 2.6 cm) surrounded by a thin margin. Attached to the sediment by a thin tuft of basalia that extends from the central lower body.

Remarks. Morphological characters were found concordant with those of the genus *Hyalonema*. The 16S sequence is very similar (99.34%) to sequences from *H. (Cyliconemaoida) ovuliferum* Schulze, 1899, being the closest match on public databases. It is recovered in a well-supported clade along with other hyalonematids (Fig. 54), supporting its placement within the genus. It was not possible to assign it any subgenus, as the different subgenera have not been recovered as monophyletic (Dohrmann 2018).

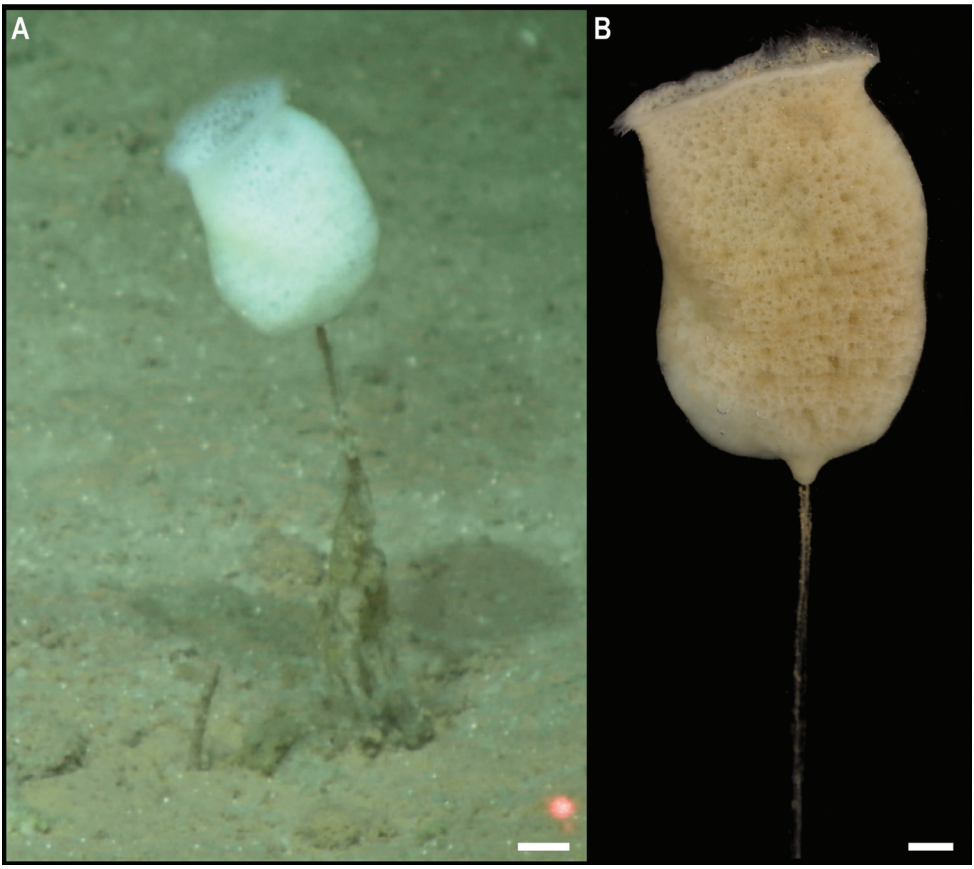

Figure 56. *Hyalonema* stet. CCZ_081 **A** in situ image, **B**. Scale bars: 1 cm (**A**); 5 mm (**B**). Image attribution: Durden and Smith (**A**); Wiklund, Durden, Drennan, and McQuaid (**B**).

Ecology. This specimen was collected anchored to the sediment on the abyssal plain of APEI 4 at 5031 m.

Comparison with image-based catalogue. A very similar hyalonematid morphotype (i.e., *Hyalonema* sp indet., HEX_003) has been commonly encountered in seabed image surveys conducted across the eastern CCZ and in abyssal areas of the Kiribati EEZ. As observed in HEX_002, the aperture width of the central osculum in HEX_003 can vary owing to body contractions or expansions (Kahn et al. 2020), and should hence not be used to guide identifications of these morphotypes based on seabed imagery.

Subclass Hexasterophora Schulze, 1886
Order Lyssacinosida Zittel, 1877
Family Euplectellidae Gray, 1867
Subfamily Euplectellinae Gray, 1867

Euplectellinae stet. CCZ_199
Fig. 57

Material. Clarion-Clipperton Zone • 1 specimen; APEI 1; 11.2518°N, 153.5853°W; 5202 m deep; 10 Jun. 2018; Smith & Durden leg.; GenBank: ON400729 (COI), ON406611 (16S); NHMUK; Voucher code: CCZ_199.

Description. Single specimen (Fig. 57A). Lophophytous white sponge with tubular habitus (L = 5 cm). There is a large, central osculum (d = 2cm), and protruding fistules with terminal suboscula, each with one or two, mostly two, openings (Fig. 57B). Long basalia (L = 6 cm) arranged as a tube, protruding from the lower end of the habitus and anchored to the sediment (Fig. 57C).

Remarks. The 16S sequence is close to *Corbitella discasterosa* Tabachnick & Lévi, 2004 (2.3% K2P distance), and it is also similar to other species within the family Euplectellidae. The closest COI match is *Docosaccus maculatus* Kahn, Geller, Reiswig & Smith Jr., 2013 (91.5% similarity). Morphological characters are concordant with those of the family Euplectellidae, and in the phylogenetic analysis it is recovered within the Euplectellidae (Fig. 54), along with other species of *Holascus* Schulze, 1886, but poorly supported. Although the subfamilies were not recovered as monophylectic, it is very likely it belongs to the subfamily Euplectillinae based on its lophophytous form.

Ecology. This specimen was found anchored to the abyssal sediments of APEI 1 at 5202 m depth.

Comparison with image-based catalogue. A very similar Euplectellidae morphotype (i.e., Euplectellidae gen. indet., HEX_005) has been commonly encountered in seabed image surveys conducted across nodule fields areas of the eastern CCZ, but not in abyssal areas of the Kiribati EEZ. Kersken et al. (2019) collected a few specimens of HEX_005 at the APEI 3 (Northeastern CCZ), identified as *Corbitella discasterosa* based on morphological characters. *Corbitella discasterosa* is basiphytous, while our specimen is lophophytous, but this would hardly be distinguished from seabed images.

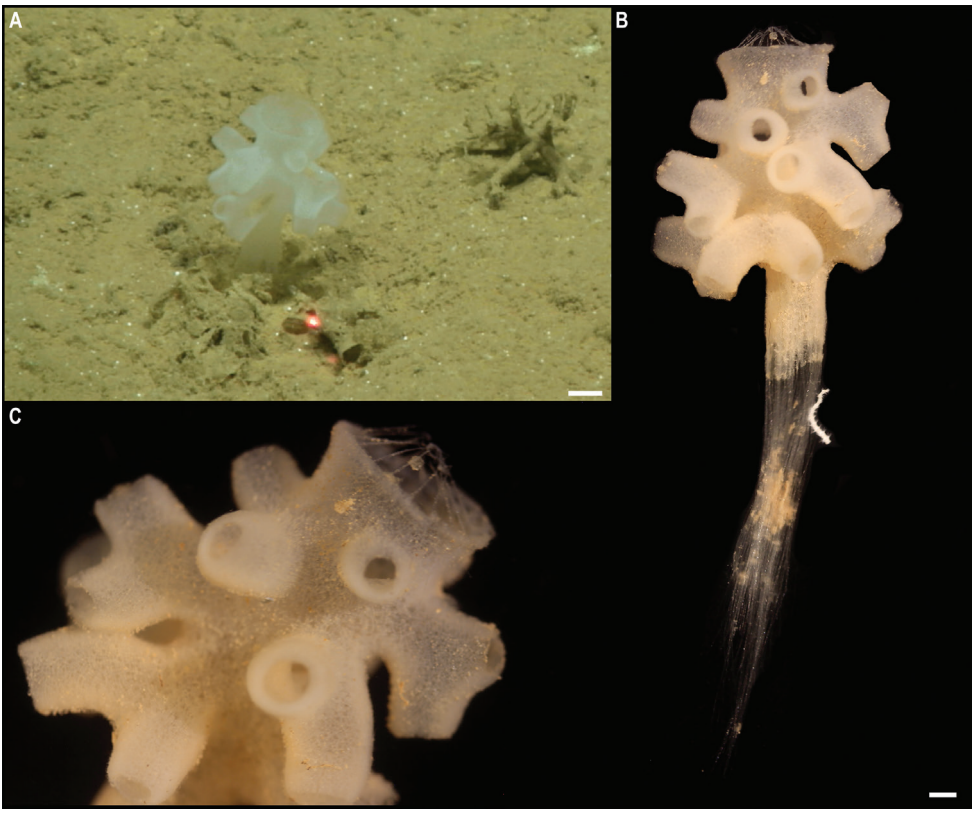

Figure 57. Euplectellinae stet. CCZ_199 **A** in situ image **B** detail of body **C** whole specimen with protruding basalia. Scale bars: 1 cm (**A**); 5 mm (**B**). Image attribution: Durden and Smith (**A**); Wiklund, Durden, Drennan, and McQuaid (**B, C**).

Genus *Docosaccus* Topsent, 1910

Docosaccus sp. CCZ_021

Fig. 58

Material. Clarion-Clipperton Zone • 1 specimen; APEI 7; 5.1043°N, 141.8867°W; 4860 m deep; 25 May. 2018; Smith & Durden leg.; GenBank: ON400684 (COI), ON406635 (18S), ON406612 (16S), ON406598 (28S), ON411255 (ALG11); NHMUK 2022.6; Voucher code: CCZ_021.

Description. Single specimen; lophophytous sponge. Plate-like, flat, subcircular body; 8.7 cm at its longest axis, 1 mm thick (Fig. 58A). Colouration is yellowish. Atrial surface facing up (Fig. 58C), and dermal surface almost in contact with the seafloor, with basalia protruding from it and anchoring it to the sediment (Fig. 58B).

Remarks. External morphological characters are concordant with the description of *D. maculatus* (Kahn et al. 2013). However, sequences for the 16S and COI genes

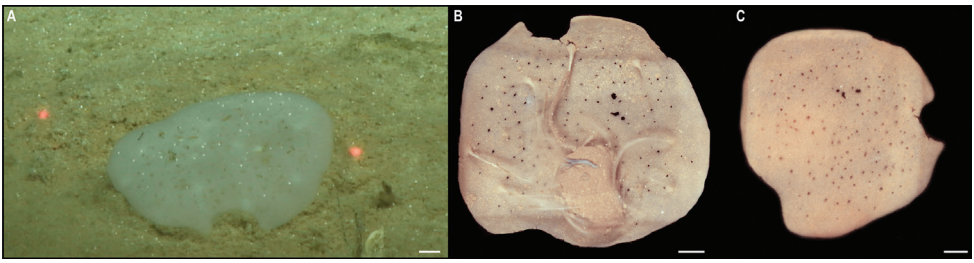

Figure 58. *Docosaccus* sp. CCZ_021 **A** in situ image **B** dermal surface **C** and atrial surface. Scale bars: 1 cm (**A, B, C**). Image attribution: Durden and Smith (**A**); Wiklund, Durden, Drennan, and McQuaid (**B, C**).

from the holotype are 2.4% and 3.9% divergent (K2P distance), respectively, from the western CCZ specimen. Sequences from 18S and 28S do not match to sequences from *D. maculatus*. The species was described from Station M, off California, in the Pacific Ocean at depths of 3,953–4,000 m, but the genus was originally thought to be restricted to Antarctica (Kahn et al. 2013). This species has been recorded in the CCZ, in the eastern IFREMER contract area and in APEI 3, from 4905–4998 m depth (Kersken et al. 2019). The specimen collected in the western CCZ differs from the holotype of *D. maculatus* in having more parietal oscula, and is smaller, and therefore considered a different species. External morphological characters also differ from the other species reported for the CCZ, *D. nidulus* Kersken, Janussen & Martínez Arbizu, 2019.

Ecology. This specimen was found anchored to abyssal sediments of APEI 7 at 4860 m depth.

Comparison with image-based catalogue. A very similar *Docosaccus* sp. morphotype (i.e., *Docosaccus maculatus* sp. inc., HEX_015) has been very frequently encountered in seabed image surveys conducted across nodule fields areas of the eastern CCZ and in abyssal areas of the Kiribati EEZ.

Genus *Holascus* Schulze, 1886

Holascus stet. CCZ_078

Fig. 59

Material. Clarion-Clipperton Zone • 1 specimen; APEI 7; 5.0443°N, 141.8162°W; 48745 m deep; 28 May. 2018; Smith & Durden leg.; GenBank: ON400700 (COI), ON406636 (18S), ON406613 (16S), ON406599 (28S), ON411256 (ALG11); NHMUK 2022.7; CCZ_078.

Description. Single specimen; lophophytous white sponge (Fig. 59A). Band-like body, collar formed from thin wall with two large openings, with lower opening being larger than upper opening (Fig. 59B, C). Body height of 4.8 cm, lower body diameter of 15.1 cm, and upper body diameter of 11.8 cm. Basalia almost as long as the body height, protruding from the lower margin and anchoring it to the sediment (Fig. 59A).

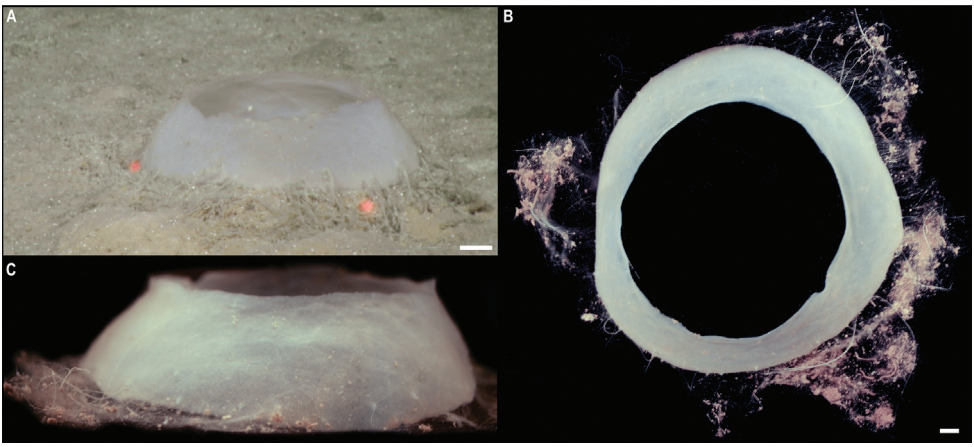

Figure 59. *Holascus* stet. CCZ_078 **A** in situ image **B** lateral view of specimen before preservation **C** top view. Scale bars: 2 cm (**A**); 1 cm (**B**). Image attribution: Durden and Smith (**A**); Wiklund, Durden, Drennan, and McQuaid (**B, C**).

Remarks. Morphological external characters are concordant with the description of *Holascus spinosus* Kersken, Janussen & Martínez Arbizu, 2019, which was described from the IOM area in the CCZ. The closest genetic matches on GenBank for the 16S correspond to species within the genus *Holascus* (2.1–3.5% genetic divergence), with the holotype of *Holascus spinosus* being the closest match (2.1% genetic divergence). There are no 18S sequences available for *H. spinosus*, but it is 0.23% divergent from another species within the genus, *H. euonyx* (Lendenfeld, 1915), from which it differs morphologically. In the phylogenetic tree it was recovered, with low support, as sister to *H. spinosus* (Fig. 54), but 16S genetic divergence suggested these to be separate species.

Ecology. This specimen was found anchored to abyssal sediments of APEI 7 at 4874 m depth.

Comparison with image-based catalogue. A very similar *Holascus* sp. morphotype (i.e., *Holascus* sp. indet., HEX_014) has been commonly encountered in seabed image surveys conducted across nodule fields areas of the eastern CCZ and in abyssal areas of the Kiribati EEZ.

Subfamily Bolosominae Tabachnick, 2002

Bolosominae stet. CCZ_198

Fig. 60

Material. Clarion-Clipperton Zone • 1 specimen; APEI 1; 11.2518°N, 153.6053°W; 5205 m deep; 10 Jun. 2018; Smith & Durden leg.; GenBank: ON400728 (COI), ON406637 (18S), ON406614 (16S), ON406600 (28S); NHMUK 2022.10; Voucher code: CCZ_198.

Description. Single specimen; lophophytous white sponge (Fig. 60A, B). Body is cup- to bell-shaped, slightly wider than long (L = 10 cm, W = 11 cm), with a long,

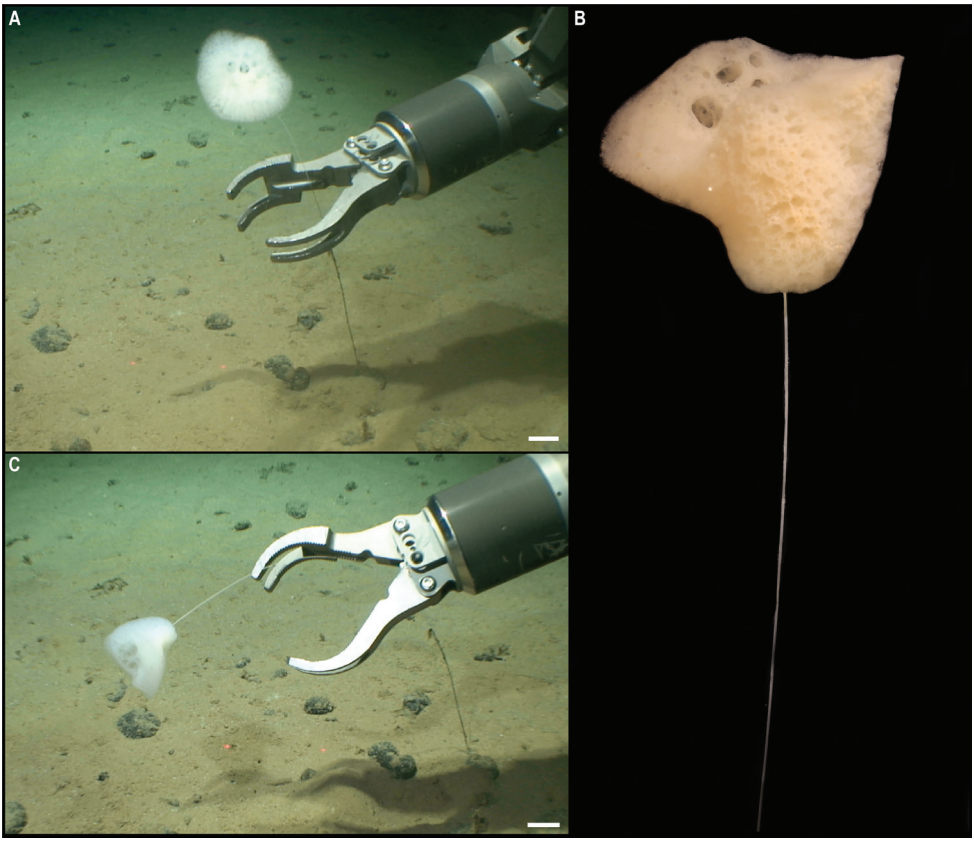

Figure 60. Bolosominae stet. CCZ_198 **A, C** in situ images **B** specimen before preservation. Scale bars: 5 cm (**A, C**). Image attribution: Durden and Smith (**A, C**); Wiklund, Durden, Drennan, and McQuaid (**B**).

slender stalk (L = 70 cm) anchored to soft sediment. Central osculum with thick body walls.

Remarks. The closest match with the 18S sequence is the holotype of *Hyalostylus microfloricomus* Kersken, Janussen & Martínez Arbizu, 2019 (99.8%), described from the Heip Mountains in the GSR contract area in the CCZ at 3788 m depth (Kersken et al. 2019). However, in the phylogenetic tree (Fig. 54) it was recovered in a well-supported clade representing the subfamily Bolosominae, but subclades were not well supported and hence the specimen is not attributed to any genera.

Ecology. This specimen was collected on abyssal sediments of APEI 1 at 5205 m depth, and was anchored to the sediment.

Comparison with image-based catalogue. A very similar stalked sponge morphotype (i.e., Hexactinellidae ord. indet., HEX_026) has been encountered in seabed image surveys conducted at the eastern CCZ, but not in abyssal areas of Kiribati's EEZ. In seabed images, HEX_026 highly resembles *Hyalonema (Cyliconemaoida) campanula* Lendenfeld, 1915, as identified by Kersken et al. (2019) based on morphological traits observed in specimens encountered in the eastern CCZ.

Order Sceptrulophora Mehl, 1992
Family Euretidae Zittel, 1877
Subfamily Chonelasmatinae Schrammen, 1912
Genus *Bathyxiphus* Schulze, 1899

***Bathyxiphus* sp. CCZ_151**
Figure 61

Material. Clarion-Clipperton Zone • 1 specimen; APEI 4; 6.9881°N, 149.9321°W; 5001 m deep; 06 Jun. 2018; Smith & Durden leg.; GenBank: ON400713 (COI), ON406638 (18S), ON406615 (16S), ON406601 (28S); NHMUK 2022.11; Voucher code: CCZ_151.

Description. Single specimen; basiphytous sponge (Fig. 61A, E). Body white, elongated (L > 60 cm, W = 10 cm), thin (W = 11 mm), upright-blade shaped habitus (Fig. 61B, C, E), attached to, possibly, a beaked-whale rostrum covered in manganese crust (Fig. 61A).

Remarks. Morphological characters are concordant with those of the genus, being very similar to *Bathyxiphus subtilis* Schulze, 1899, the only known species in the genus. However, a midrib has been suggested as a key morphological feature absent in the specimen presented here. The species was described from Isla Guadalupe at 1251 m depth, and was recently recorded in APEI 3 at 4914 m (Kersken et al. 2019). However,

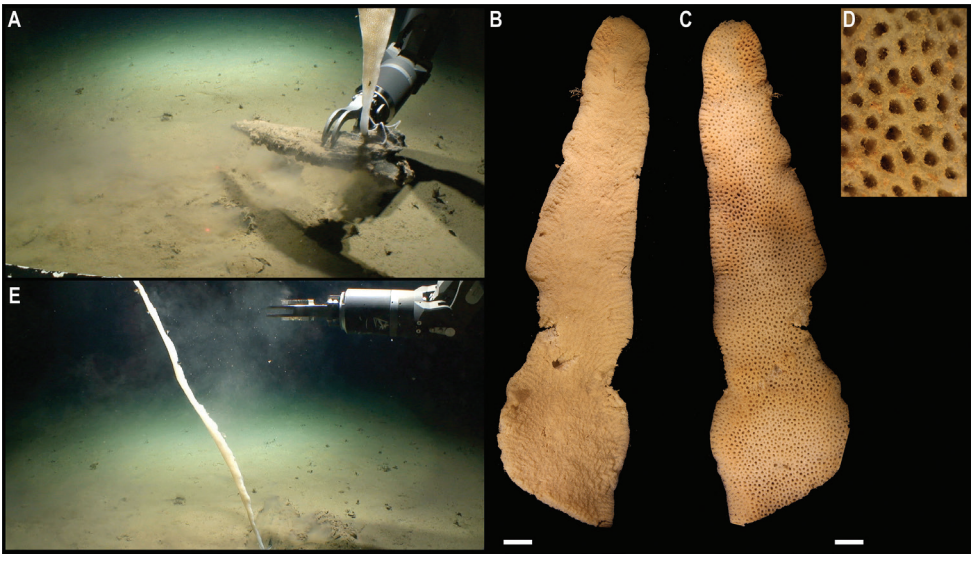

Figure 61. *Bathyxiphus* sp. CCZ_151. Specimen CCZ_151 **A, E** in situ images **B, C, D** specimen before preservation. Scale bars: 2 cm (**B, C**). Image attribution: Durden and Smith (**A, E**); Wiklund, Durden, Drennan, and McQuaid (**B–D**).

16S sequences between the APEI 3 specimen and the western CCZ specimen are 3% divergent (K2P distance). Additionally, they were not recovered as monophyletic in the phylogenetic tree (Fig. 54) and hence considered different species. Measurements of total length were estimated from in situ images as only approx. half the specimen was recovered.

Ecology. The specimen was found attached to a beaked-whale rostrum covered in polymetallic crust, on abyssal sediments of APEI 4 at 5001 m depth.

Comparison with image-based catalogue. A similar *Bathyxiphus* sp. morphotype (i.e., *Bathyxiphus* sp. indet., HEX_025), though usually much smaller-sized, has been commonly encountered in seabed image surveys conducted across nodule fields areas of the eastern CCZ, but not in abyssal areas of the Kiribati EEZ.

Discussion

The DeepCCZ expedition surveyed three APEIs on the western CCZ, targeting both abyssal seafloor and seamounts, and sampling the different megafaunal components. The ROV survey for benthic megafauna yielded a remarkably diverse collection from a small number of specimens, with 48 species from only 55 specimens (Table 1). Most species were represented by a single specimen, but whenever more than one specimen of the same species was collected, they were found at similar depths and same geoform (i.e., seamount, abyssal plain or seamount slope), even if collected in different sites. More than half of the species, 26, were sediment dwellers found both on seamounts and abyssal plains, mostly representing mobile megafauna, such as sea urchins, sea cucumbers, brittle stars, sea stars, a polychaete worm, and a jellyfish observed skimming the seafloor, and a single sessile species of cup coral. Eight species, mainly sponges, were found anchored to the sediment, five species were found attached to nodules, two species attached to polymetallic crust found on seamount slopes, and a single species of sponge was found attached to a fossilised beaked-whale rostrum covered in manganese crust. Additionally, six species were found attached to old glass sponge stalks, including scalpellids, crinoids, and actiniarians, with a few species co-occurring on the same sponge stalks.

Many of the taxa presented here had been encountered in image-based surveys from across the CCZ but never collected before, making our collections particularly important for improving taxonomic knowledge (Glover et al 2018). We were able to obtain genetic sequences for all but one specimen. The vast majority of taxa (29) could not be attributed to described species, with only four having been previously reported for the CCZ (Christodoulou et al. 2020; Glover et al. 2016b; Pawson and Foell 1986). The high number of delimited but undescribed species reported here highlights our still-limited knowledge on abyssal invertebrate megafauna in the CCZ, especially in the protected APEI regions, and illustrates the importance of publishing open DNA taxonomic data, even if full species identification and description are not always possible.

Although the CCZ is often considered a vast and relatively homogeneous abyssal plain, this region has substantial, ecologically important, seafloor heterogeneity (McQuaid et al. 2020; Washburn et al. 2021a). Variations in community structure and biodiversity have been documented across the region (Smith et al. 2021), mainly in the central and eastern CCZ, resulting from local and regional environmental conditions, such as topographical changes, food input, and nodule abundance (Stoyanova 2012; Vanreusel et al. 2016; Simon-Lledó et al. 2019c). While this study was not designed to investigate drivers of benthic megafaunal assemblages, some differences were observed between seamounts and abyssal plains. In other areas, seamounts have been found to harbour similar megafaunal taxonomic compositions as adjacent continental slopes (Clark et al. 2010). However, little overlap between seamount and abyssal plain taxa has been reported from surveys in the eastern CCZ (Cuvelier et al. 2020), and in western APEIs (Bribiesca-Contreras et al. 2021; Durden et al. 2021; Leitner et al. 2021). Due to the sampling strategy of maximising diversity, most species were represented by a single specimen, but whenever more than one specimen from the same species was collected, they were found in the same geoform (i.e., seamount or abyssal seafloor) even when collected in different APEIs (Table 1). Eight of the nine species that were assigned to previously described taxa were found in abyssal sites, except for *Calyptrophora distolos* that was originally described from a seamount (Cairns 2018). This is possibly a result of seamounts being understudied and undersampled compared to abyssal plains.

While the lack of shared species between habitats in this study could be a result of undersampling, faunistic changes between habitats have been reported in the CCZ (Cuvelier et al. 2020; Durden et al. 2021). Differences between abyssal plains and seamounts in APEIs 4 and 7 (with only 16 and 19% overlap in Operational Taxonomic Units; OTUs) have been observed from environmental-DNA sampling of sediments, with most OTUs being rare and limited to small areas (Laroche et al. 2020). Similarly, image-based surveys in the western APEIs observed very few common morphotypes shared across habitats, with several rare morphotypes observed only once (Durden et al. 2021). In addition, Leitner et al. (2021) have argued that even if some species are shared between seamounts and the abyssal seafloor, the areal coverage of seamounts is a tiny proportion compared to the areal of abyssal seafloor in the CCZ, so seamounts could supply only a very limited number of propagules for recolonisation over ecological time scales. Previous findings and our data currently suggest that CCZ seamounts could not act as viable refugia for abyssal taxa and provide propagules for recolonisation of areas disturbed by mining. Following the principles of a precautionary approach, representative and suitable refuge areas for megafaunal communities needs to be defined and protected as source of propagules for recolonisation.

The study of deep-sea ecosystems presents several challenges, from the difficulties of collecting at great depths, to the resources required for an oceanographic survey, and the labour to document and describe all the collected material (Glover et al. 2018). With the pressing need to describe the biodiversity of these habitats, taxonomic studies that synthesise morphological, ecological, and genetic information, even for undescribed and indeterminate species (e.g., Dahlgren et al. 2016; Glover et al. 2016b; Amon et al. 2017a, b; Wiklund et al. 2017; Christodoulou et al. 2020) contribute

fundamentally to the iterative building of biodiversity baselines (Engel et al. 2021; Glover et al. 2015). For instance, based on DNA sequences, we found two taxa with distributions likely spanning the entire CCZ, because they matched previously indeterminate juveniles collected in the eastern CCZ (*Ophiocymbium tanyae* as Ophioscolecidae sp. 20 in Christodoulou et al. (2020), and cf. *Porphyrocrinus* sp. CCZ_165 as Crinoidea sp. NHM_055 in Glover et al. (2016b)).

One of the limitations of this study is the scarcity of published barcodes for deep-see invertebrates. For instance, an environmental DNA study in the western APEIs found that only 25% and 1.5% of OTUs could be assigned to family level using reference libraries for 18S and COI, respectively (Laroche et al. 2020). We mainly targeted the barcoding gene COI because it has been used before to document biodiversity in the CCZ (e.g., Dahlgren et al. 2016; Glover et al. 2016b; Wiklund et al. 2017; Christodoulou et al. 2020). However, while the gene is useful for species delimitation in most groups, it is so variable that it does not accurately reflect phylogenetic relationships. Thus, in several cases it was not possible to assign our specimens to lower taxonomic levels based solely on genetic information because comparisons of our generated sequences to public databases showed that the closest taxa were only ~ 80% similar to multiple species belonging to different higher taxonomic ranks (Order or Family levels). Hence, additional genes were targeted to resolve higher rank relationships (16S, 18S, and 28S), but even for these genes, the lack of reference libraries hindered taxonomic placement. This is not surprising because the deep sea is severely undersampled and genetic sequences from bathyal and abyssal species are scarce in public databases. Even though there is much greater availability of genetic information for shallow water species, this did not inform our taxonomic assignments for most groups, because it has been found that bathyal and abyssal taxa often represent separate lineages from shallow-water ones (e.g., brittle stars: Bribiesca-Contreras et al. 2017; Christodoulou et al. 2019; isopods: Lins et al. 2012).

Additional challenges result from the documentation that COI and other mitochondrial genes show very little variation in anthozoan cnidarians (Hebert et al. 2003), preventing use of COI for species delimitation. For instance, the sequence of *Chrysogorgia* sp. CCZ_112 collected in APEI 4 differed from the COI sequence of *C. abludo* by a single nucleotide. Although the specimen was not assigned to the species because previous findings show that congeneric species of octocorals can share the same COI haplotype (McFadden et al. 2011), we also took a precautionary approach when assigning species to avoid overestimation of species ranges. In some syntheses, most deep-sea species have been assumed to have wide distributional ranges (McClain and Hardy 2010), likely resulting from the greater ease of discovering abundant, wide-ranging species than species with narrow distributions (Higgs and Attrill 2015), but also due to low or overlooked morphological variability that hinders our ability to discriminate species. Molecular studies have revealed different distinct lineages in some common, previously considered wide-ranging species. For instance, genetic sequences and further detailed morphological examination revealed at least two distinct species within the cosmopolitan *Psychropotes longicauda* Théel, 1882 (Gubili et al. 2017; Gebruk et al. 2020). One represents the cosmopolitan species *P. pawsoni* Gebruk & Kremenetskaia in Gebruk et

al. 2020 distributed in all four oceans, and the second represents a species only occurring in the northwest Pacific, *P. moskalevi* Gebruk & Kremenetskaia in Gebruk et al. 2020.

While detailed taxonomic studies can reveal an overlooked biodiversity in deep-sea taxa and are greatly improving our understanding of species ranges, they are time-consuming and usually target a small area or a few taxa (e.g., O'Loughlin and Ahearn 2005; Molodtsova and Opresko 2017; Herzog et al. 2018; Kersken et al. 2019). In contrast, the use of in situ seabed imagery to investigate megabenthic communities allows much larger area surveys, but at a lower taxonomic resolution that can potentially underestimate biodiversity and over-estimate species ranges. For instance, the sponge subfamilies Euplectellinae and Corbitellinae are differentiated by their mode of fixation to substrata. From seabed imagery, two hexactinellid sponges belonging to these subfamilies (Euplectellinae stet. CCZ_199 herein, and *Corbitella discasterosa* in (Kersken et al. 2019), respectively) were classified as the same morphotype because the mode of fixation cannot be observed when photographed from the top. However, the integration of both methods can provide key insights into species composition and connectivity of benthic communities across the CCZ, which are fundamental aspects to guide conservation strategies.

The alignment of in situ specimen images from this study with invertebrate morphotypes previously catalogued from (and standardised across) different seabed image surveys conducted in the CCZ (Amon et al. 2016; Simon-Lledó et al. 2019c, d, 2020; Cuvelier et al. 2020; Durden et al. 2021) provided preliminary insight into the connectivity of western megafauna populations. The 53 specimens that had an associated in situ image were classified into a total of 45 morphotypes, from which 11 represented new additions to the existing CCZ megafauna catalogue. Few morphotypes (9) were found to have wider distributions, being reported from both the Kiribati EEZ to the west of the CCZ, and from the eastern CCZ. Surprisingly, only two morphotypes were uniquely shared with Kiribati, while 16 were uniquely shared with the eastern CCZ. These results suggest, rather tentatively, that western CCZ megafauna communities may share a much larger species pool with (the more distant) eastern CCZ areas than with closer areas towards the west, like Kiribati's abyss. However, it is important to note that a much larger sampling effort was previously conducted in eastern CCZ areas than around Kiribati. In addition, the ROV sampling conducted for this study was limited and the number of species identified in this study (48) is much lower than the number of morphotypes that have been identified from seabed imagery in the western CCZ (143; Durden et al. 2021). Further interpretation and synthesis of existing megafauna distribution data, as well as additional sampling, will expand and contextualise these preliminary observations.

Conclusions

We provide the first megafaunal faunistic study from the western CCZ based on voucher specimens. Our findings indicate a high diversity, represented mostly by undescribed species of megafauna in the western CCZ with little overlap between abyssal plains and seamounts, and within similar habitats located in greater distances to one

another. Further studies should aim to increase our knowledge of patterns of biodiversity across the entire CCZ in order to inform environmental management plans to protect its biodiversity. Our work also highlights the need for detailed taxonomic studies, not only within the CCZ, an area targeted for deep-sea mining, but in other bathyal, abyssal, and hadal regions. While species identification through genetic markers can facilitate the generation of species inventories, this is only achievable when genetic reference libraries are representative of the area and taxon of study, and these remains limited for the CCZ megafauna.

Acknowledgements

We want to acknowledge the masters, crew and technical support staff on the R/V Kilo Moana and ROV Lu'ukai during the DeepCCZ expedition. We are very grateful for help with taxonomic identifications provided by the expert taxonomists: Estefania Rodriguez (AMNH) for anemones, Dhugal Lindsay (JAMSTEC) for scyphozoans; Chris Mah (NMNH) for sea stars; Rich Mooi (CAS) and Carlos Andres Conejeros Vargas (UNAM) for sea urchins; and Lenka Nealova (NHM) for annelids. We also acknowledge Lauren Hughes (NHM), Miranda Lowe (NHM), Tom White (NHM), Amanda Robinson (NMNH), Emma Sherlock (NHM), Andreia Salvador (NHM), and Andrew Cabrinovic (NHM) for curatorial support; and Elena Luigli (NHM) and Claire Griffin (NHM) for lab support. Primary funding was from the Gordon and Betty Moore Foundation grant no. 5596 and NOAA Office of Ocean Exploration (grant #NA17OAR0110209), and the University of Hawaii. We also acknowledge funding from UK Seabed Resources, the UK Natural Environment Research Council grant numbers NE/T003537/1 and NE/T002913/1 and through National Capability funding to NOC as part of the Climate Linked Atlantic Section Science (CLASS) programme (grant number NE/R015953/1), and The Norwegian Research Council (JPIOMining Impact 2). DJA received funding from the EU's Horizon 2020 research and innovation programme under the Marie Sklodowska-Curie grant agreement number 747946.

References

Agassiz A (1881) Report on the Echinoidea dredged by H.M.S. Challenger during the years 1873–1876. Report on the Scientific Results of the Voyage of HMS Challenger during the years 1873–76. Zoology (Jena, Germany) 3: 1–321.

Agassiz A (1898) Reports on the dredging operations off the west coast of Central America to the Galápagos, to the west coast of México, and in the Gulf of California, in charge of Alexander Agassiz, carried on by the U.S. Fish Commission Streamer "Albatross", during 1891, Lieut. Commander Z. L. Tanner, U.S.N., Commanding. XXIII. Preliminary report on the Echini. Bulletin of the Museum of Comparative Zoology 32: 71–86.

Agassiz A (1904) The Panamic deep sea echini. Memoirs of the Museum of Comparative Zoology at Harvard College 31: 1–243.

Amon DJ, Ziegler AF, Dahlgren TG, Glover AG, Goineau A, Gooday AJ, Wiklund H, Smith CR (2016) Insights into the abundance and diversity of abyssal megafauna in a polymetallic-nodule region in the eastern Clarion-Clipperton Zone. Scientific Reports 6(1): 1–12. https://doi.org/10.1038/srep30492

Amon DJ, Ziegler AF, Drazen JC, Grischenko AV, Leitner AB, Lindsay DJ, Voight JR, Wicksten MK, Young CM, Smith CR (2017a) Megafauna of the UKSRL exploration contract area and eastern Clarion-Clipperton Zone in the Pacific Ocean: Annelida, Arthropoda, Bryozoa, Chordata, Ctenophora, Mollusca. Biodiversity Data Journal 14598: e14598. https://doi.org/10.3897/BDJ.5.e14598

Amon DJ, Ziegler AF, Kremenetskaia A, Mah CL, Mooi R, O'Hara T, Pawson DL, Roux M, Smith CR (2017b) Megafauna of the UKSRL exploration contract area and eastern Clarion-Clipperton Zone in the Pacific Ocean: Echinodermata. Biodiversity Data Journal 11794: e11794. https://doi.org/10.3897/BDJ.5.e11794

Anderson OF (2016) A review of New Zealand and southeast Australian echinothurioids (Echinodermata: Echinothurioida)–excluding the subfamily Echinothuriinae–with a description of a new species of *Tromikosoma*. Zootaxa 4092: 451–488. https://doi.org/10.11646/zootaxa.4092.4.1

Bonifácio P, Martínez Arbizu P, Menot L (2020) Alpha and beta diversity patterns of polychaete assemblages across the nodule province of the eastern Clarion-Clipperton Fracture Zone (equatorial Pacific). Biogeosciences 17(4): 865–886. https://doi.org/10.5194/bg-17-865-2020

Bouckaert R, Heled J, Kuhnert D, Vaughan T, Wu CH, Xie D, Suchard MA, Rambaut A, Drummond AJ (2014) BEAST 2: A software platform for Bayesian evolutionary analysis. PLoS Computational Biology 10(4): e1003537. https://doi.org/10.1371/journal.pcbi.1003537

Bribiesca-Contreras G, Verbruggen H, Hugall AF, O'Hara TD (2017) The importance of offshore origination revealed through ophiuroid phylogenomics. Proceedings. Biological Sciences 284(1858): e20170160. https://doi.org/10.1098/rspb.2017.0160

Bribiesca-Contreras G, Dahlgren TG, Horton T, Drazen JC, Drennan R, Jones DOB, Leitner AB, McQuaid KA, Smith CR, Taboada S, Wiklund H, Glover AG (2021) Biogeography and Connectivity Across Habitat Types and Geographical Scales in Pacific Abyssal Scavenging Amphipods. Frontiers in Marine Science 8: e1028. https://doi.org/10.3389/fmars.2021.705237

Cairns SD (2015) New abyssal Primnoidae (Anthozoa: Octocorallia) from the Clarion-Clipperton Fracture Zone, equatorial northeastern Pacific. Marine Biodiversity 46(1): 141–150. https://doi.org/10.1007/s12526-015-0340-x

Cairns SD (2018) Primnoidae (Cnidaria: Octocorallia: Calcaxonia) of the Okeanos Explorer expeditions (CAPSTONE) to the central Pacific. Zootaxa 4532(1): 1–43. https://doi.org/10.11646/zootaxa.4532.1.1

Castresana J (2000) Selection of conserved blocks from multiple alignments for their use in phylogenetic analysis. Molecular Biology and Evolution 17(4): 540–552. https://doi.org/10.1093/oxfordjournals.molbev.a026334

Christodoulou M, O'Hara TD, Hugall AF, Arbizu PM (2019) Dark Ophiuroid Biodiversity in a Prospective Abyssal Mine Field. Current Biology 29(22): 3909–3912. https://doi.org/10.1016/j.cub.2019.09.012

Christodoulou M, O'Hara T, Hugall AF, Khodami S, Rodrigues CF, Hilario A, Vink A, Martinez Arbizu P (2020) Unexpected high abyssal ophiuroid diversity in polymetallic nodule fields of the northeast Pacific Ocean and implications for conservation. Biogeosciences 17(7): 1845–1876. https://doi.org/10.5194/bg-17-1845-2020

Chow S, Konishi K, Mekuchi M, Tamaki Y, Nohara K, Takagi M, Niwa K, Teramoto W, Manabe H, Kurogi H, Suzuki S, Ando D, Jinbo T, Kiyomoto M, Hirose M, Shimomura M, Kurashima A, Ishikawa T, Kiyomoto S (2016) DNA barcoding and morphological analyses revealed validity of Diadema clarki Ikeda, 1939 (Echinodermata, Echinoidea, Diadematidae). ZooKeys 585: 1–16. https://doi.org/10.3897/zookeys.585.8161

Clark MR, Rowden AA, Schlacher T, Williams A, Consalvey M, Stocks KI, Rogers AD, O'Hara TD, White M, Shank TM, Hall-Spencer JM (2010) The ecology of seamounts: Structure, function, and human impacts. Annual Review of Marine Science 2(1): 253–278. https://doi.org/10.1146/annurev-marine-120308-081109

Cuvelier D, Ribeiro PA, Ramalho SP, Kersken D, Martinez Arbizu P, Colaço A (2020) Are seamounts refuge areas for fauna from polymetallic nodule fields? Biogeosciences 17(9): 2657–2680. https://doi.org/10.5194/bg-17-2657-2020

Dahlgren TG, Wiklund H, Rabone M, Amon DJ, Ikebe C, Watling L, Smith CR, Glover AG (2016) Abyssal fauna of the UK-1 polymetallic nodule exploration area, Clarion-Clipperton Zone, central Pacific Ocean: Cnidaria. Biodiversity Data Journal 4: e9277. https://doi.org/10.3897/BDJ.4.e9277

Danovaro R, Fanelli E, Aguzzi J, Billett D, Carugati L, Corinaldesi C, Dell'Anno A, Gjerde K, Jamieson AJ, Kark S, McClain C, Levin L, Levin N, Ramirez-Llodra E, Ruhl H, Smith CR, Snelgrove PVR, Thomsen L, Van Dover CL, Yasuhara M (2020) Ecological variables for developing a global deep-ocean monitoring and conservation strategy. Nature Ecology & Evolution 4(2): 181–192. https://doi.org/10.1038/s41559-019-1091-z

Dohrmann M (2018) Progress in glass sponge phylogenetics: A comment on Kersken et al. (2018). Hydrobiologia 843(1): 51–59. https://doi.org/10.1007/s10750-018-3708-7

Downey ME (1986) Revision of the Atlantic Brisingida (Echinodermata: Asteroidea), with description of a new genus and family. Smithsonian Contributions to Zoology 435(435): 1–57. https://doi.org/10.5479/si.00810282.435

Durden JM, Putts M, Bingo S, Leitner AB, Drazen JC, Gooday AJ, Jones DOB, Sweetman AK, Washburn TW, Smith CR (2021) Megafaunal Ecology of the Western Clarion Clipperton Zone. Frontiers in Marine Science 2021: 722. https://doi.org/10.3389/fmars.2021.671062

Eléaume M, Bohn J-M, Roux M, Améziane N (2012) Stalked crinoids (Echinodermata) collected by the R/V Polarstern and Meteor in the south Atlantic and in Antarctica. Zootaxa 3425(1): 1–22. https://doi.org/10.11646/zootaxa.3425.1.1

Engel MS, Ceríaco LMP, Daniel GM, Dellapé PM, Löbl I, Marinov M, Reis RE, Young MT, Dubois A, Agarwal I, Lehmann AP, Alvarado M, Alvarez N, Andreone F, Araujo-Vieira K, Ascher JS, Baêta D, Baldo D, Bandeira SA, Barden P, Barrasso DA, Bendifallah L, Bockmann FA, Böhme W, Borkent A, Brandão CRF, Busack SD, Bybee SM, Channing

A, Chatzimanolis S, Christenhusz MJM, Crisci JV, D`elía G, Da Costa LM, Davis SR, De Lucena CAS, Deuve T, Fernandes Elizalde S, Faivovich J, Farooq H, Ferguson AW, Gippoliti S, Gonçalves FMP, Gonzalez VH, Greenbaum E, Hinojosa-Díaz IA, Ineich I, Jiang J, Kahono S, Kury AB, Lucinda PHF, Lynch JD, Malécot V, Marques MP, Marris JWM, McKellar RC, Mendes LF, Nihei SS, Nishikawa K, Ohler A, Orrico VGD, Ota H, Paiva J, Parrinha D, Pauwels OSG, Pereyra MO, Pestana LB, Pinheiro PDP, Prendini L, Prokop J, Rasmussen C, Rödel M-O, Rodrigues MT, Rodríguez SM, Salatnaya H, Sampaio Í, Sánchez-García A, Shebl MA, Santos BS, Solórzano-Kraemer MM, Sousa ACA, Stoev P, Teta P, Trape J-F, Dos Santos CV-D, Vasudevan K, Vink CJ, Vogel G, Wagner P, Wappler T, Ware JL, Wedmann S, Zacharie CK (2021) The taxonomic impediment: A shortage of taxonomists, not the lack of technical approaches. Zoological Journal of the Linnean Society 193(2): 381–387. https://doi.org/10.1093/zoolinnean/zlab072

Fauchald K (1977) The polychaete worms. Definitions and keys to the orders, families and genera. Natural History Museum of Los Angeles County, Science Series 28, 188 pp. https://repository.si.edu/bitstream/handle/10088/3435/PinkBook-plain.pdf

Forero-Mejia AC, Molodtsova T, Östman C, Bavestrello G, Rouse GW (2019) Molecular phylogeny of Ceriantharia (Cnidaria: Anthozoa) reveals non-monophyly of traditionally accepted families. Zoological Journal of the Linnean Society 190(2): 397–416. https://doi.org/10.1093/zoolinnean/zlz158

Gallo ND, Cameron J, Hardy K, Fryer P, Bartlett DH, Levin LA (2015) Submersible- and lander-observed community patterns in the Mariana and New Britain trenches: Influence of productivity and depth on epibenthic and scavenging communities. Deep-sea Research. Part I, Oceanographic Research Papers 99: 119–133. https://doi.org/10.1016/j.dsr.2014.12.012

Gebruk AV, Kremenetskaia A, Rouse GW (2020) A group of species "*Psychropotes longicauda*" (Psychropotidae, Elasipodida, Holothuroidea) from the Kuril-Kamchatka Trench area (North-West Pacific). Progress in Oceanography 180: e102222. https://doi.org/10.1016/j.pocean.2019.102222

Glover A, Dahlgren T, Wiklund H, Mohrbeck I, Smith C (2015) An End-to-End DNA Taxonomy Methodology for Benthic Biodiversity Survey in the Clarion-Clipperton Zone, Central Pacific Abyss. Journal of Marine Science and Engineering 4(1): 2. https://doi.org/10.3390/jmse4010002

Glover A, Dahlgren T, Taboada S, Paterson G, Wiklund H, Waeschenbach A, Cobley A, Martínez P, Kaiser S, Schnurr S, Khodami S, Raschka U, Kersken D, Stuckas H, Menot L, Bonifacio P, Vanreusel A, Macheriotou L, Cunha M, Hilário A, Rodrigues C, Colaço A, Ribeiro P, Błażewicz M, Gooday A, Jones D, Billett D, Goineau A, Amon D, Smith C, Patel T, McQuaid K, Spickermann R, Brager S (2016a) The London Workshop on the Biogeography and Connectivity of the Clarion-Clipperton Zone. Research Ideas and Outcomes 2: e10528. https://doi.org/10.3897/rio.2.e10528

Glover AG, Wiklund H, Rabone M, Amon DJ, Smith CR, O'Hara T, Mah CL, Dahlgren TG (2016b) Abyssal fauna of the UK-1 polymetallic nodule exploration claim, Clarion-Clipperton Zone, central Pacific Ocean: Echinodermata. Biodiversity Data Journal 4: e7251. https://doi.org/10.3897/BDJ.4.e7251

Glover AG, Wiklund H, Chen C, Dahlgren TG (2018) Managing a sustainable deep-sea 'blue economy' requires knowledge of what actually lives there. eLife 7: e41319. https://doi.org/10.7554/eLife.41319

Gong L, Li X, Xiao N, He L, Zhang H, Wang Y (2020) Rediscovery of the abyssal species *Peniagone leander* Pawson & Foell, 1986 (Holothuroidea: Elasipodida: Elpidiidae): the first record from the Mariana Trench area. Journal of Oceanology and Limnology 38(4): 1319–1327. https://doi.org/10.1007/s00343-020-0067-9

Gooday AJ, Durden JM, Holzmann M, Pawlowski J, Smith CR (2020a) Xenophyophores (Rhizaria, Foraminifera), including four new species and two new genera, from the western Clarion-Clipperton Zone (abyssal equatorial Pacific). European Journal of Protistology 75: 125715. https://doi.org/10.1016/j.ejop.2020.125715

Gooday AJ, Durden JM, Smith CR (2020b) Giant, highly diverse protists in the abyssal Pacific: Vulnerability to impacts from seabed mining and potential for recovery. Communicative & Integrative Biology 13(1): 189–197. https://doi.org/10.1080/19420889.2020.1843818

Gubili C, Ross E, Billett DSM, Yool A, Tsairidis C, Ruhl HA, Rogacheva A, Masson D, Tyler PA, Hauton C (2017) Species diversity in the cryptic abyssal holothurian *Psychropotes longicauda* (Echinodermata). Deep-sea Research. Part II, Topical Studies in Oceanography 137: 288–296. https://doi.org/10.1016/j.dsr2.2016.04.003

Hebert PD, Ratnasingham S, deWaard JR (2003) Barcoding animal life: Cytochrome c oxidase subunit 1 divergences among closely related species. Proceedings. Biological Sciences 270: S96–S99. https://doi.org/10.1098/rsbl.2003.0025

Hein JR, Koschinsky A, Kuhn T (2020) Deep-ocean polymetallic nodules as a resource for critical materials. Nature Reviews Earth & Environment 1: 158–169. https://www.nature.com/articles/s43017-020-0027-0

Herzog S, Amon DJ, Smith CR, Janussen D (2018) Two new species of *Sympagella* (Porifera: Hexactinellida: Rossellidae) collected from the Clarion-Clipperton Zone, East Pacific. Zootaxa 4466(1): 152–163. https://doi.org/10.11646/zootaxa.4466.1.12

Hestetun JT, Vacelet J, Boury-Esnault N, Borchiellini C, Kelly M, Rios P, Cristobo J, Rapp HT (2016) The systematics of carnivorous sponges. Molecular Phylogenetics and Evolution 94: 327–345. https://doi.org/10.1016/j.ympev.2015.08.022

Higgs ND, Attrill MJ (2015) Biases in biodiversity: Wide-ranging species are discovered first in the deep sea. Frontiers in Marine Science 2(61): 1–8. https://doi.org/10.3389/fmars.2015.00061

Hoek PPC (1883) Report on the Cirripedia collected by H.M.S. Challenger during the years 1873–76. Report on the Scientific Results of the Voyage of HMS Challenger during the years 1873–76 Zoology 8: 1–169. https://doi.org/10.5962/bhl.title.12873

Horton T, Marsh L, Bett BJ, Gates AR, Jones DOB, Benoist NMA, Pfeifer S, Simon-Lledó E, Durden JM, Vandepitte L, Appeltans W (2021) Recommendations for the Standardisation of Open Taxonomic Nomenclature for Image-Based Identifications. Frontiers in Marine Science 62: 1–13. https://doi.org/10.3389/fmars.2021.620702

Howell KL, Rogers AD, Tyler PA, Billett DSM (2004) Reproductive isolation among morphotypes of the Atlantic seastar species *Zoroaster fulgens* (Asteroidea: Echinodermata). Marine Biology 144(5): 977–984. https://doi.org/10.1007/s00227-003-1248-8

International Seabed Authority I (2020) Workshop Report: Deep CCZ Biodiversity Synthesis Workshop Friday Harbor, Washington, USA, 1–4 October 2019. Kingston, Jamaica.

Jones DO, Kaiser S, Sweetman AK, Smith CR, Menot L, Vink A, Trueblood D, Greinert J, Billett DS, Arbizu PM, Radziejewska T, Singh R, Ingole B, Stratmann T, Simon-Lledó E, Durden JM, Clark MR (2017) Biological responses to disturbance from simulated deep-sea polymetallic nodule mining. PLoS ONE 12: e0171750. https://doi.org/10.1371/journal.pone.0171750

Jones DOB, Simon-Lledó E, Amon DJ, Bett BJ, Caulle C, Clément L, Connelly DP, Dahlgren TG, Durden JM, Drazen JC, Felden J, Gates AR, Georgieva MN, Glover AG, Gooday AJ, Hollingsworth AL, Horton T, James RH, Jeffreys RM, Laguionie-Marchais C, Leitner AB, Lichtschlag A, Menendez A, Paterson GLJ, Peel K, Robert K, Schoening T, Shulga NA, Smith CR, Taboada S, Thurnherr AM, Wiklund H, Young CR, Huvenne VAI (2021) Environment, ecology, and potential effectiveness of an area protected from deep-sea mining (Clarion Clipperton Zone, abyssal Pacific). Progress in Oceanography 197: e102653. https://doi.org/10.1016/j.pocean.2021.102653

Kahn AS, Geller JB, Reiswig HM, Smith KL (2013) *Bathydorus laniger* and *Docosaccus maculatus* (Lyssacinosida; Hexactinellida): Two new species of glass sponge from the abyssal eastern North Pacific Ocean. Zootaxa 3646(4): 386–400. https://doi.org/10.11646/zootaxa.3646.4.4

Kahn AS, Pennelly CW, McGill PR, Leys SP (2020) Behaviors of sessile benthic animals in the abyssal northeast Pacific Ocean. Deep-sea Research. Part II, Topical Studies in Oceanography 173: e104729. https://doi.org/10.1016/j.dsr2.2019.104729

Kaiser S, Smith CR, Arbizu PM (2017) Editorial: Biodiversity of the Clarion Clipperton Fracture Zone. Marine Biodiversity 47(2): 259–264. https://doi.org/10.1007/s12526-017-0733-0

Kamenskaya OE, Melnik VF, Gooday AJ (2013) Giant protists (xenophyophores and komokiaceans) from the Clarion-Clipperton ferromanganese nodule field (eastern Pacific). Biology Bulletin Reviews 3(5): 388–398. https://doi.org/10.1134/S2079086413050046

Katoh K, Rozewicki J, Yamada KD (2019) MAFFT online service: Multiple sequence alignment, interactive sequence choice and visualization. Briefings in Bioinformatics 20(4): 1160–1166. https://doi.org/10.1093/bib/bbx108

Kersken D, Janussen D, Arbizu PM (2019) Deep-sea glass sponges (Hexactinellida) from polymetallic nodule fields in the Clarion-Clipperton Fracture Zone (CCFZ), northeastern Pacific: Part II–Hexasterophora. Marine Biodiversity 49(2): 947–987. https://doi.org/10.1007/s12526-018-0880-y

Kremenetskaia A, Gebruk A, Alt CHS, Budaeva N (2021) New and Poorly Known Species of *Peniagone* (Holothuroidea, Elpidiidae) from the Northwest Pacific Ocean with Discussion on Phylogeny of the Genus. Diversity (Basel) 13(11): e541. https://doi.org/10.3390/d13110541

Lanfear R, Frandsen PB, Wright AM, Senfeld T, Calcott B (2017) PartitionFinder 2: New methods for selecting partitioned models of evolution for molecular and morphological phylogenetic analyses. Molecular Biology and Evolution 34: 772–773. https://academic.oup.com/mbe/article-abstract/34/3/772/2738784

Laroche O, Kersten O, Smith CR, Goetze E (2020) Environmental DNA surveys detect distinct metazoan communities across abyssal plains and seamounts in the western Clarion Clipperton Zone. Molecular Ecology 29(23): 4588–4604. https://doi.org/10.1111/mec.15484

Leitner AB, Drazen JC, Smith CR (2021) Testing the Seamount Refuge Hypothesis for Predators and Scavengers in the Western Clarion-Clipperton Zone. Frontiers in Marine Science 8: 1–22. https://doi.org/10.3389/fmars.2021.636305

Li YN, Xiao N, Zhang LP, Zhang H (2018) *Benthodytes marianensis*, a new species of abyssal elasipodid sea cucumbers (Elasipodida: Psychropotidae) from the Mariana Trench area. Zootaxa 4462(3): 443–450. https://doi.org/10.11646/zootaxa.4462.3.10

Lins LS, Ho SY, Wilson GD, Lo N (2012) Evidence for Permo-Triassic colonization of the deep sea by isopods. Biology Letters 8(6): 979–982. https://doi.org/10.1098/rsbl.2012.0774

Martynov AV (2010) Reassessment of the classification of Ophiuroidea (Echinodermata), based on morphological characters. I. General character evaluation and delineation of the families Ophiomyxidae and Ophiacanthidae. Zootaxa 2697(1): 1–154. https://doi.org/10.11646/zootaxa.2697.1.1

McClain CR, Hardy SM (2010) The dynamics of biogeographic ranges in the deep sea. Proceedings. Biological Sciences 277(1700): 3533–3546. https://doi.org/10.1098/rspb.2010.1057

McFadden CS, Benayahu Y, Pante E, Thoma JN, Nevarez PA, France SC (2011) Limitations of mitochondrial gene barcoding in Octocorallia. Molecular Ecology Resources 11(1): 19–31. https://doi.org/10.1111/j.1755-0998.2010.02875.x

McQuaid KA, Attrill MJ, Clark MR, Cobley A, Glover AG, Smith CR, Howell KL (2020) Using habitat classification to assess representativity of a protected area network in a large, data-poor area targeted for deep-sea mining. Frontiers in Marine Science 7: e1066. https://doi.org/10.3389/fmars.2020.558860

Messing CG (2016) *Porphyrocrinus daniellalevyae* n. sp. (Echinodermata: Crinoidea), a sea lily from the tropical western Atlantic with a unique crown pattern. Zootaxa 4147(1): 1–35. https://doi.org/10.11646/zootaxa.4147.1.1

Miller AK, Kerr AM, Paulay G, Reich M, Wilson NG, Carvajal JI, Rouse GW (2017) Molecular phylogeny of extant Holothuroidea (Echinodermata). Molecular Phylogenetics and Evolution 111: 110–131. https://doi.org/10.1016/j.ympev.2017.02.014

Mironov AN (1971) [Soft sea urchins of the family Echinothuriidae collected by the R/V "Vityaz" and the "Academician Kurchatov" in the Pacific and Indian Oceans.] Trudy Instituta Okeanologii Akademii Nauk SSSR 92: 317–325.

Mironov AN, Minin KV, Dilman AB (2015) Abyssal echinoid and asteroid fauna of the North Pacific. Deep-sea Research. Part II, Topical Studies in Oceanography 111: 357–375. https://doi.org/10.1016/j.dsr2.2014.08.006

Molodtsova TN, Opresko DM (2017) Black corals (Anthozoa: Antipatharia) of the Clarion-Clipperton Fracture Zone. Marine Biodiversity 47(2): 349–365. https://doi.org/10.1007/s12526-017-0659-6

Mooi R, Constable H, Lockhart S, Pearse J (2004) Echinothurioid phylogeny and the phylogenetic significance of *Kamptosoma* (Echinoidea: Echinodermata). Deep-sea Research. Part II, Topical Studies in Oceanography 51(14–16): 1903–1919. https://doi.org/10.1016/j.dsr2.2004.07.020

O'Hara TD, Stöhr S, Hugall AF, Thuy B, Martynov A (2018) Morphological diagnoses of higher taxa in Ophiuroidea (Echinodermata) in support of a new classification. European Journal of Taxonomy 2018(416): 1–35. https://doi.org/10.5852/ejt.2018.416

O'Loughlin PM, Ahearn C (2005) A review of pygal-furrowed Synallactidae (Echinodermata: Holothuroidea), with new species from the Antarctic, Atlantic and Pacific oceans. Memoirs of the Museum of Victoria 62(2): 147–179. https://doi.org/10.24199/j.mmv.2005.62.5

O'Loughlin PM, Paulay G, Davey N, Michonneau F (2011) The Antarctic region as a marine biodiversity hotspot for echinoderms: Diversity and diversification of sea cucumbers. Deep-sea Research. Part II, Topical Studies in Oceanography 58(1–2): 264–275. https://doi.org/10.1016/j.dsr2.2010.10.011

OBIS (2022) Ocean Biodiversity Information System. Intergovernmental Oceanographic Commission of UNESCO.

Pante E, Watling L (2011) *Chrysogorgia* from the New England and Corner Seamounts: Atlantic–Pacific connections. Journal of the Marine Biological Association of the United Kingdom 92(5): 911–927. https://doi.org/10.1017/S0025315411001354

Pawson DL (1983) *Psychronaetes hanseni*, a new genus and species of elasipodan sea cucumber from the eastern central Pacific (Echinodermata: Holothurioidea). Proceedings of the Biological Society of Washington 96: 154–159.

Pawson DL, Foell EJ (1986) *Peniagone leander* new species, an abyssal benthopelagic sea cucumber (Echinodermata: Holothuroidea) from the eastern central Pacific Ocean. Bulletin of Marine Science 38: 293–299.

Poltarukha OP, Mel'Nik VF (2012) New records of deep-sea barnacles (Cirripedia: Thoracica: Scalpelliformes) from the Clarion-Clipperton region, Pacific Ocean. Zootaxa 3297: 34–40. https://doi.org/10.11646/zootaxa.3297.1.2

Provoost P, Bosch S (2020) robis: Ocean Biodiversity Information System (OBIS) Client. R package version 239.

Rex MA, Etter RJ (2010) Deep-sea Biodiversity. Harvard University Press, Cambridge, MA.

Rodriguez E, Barbeitos MS, Brugler MR, Crowley LM, Grajales A, Gusmao L, Haussermann V, Reft A, Daly M (2014) Hidden among sea anemones: The first comprehensive phylogenetic reconstruction of the order Actiniaria (Cnidaria, Anthozoa, Hexacorallia) reveals a novel group of hexacorals. PLoS ONE 9(5): e96998. https://doi.org/10.1371/journal.pone.0096998

Shalaeva K, Boxshall G (2014) An illustrated catalogue of the scalpellid barnacles (Crustacea: Cirripedia: Scalpellidae) collected during the HMS "Challenger" expedition and deposited in the Natural History Museum, London. Zootaxa 3804(1): 1, 4–63. https://doi.org/10.11646/zootaxa.3804.1.1

Simon-Lledó E, Bett BJ, Huvenne VAI, Koser K, Schoening T, Greinert J, Jones DOB (2019a) Biological effects 26 years after simulated deep-sea mining. Scientific Reports 9(1): 1–13. https://doi.org/10.1038/s41598-019-44492-w

Simon-Lledó E, Bett BJ, Huvenne VAI, Schoening T, Benoist NMA, Jeffreys RM, Durden JM, Jones DOB (2019b) Megafaunal variation in the abyssal landscape of the Clarion Clipperton Zone. Progress in Oceanography 170: 119–133. https://doi.org/10.1016/j.pocean.2018.11.003

Simon-Lledó E, Bett BJ, Huvenne VAI, Schoening T, Benoist NMA, Jones DOB (2019c) Ecology of a polymetallic nodule occurrence gradient: Implications for deep-sea mining. Limnology and Oceanography 64(5): 1883–1894. https://doi.org/10.1002/lno.11157

Simon-Lledó E, Thompson S, Yool A, Flynn A, Pomee C, Parianos J, Jones DOB (2019d) Preliminary Observations of the Abyssal Megafauna of Kiribati. Frontiers in Marine Science 605: e605. https://doi.org/10.3389/fmars.2019.00605

Simon-Lledó E, Pomee C, Ahokava A, Drazen JC, Leitner AB, Flynn A, Parianos J, Jones DOB (2020) Multi-scale variations in invertebrate and fish megafauna in the mid-eastern Clarion Clipperton Zone. Progress in Oceanography 187: e102405. https://doi.org/10.1016/j.pocean.2020.102405

Sladen WP (1889) Report on the Asteroidea. Report on the scientific results of the voyage of H.M.S. Challenger during the years 1873–1876. Zoology (Jena, Germany) 30: 1–893.

Smith CR, Clark MR, Goetze E, Glover AG, Howell KL (2021) Editorial: Biodiversity, Connectivity and Ecosystem Function Across the Clarion-Clipperton Zone: A Regional Synthesis for an Area Targeted for Nodule Mining. Frontiers in Marine Science 8: e797516. https://doi.org/10.3389/fmars.2021.797516

Stamatakis A (2006) RAxML-VI-HPC: Maximum likelihood-based phylogenetic analyses with thousands of taxa and mixed models. Bioinformatics (Oxford, England) 22(21): 2688–2690. https://doi.org/10.1093/bioinformatics/btl446

Stöhr S, O'Hara TD (2021) Deep-sea Ophiuroidea (Echinodermata) from the Danish Galathea II Expedition, 1950–52, with taxonomic revisions. Zootaxa 4963(3): 505–529. https://doi.org/10.11646/zootaxa.4963.3.6

Stoyanova V (2012) Megafaunal diversity associated with deep-sea nodule-bearing habitats in the eastern part of the Clarion-Clipperton Zone, NE Pacific. International Multidisciplinary Scientific GeoConference SGEM 1: 645–652. https://doi.org/10.5593/sgem2012/s03.v1032

Théel H (1879) Preliminary report on the Holothuroidae of the exploring voyage of the H.M.S. Challenger under professor Sir C. Wyville Thomson F.R.S., Part 1. Bihang Till K Svenska Vet Akad Handlingar 5: 1–20.

Théel H (1882) Report on the Holothuroidea dredged by H.M.S. 'Challenger' during the years 1873–76. Part i. Report on the scientific results of the voyage of H.M.S. Challenger during the years 1873–1876. Zoology (Jena, Germany) 4: 1–176.

Thomson CW, Murray J (1885) Report on the Scientific Results of the Voyage of H.M.S. Challenger during the years 1873–1876. Zoology (Jena, Germany) 115(48): 30.

Tilot V (2006) Biodiversity and Distribution of the Megafauna. In: Commission IO (Ed.) Technical Series 69. Project Unesco COI/Min, Vlanderen.

Vanreusel A, Hilario A, Ribeiro PA, Menot L, Arbizu PM (2016) Threatened by mining, polymetallic nodules are required to preserve abyssal epifauna. Scientific Reports 6(1): 1–6. https://doi.org/10.1038/srep26808

Washburn TW, Jones DOB, Wei C-L, Smith CR (2021a) Environmental Heterogeneity Throughout the Clarion-Clipperton Zone and the Potential Representativity of the APEI Network. Frontiers in Marine Science 8: e319. https://doi.org/10.3389/fmars.2021.661685

Washburn TW, Menot L, Bonifácio P, Pape E, Błażewicz M, Bribiesca-Contreras G, Dahlgren TG, Fukushima T, Glover AG, Ju SJ, Kaiser S, Yu OH, Smith CR (2021b) Patterns of

macrofaunal biodiversity across the Clarion-Clipperton Zone: An area targeted for deep-sea mining. Frontiers in Marine Science 8: e250. https://doi.org/10.3389/fmars.2021.626571

Wedding LM, Friedlander AM, Kittinger JN, Watling L, Gaines SD, Bennett M, Hardy SM, Smith CR (2013) From principles to practice: A spatial approach to systematic conservation planning in the deep sea. Proceedings. Biological Sciences 280(1773): e20131684. https://doi.org/10.1098/rspb.2013.1684

Wiklund H, Taylor JD, Dahlgren TG, Todt C, Ikebe C, Rabone M, Glover AG (2017) Abyssal fauna of the UK-1 polymetallic nodule exploration area, Clarion-Clipperton Zone, central Pacific Ocean: Mollusca. ZooKeys 707: 1–46. https://doi.org/10.3897/zookeys.707.13042

Wilson GDF (2017) Macrofauna abundance, species diversity and turnover at three sites in the Clipperton-Clarion Fracture Zone. Marine Biodiversity 47(2): 323–347. https://doi.org/10.1007/s12526-016-0609-8

Xiao N, Gong L, Kou Q, Li X (2019) *Psychropotes verrucicaudatus*, a new species of deep-sea holothurian (Echinodermata: Holothuroidea: Elasipodida: Psychropotidae) from a seamount in the South China Sea. Bulletin of Marine Science 95(3): 421–430. https://doi.org/10.5343/bms.2018.0041

Zevina GB, Poltarukha OP (2014) Deep-sea fauna of European seas: An annotated species check-list of benthic invertebrates living deeper than 2000 m in the seas bordering Europe. Cirripedia. Invertebrate Zoology 11: 101–111. http://oceanrep.geomar.de/id/eprint/28024

Zhang R, Wang C, Zhou Y, Zhang H (2019) Morphology and molecular phylogeny of two new species in genus *Freyastera* (Asteroidea: Brisingida: Freyellidae), with a revised key to close species and ecological remarks. Deep-sea Research. Part I, Oceanographic Research Papers 154: e103163. https://doi.org/10.1016/j.dsr.2019.103163

Supplementary material 1

Table S1

Authors: Guadalupe Bribiesca-Contreras, Thomas G. Dahlgren, Diva J. Amon, Stephen Cairns, Regan Drennan, Jennifer M. Durden, Marc P. Eléaume, Andrew Hosie, Antonina Kremenetskaia, Kirsty McQuaid, Timothy D. O'Hara, Muriel Rabone, Erik Simon-Lledó, Craig R. Smith, Les Watling, Helena Wiklund, Adrian G. Glover

Data type: phylogenetic

Explanation note: Detail of sequences included in the phylogenetic analyses including details of voucher numbers, code, GenBank accession number for different genes, details on whether specimens included are part of type material.

Link: https://doi.org/10.3897/zookeys.1113.82172.suppl1

ZooKeys 1113: 111–152 (2022)
doi: 10.3897/zookeys.1113.81240
https://zookeys.pensoft.net

RESEARCH ARTICLE

A peer-reviewed open-access journal
ZooKeys
Launched to accelerate biodiversity research

A new species of *Astronotus* (Teleostei, Cichlidae) from the Orinoco River and Gulf of Paria basins, northern South America

Alfredo Perez Lozano[1], Oscar M. Lasso-Alcalá[2], Pedro S. Bittencourt[3], Donald C. Taphorn[4], Nayibe Perez[4], Izeni Pires Farias[3]

1 *Instituto de Ciências Biológicas e da Saúde, Universidade Federal de Alagoas (UFAL), Maceió, Brazil* **2** *Museo de Historia Natural La Salle, Fundación La Salle de Ciencias Naturales (MHNLS), Caracas, Venezuela* **3** *Laboratório de Evolução e Genética Animal, Universidade Federal do Amazonas (UFAM), Manaus, Brazil* **4** *BioCentro, Universidad Nacional Experimental de los Llanos Occidentales Ezequiel Zamora (UNELLEZ), Guanare, Portuguesa, Venezuela*

Corresponding author: Alfredo Perez (piracatinga@yahoo.com.br)

Academic editor: Felipe Ottoni | Received 29 January 2022 | Accepted 15 May 2022 | Published 18 July 2022

https://zoobank.org/72D6D6BC-40CF-4FCE-96C9-C4566578C817

Citation: Perez Lozano A, Lasso-Alcalá OM, Bittencourt PS, Taphorn DC, Perez N, Farias IP (2022) A new species of *Astronotus* (Teleostei, Cichlidae) from the Orinoco River and Gulf of Paria basins, northern South America. ZooKeys 1113: 111–152. https://doi.org/10.3897/zookeys.1113.81240

Abstract

Based on morphological and molecular analysis of *Astronotus* species, a new species is described from the Orinoco River and Gulf of Paria basins in Venezuela and Colombia. Morphologically, it differs from *Astronotus crassipinnis* and *Astronotus ocellatus* in pre-orbital depth, caudal peduncle depth, head width, and caudal peduncle length, with significant differences in average percentage values. Osteologically, it differs from the two described species by lacking a hypurapophysis on the parahypural bone (hypural complex) and having two or three supraneural bones. Another characteristic that helps diagnose the new species is the morphology of the sagitta otolith, which is oval with crenulated dorsal and ventral margins and a rounded posterior edge. Genetically, the new species is distinct from all the other lineages previously proposed for the genus, delimited by five single locus species delimitation methods, and also has unique diagnostic nucleotides. Phylogenetic analyses support the monophyly of the new species as well as all other species/lineages. *Astronotus* species have considerable genetic, anatomical, and sagitta otolith shape differences, but have few significant traditional morphometric and meristic differences, because there is high variability in counts of spines, soft dorsal-fin rays, and lateral-line scales. It is clear that this new species is genetically and anatomically differentiated from all other species within the genus, and deserves recognition as a new valid species.

Keywords
DNA, fish, freshwater, morphometrics, osteology, sagitta otoliths, taxonomy

Introduction

The genus *Astronotus* Swainson, 1839 is the only known member of the tribe Astronotini widely distributed in South American river systems (Kullander 1986, 2003). It was originally considered to be a subgenus of *Crenilabrus* Oken, 1817. Kullander (1981, 1983, 1986) reviewed the taxonomy of *Astronotus* and considered only two nominal species as valid: (1) *Astronotus ocellatus* (Agassiz, 1831 in Spix and Agassiz 1829). Type locality Atlantic Ocean (error), types in ZSM (lost) distributed in western Amazon and Orinoco basins, with established populations introduced in others states of Brazil as Bahia, Ceará, Espirito Santo, Maranhão, and Piauí states (Burger et al. 2011; Leão et al. 2011; Ramos et al. 2014, 2018; Silva et al. 2020) and outside of South America e.g. Singapore (Ng et al. 1993), Canada (Coker et al. 2001), China (Ma et al. 2003), Hawaii (Mundy 2005), Poland (Solarz 2005), Australia (Hammer et al. 2012; ACTFR 2014), USA (Robins et al. 1991; Fuller et al. 1999; Nico et al. 2019; Rodríguez-Barrera et al. 2020), and Italy (Lorenzoni et al. 2019) and (2) *Astronotus crassipinnis* (Heckel, 1840). Type locality Rio Paraguay, distributed naturally in southern parts of the Amazon (upper Madeira River) and the upper Paraguay basins (Kullander 1986; Lasso et al. 2001; Kullander 2003; Fricke et al. 2019; Dos Reis et al. 2020) and introduced in Bahia and São Paulo States, and the upper Paraná River in Brazil (Kullander 1981; García et al. 2018; Lopes et al. 2022).

Kullander (1986) reviewed the taxonomy of *Astronotus* species based on morphometric and meristic data from 68 specimens from the Paraguay River basin (Paraná River basin in Paraguay), 18 specimens from several tributaries of the Amazon River basin (Brazil), six specimens from the Orinoco River Basin (Venezuela and Colombia), and 50 from the Peruvian Amazon (Ucayalí and Amazon basins); with this work he redescribed *A. ocellatus* and revalidated *A. crassipinnis*. According to Kullander (2003) both species are medium to large-sized (21–24 cm standard length), and are mainly distinguished by the presence of a group of ocelli (2–12) at the base of the dorsal fin (present in *A. ocellatus* vs. absent in *A. crassipinnis*), the pattern of bars along the sides of the body, and the dorsal-fin spine and ray count (XIII.20 in Peruvian *A. ocellatus* vs. XII.21 in Paraguayan *A. crassipinnis*). However, Colatreli et al. (2012), who molecularly diagnosed the two *Astronotus* species, found that the presence or absence of ocelli is not species-specific and varies between localities and individuals in the same locality. Furthermore, Kullander (1986) found that the meristic characters for the two valid species have significant overlap and are not discriminating.

Kullander (2003) also suggested that there were probably several additional undescribed species in the genus *Astronotus* distributed in the basins of the Amazon, Orinoco, Comté Orapu, Approuague, and Oyapock rivers (French Guiana and State

of Amapá, Brazil), and the northern part of the Paraguay River basin. Here we describe a new species of *Astronotus* from the Orinoco River and Gulf of Paria basins by using an integrative taxonomy approach, combining morphometric, meristic, internal anatomy (osteology), otolithometric, and molecular data.

Materials and methods

Specimens of *Astronotus* from the Orinoco and Gulf of Pária basins were used for morphological (n = 65) and genetic analyses (n = 5). To investigate the taxonomic status of *Astronotus* of Venezuela and Colombia, specimens of the two valid species of *Astronotus* were examined: *A. ocellatus* (n = 16) and *A. crassipinnis* (n = 21). The map was constructed in R 4.1.1 using packages 'ggspatial', 'raster', 'rgdal', 'rnaturalearth', and 'tidyverse' (R Development Core Team 2011). The final image was edited in Inkscape.

For some specimens, tissue samples were taken from the right side in the posterior region of the flanks and immediately preserved in 98% ethanol. After that, the fishes were fixed in 10% formalin for four weeks and then transferred to 70% ethanol. Specimens were purchased from fishermen or markets, and transported with permits from the Instituto Chico Mendes da Biodiversidade in Brazil (SISBIO N° 54708-1). The fish collection in Venezuela was conducted under a permit to the Universidad Nacional Experimental de los Llanos Occidentales Ezequiel Zamora (UNELLEZ). Voucher specimens are deposited in the collections of The Museo de Ciencias Naturales de Guanare (**MCNG**), Guanare, Venezuela; The Museo de Historia Natural La Salle (**MHNLS**), Caracas, Venezuela; The Museo de Biología de la Universidad Central de Venezuela (**MBUCV**), Caracas, Venezuela; The Estación Biológica Rancho Grande (**EBRG**), Maracay, Venezuela; The Instituto Nacional de Pesquisas da Amazônia (**INPA-ICT**), Manaus, Brazil. Photos of specimens were provided by the Academy of Natural Sciences of Philadelphia (**ANSP**), Pennsylvania, United States of America. Other specimens of *Astronotus* species previously deposited in these collections were also examined. All work was conducted in accordance with the guidelines of the Ethical Committee from the Conselho Nacional de Controle de Experimentação Animal (CONCEA 2016) of Brazil.

Morphological methods

We followed Kullander (1986, Fig. 1) for morphometric characters and López-Fernández and Taphorn (2004) for meristic characters and scale row nomenclature which consisted of 12 morphometric and ten meristic features, measured using digital calipers (0.10 mm) (Fig. 1). Osteological characteristics of the axial skeleton were analyzed by means of high-definition digital radiographs, in 26 MHNLS specimens of the *Astronotus* of Venezuela and Colombia, using a General Electric X-ray unit, model SenoGrate T 800, processed under the Agfa Viewer NX application. Additionally, and for comparative analysis, ten radiographs of *A. ocellatus* and four of *A. crassipinnis*

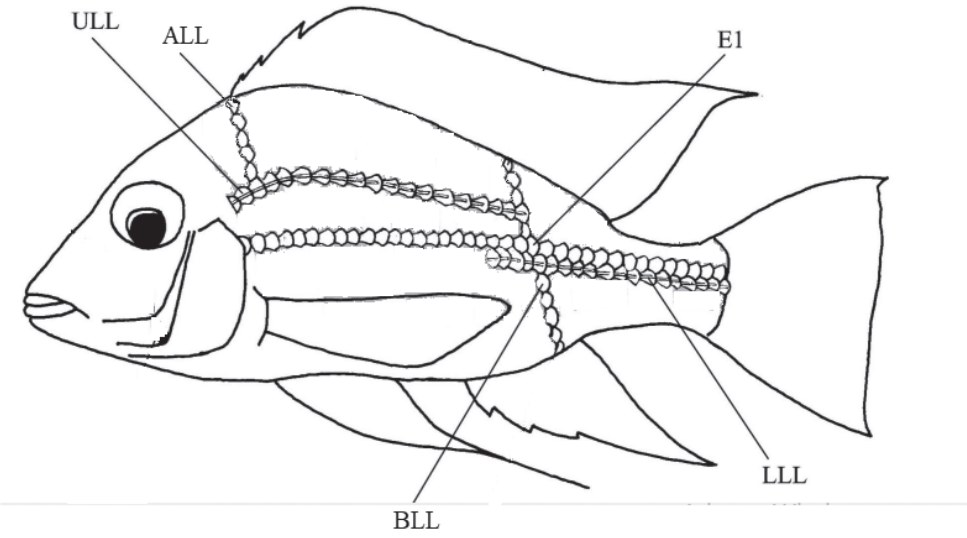

Figure 1. Meristic counts. Abbreviations: ALL - scales above upper lateral line to dorsal fin origin; BLL - scales below lower lateral line to anal-fin; E1 - scales longitudinal above the lower lateral line; LLL - lower lateral-line scales; ULL - upper lateral-line scales. Image modified from López-Fernández and Taphorn (2004).

were analyzed from specimens of the fish collections of INPA, Smithsonian Institution National Museum of Natural History, Washington D.C., U.S.A. (**USNM**) and Zoologische Staatssammlung München, München, Germany (**ZSM**).

The description and denomination of the elements of the axial and caudal skeleton, denominated hypural complex, follow Andreata (1979), Kullander (1983, 1986) and Sibilia and Andreata (1991), with some modifications: preural centrum = **CP**; hemal spine = **HEM**; ural centrum = **CU**; parahypural = **PH**; hypaxial procurrent caudal rays = **HPCR**; hypuraphophysis = **PP**; hypaxial caudal rays = **HCR**; hypurals = **H**; epaxial caudal Rays = **ECR**; diastema = **D**; epaxial procurrent caudal rays = **EPCR**; stegural = **ES**; total caudal rays = **TCR**; epurals = **E**; neural spine = **NEU**. Description of supraneural bones follows Mabee (1988). Description of the jaw teeth and color pattern follow Kullander (1986). All Institutional acronyms follow Sabaj (2016).

For the examination of otolith morphology, the sagitta otoliths (*Astronotus* from Venezuela, n = 15; *A. ocellatus*, n = 10; and *A. crassipinnis* n = 12) were cleaned with a 2% potassium hydroxide solution (10–20 min.) and washed with distilled water. The sagitta otoliths were photographed following the recommendations of AFORO (Lombarte et al. 2006), with a Leica binocular S8-APO stereomicroscope, equipped with a Leica EC3 camera, and processed using Leica Application Suite LAS-EZ digital image analysis software, v. 2.1.0. For the morphological description of the otoliths, the terminology defined by Assis (2000, 2003) and Schwarzhans (1978, 1993) was used (Fig. 2). All measurements of the otoliths were made using the IMAGEJ v. 1.49 software (Rasband 1997–2016; http://imagej.nih.gov/ij/). Otoliths used in this study are deposited in the collection of UFAL and the private collection of AP.

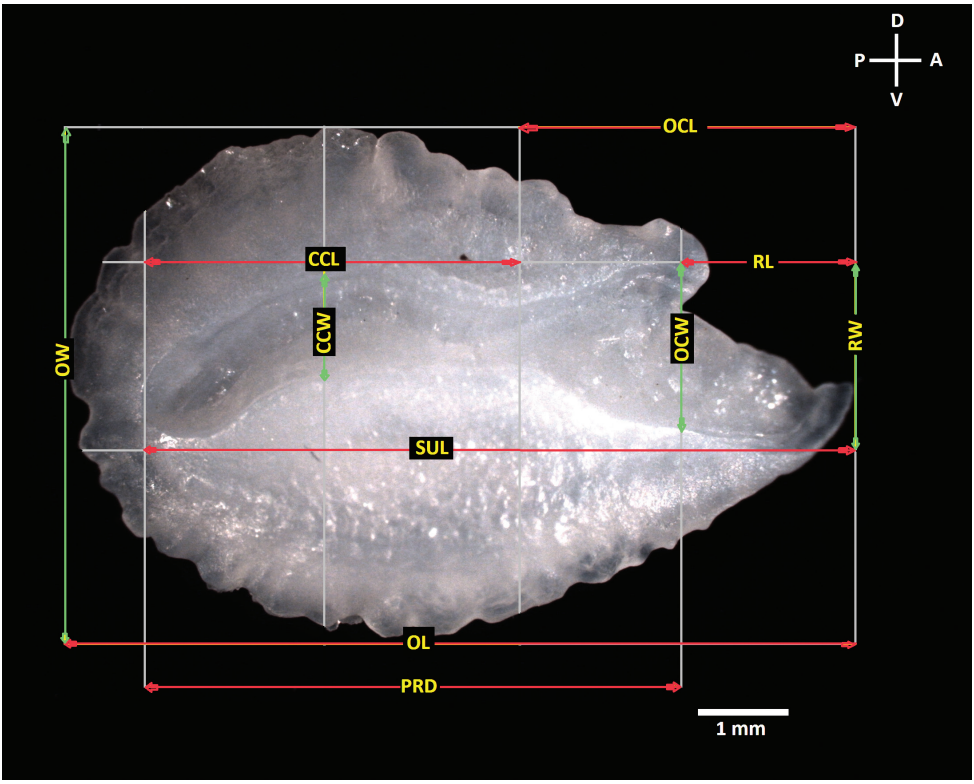

Figure 2. View lateral and internal face of sagitta otolith of *Astronotus*, illustrating measurements. Abbreviations: OL otolith length; SUL - acoustic sulcus length; OCL - ostial colliculum length; CCL - caudal colliculum length; PRD - post rostrum distance; RL - rostrum length; OW - o width; CCW - caudal colliculum width; OCW - ostial colliculum wide; RW - rostrum width.

We used the following abbreviations for standard sagitta otolith measurements and ratios: aspect ratio (**Ar**), roundness index (**Rd**), otolith width (**Ow**) morphometric index (**Ow/PRD**). In addition to the standard otolith measurement ratios we also used two new ones: colliculum width-rostrum width ratio (**CCW/RW**), proportion of the CCW of the contained in the RW and rostrum width-post-rostrum distance (**RW/PRD**), proportion of the contained in the PRD as well as standard parameters such as otolith area (**AO**), and otolith perimeter (**PO**), for the calculation of biometric and shape indexes and for the quantitative description of the otoliths (see Suppl. material 1: Table S1 for complete list and descriptions). The differences among the mean values from shape index among species were tested by analysis of variance (ANOVA-one way), using the Paleontological Statistics Software PAST v. 3.0 (Hammer et al. 2001; https://folk.uio.no/ohammer/past). In total, 12 morphometric measurements, nine meristic, and 12 otolithometric were calculated.

To test the discriminant power of biometric and shape indices of the otoliths morphometric data, a Canonical Discriminant Analysis (**CDA**) also was performed using

the Paleontological Statistics Software PAST v. 3.0. The CDA orders the groups, maximizing the multivariate variation among the groups in relation to the variance within the group, using Mahalanobis distance as a linear discriminant classifier. The classified data were attributed to the group that resulted with the least distance from Mahalanobis, and the group mean in each group was validated by the jack-knife procedure (Hammer et al. 2001).

Molecular methods

Tissue samples collected from 24 individuals (five individuals from Venezuela, seven *A. crassipinnis*, and 12 *A. ocellatus*) were used in molecular analyses. Tissues were preserved in 95% ethanol for DNA extraction and deposited in the Universidade Federal do Amazonas animal tissue collection (CTGA-UFAM). We extracted whole genomic DNA using CTAB (2% CTAB, 1.4 M NaCl, 20 mM EDTA, 100 mM Tris HCl, 1% PVP) extraction protocol plus 15 mg/mL Proteinase K. We amplified 612 bp of the cytochrome C oxidase subunit I (COI) gene via polymerase chain reaction (PCR) using the M13-tailed primer cocktails FishF2/FishR2 and VF2/VR1d (Ivanova et al. 2007) in a total of 15 µL PCR mix, which included 1.5 µL 25 mM MgCl2, 1.5 µL 10 mM dNTPs (2.5 mM each dNTP), 0.5 µL 20 mg/mL Bovine Serum Albumin (BSA), 1.5 µL 10X Taq Buffer with KCl (100 mM Tris-HCl – pH 8.8 at 25 °C – 500 mM KCl, 0.8% (v/v) Nonidet P40), 1.5 µL of primer cocktails (2 pM each), 0.5 µL of Taq DNA polymerase (1 U/µL), 1.0 µL of template DNA (50–100 ng/µL), and 7.0 µL of dd H2O. PCR cycling conditions were as follows: 94 °C (30 s), 35 cycles of 94 °C (30 s), 50 °C (35 s), and 72 °C (90 s), followed by 72 °C (5 min). Exonuclease I – Shrimp Alkaline Phosphatase (ExoSAP) was used to purify PCR products which we then used for fluorescent dye terminator sequencing using primers M13F(-21) and FishR2, following the manufacturer's recommended protocols for ABI BigDye Terminator (ThermoFisher). We precipitated the sequencing reaction products using 100% Ethanol/125 mM EDTA solution, resuspended it in Hi-Di Formamide, and resolved it on an ABI 3500XL automatic sequencer (ThermoFisher).

We combined all the COI *Astronotus* sequences obtained by Colatreli et al. (2012), with the additional 24 sequences from the present work. We also included 20 sequences obtained in the GenBank database (www.ncbi.nlm.nih.gov/Genbank), with the following accession numbers: *Astronotus crassipinnis*-JN988692, GU701855, GU701858, GU701859, GU701860, GU701861, GU701862; *Astronotus ocellatus*-MG911947, MG911948, MG911949, MH411562, MH411563, MH411564, MH411565; *Cichla ocellaris*-MZ050952, MZ051118, MZ051137, MZ051601, MZ051657, MZ051740. Sequences of *Cichla ocellaris* Bloch & Schneider, 1801 were used as outgroups for subsequent analyses. For the newly collected samples we organized and verified the nucleotide sequences using GENEIOUS 6 (Kearse et al. 2012). The forward and reverse chromatogram reads for each sample sequenced were assembled into Contigs (DNA sequences with overlapping regions, where COI fragments in both ways 5'- 3' and 3'- 5' are assembled by similarity) and verified by eye. We then

used MAFFT v. 7.07 (Katoh et al. 2002) to perform an automatic alignment using all consensus sequences, followed by a final visual verification. Sequences were also translated into putative amino acids. All new sequences generated in this study are available in GenBank under accession numbers MZ770705–MZ770728. Metadata for all the sequences used in this study are presented in Suppl. material 3: Data S1 (a spreadsheet in xls format) as a flat file following the standard Darwin core format (http://rs.tdwg.org/dwc/terms/index.htm).

Molecular and species delimitation analyses

We calculated intra and inter mean genetic distances (uncorrected p-distance, as suggested by Collins et al. (2012)) between the new *Astronotus* species proposed herein and the other two valid species using the packages ape 5.1 (Paradis et al. 2004), and spider 1.4-2 (Brown et al. 2012) of the statistical software R 4.1.1 (R Development Core Team 2011), with the pairwise deletion option set to "TRUE". Diagnostic nucleotides (Sarkar et al. 2008) for each species/lineage were also delimited using the spider function 'nuDiag'. A Neighbor-Joining tree containing all sequences is provided as Suppl. material 2: Fig. S1.

For single-locus species delimitation analyses, the total dataset was reduced to a new dataset containing unique haplotypes using the 'hapCollapse' function (available at http://github.com/legalLab/protocols-scripts) in the statistical software R. We then generated a Bayesian inference phylogeny using the software BEAST 2.6.2 (Bouckaert et al. 2019) using the following settings: nucleotide substitution model (HKY+I+G) estimated using the BEAST2 package bModelTest 1.2.1 (Bouckaert and Drummond 2017); single site model partition; strict molecular clock; coalescent constant population tree prior. We ran three independent runs with 20 million Markov chain Monte Carlo (MCMC) generations, sampling tree topologies and branch lengths every 2,000 generations, discarding the first 10% generations as burn-in. Convergence between chains was observed by checking the values of effective sample size (ESS > 200) and stationarity of the chain using the software TRACER 1.7.1 (Rambaut et al. 2018). We combined the runs, subsampled at a frequency of 6,000 generations, and burned-in the first 10% generations of each run using LogCombiner (Drummond et al. 2012) to produce a final dataset with 9,000 topologies which were used to produce a maximum credibility tree in TREEANNOTATOR (Bouckaert et al. 2019).

We used the maximum credibility tree as input for five single locus species delimitation analysis: GMYC, the Generalized Mixed Yule Coalescent model (Pons et al. 2006; Monaghan et al. 2009; Fujisawa and Barraclough 2013); bGMYC, a Bayesian implementation of GMYC (Reid and Carstens 2012); ABGD, the Automatic Barcode Gap Discovery (Puillandre et al. 2012); ASAP, Assemble Species by Automatic Partitioning (Puillandre et al. 2021); and LocMin, the local minima method which is a distance threshold optimizing and clustering method implemented in Spider 1.4-2 (Brown et al. 2012); For bGMYC, we used the package splits 1.0–19 (Fujisawa and Barraclough 2013); For ABGD, we used the online web application (https://bioinfo.mnhn.fr/abi/

public/abgd/abgdweb.html). For ASAP, we also used the online web application (https://bioinfo.mnhn.fr/abi/public/asap/asapweb.html). All analyses were carried out in the R statistical software and visualized using the package GGTREE (Yu et al. 2017).

Results

***Astronotus mikoljii* sp. nov.**
https://zoobank.org/ECF46E72-25E7-4F1A-A0FC-53581D75241E
Tables 2, 3; Figs 3–6, 8a–10, Suppl. materials 1, 2: Tables S2–S5, Fig. S1

Synonymy. *Astronotus ocellatus*. Fowler 1911: 437 (first description with specimens from Venezuela); Luengo 1963: 337 (listed); León 1966: 1127–1134 (brief note); Fernández-Yépez and Antón 1966: 83 (listed); Mago 1967: 259 (listed); Mago 1970a: 76, 78, 80, 87, 88, 92, 96 (biological data), 1970b: 20 (picture, notes), 1978: 14, 15, 17, 22 (picture, brief description); Novoa and Ramos 1978: 134–138 (note, picture); Kullander 1981: 682, 683 (morphological description of Orinoco specimens, distribution); Román 1981: 62, 136 (identification key, picture, note); Cervigón 1982: 354 (picture); Novoa et al. 1982: 312–313, fig. 62 (biological and ecological data, picture); Cervigón 1983: 118–119 (experimental aquaculture); Ginéz and Olivo 1984: 159 (note); Ginéz et al. 1984: 184 (notes); Taphorn and Lilyestrom 1984: 70, 71, 74, 75, 75, 83, 84 (ecological data); Román 1985: 33 (brief morphological description, note, picture); Kullander 1986: 68 (taxonomic status); Novoa 1986: 245 (note); Machado-Allison 1987: 30, 31, 32, 39, 42,43, 47, 48, 60, 61, 62, 94, 114 (biological and ecological data, juvenile picture); Machado-Allison et al. 1987: 136 (listed); Lasso 1988: 371, 372, 381 (list, note); Román 1988: 62 (identification key, picture); Rengifo 1989: 9–16 (note); Winemiller 1989a: 180 (ecological data), 1989b: 241 (ecological data); Novoa 1990: 396 (listed); Rodríguez and Lewis 1990: 322 (listed); Winemiller 1990: 665–672 (ecological data), 1991: 360 (ecological data); Monente 1992: 137 (note); Román 1992: 33 (picture, notes); Machado-Allison 1993: 30, 31, 39, 43, 48, 61, 94, 114 (biological and ecological data, picture); Machado-Allison and Moreno 1993: 83 (note); Royero 1993: 98 (listed); Barbarino-Duque and Taphorn 1994: 100, 101 (note, picture); Winemiller 1996: 111, 112, 129 (ecological data); Winemiller et al. 1996: 26, 38 (biological and ecological data); Rodríguez and Lewis 1997: 114 (ecological data); Fuller et al. 1999: 415 (listed); Lasso et al. 1999: 28 (listed, note); Mojica 1999: 564 (listed, note); Maldonado-Ocampo 2001; 68, 71 (listed, note): Lasso et al. 2003a: 188 (listed, note), 2003b: 244 (listed, note), 2003c: 287 (listed, brief description, note); Machado-Allison 2003: 568 (listed, note); Ajiaco-Martínez et al. 2012: 144 (listed); Herrera et al. 2012: 65 (listed); Machado-Allison et al. 2013: 305, 307, 332 (listed, note); Ortega-Lara 2016: 81 (picture, listed); Ramírez-Gil and Ajiaco-Martínez 2016: 131 (table 3: listed); DoNascimiento et al. 2017: 99 (listed, note); Winemiller et al. 2018: 5, 6 (listed, ecological data).

Astronotus cf. *ocellatus*. Lasso et al. 1999: 28 (listed); Lasso and Machado-Allison 2000: 56, 57, 154 (diagnostic features, type locality, note, picture); Lasso et al. 2003b:

Figure 3. *Astronotus mikoljii* sp. nov., preserved holotype MCNG 56677 (240.12 mm SL), Venezuela., Estado Apure, Municipio Pedro Camejo in a small stream tributary of Arauca River. Photograph: Ivan Mikolji.

244 (listed, note), 2003c: 287 (listed, taxonomic note); Lasso 2004: 377,378 (diagnostic, features, biological and ecological data); Taphorn et al. 2005: 24, 30, 32, 34 (listed, notes); Medina and Bonilla 2006: 3, 4, 6, 9 (picture, genetic data); Marcano et al. 2007: 46 (listed); Brito et al. 2011: 310 (diagnostic features, note, picture); Echeverría and Machado-Allison 2015: 81, 83 (listed), Machado-Allison et al. 2018: 442, 443, 454, 455, 483 (picture, painting, morphologic description, biological and ecological data).

Astronotus sp. Lasso et al. 2003a: 188 (ecological data); Rodríguez-Olarte et al. 2003: 205, 211 (listed ecological data); Antonio and Lasso 2004: 92, 93, 107 (diagnostic features, comparative material, note); Campo 2004: 59 (listed); Hoeinghaus et al. 2004: 88, 92 (listed, notes); Lasso et al. 2004: 148 (listed, note); López-Fernández et al. 2005: 646, 649–651 (morphological characters); Galvis et al. 2007: 272, 394 (diagnostic features, note, picture); Lasso et al. 2009a: 119 (listed, note), 2009b: 143 (listed, note), 2010: 57, 71 (listed, brief description, note); Machado-Allison et al. 2010: 223 (listed); Lasso et al. 2011a: 64 (listed, note), 2011b: 102–108 (listed, identification key); Villa-Navarro et al. 2011: 277 (listed); Machado-Allison et al. (2013): 305, 307, 332 (listed, notes); Lasso et al. 2014: 103 (note, picture); Usma et al. 2016: 117 (listed).

Type material. ***Holotype.*** MCNG 56677 (225.1 mm SL), Venezuela. Estado Apure, Pedro Camejo Municipio in a small stream (tributary of the Arauca River), 07°33'14.08"N, 67°38'44.06"W, 13 Jun 2015, Pérez A. and Alfonso R. leg. (Fig. 3; Tables 1, 2).

Paratypes. MCNG 56678 (5, 175.3–200.4 mm SL); MBUCV 35750 (1,144.4 mm SL); MHNLS 26123 (1, 140.4 mm SL); INPA-ICT 057800 (2, 112.3–143.4 mm SL); EBRG 11061 (1, 152.2 mm SL), Venezuela, Estado Apure, Municipio Pedro Camejo, small tributary stream of the Arauca River, same date and collectors as

Table 1. Comparison of morphometric data from *Astronotus mikoljii* sp. nov., *A. ocellatus* and *A. crassipinnis*. The measurements are expressed in mm; all other measurements are expressed as percentage of SL as mean (*X*); standard deviation (± SD), and range (min – max).

Morphometric variable	*A. mikoljii* sp. nov.		*A. crassipinnis*		*A. ocellatus*	
	X (± SD)	(min–max)	*X* (± SD)	(min–max)	*X* (± SD)	(min–max)
Head length (H)	36.72 ±1.85	(31.78–42.76)	35.01 ±1.25	(32.44–36.75)	33.26 ±1.65	(30.50–36.50)
Snout length (snout)	11.53 (±1.23)	(9.09–14.86)	5.36 (±0.85)	(4.12–6.97)	10.67 (±0.67)	(9.18–1.73)
Body depth (body)	46.5 (±3.43)	(39.18–53.57)	51.26 (±1.86)	(49.03–55.50)	46.19 (±3.36)	(40.38–52.29)
Orbital diameter (O)	9.06 (±1.09)	(7.25–12.35)	7.36 (±0.64)	(6.14–8.36)	7.73 (±1.18)	(6.02–11.32)
Head width (HW)	21.83 (±1.11)	(19.49–25.41)	21.53 (±1.32)	(19.65–23.78)	19.64 (±3.31)	(8.13–23.25)
Inter-orbital width (Int-Orb)	13.8 (±1.11)	(12.2–17.89)	14.19 (±1.39)	(11.49–16.78)	14.79 (±2.00)	(13.32–21.89)
Pre-orbital depth (Pre-Orb)	14.22 (±1.88)	(11.09–18.06)	10.14 (±1.13)	(8.62–13.02)	15.91 (±1.47)	(13.98–18.72)
Caudal peduncle depth	17.29 (±1.05)	(15.01–20.14)	17.1 (±0.62)	(15.65–18.22)	16.45 (±1.13)	(14.43–18.41)
Caudal peduncle length	10.32 (±2.17)	(7.41–19.79)	11.09 (±0.57)	(10.02–12.17)	12.81 (±0.74)	(11.63–14.44)
Pectoral-fin length (P1)	29.29 (±3.03)	(23.02–36.15)	30.03 (±2.33)	(24.51–34.47)	29.66 (±1.78)	(27.38–33.22)
Pelvic-fin length (P2)	23.34 (±4.45)	(16.63–34.73)	23.49 (±2.51)	(19.38–27.85)	24.22 (±4.71)	(17.21–33.97)
Last dorsal spine length	9.92 (±2.40)	(6.46–15.46)	9.72 (±1.78)	(7.24–12.59)	7.59 (±1.65)	(5.07–12.18)

Table 2. Comparison of meristic data from *Astronotus mikoljii* sp. nov., *A. ocellatus*, and *A. crassipinnis*.

Meristic variable	*A. mikoljii* sp. nov.	*A. crassipinnis*	*A. ocellatus*
	mode (min–max)	mode (min–max)	mode (min–max)
Dorsal-fin rays (D)	20 (17–21)	18 (16–24)	18 (17–21)
Anal-fin rays (A)	18 (16–20)	18 (15–21)	17 (16–20)
Longitudinal scales (E1)	38 (35–41)	35 (33–41)	33 (31–35)
Upper lateral line scales (ULL)	20 (18–21)	21 (19–22)	19 (18–22)
Lower lateral line scales (LLL)	18 (15–21)	16 (12–20)	13 (11–16)
Scales above lateral line (ALL)	7 (7–8)	7 (7–8)	6 (6–7)
Scales below lateral line (BLL)	10 (6–12)	12 (11–14)	12 (12–13)
Circumpeduncular scales (SPC)	28 (26–32)	30 (26–31)	29 (27–30)
Ceratobranchial gill rakers	10 (9–11)	9 (9–12)	11 (10–11)
Opercular scales	3 (3–5)	4 (3–5)	4 (3–5)
Cheek scales	8 (7–11)	10 (7–11)	11 (7–11)

holotype; Venezuela, ANSP 37896 (1, 124.5 mm SL). Estado Monagas, Las Piedritas Caño Uracoa, 24.9 km SW of Uracoa, 8°48'9.00"N, 62°28'25.00"W, 12 Feb 1911, Bond F. and Brown S. leg.; MHNLS 198 (5, 97.5–116.7 mm SL) Estado Apure, Achaguas, Río Apure, 7°55'35"N, 68°28'47"W, 10, Jan 1951, Fernández-Yépez A. leg.; MHNLS 3551 (2, 109.1–121.9 mm SL). Estado Anzoátegui Laguna de Mamo, 1 km south of Juasiullal, right bank of the Orinoco River, 7°25'57"N, 63°7'8"W, 22 Jan 1981, Feo G., Pérez L., Ovidio H. leg.; MHNLS 3776 (3, 98.7–115.9 mm SL) Estado Bolivar, Orinoco River, Fajardo Island Main channel, May 05, 1975, Köpke H.; MHNLS 3777 (1, 119.1 mm SL) Estado Bolivar, Orinoco River, Fajardo Island Main channel, 19 Apr 1974, Köpke H. leg.; MHNLS 4850 (1, 79.1 mm SL) Estado

Bolivar, Rio Claro Lagoon, approximately 15 Km East of San Félix, 02 Apr 1986, Pérez L. leg.; MHNLS 4914 (1, 121.7 mm SL) Estado Bolivar, Residual Lagoon, Hato Puga; approximately 25 km East of San Felix, 11 Apr 1986, Pérez L. leg.; MHNLS 4915 (1, 121.6 mm SL) Estado Bolivar, Laguna Chirere approximately 30 km west of Puerto Ordáz, 04 Apr 1986, Pérez L. leg.; MHNLS 4916 (1, 117.3 mm SL) Estado Bolivar, Laguna Río Claro approximately 15 km East of San Felix, 07 Apr 1987, Lasso C. Pérez L. leg.; MHNLS 7860 (2, 94.0–107.5 mm SL) Estado Cojedes, El Baul, 8°54'48.60"N, 68°17'17.52"W, 15 Apr 1984, B. Román leg.; MHNLS 9022 (1, 85.3 mm SL) Estado Bolivar, Caicara del Orinoco, Rio Aripao to Chaviripa River, 26 Mar 1986, B. Román leg.; MHNLS 9050 (1, 125.6 mm SL) Estado Guárico, Esteros de Camaguán, 6 May 1984, B Román leg.; MHNLS 11719 (1, 118 mm SL) Estado Apure, Caño Guaritico Hato El Frío, 7°52'35.00"N, 66°55'57.00"W, 18 Jan 1991, Lasso-Alcalá O. Lasso C. leg.; MHNLS 13094 (1, 201.5 mm SL) Estado Bolivar, Laguna Patiquín floodplain Caño Mato, tributary of Caura River, 7°9'16.00"N, 65°11'57.00"W, 23 Mar 1998, Vispo, C. leg.; MHNLS 13812 (2, 108.7–119.3 mm SL) Estado Delta Amacuro, Orinoco River Delta, Caño Ibaruma, Serranía de Imataca, 8°1'0.00"N, 60°47'0.00"W, 24 Jan 2003, Ponte V. leg.; MCNG 3608 (1, 148.9 mm SL) Estado Apure, Modules of UNELLEZ area adjacent to south of dike Caño Caicara, 7°25'30.00"N, 69°32'20.00"W, 2 Jun 1981, Donald Taphorn leg.; MCNG 2522 (1, 106.6 mm SL) Estado Apure, 3.4 km south of Bruzual bridge west side of road, 8°01'20.00"N, 69°20'50.00"W, 17 Nov 1980, Donald Taphorn leg.; MCNG 1832 (1, 118.5 mm SL) Estado Apure, 3.4 km south of Bruzual bridge 8°01'20.00"N, 69°20'50.00"W, 15 Nov 1980, Donald Taphorn leg.; MCNG 5993 (1, 101.3 mm SL) Estado Apure, Hato el Frio, 30 Sep 1979, Craig Lilyestrom leg.; MCNG 4994 (3, 193.1–210.1 mm SL) Estado Apure, Modules Fernando Corrales (UNELLEZ) dike east, 7°29'30.00"N, 69°31'W, 27 Nov 1981, Donald Taphorn leg.; MCNG 32543 (1, 101.6 mm SL) Estado Barinas, culvert 10 km NW of Libertad on road to Barinas 8°20'3.00"N, 69°43'41.00"W, 25 Jan 1995, John Armbruster leg.; MCNG 1675 (4, 197.4–240.7 mm SL) Estado Barinas, borrow pit at end of runway at Arismendi, 8°29'50.00"N, 68°21'20.00"W, 14 Sep 1980, Donald Taphorn leg.; MCNG 32596 (1, 161.9 mm SL) Estado Barinas, Río Caipe, to the east of town La Luz, 8°24'31.00"N, 69°48'19.00"W, 26 Jan 1995, John Armbruster leg.; MCNG 26930 (2, 112.50–104.90 mm SL) Estado Cojedes, San Geronimo in Hato Santa Clara, 02 Nov 1991, Manuel Gonzalez Fernandez leg.; MCNG 789 (2, 185.6–193.4 mm SL) Estado Delta Amacuro, Caño Paloma Orinoco River Delta, 21 Feb 1978, John Lundberg leg.; MCNG 32033 (1, 195 mm SL) Estado Guárico, P.N. Aguaro-Guariquito, Río Aguaro at El Paso to Médano Gómez, 7°50'27.00"N, 66°30'23.00"W, 01 Nov 1995, Donald Taphorn leg.; MCNG 32006 (2, 152.2 mm SL) Estado Guárico, P.N. Aguaro-Guariquito, Río Aguaro in Laguna Begonia, 7°52'6.00"N, 66°30'36.00"W, 01 Nov 1995, Donald Taphorn leg.; MCNG 25187 (1, 183.3 mm SL) Estado Guárico, Calabozo highway, Camaguán, 14 Jan 1982, Otto Castillo leg.; MCNG 32739 (1, 180.1 mm SL) Estado Guárico, P.N. Aguaro-Guariquito, Laguna Médano Gómez, 06 Aug 1995, Aniello Barbarino-Duque leg.; MCNG 11580 (2, 101.8–122.3 mm

SL) Estado Guárico, borrow pit in savannah 2.3 km from San Fernando de Apure between km 305 and 306, 7°55'20.00"N, 67°28'20.00"W, 22 Mar 1981, Donald Taphorn leg.; MCNG 26815 (3, 90.5–109.0 mm SL) Estado Portuguesa, Caño Maraca, 8°53'11.00"N, 69°29'18.00"W, 13 Jan 1992, Larry Page, Pat Ceas, Brooks Burr, Steve Walsh, Chris Taylor, Leo Nico, Kirk Winemiller leg.; MCNG 15461 (1, 127.4 mm SL) Estado Portuguesa, Brazo del Caño Maraca at ranch of Darío Urriola, 26 Oct 1984, Kirk Winemiller leg.; MCNG 9097 (3, 112.3–138.1 mm SL) Estado Portuguesa, borrow pit N of Moritas east of Guanare-Las Moritas road, 8°45'30.00"N, 69°34'30.00"W, 03 Jan 1979, Donald Taphorn leg.; MCNG 5740 (1, 110.6 mm SL) Estado Portuguesa, Caño Maraca at bridge via Guanarito, Km 60, 8°49'50.00"N, 69°20'20.00"W, 28 Aug 1980, Donald Taphorn leg.; MCNG 29650 (1, 112.3 mm SL) Estado Portuguesa, Caño San José between Guanarito and La Capilla, 8°41'9.00"N, 68°56'49.00"W, 01 Mar 1994, John Armbruster leg.; Colombia • MHNLS 23575 (1, 114.7 mm SL), Departamento de Vichada, Caño drainage of Laguna Cajaro right bank of the Guaviare River, 3°58'14.00"N, 67°59'8.00"W, 16 Feb 2008; C. Lasso M. Sierra. M. Patiño F. Villa. A. Ortega. leg.; MHNLS 24053 (1, 218 mm SL), Departamento de Vichada, Caño Vitina right bank affluent, Rio Inírida upstream from Caranacoa beach, 3°44'30.00"N, 67°56'10.00"W, 21 Feb 2008, C. Lasso. M. Sierra M. Patiño F. Villa A. Ortega. leg.; MHNLS 24054 (1, 227.5 mm SL), Departamento de Vichada, Caño Vitina tributary right bank Río Inírida, upstream from Playa de Caranacoa, 3°44'30.00"N, 67°56'10.00"W, 21 Feb 2008, C. Lasso M. Sierra M. Patiño F. Villa; A. Ortega leg.; MHNLS 24059 (1, 205.5 mm SL), Departamento de Vichada, Peluame Lagoon, left Bank Guaviare River, near Guaviare-Inírida Confluence, 3°57'51.00"N, 67°55'W, 17 Feb 2008, C. Lasso M. Sierra M. Patiño F. Villa A. Ortega; S. Usma leg.; MHNLS 24061 (1, 211.5 mm SL), Departamento de Vichada, Laguna Bolívar, left bank, flooded area, Orinoco River, between Guanayana and Amanaven farms, 4°7'N, 67°45'W, 26 Feb 2008, C. Lasso M. Sierra M. Patiño F. Villa leg.; MHNLS 24064 (1, 226 mm SL), Departamento de Vichada, Caño Vitina, tributary right bank Río Inírida, upstream of Playa de Caranacoa, 3°44'30.00"N, 67°56'10.00"W, 21 Feb 2008, C. Lasso M. Sierra M. Patiño F. Villa; A. Ortega leg.

Comparative material. *Astronotus ocellatus*. NPA-ICT 026472 (1) Brazil, Amazonas, Catalão, rio Solimões Bacia do Solimões, 3°9'34.00"S, 59°54'44.00"W, 20 Dec 2002; INPA-ICT 050911 (1) Brazil, Amazonas, rio Solimões, Ilha da Paciência, 3°20'5.60"S, 60°12'11.30"W, Manaquiri, 18 Dec 2011; J. Santos, R. Orta, F. Pena leg.; INPA-ICT 050912 (1) Brazil, Amazonas, rio Solimões, Ilha da Paciência, 3°20'5.60"S, 60°12'11.30"W, Manaquiri, 18 Dec 2011; J. Santos, R. Ota, F. Pena leg.; INPA-ICT 033076 (1) Brazil, Tabatinga, rio Solimões, 3°57'32.00"S, 69°20'19.00"W, town of Palmares, 02 Sept 2003; Jansen Zuanon leg.; INPA-ICT 033913 (1) Brazil, Amazonas, São Sebastião de Uatumã, rio Uatumã, 30 Oct 2009; R. Leitão, R. Lazzarotto leg.; INPA-ICT 033889 (1) Brazil, Amazonas, rio Nhamunda, 2°13'51.00"S, 56°46'23.00"W, município Nhamunda, 21 Sept 2009; R. Leitão, R. Lazzarotto leg.; INPA 050452 (2) Brazil, Amazonas, rio Preto da Eva, 2°44'38.10"S, 59°28'38.60"W, highway AM-010, km 110, 20 Aug 2014; INPA 22331 (1) Brazil, Amazonas, Lago do Boto, RDS

do lago Piranha, Manacapuru, 30 Jan 2003; Ivanildo; INPA-ICT 033437 (2) Brazil, Amazonas, Lago Ressaca Grande, rio Solimões, 2°28'26.00"S, 66°9'17.00"W, Fonte Boa, 08 Sept 2003; Jansen Zuanon leg.; INPA 17486 (1) Brazil, Amazonas, pool in Lago Secado, rio Purus, Santa Lucia, 03 Jun 2001; Lucia Rapp-Daniel leg.; INPA 17364 (3) Brazil, Amazonas, Lago Campinas, rio Purus, 05 Jun 2001; Lucia Rapp Py-Daniel leg; INPA-ICT 029312 (49) Brazil, Amazonas, RDS Uacari, stream near community of Pupunha; 5°35'47.00"S, 67°47'13.00"W; 26 Nov 2007; Martins, A.R. leg.; INPA-ICT 007143 (1) Brazil, Para, Rio Cupari, near mouth of Tapajon River, 3°44'31.00"S, 55°23'25.00"W, 27 Oct 1991; Zuanon, J.A. leg.; INPA-ICT 007170 (1) Brazil, Para, Rio Cupari, near mouth of Tapajos River; 27 Oct 1991; Zuanon, J.A. leg; INPA-ICT 007333 (1) Brazil, Tocantins, Rio Tocantins, Icangui; Brazil, Pará, Tucuruí, 3°49'49.80"S, 49°38'21.84"W, 28 Jun 1980; Equipe de Ictiologia do INPA leg.; INPA-ICT 020454 (1) Brazil, Tocantins, Lago das Ariranhas, rio Araguaia; Brazil, Tocantins, Caseara, 9°14'5.28"S, 49°57'59.76"W, 11 Nov 2000; Equipe de Ictiologia do INPA leg.; INPA-ICT 020663, (2) Brazil, Tocantins, Rio Tocantins, Jabutizão, 7°43'55.56"S, 49°28'31.80"W, 10 May 2000; Santos, G.M. leg; INPA-ICT 040585 (1) Brazil, Pará, Mercado do Porto, collected from stream tributary to Xingu River, near Vitória do Xingu, 2°52'51.00"S, 52°0'45.00"W, 23 Sept 2013; Sabaj, M. H. leg; INPA-ICT 043339 (6) Brazil, Pará, Xingu River, specimens bought in market, near Tucuri stream around Vitória do Xingu; 07 Mar 2014; Martins, A.R. leg.

Astronotus crassipinnis. INPA-ICT 021697 (1) Brazil, Rondônia, rio Novo, Guaporé, 11°29'29.00"S, 64°34'34.00"W, 27 Jul 2003; Torrente Vilara; INPA-ICT 038549 (2) Lago do Bodo, Bom Jardim, Porto Velho (Brazil, Rondônia), 8°32'31.00"S, 63°37'26.00"W, 12 Ago 2011, L. Costas, F. Viera, leg.; INPA-ICT 049921 (3) Brazil, Rondônia, Rio Guaporé, Surpresa, 10°06'11"S, 65°38'44"W, 21 Set 1985; G.M. dos Santos leg.; INPA-ICT 049922 (2) Brazil, Rondônia, mouth of Guaporé River, near Surpresa, 11°19'44"S, 64°60'11"W, 16 Jun 1984; Costa Marques, G.M. dos Santos leg.; INPA-ICT 049923 (1) Brazil, Rondônia, Rio Pacaás-Novos, blackwater flooded forest ca. 15 km upstream from mouth of Pacaás Novos River, Guajará-Mirim, 02 Apr1987, G.M. dos Santos leg.

Diagnosis. The new species is distinguished from congeners by the following combination of characters: two or three supraneural bones (Fig. 4) (vs. two); absence of the spinous process (hypurapophysis) on the anterosuperior border of the parahypural bone (hypural complex) in *Astronotus mikoljii* sp. nov. (vs. present in *A. ocellatus* and *A. crassipinnis*) (Fig. 5). The sagitta otolith in *A. mikoljii* sp. nov. is oval, with strongly crenulated ventral and dorsal margins (vs. elliptical and smooth-lobed margins in *A. crassipinnis*, and elliptical and smooth-dentate margins *A. ocellatus*); the rostrum is projected with an elongated process, in *A. mikoljii* sp. nov. (vs. rostrum process short in *A. crassipinnis* and *A. ocellatus*); the posterior region of the sagitta otolith is rounded in *A. mikoljii* sp. nov. (vs. straight or flat in *A. crassipinnis* and *A. ocellatus*) (Fig. 6). The aspect ratio of sagitta otoliths in *A. mikoljii* sp. nov. (AR = 0.665) is higher than that of *A. ocellatus* (AR = 0.606), and *A. crassipinnis* (AR = 0.585), and the differences are statistically significant at $P < 0.05$. The roundness index was highest in *A. mikoljii* sp. nov. (Rd = 0.597) vs.

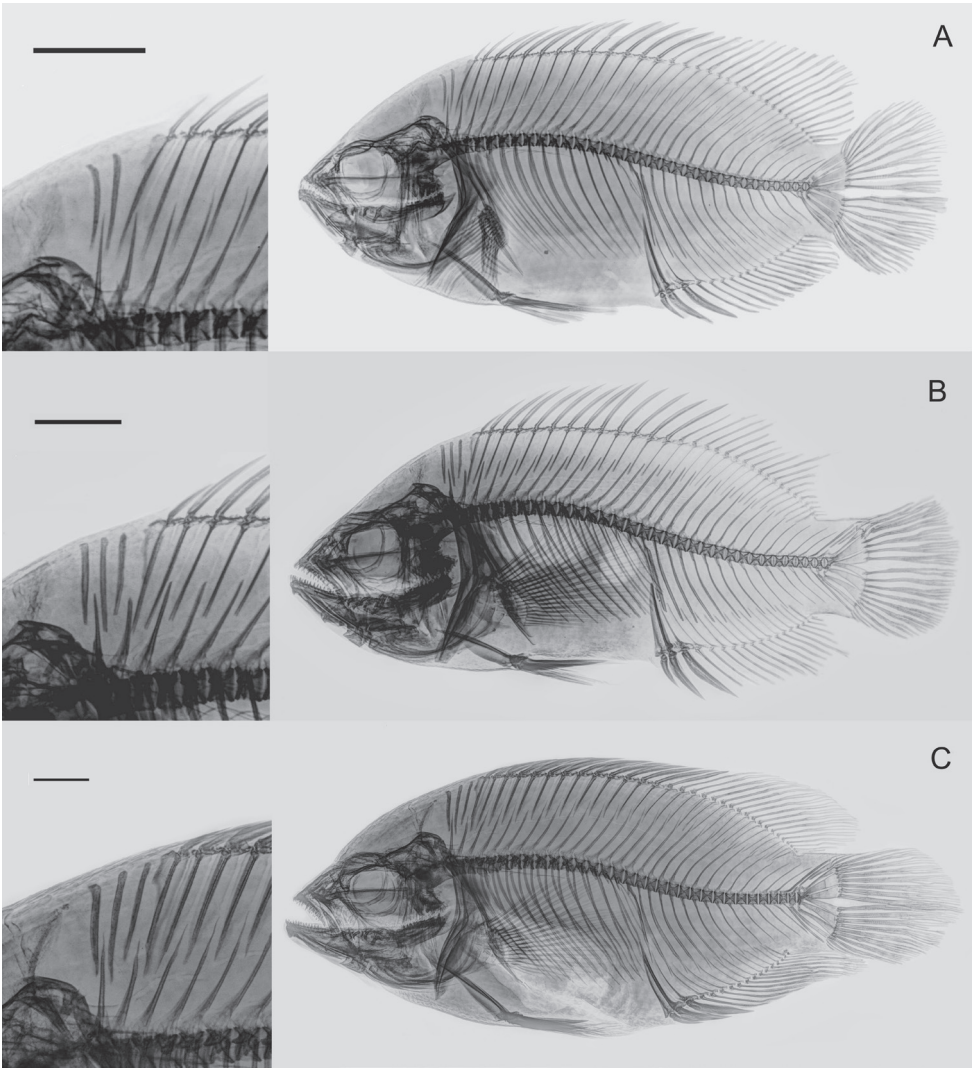

Figure 4. Radiographs of paratypes of *Astronotus mikoljii* sp. nov. and details of the supraneural bones **A** MHNLS 198 (116.7 mm SL) **B** MHNLS 26123 (140.4 mm SL) **C** MHNLS 24054 (227.5 mm SL). Scale bars: 10 mm.

A. ocellatus (Rd = 0.545) and *A. crassipinnis* (Rd = 0.543) ($P < 0.05$). Also the morphometric index showed higher values in *A. mikoljii* sp. nov. compared to *A. ocellatus* (0.837 vs. 0.767) and *A. crassipinnis* (0.735) (Suppl. material 1: Table S2). The new species also is distinguished from congeners by the following combination of morphometric characters: the mean head length of *A. mikoljii* sp. nov. (36.72% SL) is longer than that of *A. crassipinnis* (35.01% SL), and also *A. ocellatus* (33.26% SL); the mean diameter of the orbit of *A. mikoljii* sp. nov. (9.06% SL) is greater than that of *A. ocellatus* (7.36%SL) and that of *A. crassipinnis* (7.73% SL); the mean pre-orbital depth of *A. mikoljii* sp. nov. (14.22% SL) is greater than that of *A. crassipinnis* (10.14% SL) but less than that of

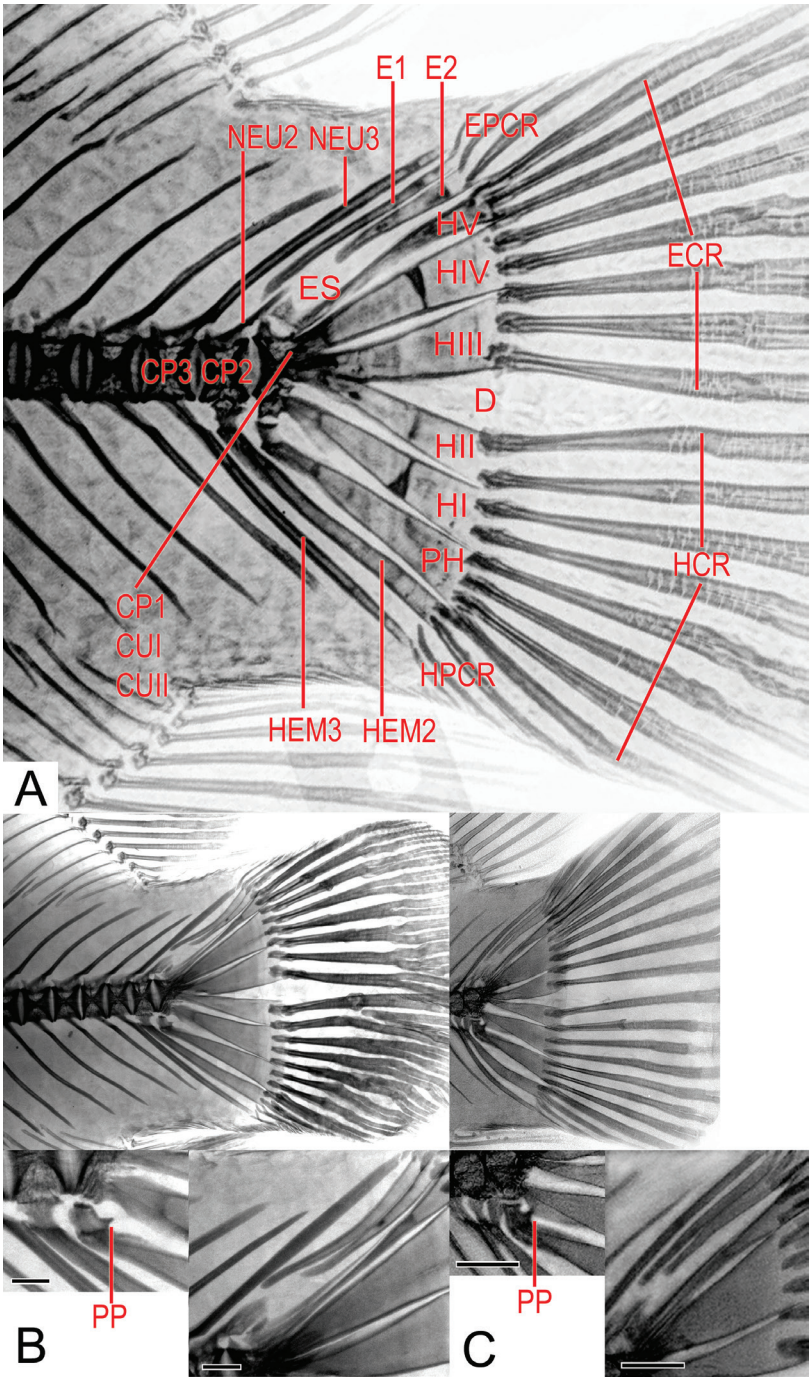

Figure 5. Radiographs of the caudal skeleton in *Astronotus* species showing magnified details **A** *A. mikoljii* sp. nov. (MHNLS 24059, 205.5 mm SL) **B** *A. crassipinnis* INPA-ICT 33889 (204.3 mm SL) **C** *A. ocellatus* USNM 284442 (79.6 mm SL). Abbreviations: hypurapophysis (PP) of parahypural bone (PH), epurals (E1 – E2) and neural spine (NEU2, diastema (D), preural centrum (CP), epaxial caudal rays (ECR), hypaxial caudal rays (HCR), epaxial procurrent caudal rays (EPCR) hypaxial procurrent caudal rays (HPCR). Scale bars: 2 mm.

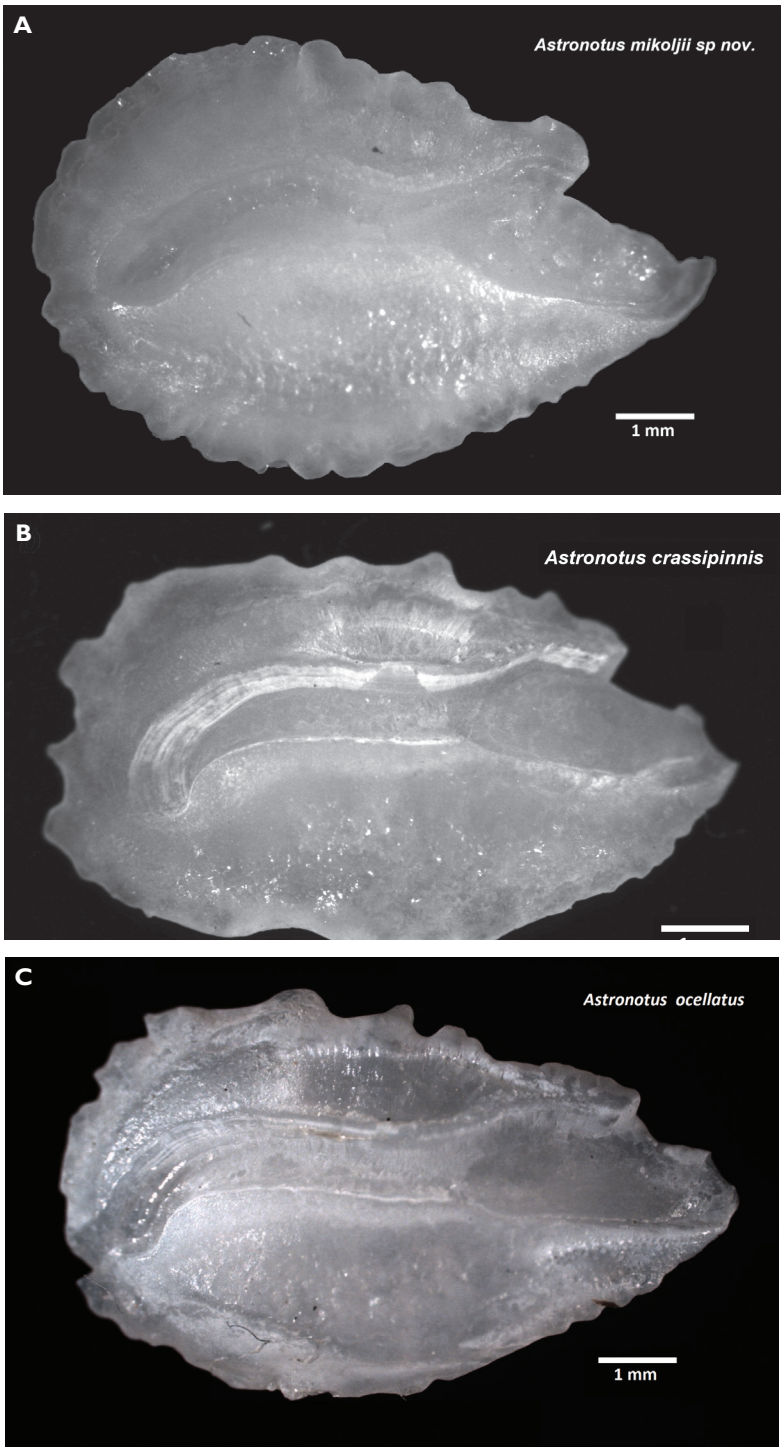

Figure 6. Left sagitta otoliths (medial view) of **A** *Astronotus mikoljii* sp. nov. **B** *A. crassipinnis* **C** *A. ocellatus.* Scale bars: 1 mm.

A. ocellatus (15.91% SL); the mean snout length of *A. mikoljii* sp. nov. (11.53% SL) is longer than that of *A. crassipinnis* (5.36% SL), and *A. ocellatus* (10.67% SL) (Tables 1, 2).

Description. *Morphology.* Morphometric and meristic data are presented in Table 3. Body moderately oval; laterally compressed, widest at region of anterior flank and posterior part of head; Dorsal-fin base contour sloping from about middle of spinous portion. Caudal peduncle edges horizontal; ventral sometimes longer than dorsal. Head and snout short; orbit slightly below forehead contour, entirely in upper and anterior halves of head. Interorbital wide, slightly convex. Tip of exposed maxilla extending to anterior edge of orbit; lower jaw articulation below middle of orbit. Both lip folds interrupted, junction of upper and lower lips African type. Opercula and pectoral girdle bones smooth. Interorbital convex; pre-pelvic contour straight; greatest body depth at pelvic-fin bases.

Table 3. Morphometric and meristic data (mm) of holotype and paratypes of *Astronotus mikoljii* sp. nov., with specimen number (n); mean (*X*); standard deviation (SD); variation coefficient (CV); minimum value (Min); maximum value (Max).

Morphometric variable (mm)	**Holotype**	**Paratypes (*n* = 65)**				
		X	**SD**	**CV**	**Min**	**Max**
Standard length	240.12	134.61	42.42	31.52	79.11	240.12
Head length	76.50	48.91	13.75	28.12	31.07	81.70
Snout length	21.90	15.47	4.67	30.20	9.72	29.10
Body depth	110.40	64.50	19.86	30.79	35.58	110.40
Orbital diameter	17.80	11.90	2.56	21.56	9.40	18.43
Head width	47.80	29.76	9.18	30.88	17.07	49.54
Inter-orbital width	30.90	18.94	6.63	35.04	10.98	37.47
Pre-orbital depth	26.70	18.85	6.33	33.62	12.44	39.22
Caudal peduncle depth	36.30	23.35	7.15	30.62	13.27	41.54
Caudal peduncle length	26.40	13.95	5.57	39.94	6.32	26.40
Pectoral-fin length	57.20	39.74	11.36	28.59	25.22	69.51
Pelvic-fin length	46.90	31.82	8.63	27.13	18.90	51.29
Length of last dorsal spine	15.90	13.35	4.520	33.84	8.30	28.40
Meristic variable	**Holotype**	**Paratypes (*n* = 65)**				
				Min	**Max**	**mode**
Dorsal-fin rays (D)	XIII,18			XII,18	XIV, 20	XIII, 19
Anal-fin rays (A)	III,18			III,14	III, 20	III, 16
Pectoral-fin rays (P1)	15			14	17	15
Pelvic-fin rays (P2)	I,5			I,5	I,5	I,5
Caudal-fin rays (C)	20			19	24	22
Longitudinal scales (E1)	37			35	42	38
Upper lateral line scales (ULL)	20			18	21	20
Lower lateral line scales (LLL)	17			16	21	18
Scales above lateral line (ALL)	7			7	8	7
Scales below lateral line (BLL)	9			6	12	10
Circumpendicular scales (SPC)	28			26	32	28
Opercular scales	4			3	5	3
Cheek scales cheek	9			7	9	8
Ceratobranchial gill rakers	10			8	11	10
Pre-dorsal midline scales	16			14	18	16
Tubed scales in lower lobe caudal	5			1	8	6

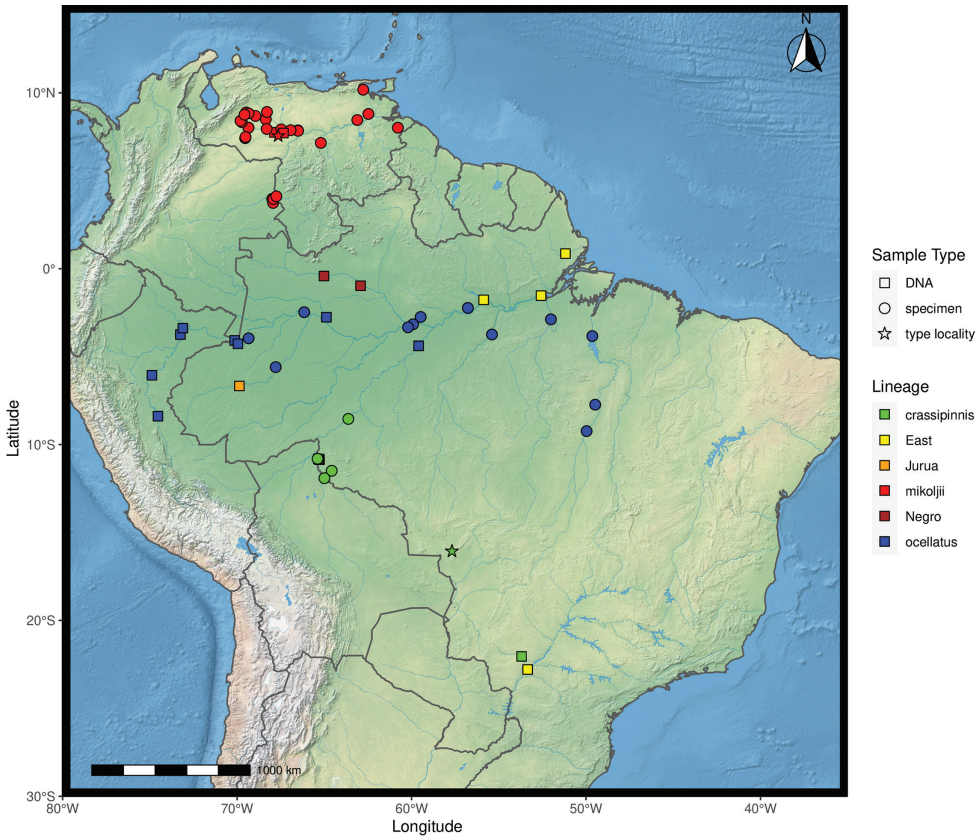

Figure 7. Map showing all the sites sampled in this study. The circles represent sampling localities based on specimen records used for morphological analyses, the squares represent sampling localities of the genetic material analyses, and the stars represent the type locality of each species. The colors represent the consensus of the species delimitation methods. *Astronotus mikoljii* sp. nov. (red), *A. crassipinnis* (green), *A. ocellatus* (blue), *Astronotus* sp. "East" (yellow), *Astronotus* sp. "Jurua" (orange), and *Astronotus* sp. "Negro" (brown).

Scales. Pre-dorsal midline scales irregularly arranged, ca. 14–18 along midline; posterior pre-pelvic scales about half size of flank scales, slightly smaller anteriorly, in ca. seven horizontal series. Scales around caudal peduncle 26–32; lower lobe of caudal fin with 1–8 tubed lateral-line scales, from base to middle usually with gaps between them, and from half to edge of fin continued by pored scales). Anterior 1/3 to 1/2 of the cheek naked, remainder with cycloid scales; cheek scale rows 3 (n = 65; range 7–9). Operculum covered with eight cycloid scales (n = 65; range 3–5); opercula scales in ca. four vertical series, sub-opercular scales in two or three series: inter-operculum with one or two scales close to pre-opercular corner and six or seven scales in principal series. Pre-operculum naked. Soft unpaired fins covered by dense scale layer. Spinous dorsal fin bordered by posteriorly progressively wider scale layer with straight margin. This basal scale layer continued onto basal 1/3 of soft dorsal fin but inter-radial scales

distal to it widen scaly layer to basal 1/2 of fin medially. Pectoral and pelvic fins naked. Inter-pelvic squamation extended laterally to cover bases. Caudal fin completely scaled save for narrow zone along hind margin; basal scales ctenoid; inter-radial scales cycloid in three or four series between rays.

Fins. One continuous dorsal fin, with anterior portion of hard rays (spines) and posterior portion with soft rays. First dorsal-fin spine inserted slightly in advance of vertical from hind margin of operculum; relative length of spines increasing to 4th then subequal to last few which are longer, twice length of first or slightly longer. Soft part of dorsal fin with rounded tip, reaching to not quite middle of caudal fin or to 3/4 of caudal fin. D. XII.18 (3), XII. 19 (4), XII. 20 (5), XIII. 17 (5), XIII. 18 (8), XIII. 19 (14), XIII. 20 (12), XIII. 21 (5), XIV. 18 (4), XIV. 19 (5), XIV. 20 (3); Anal-fin origin opposite soft dorsal-fin origin; soft portion similar to soft dorsal fin, but not reaching beyond middle of caudal fin. A. III. 14 (5), III. 15(10), III. 16 (15), III. 17 (10), III. 18 (14), III. 19 (3), III. 20 (1). Pectoral-fin with blunt dorsal tip, 4th ray longest, hind margin truncate or slightly curved; sometimes reaching to first anal-fin spine P1. 15 (n = 65; range 14–17). Pelvic-fin spine inserted below pectoral axilla; fin pointed, with outer branch of first ray longest, reaching to first anal-fin spine to 1/3 of soft-anal fin base, inner rays gradually shorter P2, 1.5 (1.5). Caudal fin with hind edge rounded, with 22 (n = 65; range 19–24), total rays (Table 3).

Gills. First gill arch with rudimentary denticles exposed laterally, two or three on epibranchial, one in angle, and 8–11 on ceratobranchial. Tiny gill-rakers present externally on medial side short, compressed and heavily denticulate (Table 3).

Teeth. Lower jaw with two teeth rows on each side (external and internal). External tooth row in both jaws extends from tip to end of each bone (dentary and maxilla). Teeth in outer series stout, conical, pointed, little recurved; anterior three or four in each jaw half as strong as rest; outer series to near end of upper jaw (20) and of corresponding length in lower jaw; inner band of very small weak teeth, less than 0.4 mm long, only anteriorly in jaws.

Otoliths. Sagitta otoliths oval with crenulate posterior, dorsal, ventral margins; Ar was greater than 0.66, otolith Rd 0.59 (Suppl. material 1: Table S2). Anterior region (rostrum) projected with elongated process and rounded posterior region. Anti-rostrum short and rounded, moderately broad ostium incisure with notch. Acoustic canal (sulcus acoustics) heterosulcoid, ostial, medial; ostium rectangular and shorter than caudal colliculum, which is tubular, closed, and strongly curved along its posterior margin.

Dorsal and vertebral skeleton. Pre-caudal vertebrae 15, caudal vertebrae 17, and total vertebrae 32. Range in vertebral counts (pre-caudal, caudal, and total) is wide (14–16, 15–18, 30–33). Two or three supraneural bones present, first anterior to neural spine of first pre-caudal vertebrae, second and third, between that spine and second neural spine of second pre-caudal vertebrae (Fig. 4, Suppl. material 1: Table S3).

Caudal skeleton. Includes hypural complex and 20–24 caudal rays. This complex has five vertebral elements, CP1, CUI, and CUII or urostyle (all fused), CP2 and CP3. This last element has HEM3 that can support one or two HPCR and a NEU3 that can be free or support up to two EPCR. The CP2 is articulated with HEM2, which

can be free or articulated with up to two HPCR or one or two HC = R. Likewise, CP2 on its upper side almost converges with bone E1 that is free or articulated with EPCR or ECR. The complex CP1 + CUI + CUII, is articulated on its lower side with four elements, PH and HI, which are articulated with two to four HCR each, the HII, which is articulated with one or two HCR and the HIII, which can support two or three ECR. Complex CP1 + CUI + CUII articulated on its anterior side with bone HIV, which in turn can support two to five ECR. On its upper side this complex is articulated with the ES bone that is fused with HV and can support between one to three ECR. Above HV, and always separated from Complex CP1 + CUI + CUII, E2 is positioned, which can be found without rays or an EPCR or ECR. Next and always separated from the E2, E1 is found which along its upper side only supports an EPCR and on the lower edge may be articulated and even fused with NEU2. Finally, NEU3 is observed, originating along the upper edge of CP3, which can be free or articulated with up to two EPCR (Fig. 5, Suppl. material 1: Table S4).

Color in alcohol. The background color varies from dark yellow to dark brown; chest color varies from pale to dark brown; abdomen whitish. Operculum and cheek pale brown. Snout and forehead chestnut. Sides of the body with irregular vertical bars (chestnut or pale brown) sometimes difficult to see, of different widths, individually variable. Sometimes with pattern of 1–3 pale and dark vertical bars, normally with pale, lambda-shaped bars; central part of these bars is usually divided at level of abdomen, forming lambda (λ) figure with bases extending to pelvic fins. Dorsal and anal fins pale or dark brown with paler edges on both. Caudal fin dark brown, darker on base, always with black ocellus surrounded by narrow white or grey ring, placed in superior part of caudal-fin base, and marginally extending onto caudal peduncle. Pectoral and pelvic fins hyaline. Dorsal fin without rings or ocelli (Fig. 3).

Color in life. Sexual dimorphism not observed. Ventrum pale grey, chest dark grey, abdomen whitish, operculum and cheek grey to brown, snout and forehead chestnut, underside of head dark grey with greyish or greenish tinge over chestnut. Sides of body with barely visible irregular vertical bars (chestnut or dark grey) of different widths and patterns, which may vary from one individual to another. Wide vertical bar of dark brown color crosses central part of body and reaches spinous portion of anal fin. Central part of said bar usually divided at level of abdomen, forming lambda (λ) shape with bases extending to pelvic fins. Posterior side of the body with abundant iridescent orange spots that can appear longitudinally. Dorsal and anal fins dark brown with paler edges. Caudal fin dark grey, darker on base. Always with black ocellus surrounded by orange or yellow ring that reaches center of lateral line of caudal fin and extends onto caudal peduncle. Pectoral fins hyaline, dorsal and pelvic fins without spots or ocelli (Fig. 8a).

Molecular analysis. We amplified 612 bp of the COI gene for the 24 *Astronotus* specimens used for genetic analyses. The addition of sequence data (58 sequences) of Colatreli et al. (2012) and the sequences obtained in GenBank (20 sequences) increased this dataset to 102 specimens. This alignment was then reduced to a total of 22 unique haplotypes of *Astronotus* plus two haplotypes of *Cichla ocellaris* as outgroups. Sequence length varied from 468 to 664 bp, with a mean sequence length of 626 bp;

Figure 8. *Astronotus mikoljii* sp. nov. **A** live coloration of specimens collected with holotype **B** Natural shallow pond and type locality in floodplain of Arauca River Venezuela. Photographs: Ivan Mikolji.

23 sites were parsimony-informative. No indels were observed. No internal stop codons were found. All *Astronotus* species (*A. ocellatus*, *A. crassipinnis*, and *A. mikoljii* sp. nov.) and additional suggested distinct lineages (*Astronotus* sp. "Jurua", *Astronotus* sp. "East", and *Astronotus* sp. "Negro") shows reciprocal monophyly in the maximum credibility tree, with high posterior probability support (≥ 0.95) (Fig. 9).

All five single-locus species delimitation methods delimited *Astronotus mikoljii* sp. nov. as a distinct lineage and, overall, the only discrepancy between the methods occurred in the method bGMYC, which identified *A. crassipinnis* and *Astronotus* sp. "East" as a single lineage. The maximum intraspecific distance within *A. mikoljii* sp. nov. was

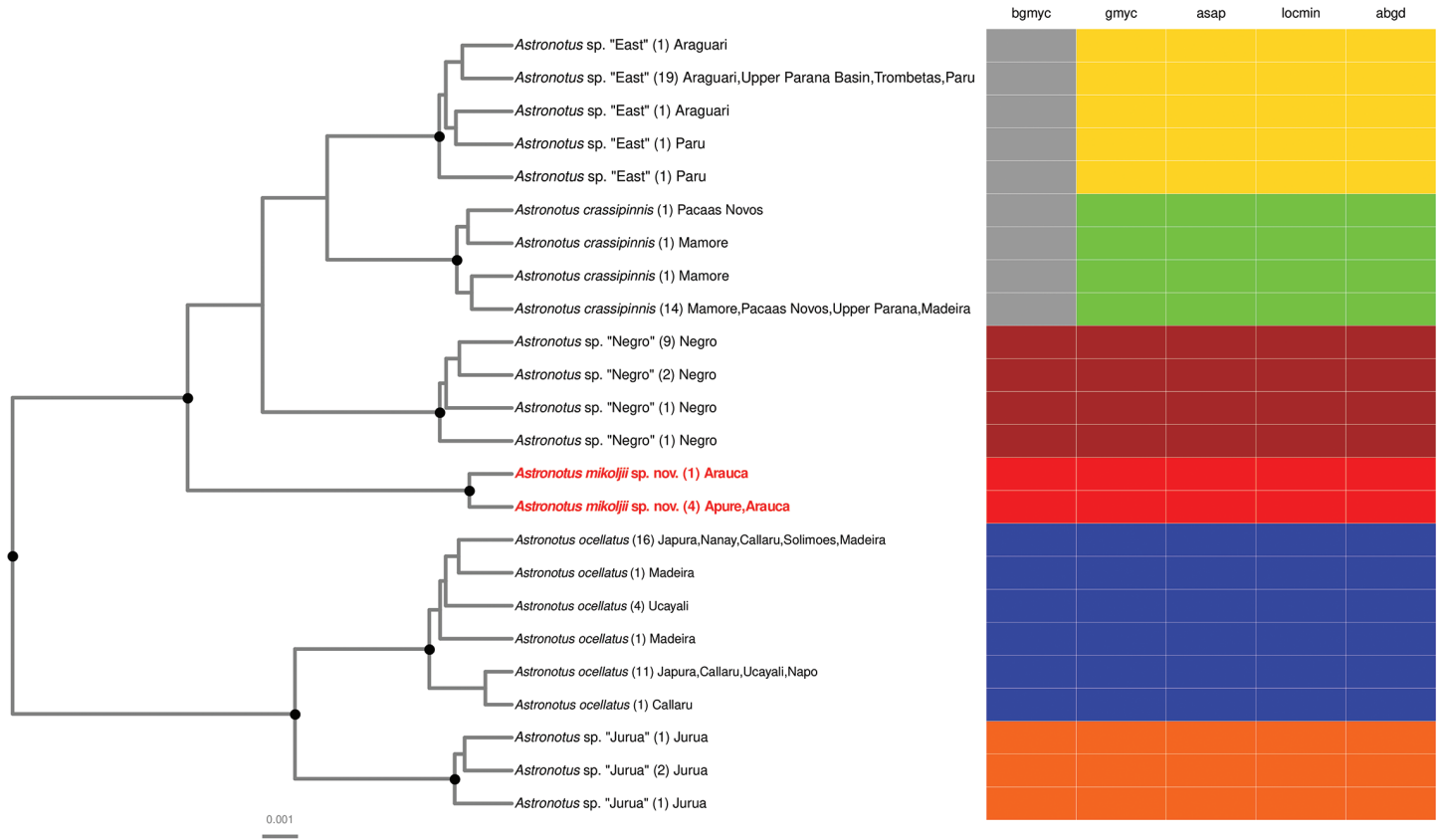

Figure 9. Maximum clade credibility tree from 9,000 posterior trees generated using BEAST 2.6. Dataset comprised 22 unique haplotypes (from a total of 102) of *Astronotus* COI sequences. Bayesian posterior probabilities above 0.95 are shown as dark nodes. Species delimitations are shown by method as colored boxes. The number of collapsed individuals is indicated in parentheses and outside of it the locations where they were sampled. The scientific name of the new species is red. The figure was created in R 4.1.1 using the package 'ggtree' and the final graphic in Inkscape.

Table 4. Max intra/inter-specific distances, Nearest Neighbor, and diagnostic nucleotides between *Astronotus* delimited lineages and species.

Species/Lineage	max_ intra (%)	min_ inter (%)	Nearest Neighbor	Diagnostic nucleotides									
				89	272	395	447	512	539	578	596	662	total
***A. mikoljii* sp. nov.**	0.163	0.98	***Astronotus* sp. "Negro"**	g	**T**	**A**	c	**G**	a	g	c	t	3
A. crassipinnis	0.388	0.904	***Astronotus* sp. "East"**	g	c	g	c	a	**G**	g	**A**	**C**	3
A. ocellatus	0.546	0.753	***Astronotus* sp. "Jurua"**	g	c	g	**T**	a	a	g	c	t	1
***Astronotus* sp. "East"**	0.301	0.753	***A. crassipinnis*, *Astronotus* sp. "Negro"**	g	c	g	c	a	a	**A**	c	t	1
***Astronotus* sp. "Jurua"**	0.151	0.753	***A. ocellatus***	g	c	g	c	a	a	g	c	t	0
***Astronotus* sp. "Negro"**	0.301	0.753	***Astronotus* sp. "East"**	**A**	c	g	c	a	a	g	c	t	1

Table 5. Mean inter-specific distances between *Astronotus* delimited lineages and species.

Mean_inter (%)	*A. mikoljii* sp. nov.	*A. crassipinnis*	*A. ocellatus*	*Astronotus* sp. "East"	*Astronotus* sp. "Jurua"	*Astronotus* sp. "Negro"
***A. mikoljii* sp. nov.**	-	2.15	1.75	1.36	2.09	1.04
A. crassipinnis	2.15	-	2.2	2.15	0.92	2.08
A. ocellatus	1.75	2.2	-	1.03	2.51	1.32
***Astronotus* sp. "East"**	1.36	2.15	1.03	-	2.07	0.97
***Astronotus* sp. "Jurua"**	2.09	0.92	2.51	2.07	-	1.78
***Astronotus* sp. "Negro"**	1.04	2.08	1.32	0.97	1.78	-

0.163%, while minimum inter-specific distance was 0.98% (Table 4). The lineage *Astronotus* sp. "Negro" is the closest lineage to *A. mikoljii* sp. nov. The mean genetic distance between *A. mikoljii* sp. nov. and the currently valid species (*A. crassipinnis* and *A. ocellatus*) had values of 1.75% and 2.15%, respectively (Table 5). A total of three diagnostic sites segregates *A. mikoljii* sp. nov. from *A. ocellatus* and *A. crassipinnis* (Table 4).

Multivariate analysis. The Canonical Discriminant Analysis (CDA) using morphometric data of the sagitta otoliths clearly identified three groups corresponding to each of the described species of the genus *Astronotus* (Fig. 10). A high level of successful classification among the species was obtained using the jack-knife procedure, reaching a value ± 90% in both cases (Suppl. material 1: Table S5). In this statistical analysis, including the measurements on the geometric shape of the sagitta otoliths separated *A. mikoljii* sp. nov. from *A. ocellatus* and *A. crassipinnis*.

Etymology. The specific name is given to honor Mr. Ivan Mikolji, Venezuelan explorer, artist, author, underwater photographer, and audiovisual producer, in recognition for being a tireless and enthusiastic diffuser of the biodiversity and natural history of freshwater fishes, conservation of aquatic ecosystems of Venezuela and Colombia, and for logistic support for this work. Since 2020, Ivan Mikolji has been recognized as Associate Researcher of the Museo de Historia Natural La Salle, from the Fundación La Salle de Ciencias Naturales, in Caracas, Venezuela.

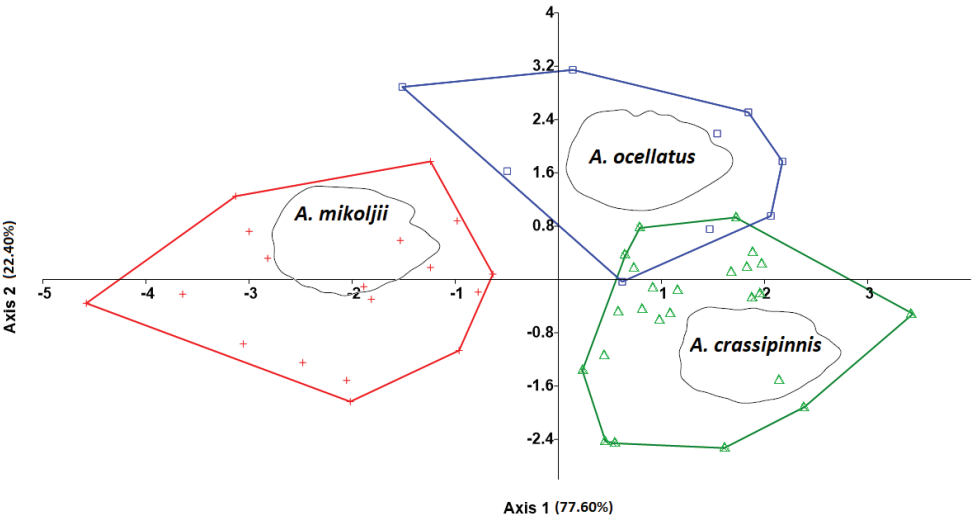

Figure 10. Plot of scores of Canonical Variants Analysis (CVA), from comparative sagitta otoliths morphometric data of *Astronotus mikoljii* sp. nov. (red crosses), *A. ocellatus* (blue squares), and *A. crassipinnis* (green triangles).

Distribution. *Astronotus mikoljii* sp. nov. is distributed in all parts of the lower Orinoco River basin (Fig. 7), along the floodplain of its main channel and in the drainages of the following rivers (or sub-basins): Atabapo, Inírida, Guaviare, Vichada, Bita, Meta, Tomo, Arauca, Apure, Caura, Morichal Largo and Delta, in Venezuela and Colombia (Fowler 1911; Novoa and Ramos 1978; Kullander 1981; Novoa et al. 1982; Román 1985; Novoa 1986; Román 1988; Winemiller 1989a, b, 1990; Lasso and Castroviejo 1992; Monente 1992; Machado-Allison 1993; Lasso et al. 1999; Mojica 1999; Ponte et al. 1999; Lasso and Machado-Allison 2000; Lasso et al. 2003a, b, c, 2004; Campo 2004, Lasso 2004; Machado-Allison 2003; Antonio and Lasso 2004; Taphorn et al. 2005; Galvis et al. 2007; Marcano et al. 2007; Lasso et al. 2009a, b; Brito et al. 2011; Lasso et al. 2011a, b; 2014; Echeverría and Machado-Allison 2015; Ortega-Lara 2016; DoNascimiento et al. 2017; Machado-Allison et al. 2018; Winemiller et al. 2018). It also occurs in the Gulf of Paria basin (Caño La Brea, Forest Reserve of Guarapiche, sub-basin San Juan River, EBRG 5055) in Venezuela (Lasso et al. 2010). It has been introduced in other watersheds of Venezuela such as Lago de Valencia and in reservoirs of the Mar Caribe basin (drainages of the Unare, Tuy, Coro and San Juan rivers (Isla de Margarita)) (Luengo 1963; León 1966; Cervigón 1983; Ginéz and Olivo 1984; Ginéz et al. 1984).

Ecology. *Astronotus mikoljii* sp. nov. usually inhabits the middle and lower reaches of the Orinoco River and the Gulf of Paria basin, at altitudes not exceeding 250 m a.s.l. (Fig. 8b). It can be found in either lotic or lentic water bodies, large or small rivers, culverts, lagoons, and floodplains, with white, clear, and black waters (sensu Sioli 1965). In the Orinoco River Delta, it lives in slow-flowing channels and flooded

forests, while in the middle Orinoco region; it has only been captured in flood and floodplain lagoons, on both banks of the river (Novoa et al. 1982; Novoa 1986). In its first stages of development, it is associated with floating vegetation and semi-rooted plants formed mainly in grasses and water hyacinth (*Paspalum repens*, *Eichhornia crassipes*). In the adult phase they are located in riparian zones, generally among grasses and sedges (Machado-Allison 1993; Lasso 2004; Lasso et al. 2011b; Echeverría and Machado-Allison 2015). Part of the type material was captured in the flooded savannah of a minor tributary of the Arauca River, in the floodplains of Apure State, Venezuela (Fig. 8b). During sampling, the body of water was almost stagnant and the water temperature was 27 °C with abundant aquatic vegetation and muddy bottom.

This species was probably negatively impacted by the invasion of the Orinoco River Basin by transferred invasive cichlid *Caquetaia kraussii* (Steindachner, 1878) (Royero and Lasso 1992; Señaris and Lasso 1993; Lasso and Machado-Allison 2000). For example, in one lagoon in the Portuguesa River drainage between Guanare and Guanarito, where one of the authors (DCT) commonly collected *A. mikoljii* sp. nov. (on many occasions over many years during student field trips from 1978 to 1988) it is now absent, having been completely replaced by *C. kraussii*.

Common names. In Spanish and indigenous local languages, names which are known for *Astronotus mikoljii* sp. nov. in Venezuela are pavona, vieja, cupaneca, Oscar, mijsho (Kariña), boisikuajaba (Warao), hácho (Pumé = Yaruro), phadeewa, jadaewa (Ye'Kuana = Makiritare), perewa, parawa (Eñepá = Panare), yawirra (Kúrrim = Kurripako), kohukohurimï, kohokohorimï, owënawë kohoromï" (Yanomami = Yanomamï) (Barandiarán 1962; Mago 1967, 1970c; Novoa et al. 1982; Obregón et al. 1984; Román 1985; Novoa 1986; Román 1988; Bedoya 1992; Mattei-Müller et al. 1994; Lasso and Machado-Allison 2000; Mosonyi 2002; Machado-Allison 2003; Vispo and Knab-Vispo 2003; Mattei-Müller and Serowe 2007; Brito et al. 2011) and pavo real, carabazú, Oscar, mojarra, mojarra negra, eba (Puinave), Itapukunda (Kurripako), uan (Tucano) in Colombia (Sánchez 2008). The suggested common name for this species in the aquarium hobby is "Mikolji's Oscar" in English, "Oscar de Mikolji ‘' in Spanish.

Discussion

Through an integrative taxonomic approach, our results demonstrate the distinctiveness of *Astronotus mikoljii* sp. nov. from *A. ocellatus* and *A. crassipinnis*, using genetic characters (DNAm), skeletal characters (presence of two or three supraneural bones and absence of spinous process in upper border of parahypural bone of caudal fin), and anatomical characters (sagitta otolith shape). Although sagitta otolith morphology has not been previously used as a diagnostic character in *Astronotus*, as shown in the CDA, each species of *Astronotus* has a differently shaped, distinct sagitta otolith that can be used to distinguish not only the new species, but also between *A. ocellatus* and *A. crassipinnis*.

The molecular analyses also show significant differences among *Astronotus mikoljii* sp. nov. *A. crassipinnis*, and *A. ocellatus*, in addition to identifying that all lineages/

species are reciprocally monophyletic in mitochondrial DNA (Fig. 9), with mean genetic p-distance of 2.15 and 1.75% respectively (Table 4). Although *A. mikoljii* sp. nov. can be diagnosed by otolithometrics and molecular data (Figs 9, 10), its differentiation by morphometry and body meristics shows little promise. Comparison of *A. ocellatus* specimens from the western and Central Amazon, as well as specimens of *A. crassipinnis* from Madeira rivers basins with *A. mikoljii* sp. nov., revealed the difficulty in distinguishing these three species using external morphometric characters. Only four morphometric characters showed significant differences (head length, snout, orbital diameter and pre-orbital distance) between the three species.

Other characteristics of the axial skeleton anatomy also support the validity of the new species. The presence of up to three supraneural elements in at least 30% of the examined x-ray specimens (n = 26) of *Astronotus mikoljii* sp. nov. (Fig. 4b, c, Suppl. material 1: Table S3), is highly unusual and distinctive. The supraneural bones, formerly known as predorsal spines, are a character of great importance in the phylogenetic classification of Teleost fishes (Fink and Fink 1981; Mabee 1988). In some groups of the family Cichlidae, the number of supraneural bones has been used to separate genera and species (Gosse 1975; López-Fernández and Taphorn 2004; López-Fernández et al. 2006; Sparks and Stiassny 2010; Arbour and López-Fernández 2011; Martinez et al. 2015). According to our review, it is not common to find members of the Cichlidae family in America that have three supraneural bones, since most of the Neotropical species have only two or sometimes just one element (e.g., Kullander 1986, 1998; López-Fernández et al. 2005; Kullander and Ferreira 2006; Chakrabarty and Sparks 2007). However, Kullander (1986), when describing the genus *Bujurquina*, indicates that it presents exceptional cases with one or three elements that represent abnormal conditions, in which the third supraneural seems to be a pterygiophore without spines. In our case, without doubt, the third element in *A. mikoljii* sp. nov. is clearly a supraneural bone, clearly separated from the first pterygiophore (Fig. 4b, c). Wijkmark et al. (2012) apparently found a specimen (28 specimens had only two elements) of *Andinoacara blombergi* with three supraneural bones, but they do not present any supporting illustration. The presence of such a high number of supraneural elements is best known in Ostariophysan fishes (Fink and Fink 1981; Chuctaya et al. 2020; Stiassny et al. 2021), but not in American cichlids. This is an important and new topic that should be studied further. These bones intervene in the dorsal flexion of the joints of the axial skeleton, when the neurocranial elevation occurs, to expand the oral cavity, at the time of suction feeding (Jimenez et al. 2018).

In the new species, there is no spinous process on the antero-superior border of the parahypural bone (Fig. 5a) of the caudal skeleton (vs. PP with a small spine in *Astronotus ocellatus* and *A. crassipinnis*), and the elements of the hypural complex in *A. mikoljii* sp. nov., are more separated and are a little less robust than in the other two species (Fig. 5b, c). In addition, some spaces such as the diastema (D) are wider in *A. mikoljii* sp. nov. than in *A. crassipinnis* and *A. ocellatus*). Monod (1968), Sibilia and Andreata (1991), and Thieme et al. (2022) described all bones of the hypural complex of *A. ocellatus* as robust and less spaced. Elements such as E2 and E3 are represented as very close and even fused by these authors, something observed in the material

examined (Fig. 5b, c), unlike *A. mikoljii* sp. nov. where these elements are more separated (Fig. 5a). Also, the E2 bone in *A. mikoljii* sp. nov. is articulated with the NEU2 spine, whereas in *A. ocellatus* they do not come into contact (Fig. 5b, c).

The analysis of the morphology of the sagitta otolith supports the distinctive taxonomic status of several fish species (Mereles et al. 2021, Reichenbacher et al. 2007, 2009a, b). However, the morphology of the sagitta otoliths was never used in previous studies for *Astronotus* species. Here, we compared the sagitta otoliths of *A. ocellatus* and *A. crassipinnis* (Figs 6, 10). The morphology of the sagitta otolith in *A. mikoljii* sp. nov. has an oval shape with strongly crenulated ventral and dorsal margins, while that in *A. crassipinnis* is elliptical with smooth-lobed margins and in *A. ocellatus*, it is elliptical with smooth-dentate margins. The rostrum of the sagitta otolith also showed differences: in *A. mikoljii* sp. nov. it is projected and larger than in *A. crassipinnis* and *A. ocellatus*; on the other hand, the posterior region of the sagitta otolith is rounded in *A. mikoljii* but straight or flat in *A. crassipinnis* and *A. ocellatus*. The biometric index and the morphometric index of sagitta otoliths in *A. mikoljii* sp. nov. also showed significant differences compared to *A. ocellatus* and *A. crassipinnis*. These results show that these species are clearly different in relation to the morphology of the sagitta otolith of *A. mikoljii* sp. nov. and the results of the genetic analysis showed the complete segregation of *A. mikoljii* sp. nov. from the other two recognized species of *Astronotus* (Fig. 9, Tables 4, 5).

In the Neotropical ichthyological literature there are several examples of species that initially had a pan-Neotropical or pan-Amazon distributions, which were later segregated into several species, including the genus *Cichla* Bloch & Schneider, 1801 (Kullander and Ferreira 2006). Likewise, Buitrago-Suárez and Burr (2007) described seven new species of *Pseudoplatystoma* Bleeker, 1862 from two species, which were previously considered to have a pan-Amazonian distribution, and Escobar et al. (2019) described a new species of *Piaractus* Eigenmann, 1903 from the Orinoco River basin, from a species previously thought widely distributed in the Amazon basin. More recently, Loboda et al. (2021) described two new species of freshwater rays of the genus *Paratrygon* Duméril 1865 from the Orinoco River basin from a single species with a shared distribution for the Orinoco and Amazon river basins.

Kullander (1986) and Colatreli et al. (2012) considered that there may be several species within the genus *Astronotus*, and particularly Colatreli et al. (2012) tested this hypothesis by using the ABGD method, delimiting five different lineages in *Astronotus* populations from the Amazon River basin that could represent candidate species. Our results using five distinct single-locus species delimitation methods also corroborate the findings of Colatreli et al. (2012) and indicate *A. mikoljii* sp. nov. as a novel and distinct lineage, more related to *Astronotus* sp. "Negro", *A. crassipinnis*, and *Astronotus* sp. "East" lineages than to *A. ocellatus* (Fig. 9, Suppl. material 3: Data S1). Although the maximum credibility tree was able to recover two main clades of *Astronotus* with high posterior probability support, relationships among the lineages of the *A. crassipinnis* clade could not be fully resolved.

Considering that the new species is described from the Orinoco basin and that this basin is connected with the Negro basin by the Casiquiare channel, the strategy

of including the Colatreli et al. (2012) sequences of individuals from the Negro River was essential for comparisons between these lineages and discussing the possibility of their being the same species. Thus, our delimitation analyses corroborate the findings of Colatreli et al. (2012) that the Negro River drainage has a distinct lineage, being also delimited by all the five methods used in this study. This lineage is probably *Astronotus rubroocellata* (originally *Cycla rubro-ocellata* Jardine & Schomburgk, 1843 in Schomburgk 1843): however, we emphasize that the revalidation of this species is beyond the scope of this study and should be the object of future studies.

Phylogenetic resolutions between *Astronotus* lineages/species were mostly well supported. Two large clades are observed, one formed by *A. ocellatus* and the *Astronotus* sp. "Jurua" lineage, and the other formed by *A. mikoljii* sp. nov. having as sister groups the *Astronotus* sp. "Negro", *A. crassipinnis*, and *Astronotus* sp. "East" lineages. Despite the monophyly of all lineages/species being well supported, the phylogenetic relationships of these last three lineages showed low support values, which prevent us from discussing their relationships. It is clear that *A. mikoljii* sp. nov. is both genetically and morphologically differentiated from all other species/lineages within the genus and merits the status of a valid species. Although interspecific genetic distance is low (Table 4), other studies suggested that the low genetic distance pattern found in other Neotropical fish groups is indicative of recent diversification (Toffoli et al. 2008; Andrade et al. 2017).

Acknowledgements

The authors would like to thank Felipe P. Ottoni, Universidade Federal de Maranhão (UFMA, Brazil) and Jonathan Ready, Universidade Federal de Pará (UFPA, Brazil) for their comments and suggestions on the manuscript. Otto Castillo and Oscar León Mata (*in memoriam*) for allowing access to the fish collection of the Museo de Ciencias Naturales de Guanare (UNELLEZ-Venezuela). Lúcia Rapp for allowing access to the fish collection of the Instituto Nacional de Pesquisas da Amazônia (INPA-Brazil). To Edwin Agudelo and Ivone Aricari Damaso of the Instituto Amazónico de Investigaciones Científicas (SINCHI-Colombia) for the collection and biological data extraction of the specimens. Ivan Mikolji of the Museo de Historia Natural La Salle, Fundación La Salle de Ciencias Naturales (MHNLS, FLASA, Caracas, Venezuela), provided images of the species in its natural environment and Holotype, provided materials, supplies, as well as logistical and economic support for this work. Rafael Alfonso, for his help in the field work in Venezuela. Mark Sabaj, Academy of Natural Sciences of Philadelphia, for the photograph and data of the first specimen of *Astronotus mikoljii* sp. nov. cited for Venezuela (ANSP 37896). Ivonne Rivas, Mirta Perdomo and Luis Ojeda, of the Radio Diagnóstico and Estudio Médico Tomograf (Instituto Clinico La Florida), Caracas, Venezuela, for radiographs of the type Material of the MHNLS. Sandra Raredon (USNM), for elaborating by our request radiographs of specimens of *A. ocellatus* and Renildo Ribeiro de Oliveira and Cárlison Silva de Oliveira (INPA) for radiographs of the species *A. ocellatus* and *A. crassipinnis*. Pedro Rivas, Instituto Caribe

de Antropología y Sociología (ICAS, Fundación La Salle de Ciencias Naturales), for research of the common names in indigenous languages of *A. mikoljii* sp. nov. José Andreata (Universidade Santa Úrsula), Telton Ramos (Universidade Estadual de Paraíba), Philippe Béarez and Aurélien Miralles (Muséum National d'Histoire Naturelle), for the bibliographical references. This study had the financial support of the Universidade Federal de Alagoas (UFAL), Conselho Nacional de Pesquisas (CNPq), Fundação de Amparo da Pesquisa do Estado de Alagoas (FAPEAL) of Brazil.

References

ACTFR (2014) Australian Centre for Tropical Freshwater Research. Pest fish profiles - *Astronotus ocellatus*. Australian Centre for Tropical Freshwater Research, Townsville, Australia, 3 pp. https://research.jcu.edu.au/tropwater/resources/Oscars.pdf

Ajiaco-Martínez RE, Ramírez-Gil H, Sánchez-Duarte P, Lasso CA, Trujillo F (2012) IV. Diagnóstico de la pesca ornamental en Colombia. Serie Editorial Recursos Hidrobiológicos y Pesqueros Continentales de Colombia. Instituto de Investigación de Los Recursos Biológicos Alexander von Humboldt, Bogotá, 152 pp.

Andrade MC, Machado VN, Jégu M, Farias IP, Giarrizzo T (2017) A new species of Tometes Valenciennes 1850 (Characiformes: Serrasalmidae) from Tocantins-Araguaia River Basin based on integrative analysis of molecular and morphological data. PLoS ONE 12(4): e0170053. https://doi.org/10.1371/journal.pone.0170053

Andreata J (1979) Osteologia da Nadadeira Caudal de *Diapterus* Ranzani e *Eucinostomus* Baird & Girard (Perciformes-Percoidei-Gerridae). Revista Brasileira de Biologia 39(1): 237–258.

Antonio ME, Lasso C (2004) Los peces del río Morichal Largo, estados Monagas y Anzoátegui, Cuenca del río Orinoco, Venezuela. Memoria de la Fundación La Salle de Ciencias Naturales 156: 5–118.

Arbour JH, López-Fernández H (2011) *Guianacara dacrya*, a new species from the Rio Branco and Essequibo River drainages of the Guiana Shield (Perciformes: Cichlidae). Neotropical Ichthyology 9(1): 87–96. https://doi.org/10.1590/S1679-62252011000100006

Assis CA (2000) Estudo morfológico dos otólitos *sagitta*, *asteriscus* e *lapillus* de teleósteos (Actinopterygii, Teleostei) de portugal continental. Ph.D. thesis, Universidade de Lisboa, Lisboa, 1005 pp.

Assis CA (2003) The lagenar otoliths of teleosts: Their morphology and its application in species identification, phylogeny and systematics. Journal of Fish Biology 62(6): 1268–1295. https://doi.org/10.1046/j.1095-8649.2003.00106.x

Barandiarán D (1962) Shamanismo yekuana o makiritare. Antropológica 11: 61–90.

Barbarino-Duque A, Taphorn DC (1994) Especies de la Pesca Deportiva, Una Guía de Identificación y Reglamentación de los Peces de Agua Dulce en Venezuela. UNELLEZ y Fundación Polar, Caracas, 155 pp.

Bedoya O (1992) Diccionario kurripako (versión experimental sujeta a revisión). Inírida: Dirección de Asuntos Indígenas del Ministerio de Educación-Venezuela/Centro Experimental Piloto de Guainía-Fundación Etnollano-Programa Coama-Colombia, Caracas, 388 pp.

Bouckaert RR, Drummond AJ (2017) Model Test: Bayesian phylogenetic site model averaging and model comparison. BMC Evolutionary Biology 17(1): 1–11. https://doi.org/10.1186/s12862-017-0890-6

Bouckaert R, Vaughan TG, Barido-Sottani J, Duchêne S, Fourment M, Gavryushkina A, Heled J, Jones G, Kuhnert D, De Maio N, Matschiner M, Mendes F, Muller NF, Ogilvie HA, Du Plessis L, Popinga A, Rambaut A, Rasmussen D, Siveroni I, Suchard MA, Wu C, Xie D, Zhang C, Stadler T, Drummond AJ (2019) BEAST 2.5: An advanced software platform for Bayesian evolutionary analysis. PLoS Computational Biology 15(4): 1–28. https://doi.org/10.1371/journal.pcbi.1006650

Brito A, Lasso C, Sanchez-Duarte P (2011) Pavona, cupaneca, Oscar, *Astronotus* cf. *ocellatus*. In: Lasso C, Sánchez-Duarte P (Eds) Los peces del delta del Orinoco. Diversidad, bio-ecología, uso y conservación. Fundación La Salle de Ciencias Naturales y Chevron C.A., Caracas, 500 pp.

Brown SDJ, Collins RA, Boyer S, Lefort MC, Malumbres-Olarte J, Vink CJ, Cruickshank RH (2012) Spider: An R package for the analysis of species identity and evolution, with particular reference to DNA barcoding. Molecular Ecology Resources 12(3): 562–565. https://doi.org/10.1111/j.1755-0998.2011.03108.x

Buitrago-Suárez UA, Burr BM (2007) Taxonomy of the catfish genus *Pseudoplatystoma* Bleeker (Siluriformes: Pimelodidae) with recognition of eight species. Zootaxa 1512(1): 1–38. https://doi.org/10.11646/zootaxa.1512.1.1

Burger R, Zanata AM, Camelier P (2011) Taxonomic study of the freshwater ichthyofauna from Recôncavo Sul basin, Bahia, Brazil. Biota Neotropica 11(4): 273–290. https://doi.org/10.1590/S1676-06032011000400024

Campo M (2004) Inventario preliminar de la íctiofauna de la Reserva de Fauna Silvestre Gran Morichal, Estado Monagas, Venezuela. Memoria de la Fundación La Salle de Ciencias Naturales 161–162: 41–60.

Cervigón F (1982) Ilustraciones: *Astronotus ocellatus*, pavona o cupaneca. P.:354. In: Novoa D (Ed.) Los Recursos Pesqueros del Río Orinoco y su Explotación. Corporación Venezolana de Guayana, Caracas, 386 pp.

Cervigón F (1983) La Acuicultura en Venezuela. Estado Actual y Perspectivas. Editorial Arte, Caracas, 121 pp.

Chakrabarty P, Sparks JS (2007) Relationships of the New World cichlid genus *Hypsophrys* Agassiz 1859 (Teleostei: Cichlidae), with diagnoses for the genus and its species. Zootaxa 1523(1): 59–64. https://doi.org/10.11646/zootaxa.1523.1.3

Chuctaya J, Ohara WM, Malabarba LR (2020) A new species of *Odontostilbe* Cope (Characiformes: Cheirodontinae) from rio Madeira basin diagnosed based on morphological and molecular data. Journal of Fish Biology 97(6): 1701–1712. https://doi.org/10.1111/jfb.14533

Coker GA, Portt CB, Minns CK (2001) Morphological and ecological characteristics of Canadian freshwater fishes. Canadian Fisheries Aquatic Sciences 2554: [iv +] 89 pp.

Colatreli O, Meliciano N, Toffoli D, Farias I, Hrbek T (2012) Deep Phylogenetic Divergence and Lack of Taxonomic Concordance in Species of *Astronotus* (Cichlidae). International Journal of Evolutionary Biology 915265: 1–8. https://doi.org/10.1155/2012/915265

Collins RA, Boykin LM, Cruickshank RH, Armstrong KF (2012) Barcoding's next top model: An evaluation of nucleotide substitution models for specimen identification. Methods in Ecology and Evolution 3(3): 457–465. https://doi.org/10.1111/j.2041-210X.2011.00176.x

CONCEA (2016) Normativas do CONCEA: Lei, Decretos, Portarias, Resoluçoes Normativas e Orientaçoes tecnicas. 3rd ed. Brasilia, 385 pp.

DoNascimiento C, Herrera EE, Herrera GA, Ortega A, Villa FA, Usma JS, Maldonado-Ocampo JA (2017) Checklist of the freshwater fishes of Colombia: A Darwin Core alternative to the updating problem. ZooKeys 708: 25–138. https://doi.org/10.3897/zookeys.708.13897

Dos Reis RB, Frota A, Deprá GC, Ota RR, da Graça WJ (2020) Freshwater fishes from Paraná State, Brazil: An annotated list, with comments on biogeographic patterns, threats, and future perspectives. Zootaxa 4868(4): 451–494. https://doi.org/10.11646/zootaxa.4868.4.1

Drummond AJ, Suchard MA, Xie D, Rambaut A (2012) Bayesian phylogenetics with BEAUti and the BEAST 1.7. Molecular Biology and Evolution 29(8): 1969–1973. https://doi.org/10.1093/molbev/mss075

Echeverría G, Machado-Allison A (2015) La íctiofauna de los Esteros de Camaguán (río Portuguesa), Estado Guárico, Venezuela. Acta Biologica Venezuelica 35(1): 75–87.

Escobar MD, Ota RP, Machado-Allison A, Andrade-López J, Farias IP, Hrbek T (2019) A new species of *Piaractus* (Characiformes: Serrasalmidae) from the Orinoco Basin with a redescription of *Piaractus brachypomus*. Journal of Fish Biology 95(2): 411–442. https://doi.org/10.1111/jfb.13990

Fernández-Yépez A, Anton JR (1966) Análisis ictiológico "Las Majaguas". Dirección de Obras Hidráulicas, Ministerio de Obras Públicas, Caracas, 107 pp.

Fink SV, Fink WL (1981) Interrelationships of the ostariophysan fishes (Teleostei). Zoological Journal of the Linnean Society 72(4): 297–353. https://doi.org/10.1111/j.1096-3642.1981.tb01575.x

Fowler H (1911) Some Fishes from Venezuela. Proceedings. Academy of Natural Sciences of Philadelphia 63(2): 419–437.

Fricke R, Eschmeyer WN, Van der Laan R (2019) Catalog of Fishes: Genera, Species, References. https://www.calacademy.org/scientists/projects/eschmeyers-catalog-of-fishes [accessed on 09 Jan 2019]

Fujisawa T, Barraclough TG (2013) Delimiting species using single-locus data and the generalized mixed yule coalescent approach: A revised method and evaluation on simulated data sets. Systematic Biology 62(5): 707–724. https://doi.org/10.1093/sysbio/syt033

Fuller PL, Nico LG, William JD (1999) Non indigenous fishes introduced into inland waters of the United States. American Fisheries Society, Special Publication 27, Maryland, 613 pp.

Galvis G, Mojica JI, Provenzano F, Lasso C, Taphorn DC, Royero R, Castillo C, Gutiérrez A, Gutiérrez MA, López Pinto Y, Mesa LM, Sánchez-Duarte P, Cipamocha C (2007) Peces de la Orinoquia colombiana con énfasis en especies de interés ornamental. Ministerio de Agricultura y Desarrollo Rural, INCODER, Universidad Nacional de Colombia - Departamento de Biología - Instituto de Ciencias Naturales, Bogotá, 425 pp.

García D, Britton J, Vidotto-Magnoni A, Orsi M (2018) Introductions of non-native fishes into a heavily modified river: Rates, patterns and management issues in the Paranapanema River (Upper Paraná ecoregion, Brazil). Biological Invasions 20(5): 1229–1241. https://doi.org/10.1007/s10530-017-1623-x

Ginéz A, Olivo M (1984) Inventario de los embalses con información básica para la actividad piscícola, Parte I: Sinopsis de los embalses administrados por el MARNR. División General de Planificación Ambiental, Serie de Informes Técnicos, DGSPOA/ IT/ 183, Caracas, 159 pp.

Ginéz A, Olivo M, Rodríguez A (1984) Inventario de los embalses con información básica para la actividad piscícola, Parte III: Sinopsis de los embalses administrados por el INOS. División General de Planificación Ambiental, Serie de Informes Técnicos, DGSPOA/ IT/ 185, Caracas, 184 pp.

Gosse JP (1975) Révision du genre *Geophagus* (Pisces, Cichlidae). Memoires de l'Académie Royale des Sciences d'Outre-Mer, Classe des Sciences Naturelles et Médicales 19(3): 1–172[+ 18].

Hammer Ø, Harper DAT, Ryan PD (2001) PAST: Paleontological Statistics Software Package for Education and Data Analysis. Palaeontologia Electronica 4: 1–9. https://palaeoelectronica.org/2001/past/issue1_01.htm [accessed on 15 May 2019]

Hammer MP, Adams M, Foster R (2012) Update to the catalogue of South Australian freshwater fishes (Petromyzontida and Actinopterygii). Zootaxa 3593(1): 59–74. https://doi.org/10.11646/zootaxa.3593.1.3

Herrera M, Segnini S, Machado-Allison A (2012) Comparación entre las comunidades de peces en dos tipos de ríos en la región oriental de Venezuela. Boletín de la Academia de Ciencias Físicas Matemáticas y Naturales 84(1): 47–67.

Hoeinghaus D, Winemiller KO, Taphorn DC (2004) Compositional change in fish assemblages along the Andean piedmont – Llanos floodplain gradient of the río Portuguesa, Venezuela. Neotropical Ichthyology 2(2): 85–92. https://doi.org/10.1590/S1679-62252004000200005

Ivanova NV, Zemlak TS, Hanner RH, Hebert PD (2007) Universal primer cocktails for fish DNA barcoding. Molecular Ecology Notes 7(4): 544–548. https://doi.org/10.1111/j.1471-8286.2007.01748.x

Jimenez YE, Camp AL, Grindall JD, Brainerd EL (2018) Axial morphology and 3D neurocranial kinematics in suction-feeding fishes. Biology Open 7(9): bio036335. https://doi.org/10.1242/bio.036335

Katoh K, Misawa K, Kuma K, Miyata T (2002) MAFFT a novel method for rapid multiple sequence alignment based on fast Fourier transform. Nucleic Acids Research 30(14): 3059–3066. https://doi.org/10.1093/nar/gkf436

Kearse M, Moir R, Wilson A, Stones-Havas S, Cheung M, Sturrock S, Buxton S, Cooper A, Markowitz S, Duran C, Thierer T, Ashton B, Meintjes P, Drummond A (2012) Geneious Basic: An integrated and extendable desktop software platform for the organization and analysis of sequence data. Bioinformatics (Oxford, England) 28(12): 1647–1649. https://doi.org/10.1093/bioinformatics/bts199

Kullander SO (1981) Cichlid fishes from the La Plata basin. Part I. Collections from Paraguay in the Musèum d'Histoire Naturelle de Genève. Revue Suisse de Zoologie 88: 675–692. https://doi.org/10.5962/bhl.part.82400

Kullander SO (1983) Taxonomic studies on the Percoid freshwater fish Family Cichlidae in South America. Part II: Review of the South American Cichlidae. Ph.D. Thesis, University of Stockholm, Stockholm, 440 pp.

Kullander SO (1986) Cichlid Fishes from the Amazon River Drainage of Peru. Swedish Museum of Natural History, Stockholm, 431 pp.

Kullander SO (1998) A phylogeny and classification of the Neotropical Cichlidae (Teleostei: Perciformes). In: Malabarba L, Reis R, Vari R, Lucena Z, Lucena C (Eds) Phylogeny and Classification of Neotropical Fishes. EDIPUCRS, Porto Alegre, 461–498.

Kullander SO (2003) Family Cichlidae (Cichlids) In: Reis RE, Kullander SO, Ferraris Jr CJ (Eds) Check list of the freshwater fishes of South and Central America. EDIPUCRS, Porto Alegre, 605–654.

Kullander SO, Ferreira EJG (2006) A review of the South American cichlid genus *Cichla*, with descriptions of nine new species (Teleostei: Cichlidae). Ichthyological Exploration of Freshwaters 17(4): 289–398.

Lasso C (1988) Inventario de la íctiofauna de nueve lagunas de inundación del Bajo Orinoco, Venezuela. Parte II: (Siluriformes-Gymnotiformes) - ACANTHOPTERYGII. Memorias de la Sociedad de Ciencias Naturales La Salle 48(Suplemento 2): 355–385.

Lasso C (2004) Los peces de la Estación Biológica El Frío y Caño Guaritico, Estado Apure, Llanos del Orinoco, Venezuela. Publicaciones del Comité Español del Programa MAB y de la Red IberoMAB de la UNESCO, N°5, 454 pp.

Lasso C, Castroviejo J (1992) Composition, abundance and biomass of the benthic fish fauna from the Guaritico River of a Venezuelan floodplain. Annales de Limnologie 28(1): 71–84. https://doi.org/10.1051/limn/1992006

Lasso C, Machado-Allison A (2000) Sinopsis de las especies de peces de la familia Cichlidae presentes en la cuenca del Río Orinoco. Claves, diagnosis, aspectos bio-ecológicos e ilustraciones. Serie Peces de Venezuela. Universidad Central de Venezuela, 150 pp.

Lasso C, Rial A, Lasso-Alcalá O (1999) Composición y variabilidad espacio-temporal de las comunidades de peces en ambientes inundables de los Llanos de Venezuela. Acta Biologica Venezuelica 19(2): 1–28.

Lasso CA, Castelló V, Canales-Tilve T, Cabot-Nieves J (2001) Contribución al conocimiento de la íctiofauna del Río Paraguá, cuenca del Río Itenez o Guaporé, Amazonía Boliviana. Memoria de la Fundación La Salle de Ciencias Naturales 59(152): 89–103.

Lasso CA, Lew D, Taphorn D, DoNascimiento C, Lasso-Alcalá O, Provenzano F, Machado-Allison A (2003a) Biodiversidad ictiológica continental de Venezuela. Parte I. Lista de especies y distribución por cuencas. Memoria de la Fundación La Salle de Ciencias Naturales 159–160: 105–195.

Lasso C, Machado-Allison A, Taphorn D, Rodríguez-Olarte D, Vispo C, Chernoff B, Provenzano F, Lasso-Alcalá O, Cervó A, Nakamura K, Gonzalez N, Meri J, Silvera C, Bonilla A, López-Rojas H, Machado-Aranda D (2003b) The fishes of the Caura River, Orinoco Basin, Venezuela: Annotated Checklist. In: Vispo C, Knab-Vispo C (Eds) Plants and Vertebrates of the Caura's Riparian Corridor: Their Biology, Use and Conservation. Scientia Guianae 12(Special Issue): 223–246.

Lasso C, Vispo C, Lasso-Alcalá O (2003c) Composition of the ichthyofauna of nine floodplain lakes of the Caura River, Southern Venezuela. In: Vispo C, Knab-Vispo C (Eds) Plants and Vertebrates of the Caura's Riparian Corridor: Their Biology, Use and Conservation. Scientia Guianae 12(Special Issue): 273–296.

Lasso C, Mojica JI, Usma JS, Maldonado J, Donascimiento C, Taphorn D, Provenzano F, Lasso-Alcalá O, Galvis G, Vásquez L, Lugo M, Machado-Allison A, Royero R, Suárez C, Ortega-Lara A (2004) Peces de la Cuenca del Río Orinoco. Parte I: Lista de especies y distribución por subcuencas. Biota Colombiana 5(2): 95–158.

Lasso C, Usma Oviedo J, Villa F, Sierra-Quintero MT, Ortega-Lara A, Mesa LM, Patiño M, Lasso-Alcalá O, Morales-Betancourt M, González-Oropesa K, Quiceno M, Ferrer A,

Suárez C (2009a) Peces de la Estrella Fluvial Inírida: Ríos Guaviare, Inírida, Atabapo y Orinoco, Orinoquía Colombiana. Biota Colombiana 10(1–2): 89–122.

Lasso C, Sánchez-Duarte P, Lasso-Alcalá O, Martín R, Samudio H, González-Oropeza K, Hernández-Acevedo J, Mesa L (2009b) Lista de los Peces del Delta del Río Orinoco, Venezuela. Biota Colombiana 10(1–2): 123–148.

Lasso C, Provenzano F, Lasso-Alcalá O, Marcano A (2010) Íctiofauna dulceacuícola y estuarina de la cuenca del golfo de Paria, Venezuela: Composición y relaciones biogeográficas con la cuenca del Orinoco. Biota Colombiana 11(1–2): 53–73.

Lasso C, Sanchez-Duarte MP, Morales-Betancourt M (2011a) Recursos pesqueros continentales de Colombia: Lista de especies. In: Lasso C, Agudelo Córdoba E, Jiménez-Segura LF, Ramírez-Gil H, Morales-Betancourt M, Ajiaco-Martínez RE, De Paula Gutiérrez F, Usma JS, Muñoz-Torres SE, Sanabria AI (Eds) I. Catálogo de los recursos pesqueros continentales de Colombia. Serie Editorial Recursos Hidrobiológicos y Pesqueros Continentales de Colombia. Instituto de Investigación de los Recursos Biológicos Alexander von Humboldt. Bogotá, 57–67.

Lasso C, Morales-Betancourt M, Sierra-Quintero M (2011b) *Astronotus* sp. y *Astronotus ocellatus* (Perciformes, Cichlidae) In: Lasso C, Agudelo Córdoba E, Jiménez-Segura LF, Ramírez-Gil H, Morales-Betancourt M, Ajiaco-Martínez RE, De Paula Gutiérrez F, Usma JS, Muñoz-Torres SE, Sanabria AI (Eds) I. Catálogo de los recursos pesqueros continentales de Colombia. Serie Editorial Recursos Hidrobiológicos y Pesqueros Continentales de Colombia. Instituto de Investigación de los Recursos Biológicos Alexander von Humboldt. Bogotá, 596–598.

Lasso C, Usma J, Villa-Navarro F, Sierra Quintero M, Ortega-Lara A, Mesa L, Morales-Betancourt M, Lasso-Alcalá O, Patiño M (2014) Peces de la Estrella Fluvial Inírida: ríos Guaviare, Inírida, Atabapo y su confluencia en el Orinoco. In: Trujillo F, Usma J, Lasso C (Eds) Biodiversidad de la Estrella Fluvial Inírida. WWF Colombia, Fundación Omacha, Instituto de Investigación de Los Recursos Biológicos Alexander von Humboldt, Bogotá, 100–127.

Leão TCC, Almeida WR, Dechoum M, Ziller SR (2011) Espécies Exóticas Invasoras no Nordeste do Brasil: Contextualização, Manejo e Políticas Públicas. Centro de Pesquisas Ambientais do Nordeste e Instituto Hórus de Desenvolvimento e Conservação Ambiental. Recife, PE, 99 pp.

León J (1966) Piscicultura rural en Venezuela. Bulletin - Office International des Epizooties 65(7–8): 1127–1134.

Loboda TS, Lasso CA, Rosa RS, de Carvalho MR (2021) Two new species of freshwater stingrays of the genus *Paratrygon* (Chondrichthyes: Potamotrygonidae) from the Orinoco basin, with comments on the taxonomy of *Paratrygon aiereba*. Neotropical Ichthyology 19(2): 1–80. https://doi.org/10.1590/1982-0224-2020-0083

Lombarte A, Chic Ò, Parisi-Baradad V, Olivella R, Piera J, García-Ladona E (2006) A web-based environment from shape analysis of fish otoliths. The AFORO database. Scientia Marina 70(1): 147–152. https://doi.org/10.3989/scimar.2006.70n1147

Lopes TM, Ganassin MJM, de Oliveira AG, Affonso IP, Gomes LC (2022) Feeding strategy of the introduced *Astronotus crassipinnis* (Cichlidae) in upper Paraná river floodplain. Iheringia. Série Zoologia 112: e2022001. https://doi.org/10.1590/1678-4766e2022001

López-Fernández H, Taphorn DC (2004) *Geophagus abalios*, *G. dicrozoster* and *G. winemilleri* (Perciformes: Cichlidae), three new species from Venezuela. Zootaxa 439(1): 1–27. https://doi.org/10.11646/zootaxa.439.1.1

López-Fernández H, Honeycutt RL, Stiassny MLJ, Winemiller KO (2005) Morphology, molecules, and character congruence in the phylogeny of South American geophagine cichlids (Perciformes, Labroidei). Zoologica Scripta 34(6): 627–651. https://doi.org/10.1111/j.1463-6409.2005.00209.x

López-Fernández H, Taphorn DC, Kullander SO (2006) Two New Species of *Guianacara* from the Guiana Shield of Eastern Venezuela (Perciformes: Cichlidae). Copeia 3(3): 384–395. https://doi.org/10.1643/0045-8511(2006)2006[384:TNSOGF]2.0.CO;2

Lorenzoni M, Borghesan F, Carosi A, Ciuffardi L, de Curtis O, Delmastro GB, di Tizio L, Franzoi P, Maio G, Mojetta A, Nonnis MF, Pizzul E, Rossi G, Scalici M, Tancioni L, Zanetti M (2019) Check-list dell'ittiofauna delle acque dolci italiane. Italian Journal of Freshwater Ichthyology 5(1): 239–254.

Luengo J (1963) La fauna ictiológica del Lago de Valencia (Venezuela) y algunas consideraciones sobre las demás hoyas del país y Trinidad. Acta Biologica Venezuelica 3: 319–339.

Ma X, Bangxi X, Yindong W, Mingxue W (2003) Intentionally introduced and transferred fishes in China's inland waters. Asian Fisheries Science 16(3–4): 279–290. https://doi.org/10.33997/j.afs.2003.16.4.001

Mabee PM (1988) Supraneural and Predorsal Bones in Fishes: Development and Homologies. Copeia 1(4): 827–838. https://doi.org/10.2307/1445705

Machado-Allison A (1993) Los Peces de los Llanos de Venezuela: Un Ensayo sobre su Historia Natural. CDCH. Universidad Central de Venezuela, Caracas, 222 pp.

Machado-Allison A (2003) Peces de agua dulce. In: Aguilera M, Azocar A, González E (Eds) Biodiversidad en Venezuela. Fundación Polar, Caracas, 562–581.

Machado-Allison A, Moreno H (1993) Inventario y aspectos de la comunidad de peces del río Orituco (Edo. Guárico). Acta Biologica Venezuelica 14(4): 77–94.

Machado-Allison A, Mago-Leccia F, Castillo O, Royero R, Marrero C (1987) Lista de especies de peces reportadas en los diferentes cuerpos de agua de los Bajos Llanos de Venezuela. In: Machado-Allison A (Ed.) Los Peces de los Llanos de Venezuela: Un Ensayo sobre su Historia Natural. Universidad Central de Venezuela, Caracas, 129–136.

Machado-Allison A, Lasso C, Usma JS, Sánchez-Duarte P, Lasso-Alcalá O (2010) Peces. Capítulo 7. In: Lasso C, Usma JS, Trujillo F, Rial A (Eds) Biodiversidad de la Cuenca del río Orinoco: Bases científicas para la identificación de áreas prioritarias para la conservación y uso sostenible de la biodiversidad. Instituto de Investigación de Los Recursos Biológicos Alexander von Humboldt, WWF Colombia, Fundación Omacha, Fundación La Salle de Ciencias Naturales, Instituto de Estudios de la Orinoquia (Universidad Nacional de Colombia). Bogotá D.C., Colombia, 216–257. [609 pp]

Machado-Allison A, Mesa L, Lasso C (2013) Peces de los morichales y cananguchales de la Orinoquia y Amazonia colombo-venezolana: una aproximación a su conocimiento, uso y conservación. Capítulo 15. In: Lasso C, Rial A, González-B. V (Eds) VII. Morichales y cananguchales de la Orinoquia y Amazonia: Colombia – Venezuela. Parte I. Serie Editorial Recursos Hidrobiológicos y Pesqueros Continentales de Colombia. Instituto

de Investigación de Los Recursos Biológicos Alexander von Humboldt (IAvH). Bogotá, 289–334. [344 pp]

Machado-Allison A, De La Fuente R, Mikolji I (2018) Catálogo Ilustrado de los Peces del Parque Nacional "Aguaro-Guariquito". Serie Peces de Venezuela. Academia de Ciencias Físicas, Matemáticas y Naturales. Museo de Biología, Instituto de Zoología y Ecología Tropical, Universidad Central de Venezuela. Fundación de la Academia de Ciencias Físicas, Matemáticas y Naturales. Caracas, 528 pp.

Mago F (1967) Notas preliminares sobre los peces de los llanos de Venezuela. Boletín de la Sociedad Venezolana de Ciencias Naturales 27(112): 237–262.

Mago F (1970a) Estudios preliminares sobre la ecología de los peces de los llanos de Venezuela. Acta Biológica Venezuélica 7(1): 71–102.

Mago F (1970b) Informe sobre las poblaciones de peces del bajo llano en Venezuela. Defensa de la Naturaleza 1: 20, 21, 32.

Mago F (1970c) Lista de los Peces de Venezuela, incluyendo un estudio preliminar sobre la ictiogeografía del país. Ministerio de Agricultura y Cría, Oficina Nacional de Pesca, Caracas, 283 pp.

Mago F (1978) Lista de los Peces de Agua Dulce de Venezuela. Cuadernos Lagoven. Caracas, 35 pp.

Maldonado-Ocampo J (2001) Peces del área de confluencia de los ríos Meta, Bita y Orinoco en Puerto Carreño, Vichada, Colombia. Dahlia 2: 61–74.

Marcano A, Mesa L, Paz J, Machado-Allison A (2007) Adiciones al conocimiento de los peces del sistema Aguaro-Guariquito y río Manapire, cuenca del río Orinoco, estado Guárico, Venezuela. Acta Biologica Venezuelica 27(1): 36–49.

Martinez CM, Arroyave J, Sparks JS (2015) A new species of *Ptychochromis* from southeastern Madagascar (Teleostei: Cichlidae). Zootaxa 4044(1): 79–92. https://doi.org/10.11646/zootaxa.4044.1.4

Mattei-Müller MC, Serowe J (2007) Lengua y cultura yanomamï. Diccionario ilustrado Yanomamï-español/ Español-Yanomamï. Ministerio del Poder Popular para la Cultura de Venezuela, UNESCO, Embajada de España en Venezuela, Agencia Española de Cooperación Internacional, Caracas, 703 pp.

Mattei-Müller MC, Henley P, Salas P (1994) Diccionario ilustrado panare-español/ índice/ español-panare. Un aporte al estudio de los Panares-E'ñepá. Caracas-Venezuela: Comisión Nacional para la Conmemoración del Quinto Centenario del Descubrimiento de América. Comisión Quinto Centenario, 417 pp.

Medina J, Bonilla A (2006) Variabilidad genética en poblaciones silvestres y lotes cultivados de *Caquetaia kraussii* (petenia) y *Astronotus* cf. *ocellatus* (pavona) (Perciformes: Cichlidae). Acta Biologica Venezuelica 26(1): 1–12.

Mereles M, Sousa R, Barroco L, Campos C, Pouilly M, Freitas C (2021) Discrimination of species and populations of the genus *Cichla* (Cichliformes: Cichlidae) in rivers of the Amazon basin using otolithic morphometry. Neotropical Ichthyology 19(4): 1–18. https://doi.org/10.1590/1982-0224-2020-0149

Mojica JI (1999) Lista preliminar de las especies de peces dulceacuícolas de Colombia. Revista de la Academia Colombiana de Ciencias 23(Suplemento Especial): 547–566.

Monaghan MT, Wild R, Elliot M, Fujisawa T, Balke M, Inward DJG, Lees DC, Ranaivosolo R, Eggleton P, Barraclough TG, Vogler AP (2009) Accelerated species Inventory on Madagascar using coalescent-based models of species Delineation. Systematic Biology 58(3): 298–311. https://doi.org/10.1093/sysbio/syp027

Monente JA (1992) Las Pesquerías del Estado Cojedes. Monografía 40. Fundación La Salle de Ciencias Naturales, Caracas, 148 pp.

Monod T (1968) Le complexe urophore des poissons teleosteens. Mémoires de l'Institut français d'Afrique noire, IFAN, Dakar 81, 705 pp.

Mosonyi JC (2002) Diccionario básico del idioma kariña. Barcelona-Venezuela: Dirección de Cultura de la Gobernación del Estado Anzoátegui/Fundación Fondo Editorial del Caribe, 187 pp.

Mundy BC (2005) Checklist of the fishes of the Hawaiian Archipelago. Bishop Museum Bulletins in Zoology (6): 1–703.

Ng PKL, Chou LM, Lam TJ (1993) The status and impact of introduced freshwater animals in Singapore. Biological Conservation 64(1): 19–24. https://doi.org/10.1016/0006-3207(93)90379-F

Nico L, Fuller P, Neilson M (2019) *Astronotus ocellatus* (Agassiz in Spix and Agassiz, 1831): U.S. Geological Survey, Nonindigenous Aquatic Species Database, Gainesville, FL. https://nas.er.usgs.gov/queries/FactSheet.aspx?SpeciesID=436 [accessed on 13 Jan 2019]

Novoa D (1986) Los peces de agua dulce. In: Gremone C, Cervigón F, Gorzula S, Medina G, Novoa D (Eds) Fauna de Venezuela, Vertebrados. Editorial Biósfera, Caracas, 223–246.

Novoa D (1990) El río Orinoco y sus Pesquerías: estado actual, perspectivas futuras y las investigaciones necesarias. In: Weibezahn F, Álvarez H, Lewis W (Eds) El Orinoco como Ecosistema. Fondo Editorial Acta Científica Venezolana, Caracas, 387–406.

Novoa D, Ramos F (1978) Las Pesquerías comerciales del río Orinoco. Corporación Venezolana de Guayana, Caracas, 168 pp.

Novoa D, Cervigón F, Ramos F (1982) Catálogo de los Recursos Pesqueros del Delta del Río Orinoco. In: Novoa D (Ed.) Los Recursos Pesqueros del Río Orinoco y su Explotación. Corporación Venezolana de Guayana, Caracas, 263–324.

Obregón H, Díaz J, Pérez L (1984) Léxico yaruro-español español-yaruro. Gobernación del Estado Apure. Corporación de Desarrollo de la Región de los Llanos, Maracay, 293 pp.

Ortega-Lara A (2016) Peces ornamentales de Colombia. Serie Recursos Pesqueros de Colombia. AUNAP. In: Ortega-Lara A, Puntes V, Barbosa L, Mojica H, Gomez S, Polanco-Rengifo O (Eds) Autoridad Nacional de Pesca y Acuicultura (AUNAP), Fundación FUNINDES, Cali, 112 pp.

Paradis E, Claude J, Strimmer K (2004) APE: Analyses of phylogenetics and evolution in R language. Bioinformatics (Oxford, England) 20(2): 289–290. https://doi.org/10.1093/bioinformatics/btg412

Pons J, Barraclough TG, Gomez-Zurita J, Cardoso A, Duran DP, Hazell S, Kamoun S, Sumlin WD, Vogler AP (2006) Sequence based species delimitation for the DNA taxonomy of undescribed insects. Systematic Biology 55(4): 595–609. https://doi.org/10.1080/10635150600852011

Ponte V, Machado-Allison A, Lasso C (1999) La íctiofauna del delta del Río Orinoco, Venezuela: Una aproximación a su diversidad. Acta Biologica Venezuelica 19(3): 25–46.

Puillandre N, Lambert A, Brouillet S, Achaz G (2012) ABGD, Automatic Barcode Gap Discovery for primary species delimitation. Molecular Ecology 21(8): 1864–1877. https://doi.org/10.1111/j.1365-294X.2011.05239.x

Puillandre N, Brouillet S, Achaz G (2021) ASAP: Assemble species by automatic partitioning. Molecular Ecology Resources 21(2): 609–620. https://doi.org/10.1111/1755-0998.13281

R Development Core Team (2011) R: A language and environment for statistical computing. R Foundation for Statistical Computing, Vienna. http://www.R-project.org [accessed on 18 Jan 2022]

Rambaut A, Drummond AJ, Xie D, Baele G, Suchard MA (2018) Posterior summarization in Bayesian phylogenetics using Tracer 1.7. Systematic Biology 67(5): 901–904. https://doi.org/10.1093/sysbio/syy032

Ramírez-Gil H, Ajiaco-Martínez RE (2016) Pesquerías del río Meta y la parte baja del río Bita. In: Trujillo F, Antelo R, Usma S (Eds) Biodiversidad de la cuenca baja y media del río Meta. Fundación Omacha, Fundación Palmarito, WWF, Bogotá, 122–139. [336 pp]

Ramos TPA, Ramos RTC, Ramos SAQA (2014) Ichthyofauna of the Parnaíba River Basin, Northeastern Brazil. Biota Neotropica 14(1): e20130039. https://doi.org/10.1590/S1676-06020140039

Ramos TPA, Lima JAS, Costa SYL, Silva MJ, Avellar RC, Oliveira-Silva L (2018) Continental ichthyofauna from the Paraíba do Norte River basin pre-transposition of the São Francisco River, Northeastern Brazil. Biota Neotropica 18(4): e20170471. https://doi.org/10.1590/1676-0611-bn-2017-0471

Rasband WS (1997–2016) IMAGEJ, U.S. National Institutes of Health, Bethesda, Maryland, USA. http://imagej.nih.gov/ij/ [accessed on 15 Mar 2019]

Reichenbacher B, Sienknecht U, Küchenhoff H, Fenske N (2007) Combined otolith morphology and morphometry for assessing taxonomy and diversity in fossil and extant killifish (*Aphanius*, †*Prolebias*). Journal of Morphology 268(10): 898–915. https://doi.org/10.1002/jmor.10561

Reichenbacher B, Kamrani E, Esmaeili HR, Teimori A (2009a) The endangered cyprinodont *Aphanius ginaonis* (Holly, 1929) from southern Iran is a valid species: Evidence from otolith morphology. Environmental Biology of Fishes 86(4): 507–521. https://doi.org/10.1007/s10641-009-9549-5

Reichenbacher B, Feulner GR, Schulz-Mirbach T (2009b) Geographic variation in otolith morphology among freshwater populations of *Aphanius dispar* (Teleostei, Cyprinodontiformes) from the southeastern Arabian Peninsula. Journal of Morphology 270(4): 469–484. https://doi.org/10.1002/jmor.10702

Reid NM, Carstens BC (2012) Phylogenetic estimation error can decrease the accuracy of species delimitation: A Bayesian implementation of the general mixed Yule-coalescent model. BMC Evolutionary Biology 12(1): 1–11. https://doi.org/10.1186/1471-2148-12-196

Rengifo A (1989) Diagnóstico preliminar de la situación actual de la íctiofauna con valor ornamental. Serie de Informes Técnicos. PROFAUNA/IT/01, Ministerio del Ambiente y los Recursos Naturales Renovables, Caracas, 50 pp.

Robins CR, Bailey RM, Bond CE, Brooker JR, Lachner EA, Lea RN, Scott WB (1991) World fishes important to North Americans. Exclusive of species from the continental waters of the United States and Canada. American Fisheries Society Special Publication 21, 243 pp.

Rodríguez MA, Lewis Jr WM (1990) Diversity and species composition of fish communities of Orinoco floodplain lakes. National Geographic Research 6: 319–328.

Rodríguez MA, Lewis Jr WM (1997) Structure of fish assemblages along environmental gradients in floodplain lakes of the Orinoco River. Ecological Monographs 67(1): 109–128. https://doi.org/10.1890/0012-9615(1997)067[0109:SOFAAE]2.0.CO;2

Rodríguez-Barrera R, Zapata-Arroyo C, Falcón W, Olmeda ML (2020) An island invaded by exotics: A review of freshwater fish in Puerto Rico. Neotropical Biodiversity 6(1): 42–59. https://doi.org/10.1080/23766808.2020.1729303

Rodríguez-Olarte D, Taphorn DC, Lasso C, Vispo C (2003) Fishes of the lower Caura River, Orinoco Basin, Venezuela. In: Vispo C, Knab-Vispo C (Eds) Plants and Vertebrates of the Caura's Riparian Corridor: Their Biology, Use and Conservation. Scientia Guianae 12: 181–221.

Román B (1981) Los Pavones. Colección: Los peces de los Llanos de Venezuela. Fundación Científica Fluvial de los Llanos, Caracas, 143 pp.

Román B (1985) Peces de agua dulce de Venezuela. Editorial Biosfera, Caracas, 192 pp.

Román B (1988) Los Pavones. Colección: Los peces de los Llanos de Venezuela. Fundación Científica Fluvial de los Llanos, Caracas, 143 pp.

Román B (1992) Peces ornamentales de Venezuela. Monografía 39, Fundación La Salle de Ciencias Naturales, Caracas, 223 pp.

Royero R (1993) Peces ornamentales de Venezuela. Cuadernos Lagoven. Caracas, 106 pp.

Royero R, Lasso C (1992) Distribución actual de la mojarra de río *Caquetaia kraussii* (Steindachner, 1878) (Perciformes: Cichlidae) en Venezuela: un ejemplo del problema de la introducción de especies. Memorias de la Sociedad de Ciencias Naturales La Salle 52(138): 163–180.

Sabaj MH (2016) Standard Symbolic Codes for Institutional Resource Collections in Herpetology and Ichthyology. Washington, DC: American Society of Ichthyologists and Herpetologists. www.asih.org/sites/default/files/documents/symbolic_codes_for_collections_v6.5_201 [accessed on 08/04/2018]

Sánchez E (2008) Diccionario puinave-español y la oración gramatical. s.l. CIRCUI/Centro de Investigaciones del Rescate Cultural Puinave Autóctonos, Inírida, 104 pp.

Sarkar IN, Planet PJ, DeSalle R (2008) CAOS software for use in character-based DNA barcoding. Molecular Ecology Resources 8(6): 1256–1259. https://doi.org/10.1111/j.1755-0998.2008.02235.x

Schomburgk RH (1843) The natural history of fishes of Guiana, part II. In: Jardine W (Ed.) The Naturalists' Library. Vol. 5. W. H. Lizars, Edinburgh.

Schwarzhans W (1978) Otolith-morphology and its usage for higher systematical units, with special reference to the Myctophiformes s.l. Mededelingen van de Werkgroep voor Tertiaire Kwartaire Geologie 15: 167–185.

Schwarzhans W (1993) A comparative morphological treatise of recent and fossil otoliths of the family Sciaenidae (Perciformes). Piscium Catalogas Part Otolithi. Piscium 1: 1–245.

Señaris JC, Lasso C (1993) Ecología alimentaria y reproductiva de la mojarra de río *Caquetaia kraussii* (Steindachner 1878) (Cichlidae) en los Llanos inundables de Venezuela. Publicaciones de la Asociación Amigos de Doñana 2: 1–58.

Sibilia A, Andreata J (1991) Osteology of the caudal fin of some species of Cichlidae (Pisces, Perciformes, Labroidei). Revista Brasileira de Zoologia 7(3): 307–318. https://doi.org/10.1590/S0101-81751990000300013

Silva AT, Chagas RJ, Santos AC de A, Zanata AM, Rodrigues BK, Polaz CNM, Alves CBM, Vieira CS, Souza FB, Vieira F, Sampaio FAC, Ferreira H, Alves HSR, Sarmento-Soares LM, Pinho M, Martins-Pinheiro RF, Lima SMQ, Campiolo S, Camelier P (2020) Freshwater fishes of the Bahia State, northeastern Brazil. Biota Neotropica 20(4): e20200969. [21 pp] https://doi.org/10.1590/1676-0611-bn-2020-0969

Sioli H (1965) Bemerkung zur typologie amazonischer flussen. Amazoniana 1(1): 74–83.

Solarz W (2005) Alien Species in Poland: Institute of Nature Conservation, Polish Academy of Sciences, Warsaw, 43–51.

Sparks JS, Stiassny MLJ (2010) A new species of *Ptychochromis* from northeastern Madagascar (Teleostei: Cichlidae), with an updated phylogeny and revised diagnosis for the genus. Zootaxa 2341(1): 33–51. https://doi.org/10.11646/zootaxa.2341.1.1

Spix JB, von Agassiz L (1829) Selecta genera et species piscium quos in itinere per Brasiliam annis MDCCCXVII–MDCCCXX jussu et auspiciis Maximiliani Josephi I.... collegit et pingendos curavit Dr J. B. de Spix.... Monachii. Part 1: [i–xvi + i–ii + 1–6 +] 1–82[, Pls. 1–48], Part 2: 83–138[, Pls. 49–101]. https://doi.org/10.5962/bhl.title.9366

Stiassny MLJ, Alter SE, Monsembula Iyaba RJC, Liyandja TLD (2021) Two new *Phenacogrammus* (Characoidei; Alestidae) from the Ndzaa River (Mfimi-Lukenie basin) of Central Africa, Democratic Republic of Congo. American Museum Novitates 3980(3980): 1–22. https://doi.org/10.1206/3980.1

Taphorn DC, Lilyestrom CG (1984) Los peces del módulo “Fernando Corrales”. Resultados ictiológicos del proyecto de investigación del CONICIT - PIMA 18. Biollania 2: 55–86.

Taphorn DC, Rodriguez-Olarte D, Hurtado N, Barbarino D (2005) Los peces y las pesquerías en el Parque Nacional Aguarico-Guariquito, Estado Guárico, Venezuela. Memoria de la Fundación la Salle de Ciencias Naturales 161–162: 19–40.

Thieme P, Schnell NK, Parkinson K, Moritz T (2022) Morphological characters in light of new molecular phylogenies: The caudal-fin skeleton of Ovalentaria. Royal Society Open Science 9(1): e211605. [27 pp] https://doi.org/10.1098/rsos.211605

Toffoli D, Hrbek T, de Araujo ML, de Almeida MP, Charvet-Almeida P, Farias IP (2008) A test of the utility of DNA barcoding in the radiation of the freshwater stingray genus *Potamotrygon* (Potamotrygonidae, Myliobatiformes). Genetics and Molecular Biology 31(1): 324–336. https://doi.org/10.1590/S1415-47572008000200028

Usma S, Maldonado-Ocampo JA, Villa-Navarro FA, Ortega-Lara A, Taphorn D, Urbano-Bonilla A, Zamudio JE, DoNascimiento C (2016) Peces de la cuenca del río Meta. In: Trujillo F, Antelo R, Usma S (Eds) Biodiversidad de la cuenca baja y media del río Meta. Fundación Omacha, Fundación Palmarito, WWF. Bogotá, 104–121. [336 pp]

Villa-Navarro F, Urbano-Bonilla A, Ortega-Lara A, Taphorn DC, Usma JS (2011) Peces del Casanare. In: Usma JS, Trujillo F (Eds) Biodiversidad del Casanare: Ecosistemas Estratégicos del Departamento. Gobernación de Casanare – WWF Colombia. Bogotá, 120–137. [286 pp]

Vispo C, Knab-Vispo C (2003) A general description of the lower Caura. plantas and vertebrates of the Cauras riparian corridor: their biology, use and conservation. Scientia Guianæ 12: 1–34.

Wijkmark N, Kullander S, Barriga R (2012) *Andinoacara blombergi*, a new species from the río Esmeraldas basin in Ecuador and a review of *A. rivulatus* (Teleostei: Cichlidae). Ichthyological Exploration of Freshwaters 23(2): 117–137.

Winemiller KO (1989a) Ontogenetic diet shifts and resource partitioning among piscivorous fishes in the Venezuelan llanos. Environmental Biology of Fishes 26(3): 177–199. https://doi.org/10.1007/BF00004815

Winemiller KO (1989b) Patterns of variation in life history among South American fishes in seasonal environments. Oecologia 81(2): 225–241. https://doi.org/10.1007/BF00379810

Winemiller KO (1990) Caudal Eyespots as Deterrents against Fin Predation in the Neotropical Cichlid *Astronotus ocellatus*. Copeia 3(3): 665–673. https://doi.org/10.2307/1446432

Winemiller KO (1991) Ecomorphological diversification in lowland freshwater fish from five biotic regions. Ecological Monographs 61(4): 343–365. https://doi.org/10.2307/2937046

Winemiller KO (1996) Dynamic Diversity in Fish Assemblages of Tropical Rivers. In: Cody ML, Smallwood JA (Eds) Long-term Studies of Vertebrate Communities. Academic Press, Orlando, Florida, 99–134. https://doi.org/10.1016/B978-012178075-3/50006-4

Winemiller KO, Marrero C, Taphorn DC (1996) Perturbaciones causadas por el hombre a las poblaciones de peces de los llanos y del piedemonte andino de Venezuela. Biollania 12: 13–48.

Winemiller KO, Taphorn DC, Kelso-Winemiller LC, López-Delgado EO, Keppeler FW, Montaña CG (2018) Fish metacommunity structure in Caño Maraca, an important nursery habitat in the Western Llanos of Venezuela. Neotropical Ichthyology 16(4): e180074. https://doi.org/10.1590/1982-0224-20180074

Yu G, Smith DK, Zhu H, Guan Y, Lam TTY (2017) Ggtree: An R package for visualization and annotation of phylogenetic trees with their covariates and other associated data. Methods in Ecology and Evolution 8(1): 28–36. https://doi.org/10.1111/2041-210X.12628

Supplementary material 1

Table S1–S5

Authors: Alfredo Perez, Oscar M. Lasso-Alcalá, Pedro S. Bittencourt, Donald C. Taphorn, Nayibe Perez, Izeni Pires Farias

Data type: Description of biometric indices used in otoliths

Explanatory note: Ratio and shape index used in morphometric analysis of otoliths from species of genus *Astronotus*.

Link: https://doi.org/10.3897/zookeys.1113.81240.suppl1

Supplementary material 2

Figure S1

Authors: Alfredo Perez, Oscar M. Lasso-Alcalá, Pedro S. Bittencourt, Donald C. Taphorn, Nayibe Perez, Izeni Pires Farias

Data type: Phylogenetic cladogram of all *Astronotus* species

Explanatory note: Neighbour Joining phylogenetic tree showing relationships among all 102 COI sequences of *Astronotus* plus five *Cichla ocellaris* sequences as outgroup.

Link: https://doi.org/10.3897/zookeys.1113.81240.suppl2

Supplementary material 3

Data S1

Authors: Alfredo Perez, Oscar M. Lasso-Alcalá, Pedro S. Bittencourt, Donald C. Taphorn, Nayibe Perez, Izeni Pires Farias

Data type: Metadata for all the sequences DNA used in this study are presented as a spreadsheet format xls, following the standard Darwin core format

Explanatory note: Metadata for all sequences generated in this study, sequences obtained from Colatreli et. al. (2012), and sequences downloaded from the GenBank nucleotide database.

Link: https://doi.org/10.3897/zookeys.1113.81240.suppl3

ZooKeys 1113: 153–166 (2022)
doi: 10.3897/zookeys.1113.79721
https://zookeys.pensoft.net

RESEARCH ARTICLE

A peer-reviewed open-access journal
ZooKeys
Launched to accelerate biodiversity research

Systematic review of the firefly genus *Emeia* Fu, Ballantyne & Lambkin, 2012 (Coleoptera, Lampyridae) from China

Cheng-Qi Zhu[1,2,3], Xiao-Dong Xu[2,3], Ying Zhen[2,3]

1 *College of Life Sciences, Zhejiang University, Hangzhou, Zhejiang, China* **2** *Westlake Laboratory of Life Sciences and Biomedicine, Key Laboratory of Structural Biology of Zhejiang Province, School of Life Sciences, Westlake University, Hangzhou, Zhejiang, China* **3** *Institute of Biology, Westlake Institute for Advanced Study, Hangzhou, Zhejiang Province, China*

Corresponding authors: Cheng-Qi Zhu (zhuchengqi@westlake.edu.cn), Ying Zhen (zhenying@westlake.edu.cn)

Academic editor: Hume Douglas | Received 23 December 2021 | Accepted 26 May 2022 | Published 18 July 2022

https://zoobank.org/05FD427F-8311-48F9-BB65-A490BC674622

Citation: Zhu C-Q, Xu X-D, Zhen Y (2022) Systematic review of the firefly genus *Emeia* Fu, Ballantyne & Lambkin, 2012 (Coleoptera, Lampyridae) from China. ZooKeys 1113: 153–166. https://doi.org/10.3897/zookeys.1113.79721

Abstract

The Luciolinae genus *Emeia* Fu, Ballantyne & Lambkin, 2012 is reviewed. Phylogenetic relationships based on *cox1* DNA barcoding sequences from 42 fireflies and 2 outgroup species are reconstructed. The dataset included three main Lampyridae subfamilies: Luciolinae, Photurinae and Lampyrinae, and *Emeia* was recovered within Luciolinae. A new species, *Emeia pulchra* Zhu & Zhen **sp. nov.**, is described from the wetland of Lishui, Zhejiang, China. *Emeia pulchra* is sister species to *E. pseudosauteri* from Sichuan, which is supported by morphological characters and a phylogeny based on DNA barcoding sequences. The two species are separated geographically as shown on the distribution map. A key to species of *Emeia* using males is provided.

Keywords

Cytochrome c oxidase subunit I , DNA barcoding, *Emeia*, firefly, Lampyridae

Introduction

Emeia Fu, Ballantyne & Lambkin, 2012 (Luciolinae) was established as a monotypic genus (Fu et al. 2012) with *Emeia pseudosauteri* (Geisthardt 2004) as the type species. *Emeia pseudosauteri* was first described from Mount Emei, Sichuan, China by Michael

Geisthardt in the genus *Curtos* Motschulsky, 1845 (Geisthardt 2004), and then transferred to *Emeia* based on morphological evidence (Fu et al. 2012). The genus *Emeia* Fu, Ballantyne & Lambkin had only one species (*E. pseudosauteri*) recorded in China before this study. The primary phenotypic feature of *Emeia* was the trilobite-like larva. The thoracic and abdominal terga of *Emeia* larvae are distinct. The lateral thoracic tergal margins are broad, similar to those of a trilobite "cephalon", while the abdomen is narrow and curls ventrad in the posterior part. At present, definition of the genus *Emeia* is based on the morphology of *E. pseudosauteri*, which makes it insufficient in light of the discovery of a second species.

In this study, based on specimens collected from Lishui, Zhejiang, China, we describe adults of *Emeia pulchra* Zhu & Zhen sp. nov. based on morphological and molecular data. We compare it with the previously described *E. pseudosauteri*. We also provide new information on the adult male hind wing venation of the type species *E.pseudosauteri.* With our detailed examination of both species, we present a systematic review of the genus *Emeia* and a key to species.

Materials and methods

Abbreviations

EL elytral length;
EW elytral width;
PL pronotal length;
BL body length (the sum of PL, EL and the length of the exposed portions of the head from the pronotum);
BW body width (the greatest distance across the elytra, BW=2EW);
T7, 8 abdominal tergite numbers;
V6, 7 abdominal ventrite numbers.

Adult males of *Emeia pulchra* Zhu & Zhen sp. nov. were collected from Jiulong National Wetland Park, Lishui, Zhejiang Province in April, 2020. The holotype and paratypes of the new species are stored at School of Life Sciences, Westlake University, Hangzhou, Zhejiang. Samples of both male and female *Emeia pseudosauteri* were collected from Mt. Tian Tai, Sichuan Province in April, 2021.

Habitus images were taken using a Nikon D7500 camera. Images of genitalia were taken using a Nikon D7500 camera mounted on an SZ650 microscope (Chongqing Optec Instrument Co., Ltd.) under reflection or transmission light. Images were edited using Adobe Photoshop CS6. Morphological terminology and measurements follow those decribed in Douglas (2017). The body length (**BL**) is the sum of the pronotal length (**PL**) and elytral length (**EL**) plus the length of the exposed portions of the head from the pronotum. The abbreviations **EW** and **BW** (**BW=2EW**) denote elytral width and body width, respectively (Fig. 1A). The length

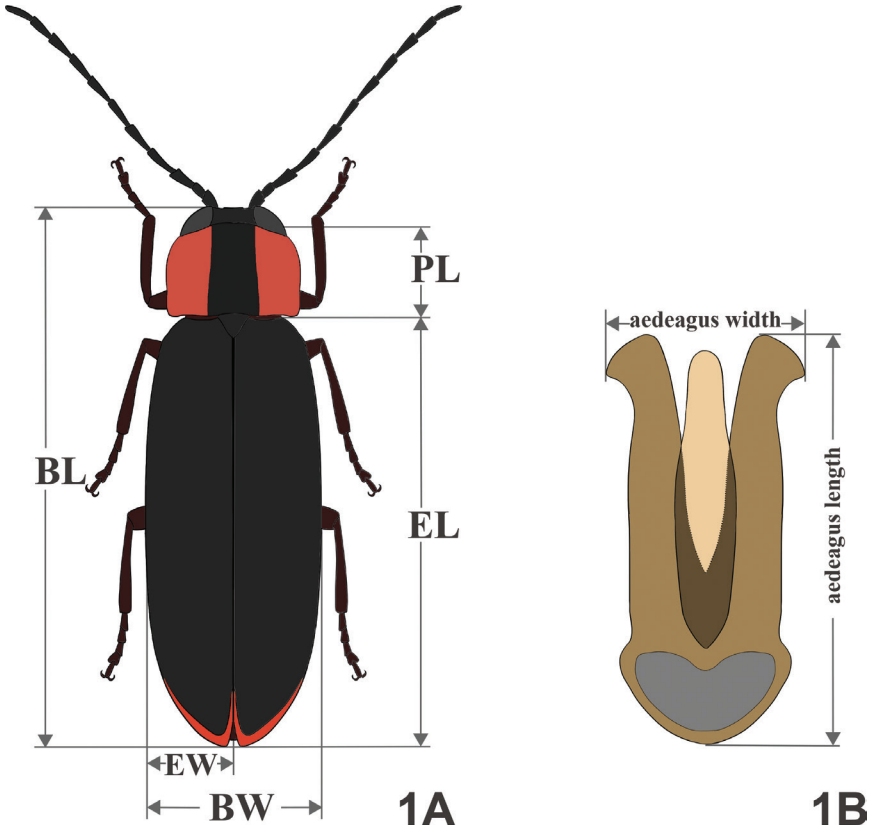

Figure 1. Measurement methods and terminology **A** male habitus, dorsal view **B** aedeagus, ventral view.

and width of the aedeagus and aedeagal sheath were measured under the microscope using the OLYMPUS cellSens Dimension software (v 3.1.1) (Fig. 1B). The dissected aedeagus and aedeagal sheath structures are preserved in pure glycerol in small vials with the corresponding specimens.

We sequenced the *cox1* gene barcode fragment from *Emeia pseudosauteri* and *E. pulchra*. Specifically, total DNA of the two *Emeia* species was isolated using the DNeasy Blood and Tissue Kit (Zhejiang Easy-Do Biotech CO., Ltd.), according to the manufacturer's protocol. The primers LCO 1490 and HCO 2198 (Folmer et al. 1994) were used to amplify the barcode fragments of the mitochondrial gene cytochrome c oxidase subunit I (*cox1*). We performed the PCR reaction in a 25 μL reaction mix containing 1× PCR buffer, 1 μL of each primer in a final concentration of 1 μM, 1 μL of template, 0.2 mM of each dNTP and 0.5 units of Taq polymerase (Takara Biomedical Technology CO., Ltd). The PCR thermal regime consisted of an initial denaturation at 95 °C for 3 min; 30 cycles of 30 s at 94 °C, 30 s at 48 °C and 30 s at 72 °C, followed by a 5 min final extension at 72 °C. PCR products were checked by electrophoresis in 1% agarose gel at 170 V for 20 min, and visualized under a UV transilluminator with nucleic acid dye (Cofitt Life Science, Hong Kong). The PCR products were cleaned

using Easy Gel Extraction & Clean-up kit (Zhejiang Easy-Do Biotech CO., Ltd.). The cleaned products were sequenced with an ABI 3730XL sequencer (Applied Biosystems, California, USA) by Zhejiang Sunya Biotechnology Co., Ltd.

MEGA6 (Tamura et al. 2013) was used for phylogenetic reconstruction. *Cox1* barcode sequences from three main subfamilies, *i.e.*, Luciolinae, Photurinae and Lampyrinae, were included, and sequences from the family Rhagophthalmidae were used as an outgroup (Table 1). The maximum likelihood method was used with 1000 boot-

Table 1. Genbank accession numbers for *cox1* sequences used for the phylogenetic analysis.

Species	Family	Sub-family	GenBank id
Pyrocoelia pectoralis	Lampyridae	Lampyrinae	KP763467.1
Pyrocoelia rufa	Lampyridae	Lampyrinae	AF452048.1
Pyrocoelia abdominalis	Lampyridae	Lampyrinae	AB608766.1
Pyrocoelia atripennis	Lampyridae	Lampyrinae	AB608767.1
Pyrocoelia discicollis	Lampyridae	Lampyrinae	AB608768.1
Pyrocoelia fumosa	Lampyridae	Lampyrinae	AB608769.1
Pyrocoelia matsumurai	Lampyridae	Lampyrinae	AB608770.1
Diaphanes nubilus	Lampyridae	Lampyrinae	MG200080.1
Diaphanes pectinealis	Lampyridae	Lampyrinae	NC_044793.1
Photinus pyralis	Lampyridae	Lampyrinae	KY778696.1
Ellychnia corrusca	Lampyridae	Lampyrinae	KR483038.1
Ellychnia hatchi	Lampyridae	Lampyrinae	JF887410.1
Pyractomena lucifera	Lampyridae	Lampyrinae	MF640134.1
Pyractomena borealis	Lampyridae	Lampyrinae	HQ928227.1
Pyractomena angulata	Lampyridae	Lampyrinae	JN290381.1
Aspisoma sp.	Lampyridae	Lampyrinae	EU009322.1
Lucidina accensa	Lampyridae	Lampyrinae	AB608771.1
Lucidina kotbandia	Lampyridae	Lampyrinae	FJ462784.1
Lucidota atra	Lampyridae	Lampyrinae	HQ984304.1
Photuris pensylvanica	Lampyridae	Photurinae	MF634963.1
Photuris quadrifulgens	Lampyridae	Photurinae	HM433520.1
Bicellonycha lividipennis	Lampyridae	Photurinae	KJ922151.1
Bicellonycha wickershamorum	Lampyridae	Photurinae	EU009302.1
Pristolycus sp.	Lampyridae	Luciolinae	MK292099.1
Sclerotia flavida	Lampyridae	Luciolinae	KP763460.1
Sclerotia aquatilis	Lampyridae	Luciolinae	KP763466.1
Pygoluciola dunguna	Lampyridae	Luciolinae	MT106243.1
Pygoluciola qingyu	Lampyridae	Luciolinae	MK292093.1
Curtos bilineatus	Lampyridae	Luciolinae	NC_044789.1
Curtos costipennis	Lampyridae	Luciolinae	AB608764.1
Abscondita terminalis	Lampyridae	Luciolinae	NC_044776.1
Abscondita anceyi	Lampyridae	Luciolinae	NC_039706.1
Emeia pseudosauteri 1	Lampyridae	Luciolinae	MN722654.1
Emeia pseudosauteri 2	Lampyridae	Luciolinae	OK103803
Emeia pulchra	Lampyridae	Luciolinae	OK144132
Luciola italica	Lampyridae	Luciolinae	KM448530.1
Asymmetricata circumdata	Lampyridae	Luciolinae	NC_032062.1
Drilaster axillaris	Lampyridae	Ototretinae	AB608756.1
Drilaster okinawensis	Lampyridae	Ototretinae	AB608758.1
Stenocladius yoshikawai	Lampyridae	Ototretinae	AB608759.1
Lamprigera yunnana	Lampyridae	*incertae_sedis*	MG200082.1
Cyphonocerus marginatus	Lampyridae	Cyphonocerinae	AB608754.1
Rhagophthalmus lufengensis	Rhagophthalmidae	–	DQ888607.1
Rhagophthalmus ohbai	Rhagophthalmidae	–	AB608775.1

strap replicates (Fig. 2). The phylogenetic relationships were displayed using iTOL (v6; https://itol.embl.de/). The new *cox1* sequences from *Emeia* have been deposited in GenBank (accession numbers OK144132 and OK103803).

Results

Phylogenetic analysis

The *cox1* barcode sequences of *E. pseudosauteri* and *E. pulchra* share a 94% sequence identity over the 658 bp segment. The phylogeny constructed from *cox1* of fireflies showed three main clades corresponding to Lampyrinae, Photurinae and Luciolinae (Fig. 2). *Emeia pseudosauteri* was recovered as sister to *E. pulchra* Zhu & Zhen sp. nov. within the subfamily Luciolinae, with strong support (100%).

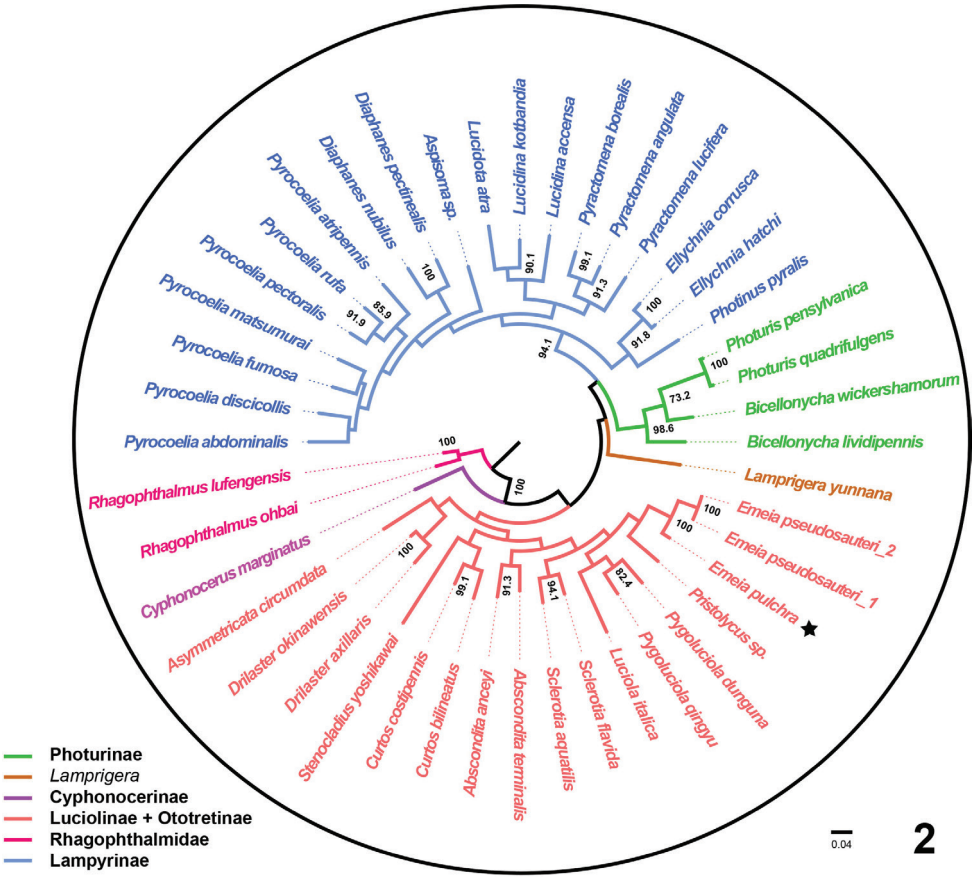

Figure 2. Maximum likelihood *cox1* gene tree of *Emeia* and related genera. The star highlights the new species, *E. pulchra* Zhu & Zhen sp. nov. *Emeia pseudosauteri*_1 was downloaded from GenBank (MN722654.1). *Emeia pseudosauteri*_2 was sequenced during this study. Bootstrap values greater than 0.7 from 1000 replicates are shown.

Taxonomic treatment

Emeia Fu, Ballantyne & Lambkin, 2012

Type species. *Emeia pseudosauteri* Geisthardt, 2004 (designated by Fu, Ballantyne and Lambkin 2012).

Diagnosis (based on adult male). *Emeia* belongs to a group of Luciolinae in which the males have aedeagal parameres widely visible beside the phallus (Ballantyne et al. 2013). *Emeia* differs from *Aquatica wuhana* Fu & Ballantyne, 2010 and *A. lateralis* Motschulsky, 1860, which have black marks on the pronotum (Fu et al. 2010). *Emeia* is distinguished from *Curtos* Motschulsky, 1845, as the species in *Curtos* have a distinctive longitudinal elytral humeral carina and parameres unequal in length (Fu et al. 2012). *Emeia* is closely related to *Pygoluciola* based on our *cox1* phylogeny (Fig. 2), but the two genera can be distinguished by the shape of the pronotum, with median anterior margin gently rounded or slightly medianly emarginate in *Pygoluciola* (Ballantyne and Lambkin 2006) versus lateral margins of pronotum almost parallel in *Emeia*.

Description (based on adult male). Body length 6.5–10.5 mm. Body width 2.7–4.0 mm. Integument black or dark brown, with a narrow (e.g., in *E. pulchra*, see Fig. 3A) or thick (e.g., in *E. pseudosauteri*, see Fig. 8A) black stripe on pronotum.

Head. Hypognathous; head depressed between eyes, eyes exposed in front of pronotum; antennae filiform, with 11 antennomeres (Figs 3B, 8B).

Thorax. Pronotum in dorsal view appearing pink-red or orange-red, with a black median stripe, lateral margins almost parallel (Figs 3A, 8A); surface of elytra smooth, longitudinal carina absent (Figs 3A, 8A); legs long and straight, no femora or tibiae swollen or curved (Figs 3B, 8B).

Abdomen. V2–V5 dark brown or black. Light organs present in V6 and V7, entirely occupying V6; V7 semitransparent (Figs 3B, 8B).

Male genitalia. Trilobate, parameres extending ~0.14 mm (n = 3) beyond phallus; both parameres equal in length (Figs 6A, 12A).

Emeia pulchra Zhu & Zhen, sp. nov.

https://zoobank.org/45330183-64CB-45CE-A2E4-7E013ECECB00
Figs 3–6

Diagnosis (based on adult male). The new species can be differentiated from *E. pseudosauteri* Fu, Ballantyne & Lambkinby the elytron, hindwing venation and aedeagus. In fresh specimens, the elytral apices are black in *E. pulchra* (Fig. 3), but with a narrow orange stripe in *E. pseudosauteri* (Fig. 8). In the male hindwing, the upper vein of the MP_{3+4} venation in *E. pulchra* reaches the margin of the hind wings without

forks (n=2) (Fig. 4). In *E. pseudosauteri*, the upper vein of MP_{3+4} forks and reaches the margin of the hind wings (n=2) (Fig. 10). The aedeagus in *E. pulchra* is approx. 3 times as long as wide (length 1.77 mm: width 0.58 mm) (Fig. 6A), versus approx. 2 times as long as wide (length 1.66 mm: width 0.84 mm) in *E. pseudosauteri* (Fig. 12A).

Description. Male: BL 10.0–10.4 mm; BW 3.5–3.7 mm (three individuals).

Head. Antennae filiform, black, almost 2/3 as long as body length; antennomere 1 cone-shaped; 2 short and cylindrical; 3 to 10 compressed, not bifurcate; 11th antennomere almost 1.5 times longer than 10th, slightly dilated from base to apex. Concave between eyes dorsally in cross section, both eyes occupying about 2/3 width of whole head in ventral view. Eyes spherical, so that head cannot fully contract into pronotum. Mouthparts fully developed, clypeolabral suture flexible, outer edges of labrum reaching inner edges of closed mandibles.

Thorax. Scutellum black and slightly emarginate distally. Elytra elongated, dark brown to black, apices not deflexed in dorsal view, sides slightly convex. Hind wing well developed, r3 half the length of r4 (Fig. 4). Legs long and straight, without swelling on any part, dark brown to black, with dense white hairs.

Abdomen. Dark brown, ventrites gradually diminishing in length posterad. Light organs yellow-white, occupying almost all of V6 and half of V7, not reaching to posterior edges of V7. V6 and V7 rounded laterally (Fig. 5), posterior half of V7 not arched in dorsal view, abruptly narrowed to truncate posterior apex, apex emarginate (Fig. 5C). T7 rounded, without anterolateral corners (Fig. 5A); T8 symmetrical with concealed anterolateral arms, widest across middle with lateral margins subparallel-sided in anterior half, tapering evenly in posterior half to a rounded and partly truncate posterior margin (Fig. 5B). Abdominal spiracles on lateral edges of each abdominal segments. EL/EW = 4.7–4.8; EL/PL= 4.7–5.0 (n=3).

Male genitalia (Fig. 6): Aedeagal sheath (T9, T10, S9) (Fig. 6D, E) 3.15 mm long; anterior half of sternite broad, apically rounded; tergite without protrusion along posterior margin of T9. Aedeagus (Fig. 6A–C) 1.61 mm long. Phallus short (~1.2 mm) and thick, broadest at midlength, becoming thinner at apex and base, parameres (lateral lobes) extending about 0.14 mm beyond phallus. Parameres robust, subparallel-sided, symmetrical, with blunt preapical lateral expansion.

Etymology. The specific name *pulchra* refers to the bright pronotum coloration.

Holotype. China • 1♂; Zhejiang, Lishui; 28°37.56'N, 119°49.7'E; H: 60 m, 2. IV. 2020; Chengqi Zhu leg.; 'HOLOTYPE (red), ♂, *Emeia pulchra* sp. nov., det. Zhu, Zhen, 2021' (Westlake University).

Paratype. China • 1♂; Zhejiang, Lishui; 28°37.56'N, 119°49.7'E; H: 60 m, 2. IV. 2020; Chengqi Zhu leg.; 'PARATYPE (yellow), ♂, *Emeia pulchra* sp. nov., det. Zhu, Zhen, 2021' (Westlake University).

Distribution. China: Zhejiang Province.

Habitat and occurrence. The males were found in an open forest of mainly Chinese wingnut, of the family Juglandaceae [*Pterocarya stenoptera* C. DC.] (Fig.

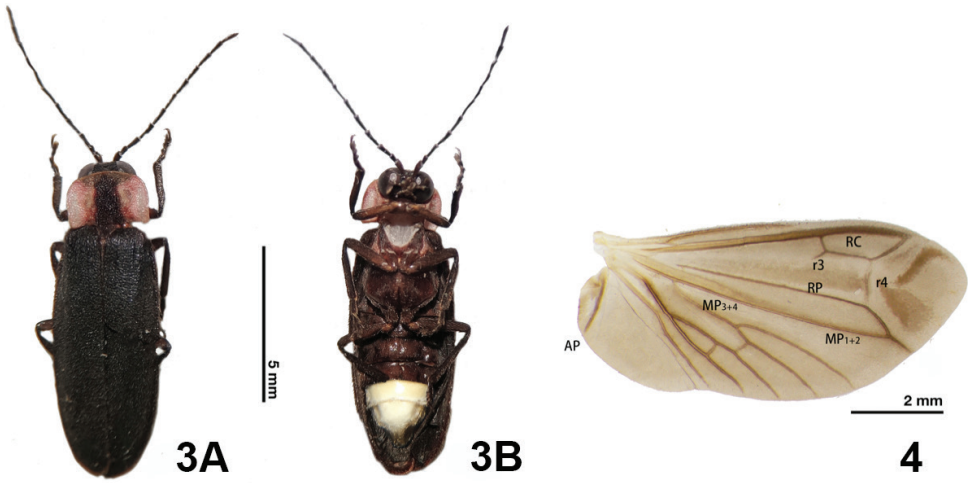

Figures 3–4. *Emeia pulchra* Zhu & Zhen sp. nov., male **3** habitus of holotype **A** dorsal view **B** ventral view **4** right wing, dorsal view. Scale bars: 5 mm (**3**); 2 mm (**4**).

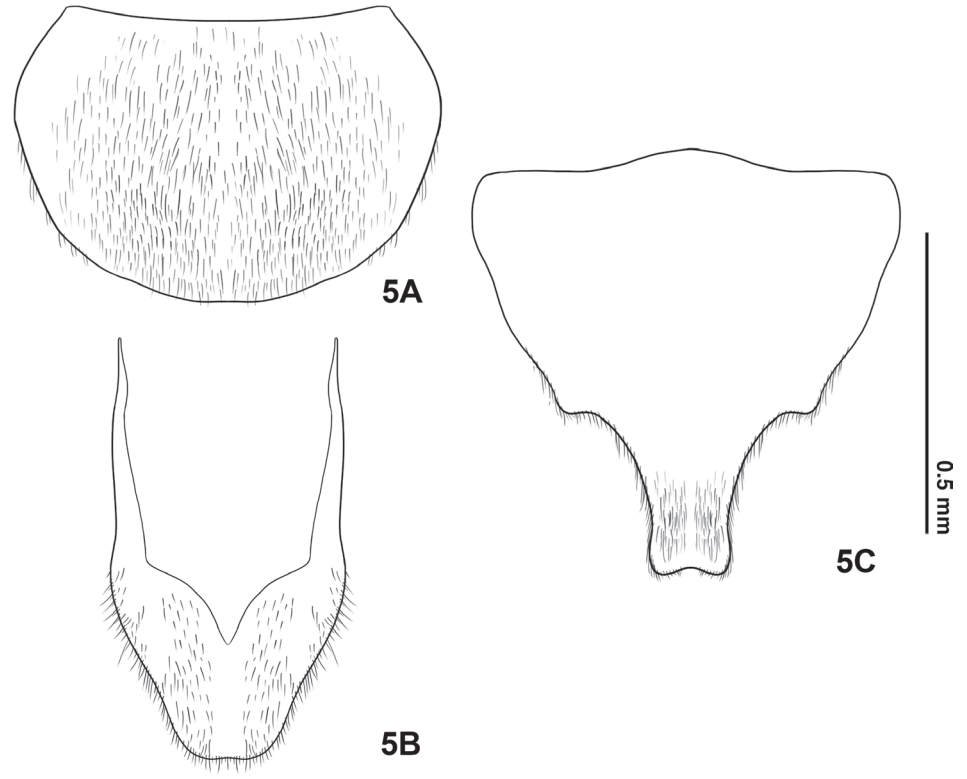

Figure 5. Male abdominal ventrites (V) and tergites (T) of *Emeia pulchra* Zhu & Zhen, sp. nov. **A** T7 **B** T8 **C** V7. Scale bar: 0.5 mm.

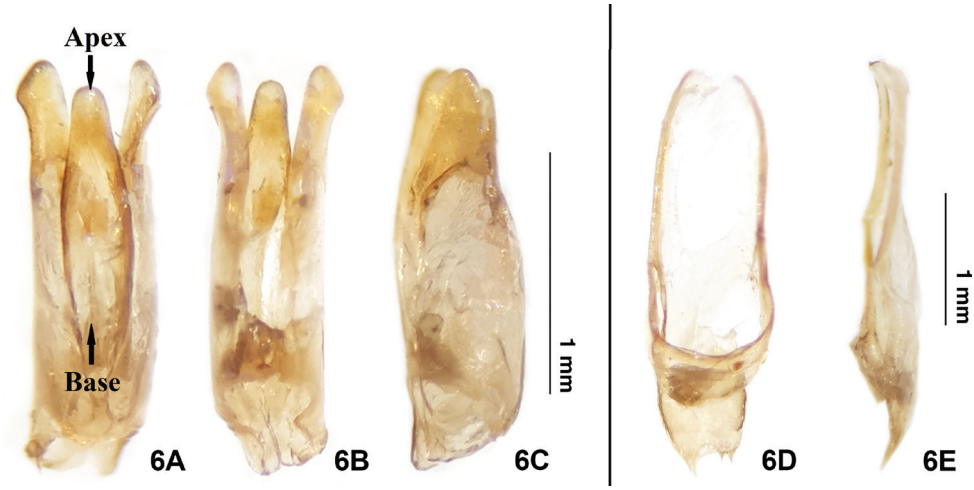

Figure 6. Aedeagusof *Emeia pulchra* Zhu & Zhen sp. nov. **A** dorsal view **B** ventral view **C** lateral view. Aedeagal sheath of *E. pulchra* **D** dorsal view **E** ventral view. Scale bar: 1 mm.

Figure 7. Habitat of *Emeia pulchra* Zhu & Zhen sp. nov. in Jiulong National Wetland Park.

7). The floor of the *Emeia pulchra* habitat was covered with a lush herbaceous layer 20–30 cm high.

There are many terrestrial snails and slugs in this habitat, which may be potential food for *Emeia pulchra* larvae. Combining descriptions from local people and our field observations, adult fireflies are usually observed mid-March. The protection of fireflies has been supported by the Lishui government and Jiulong National Wetland

Park management departments, and this area has been protected as Jiulong National Wetland Park (Fig. 7). Fan (2019) reported that the population size of *E. pulchra* has increased from 2014 to 2019 with the protection efforts.

Behavioral remarks. There are two obvious luminous bands at the terminal end of the adult male abdomen. The two bands both emit intermittent bright light during courtship. The male courtship behavior usually starts at 19:00 (approximately 1h after sunset), and peaks at about 20:30. Adult males rest on higher herbs and emit yellow and green flashing light. Males are reluctant flyers; the distance of each flight ranges from 0.5 to 5 m.

Emeia pseudosauteri (Geisthardt 2004)

Figs 8–12

Emeia pseudosauteri (Geisthardt 2004). *Zootaxa* (3403), 1–53. TL: 'Mt. Tian Tai, Sichuan Province, China'.

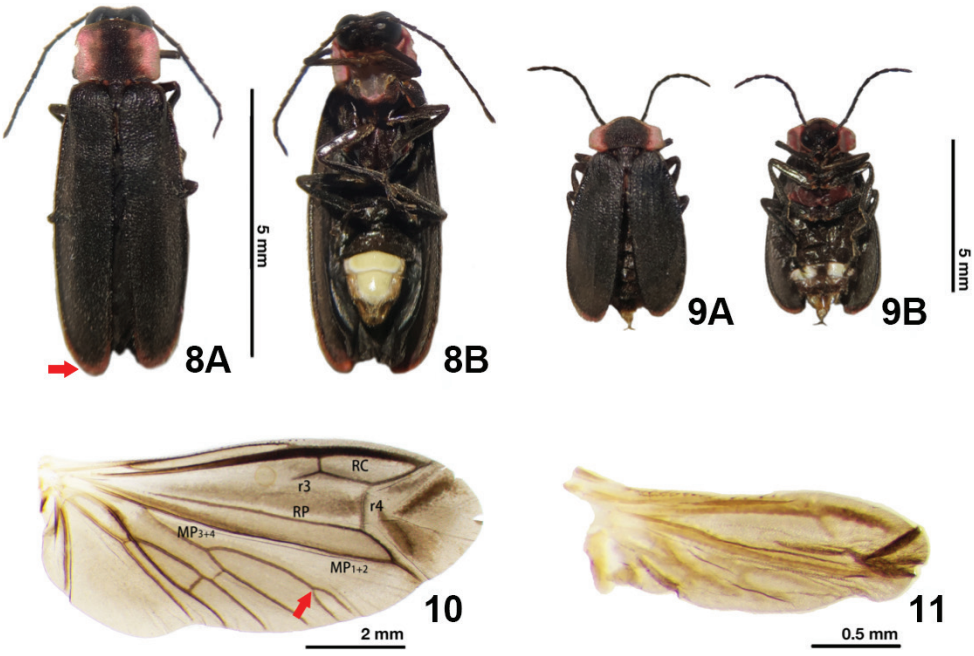

Figures 8–11. *Emeia pseudosauteri* Fu, Ballantyne & Lambkin, 2012. Male and female **8** habitus of male **A** dorsal view. Arrow highlights narrow orange stripe on elytral apices. The color appears darker in this photo, but it is orange and easily seen in both dried and fresh samples **B** ventral view **9** habitus of female. **A** dorsal view **B** ventral view **10** right wing of male. Dorsal view. Arrow points to wing venation, which differs between the two *Emeia* species **11** right wing of female. Dorsal view. Scale bars: 5 mm (**8, 9**); 2 mm (**10**); 0.5 mm (**11**).

Specimens examined. China: 6♂♂,1♀, Sichuan, Mt. Tian Tai, 3.IV. 2021, Chengquan Cao leg. We herein examined specimens of *E. pseudosauteri* from Mt. Tian Tai (the type locality), and their identity was further verified using *cox1* barcode sequences (Fig. 2) and morphological examination (Figs 8–12).

Figure 12. Aedeagus of *Emeia pseudosauteri.* **A** dorsal view **B** ventral view **C** lateral view. Male aedeagal sheath of *E. pseudosauteri* **D** dorsal view **E** ventral view. Scale bars: 1 mm.

Figure 13. Distribution map of the genus *Emeia* in China. The black star indicates *E. pulchra* Zhu & Chen sp. nov., the black dot *E. pseudosauteri* (map of China from: http://bzdt.ch.mnr.gov.cn/).

Key to species (adult males)

1 The elytral apices have a narrow orange stripe in both fresh and dried specimens; upper vein of MP_{3+4} forked and reaching edge of hind wing (Fig. 10); phallus and parameres broad, 2 times as long as wide (Fig.12A)..... ..... ***E. pseudosauteri*** **Fu, Ballantyne & Lambkin**

– The elytral apices are black in fresh and preserved specimens (Fig. 3A); upper vein of MP_{3+4} reaching margin of hind wings, but without forks (Fig. 4); phallus and parameres slender, 3 times as long as wide (Fig. 6A)..... ..... ***E. pulchra*** **Zhu & Zhen, sp. nov.**

Discussion

In this study, we summarized the diagnostic features of the genus *Emeia*. *Emeia pulchra* Zhu & Zhen, sp. nov. is morphologically similar to *E. pseudosauteri* Fu, Ballantyne & Lambkin, 2012 from Sichuan Province. However, we found differences in the antennal length and body size between the two species. The body size of a species may vary due to nutrition and environmental factors, so we did not include size in the diagnosis to the new species. The antenna of male *E. pulchra* (Fig. 3) is narrower than that of *E. pseudosauteri* (Fig. 8) in lateral view. Females of *E. pseudosauteri* have body length about 2/3 of that of the male and have normal elytra (Fig. 9), but their hind wings are small and shrunken, about 1/4 length of the male hind wings (Figs 10, 11). In the male, we found that the hind wing of *E. pseudosauteri* was relatively narrower and longer than that of *E. pulchra*. The elytral apice has a narrow orange stripe in both fresh and dried specimens of *E. pseudosauteri*, whereas it is black in *E. pulchra* (in three *E. pulchra* and six *E. pseudosauteri* examined). The observed body size of *E. pseudosauteri* (BL 6.6–7.2 mm; BW 2.7–2.9 mm; six individuals measured) was smaller than for *E. pulchra* (BL 10.0–10.4 mm; BW 3.5–3.7 mm; three individuals measured). In the male genitalia, the aedeagus of *E. pulchra* (Fig. 6A) is narrower than that of *E. pseudosauteri* (Fig. 12A), and the parameres are less curved (Figs 6B, 12B). In addition, the new species is only known from S. Zhejiang, whereas *E. pseudosauteri* is only found 1600 km westward, in the Sichuan Province (Fig. 13).

The "barcode region" of *cox1* is often used as an aid to new species' identification and distinction from close relatives in the Barcode of Life Data system (Ratnasingham and Hebert 2007; Lin et al. 2009). Currently, this method has been widely and successfully used to identify closely-related species and conspecific individuals. Our *cox1* gene tree recovered the major subdivisions within Lampyridae, including Lampyrinae, Photurinae and Luciolinae. This tree is consistent with recent studies using 436 loci (Martin et al. 2019) or 15 mitochondrial genes (Chen et al. 2019), and supports that the placement of *Emeia* in Luciolinae (Fig. 2). Both the *cox1* tree and morphology support *E. pulchra* as the closest sister species of *E. pseudosauteri*.

Acknowledgements

We are obliged to Ms. Dan-Dan Tu for assistance with DNA amplification and Mr. Zhuo-Heng Jiang for helpful comments on our manuscript. We thank Dr. Cheng-Quan Cao and Dr. Fang-Zhou Ma for specimen collection and sampling information. This work was supported by the National Natural Science Foundation of China [grant number 31900315 to Y.Z.], the Zhejiang Provincial Natural Science Foundation of China [grant numbers LR21C030001 to Y.Z.] and the Westlake Education Foundation.

References

Ballantyne LA, Lambkin CL (2006) A phylogenetic reassessment of the rare SE Asian firefly genus *Pygoluciola* Wittmer (Coleoptera: Lampyridae: Luciolinae). The Raffles Bulletin of Zoology 54: 21–48.

Ballantyne L, Fu XH, Lambkin C, Jeng ML, Faust L, Wijekoon W, Li DQ, Zhu TF (2013) Studies on South-east Asian fireflies: *Abscondita*, a new genus with details of life history, flashing patterns and behaviour of *Abs. chinensis* (L.) and *Abs. terminalis* (Olivier) (Coleoptera: Lampyridae: Luciolinae). Zootaxa 3721(1): 1–48. https://doi.org/10.11646/zootaxa.3721.1.1

Chen X, Dong Z, Liu G, He J, Zhao R, Wang W, Peng Y, Li X (2019) Phylogenetic analysis provides insights into the evolution of Asian fireflies and adult bioluminescence. Molecular Phylogenetics and Evolution 140: e106600. https://doi.org/10.1016/j.ympev.2019.106600

Douglas HB (2017) World reclassification of the Cardiophorinae (Coleoptera,Elateridae), based on phyloogenetic analyses of morphological characters. ZooKeys 655: 1–130. https://doi.org/10.3897/zookeys.655.11894

Fan L (2019) Inverstigation and Analysis of Insect Resources in Lishui Jiulong National Wetland Park. In: Zhejiang A&F University, Zhejinag, China, 1–35.

Folmer O, Black M, Hoeh W, Lutz R, Vrijenhoek R (1994) DNA primers for amplification of mitochondrial cytochrome c oxidase subunit I from diverse metazoan invertebrates. Molecular Marine Biology and Biotechnology 3: 294–299.

Fu XH, Ballantyne L, Lambkin CL (2010) *Aquatica* gen. nov. from mainland China with a description of *Aquatica wuhana* sp. nov. (Coleoptera: Lampyridae: Luciolinae). Zootaxa 2530(1): 1–18. https://doi.org/10.11646/zootaxa.2530.1.1

Fu XH, Ballantyne L, Lambkin CL (2012) *Emeia* gen. nov., a new genus of Luciolinae fireflies from China (Coleoptera: Lampyridae) with an unusual trilobite-like larva, and a redescription of the genus *Curtos* Motschulsky. Zootaxa 3403(1): 1–53. https://doi.org/10.11646/zootaxa.3403.1.1

Geisthardt M (2004) New and known fireflies from Mount Emei (China) (Coleoptera: Lampyridae). Mitteilungen des Internationalen entomologischen Vereins 29: 1–10.

Lin S, Zhang H, Hou Y, Zhuang Y, Miranda L (2009) High-level diversity of dinoflagellates in the natural environment, revealed by assessment of mitochondrial *cox1* and *cob* genes for

dinoflagellate DNA barcoding. Applied and Environmental Microbiology 75(5): 1279–1290. https://doi.org/10.1128/AEM.01578-08

Martin GJ, Stanger-Hall KF, Branham MA, Da Silveira LF, Lower SE, Hall DW, Li XY, Lemmon AR, Lemmon EM, Bybee SM (2019) Higher-level phylogeny and reclassification of Lampyridae (Coleoptera: Elateroidea). Insect Systematics and Diversity 3(6): 11. https://doi.org/10.1093/isd/ixz024

Ratnasingham S, Hebert PD (2007) BOLD: The Barcode of Life Data System (http://www.barcodinglife.org). Molecular Ecology Notes 7(3): 355–364. https://doi.org/10.1111/j.1471-8286.2007.01678.x

Tamura K, Stecher G, Peterson D, Filipski A, Kumar S (2013) MEGA6: Molecular Evolutionary Genetics Analysis Version 6.0. Molecular Biology and Evolution 30(12): 2725–2729. https://doi.org/10.1093/molbev/mst197

ZooKeys 1113: 167–197 (2022)
doi: 10.3897/zookeys.1113.85448
https://zookeys.pensoft.net

RESEARCH ARTICLE

A peer-reviewed open-access journal
ZooKeys
Launched to accelerate biodiversity research

Contribution to the knowledge of Teloganodidae (Ephemeroptera, Ephemerelloidea) of India

Alexander V. Martynov[1], T. Sivaruban[2], Dmitry M. Palatov[3], Pandiarajan Srinivasan[2], S. Barathy[4], Rajasekaran Isack[2], Michel Sartori[5,6]

1 *National Museum of Natural History, National Academy of Sciences of Ukraine, Bohdan Khmelnytsky str., 15, 01030, Kyiv, Ukraine* **2** *PG & Research Department of Zoology, The American College, Madurai-625002, India* **3** *Independent researcher, Lviv, Ukraine* **4** *Department of Zoology, Fatima College, Madurai-625018, India* **5** *Musée cantonal de zoologie, Palais de Rumine, Place de la Riponne 6, 1014 Lausanne, Switzerland* **6** *Department of Ecology and Evolution, Biophore, University of Lausanne, 1015 Lausanne, Switzerland*

Corresponding author: Alexander V. Martynov (centroptilum@gmail.com)

Academic editor: Ben Price | Received 17 April 2022 | Accepted 17 June 2022 | Published 18 July 2022

https://zoobank.org/AF6603AD-BD03-47EE-AFD0-05459C3CCC9E

Citation: Martynov AV, Sivaruban T, Palatov DM, Srinivasan P, Barathy S, Isack R, Sartori M (2022) Contribution to the knowledge of Teloganodidae (Ephemeroptera, Ephemerelloidea) of India. ZooKeys 1113: 167–197. https://doi.org/10.3897/zookeys.1113.85448

Abstract

Two new species of *Dudgeodes* Sartori, 2008 and a new species of *Teloganodes* Eaton, 1882 are described from India; they are *Dudgeodes selvakumari* Martynov & Palatov, **sp. nov.** from Himalayan region (Uttarakhand), *Dudgeodes molinerii* Sivaruban, Martynov, Srinivasan, Barathy & Isack, **sp. nov.**, and *Teloganodes barathyae* Sivaruban, Martynov, Srinivasan & Isack, **sp. nov.** from the Tamil Nadu part of the Western Ghats. Thus, for now, the Teloganodidae fauna of India includes 11 species. *Dudgeodes selvakumari* **sp. nov.** appears to be significantly extend northward the known distribution of *Dudgeodes*. Partial COI sequences were used as an initial clustering method to show the relationships of *D. selvakumari* **sp. nov.** with other sequenced operational taxonomic units (OTU) of the genus.

Keywords

COI, distribution, imago, larva, morphology, Pannota, Tamil Nadu, Uttarakhand

Introduction

The superfamily Ephemerelloidea is a relatively diverse group within Indian subcontinent. This article is the next contribution in a series of papers on the superfamily of the region. Ephemerelloidea has been actively studied during the last years, and, as a result, series of new species mainly of the family Ephemerellidae have been described from this territory (Selvakumar et al. 2014, 2018a, 2018b; Anbalagan et al. 2015; Martynov et al. 2019, 2021a, 2021b; Sivaruban et al. 2021; Srinivasan et al. 2021). Teloganodidae are less diverse than Ephemerellidae and more poorly studied in Indian subcontinent. Within India, the Teloganodidae were known until now by seven species in four genera: *Teloganodes* Eaton, 1882 (three species), *Dudgeodes* Sartori, 2008 (three species), *Derlethina* Sartori, 2008 (one species), *Indoganodes* Selvakumar, Sivaramakrishnan & Jacobus, 2014 (one species) (Selvakumar et al. 2014; Anbalagan et al. 2015; Srinivasan et al. 2021).

Teloganodes and *Dudgeodes* occur within Indomalayan realm only. *Teloganodes* consists of eight species distributed in the Indian subcontinent (Sartori et al. 2008; Selvakumar et al. 2014). Three of these species are known from India: *T. kodai* Sartori, 2008 and *T. dentatus* Navás, 1931 are endemic to the Western Ghats; *T. sartorii* Selvakumar, Sivaramakrishnan & Jacobus, 2014 is endemic to the Eastern Ghats (Selvakumar et al. 2018a). The genus *Dudgeodes* currently contains 16 species, and three of them are known from India: *D. bharathidasani* Anbalagan, 2015, *D. palnius* Selvakumar, Sivaramakrishnan & Jacobus, 2014, and *D. sartorii* Srinivasan, Sivaruban, Barathy & Isack, 2021 – all endemic to the Western Ghats (Sartori et al. 2008; Selvakumar et al. 2014, 2018a; Anbalagan et al. 2015; Martynov et al. 2016; Garces et al. 2020; Srinivasan et al. 2021).

Representatives of *Teloganodes* are well distinguished at larval stages from other genera of the family (Sartori et al. 2008). Nevertheless, the winged stages of teloganodids are poorly known, as they have been described for only two species: only the male imago is known for *T. dentatus* Navás, 1931 (the larval stage remains unknown), and the female imago and male subimago have been described for *T. tristis* (Hagen, 1858) (the larval stage remains unknown). Despite the large number of species of *Dudgeodes*, only four are known from the winged stages: *D. hutanis* Sartori, 2008 (female subimago, Indonesia), *D. ulmeri* Sartori, 2008 (male subimago, Indonesia), *D. lugens* (Navás, 1933) (female subimago, China), and *D. pescadori* Sartori, 2008 (male and female imago and subimago, Philippines) (Sartori et al. 2008). Thus, the winged stages of all Indian species have not yet been described.

In the present contribution we describe three new species from India: *Dudgeodes selvakumari* Martynov & Palatov, sp. nov. based on larval, imaginal, and egg stages; *Dudgeodes molinerii* Sivaruban, Martynov, Srinivasan, Barathy & Isack, sp. nov. based on larval and egg stages, and *Teloganodes barathyae* Sivaruban, Martynov, Srinivasan & Isack, sp. nov. based on the larval stage only.

Materials and methods

Larvae were collected by hand picking and kick-net sampling in Uttarakhand Pradesh and Tamil Nadu, India. Winged stages were reared from larvae in Martynov-designed

grow nets (Fig. 16A–C). All material is stored in 80–95% ethanol. Some specimens were mounted on slides with Canada balsam.

Specimens of *Dudgeodes selvakumari* sp. nov. and their body parts unmounted on slides were photographed using a Leica M205A microscope with a Leica Z16 APO apochromatic zoom system and Leica DFC450 camera. The photographs were processed with LAS Core v. 3.8. Body parts mounted on slides were photographed with a Ulab XY-B2T microscope with a Canon Power Shot A 630 camera. These photographs were processed with Adobe Photoshop CS5 and Helicon Focus v. 6. Larvae studied with a scanning electron microscope were dehydrated in ethanol and then critical-point dried. Scanning electron microscopy was done on a Vega3 Tescan SEM.

Larval morphological characters of *D. molinerii* sp. nov. and *Teloganodes barathyae* sp. nov. were studied using a LABOMED Luzeo 6Z stereo zoom microscope with an AR 6 Pro camera. Specimens studied under SEM were dehydrated in ethanol and critical-point dried, then examined using a Zeiss EVO 18 SEM. The photographs were processed using Adobe Photoshop 7.0 when necessary.

Names of protuberances of thorax (excluding lateral anterior tubercles, LAs) are given according to Auychinda et al. (2020).

Type material on *D. selvakumari* sp. nov. is deposited in collection of first author in the National Museum of Natural History of the National Academy of Sciences of Ukraine, Kyiv, Ukraine (NMNH NASU; holotype and paratypes); collection of Dmitry Palatov (paratypes); Museum of Zoology, Lausanne, Switzerland (MZL; paratypes). The type specimens of *D. molinerii* sp. nov. and *T. barathyae* sp. nov. are deposited in the Zoological Survey of India, Southern Regional Centre (ZSI-SRC; Chennai, Tamil Nadu, India) and The American College Museum (AMC; Madurai, Tamil Nadu, India).

Molecular study

Total genomic DNA was extracted from three specimens of *D. selvakumari* sp. nov. using the BioSprint 96 extraction robot (Qiagen Inc., Hilden, Germany) following the supplier's instructions. We used the non-destructive protocol described by Vuataz et al. (2011), which enables post-extraction morphological study of specimens. We then amplified a 658-bp fragment at the 5' end of the mitochondrial cytochrome c oxidase subunit I (COI) gene, corresponding to the standard animal barcode region, using the HCO2198 and LCO1490 primers (Folmer et al. 1994). Polymerase Chain Reaction (PCR) was conducted in a volume of 25 µl, consisting of 5 µl (unknown concentration) of template DNA, 1.3 µl (10 µM) of each primer, 0.2 µl (25 mM) of dNTP solution (Promega), 5 µl of 5× buffer (Promega) containing 7.5 mM of $MgCl_2$, 2.5 µl (25 mM) of $MgCl_2$, 1 U of Taq polymerase (Promega), and 9.7 µl of sterile ddH_2O. Optimized PCR conditions included initial denaturation at 95 °C for 5 min, 40 cycles of denaturation at 95 °C for 30 s, annealing at 50 °C for 30 s, and extension at 72 °C for 40 s, with final extension at 72 °C for 7 min. Purification and automated sequencing was carried out in Microsynth (Balgach, Switzerland).

Alignment of analyzed sequences was made in BioEdit v. 7.0.5.3. Recently, both tree- and distance-based methods of species delimitation based on single-locus data have been used.

We calculated genetic distances within and between species and other taxa were calculated in MEGA v. 11 (Tamura et al. 2021). IQ-Tree and FigTree v. 1.4.4 were used for constructing phylogenetic trees from sequence data using a maximum-likelihood (ML) analysis. We used two models of molecular evolution: Tamura-Nei (TN93) (Tamura and Nei 1993) and Kimura 2-parameter (K2) (Kimura 1980) models with a gamma distribution (shape parameter = 0.19). This analysis involved eight nucleotide sequences. Codon positions included were $1^{st}+2^{nd}+3^{rd}$+Noncoding. All ambiguous positions were removed for each sequence pair (pairwise deletion option). There were 655 positions in the final dataset.

GenBank accession numbers for newly derived sequences are given in Table 1, with the nomenclature of gene sequences following Chakrabarty et al. (2013). Other used sequences of Teloganodidae were taken from Selvakumar et al. (2016), Garces et al. (2020), and GenBank (unpublished data). *Indoganodes jobini* Selvakumar, Sivaramakrishnan & Jacobus, 2014, *Teloganodes sartorii* Selvakumar, Sivaramakrishnan & Jacobus, 2014, and *T. kodai* Sartori, 2008 were chosen as the outgroup (Selvakumar et al. 2016).

Table 1. Codes and origin of new sequences used in molecular study.

Species	Specimen catalogue number	Locality	GPS Coordinates	Date	GenBank ID	GenSeq nomenclature
Dudgeodes selvakumari sp. nov.	GBIFCH00970940	India, Uttarakhand, Mailani Range, vicinity of Garjiya village, unnamed river – left tributary of Kosi River	29.4732°N, 79.1640°E	1.v.2018	ON255658	genseq-2 COI
Dudgeodes selvakumari sp. nov.	GBIFCH00970941				ON255659	genseq-2 COI
Dudgeodes selvakumari sp. nov.	GBIFCH00970942				ON255660	genseq-2 COI

Results and discussion

Taxonomy

***Dudgeodes selvakumari* Martynov & Palatov, sp. nov.**
https://zoobank.org/20B9E573-1D83-40E0-9191-F26480F7A7CE
Figs 1–8

Material examined. *Holotype*: imago ♂, with corresponding larval and subimaginal exuviae, India, Uttarakhand, Mailani Range, vicinity of Garjiya village, unnamed river – left tributary of Kosi River, 29.4732°N, 79.1640°E, 430 m a.s.l., 22.v.2018, A.V. Martynov & D.M. Palatov leg., Indi9Telsp/1 (NMNH NASU). ***Paratypes*:** 27 larvae, 9 larvae exuviae, 6 imagos with subimaginal exuviae, including 5♂ and 1♀), ibid., 22.v.2018, A.V. Martynov & D.M. Palatov leg., Indi9Telsp/2–11 (NMNH NASU); 51 larvae, ibid., 1–2.v.2018, A.V. Martynov & D.M. Palatov leg. – NMNH NASU (25 larvae, Indi8Telsp/1–11), MZL (6 larvae), Palatov's collection (20 larvae).

Etymology. The new species is named in honour of Dr C. Selvakumar of India, who contributed significantly to the study of mayflies in India.

Figure 1. Larva of *Dudgeodes selvakumari* Martynov & Palatov, sp. nov., paratypes **A** total dorsal view **B** total ventral view **C** male head, dorsal view **D** abdomen, dorsal view. Scale bars: 0.5 mm (**A, C, D**); 1 mm (**B**).

Figure 2. Larva of *Dudgeodes selvakumari* Martynov & Palatov, sp. nov., paratypes **A, B** mandibles **C** labrum **D** hypopharynx **E** maxilla **F** apical part of maxilla **G** labium.

Description. ***Mature larva.*** Body length 3.0–5.5 mm; cerci length 3.5–6.2mm. Dorsal surface of body yellowish with brown-black spots and strokes (Fig. 1A); ventral surface yellowish white, with indistinct median gray smudges on sternites (Fig. 1B).

Head dirty yellow with indistinct brown smudges. Antennae also dirty yellow, distal segments of flagellum and distal part of scapus blackish. Dorsal part of male eyes brown (Fig. 1C). Occipital and suboccipital tubercles absent. Genae moderately developed. Antennae length 1.15 times head width, flagellum with about 15 or more segments. Lateral margin of head fringed with a row of long, stout setae, forked near base

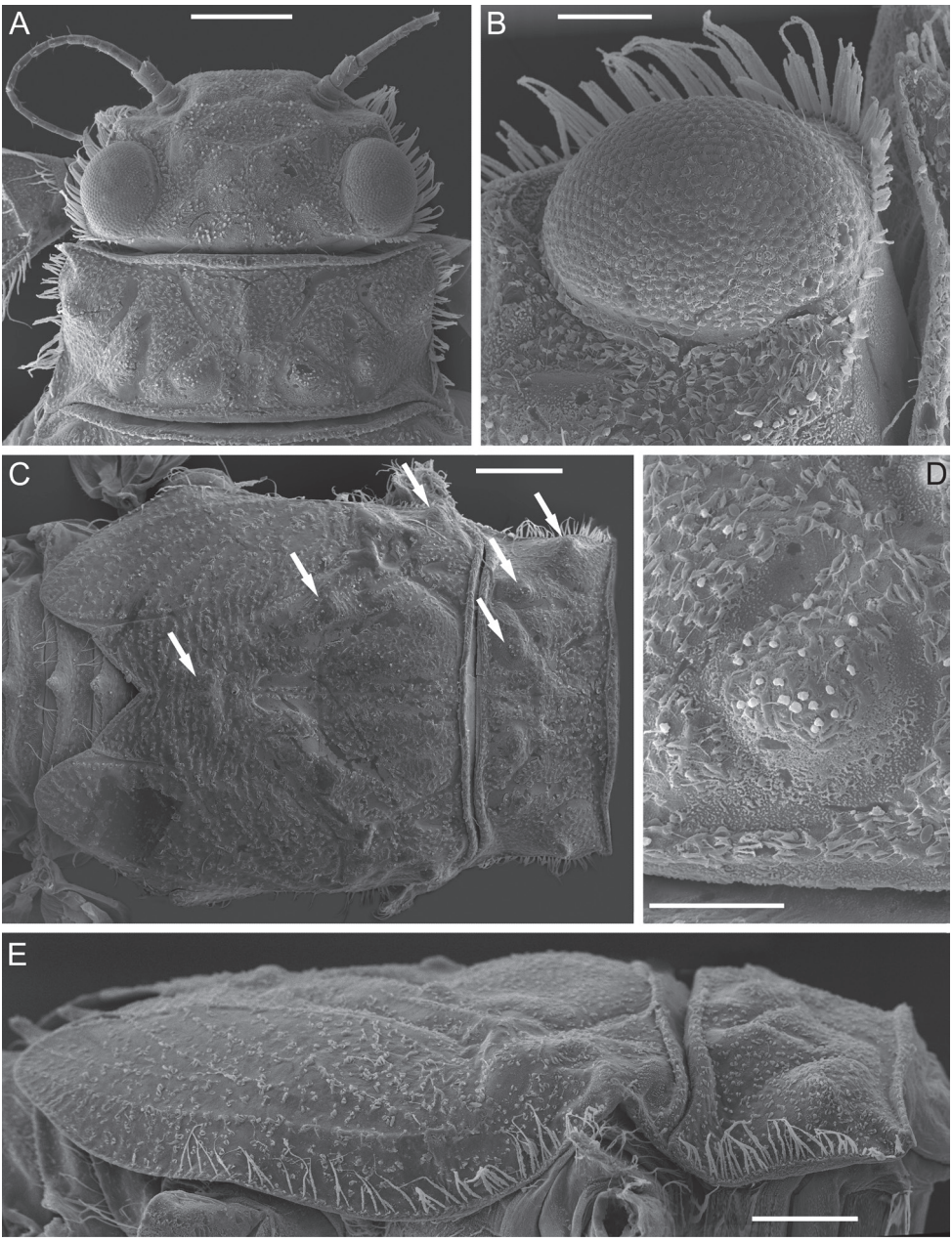

Figure 3. Larva of *Dudgeodes selvakumari* Martynov & Palatov, sp. nov., paratypes **A** head and pronotum, dorsal view **B** row of setae at outer margin of head **C** thorax, dorsal view **D** sub-median tubercle (SM) of pronotum **E** thorax, lateral view. Abbreviations: white arrows show tubercles of pronotum and mesonotum. Scale bars: 0.3 mm (**A, C, E**); 0.1 mm (**B, D**).

and with pointed apices, a row extending from posterior margin of eyes to labrum; stout setae on posterior margin of eyes distinctly shorter (Fig. 3B). Head covered with scattered, short, hair-like setae and short, stout setae with slightly divided margins.

***Mouthparts*.** Labrum wide and compact, width/length ratio 2.64–2.65, with smooth medial concavity on anterior margin (Fig. 2C). Dorsal surface covered with transversal band of long, stout, hair-like setae. Anterior area and margin densely covered with variously sized feathered setae.

Mandibles slender with few small setae along outer margin and one stout, hair-like seta in middle of margin. Right mandible (Fig. 2A): outer incisor composed of three teeth, one of them located remotely from others; inner incisor with two teeth; prostheca reduced, consisting of a bunch of thin setae; row of 6–8 long, stout, hair-like setae below mola and some short setae above mola. Left mandible (Fig. 2B): outer incisor with three teeth; inner incisor with two subequal teeth inserted transversely; prostheca small with a group of small setae; no setae below mola; base of mola with 2–3 small, apically pointed, stout setae.

Maxilla (Fig. 2E, F) slender, with well-developed canine, two dentisetae, and four long stout setae on inner apical part; crown with bunch of long setae; inner margin of lacinia base with 1+4 feathered, long, stout setae; maxillary palp reduced to a protuberance with single hair-like seta.

Hypopharynx with long, feathered setae on the rounded apexes of superlinguae, and very short setae on lingua (Fig. 2D).

Labial palp three-segmented, slightly constricted towards apex; articulation between segments clearly visible; segment III elongate and rounded apically, length/width at base ratio 1.9–2.2 (Fig. 2G). Outer margins of segments I and II covered with sparse, long, stout, hair-like setae; segment III with several fine setae only. Submentum well developed laterally. Glossae and paraglossae short and broad, rounded apically, their apexes densely covered with variously sized, feathered, stout setae; outer margins of paraglossae covered with long, feathered, stout setae.

***Thorax*.** Pronotum with three pairs of tubercles: SMs, SLs, and Ls; with a few short globular stout setae; M tubercle absent (Fig. 3C–E). Lateral margins of pronotum and mesonotum with a row of long, stout setae, some of them forked (Fig. 3E). Surface of mesonotum with an MP, pair of SMMs and pair of LAs (lateral anterior tubercles) (Fig. 3C, E); these tubercles also bear a few short, stout setae with slightly divided margins.

Forefemur moderately slender, ca 2.1 times longer than wide; outer margin covered with regular row of long, stout, hair-like setae, and few thin, hair-like setae (some setae in bunches); submarginal row of setae distinct, composed of stout setae (elongate and short) with slightly divergent margins (Fig. 4D); inner margin with row of long, stout, hair-like setae. Transverse row on dorsal surface consists of about 20 long, apically pointed, stout setae (Fig. 4A). Irregular row of short, stout setae with slightly divergent margins located parallel to longitudinal indistinct ridge (Fig. 4A–C). Dorsal surface of fore tibia with few scattered, short, stout setae of same kind, solitary hair-like setae, and hair-like setae in bunches (consisting of 2–4 setae), oblique regular row of long, stout, hair-like setae. Outer and inner margins of tibia with relatively short hair-like setae; inner margin with several elongate, pointed, stout setae.

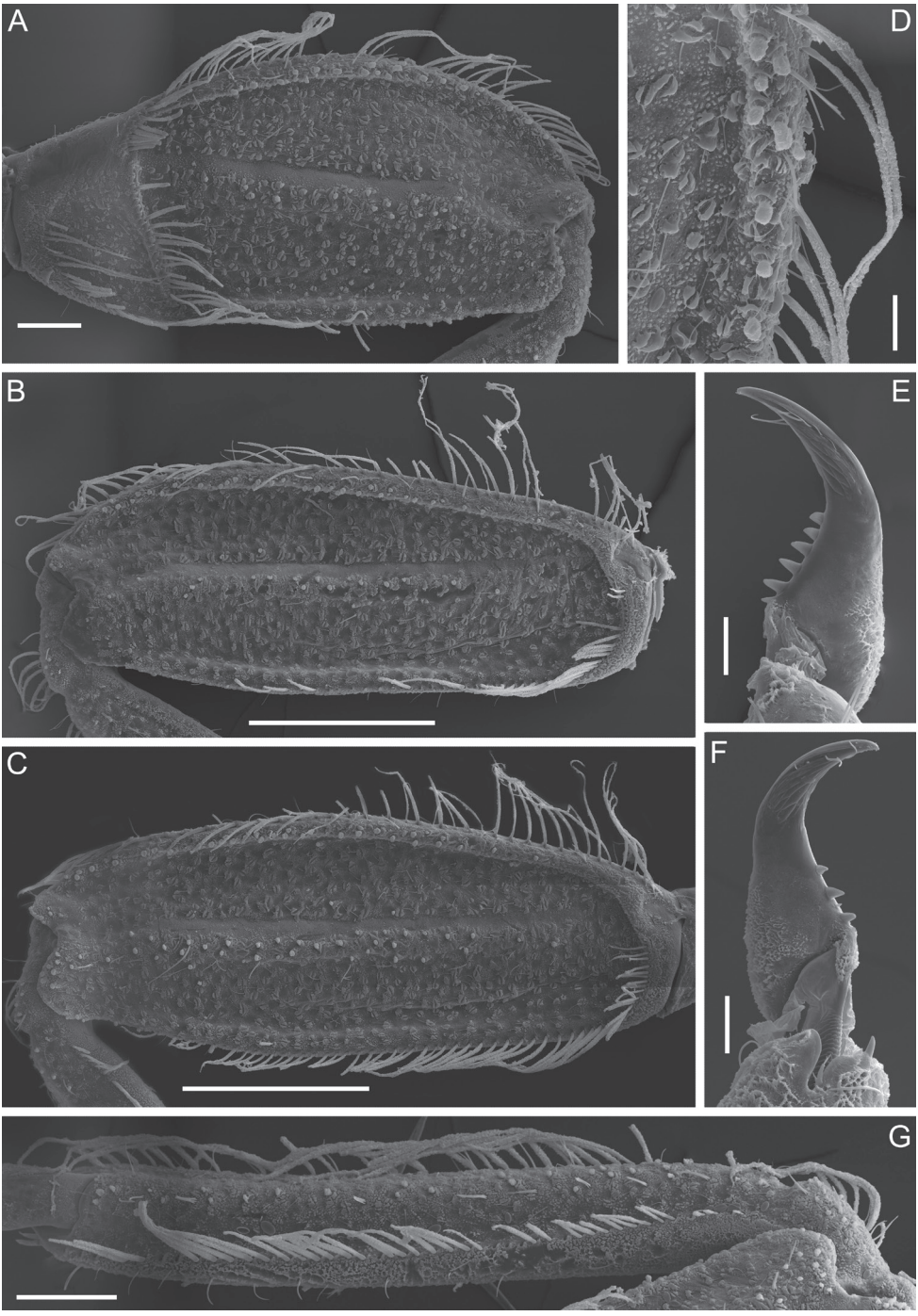

Figure 4. Larva of *Dudgeodes selvakumari* Martynov & Palatov, sp. nov., paratypes **A** fore femur **B** middle femur **C** hind femur **D** outer margin of fore femur **E, F** tarsal claws **G** middle tibia. Scale bars: 0.1 mm (**A, G**); 0.3 mm (**B, C**); 0.03 mm (**D–F**).

Middle and hind femora (Fig. 4B, C), in contrast to fore femur, more slender, ca 2.6–2.7 times longer than wide, with denser submarginal row of stout setae, inner margin with regular row of long, stout, hair-like setae. Outer margins of middle and hind femora and tibiae with a regular row of long, stout, hair-like setae (Fig. 4D, G). Setation of dorsal surface of middle and hind tibiae most similar to those of fore leg, but oblique regular row of long, stout setae longer, and reaching distal end of tibia (Fig. 4G).

Tarsal claws moderately hooked, lacking subapical denticles, with 4–6 medial denticles and several (3–5) subapical setae (Fig. 4E, F).

Abdomen. All terga with moderately developed, narrowed (especially on terga V–X) median tubercles (Fig. 5A, F); the largest on terga V–VIII; tubercle of tergum X narrow and pointed. Median tubercles of terga I–IX distinctly elongate in lateral view (Fig. 5C). Median tubercles covered with short stout setae with divergent margins (Fig. 5E). Posterolateral projections moderately developed on segments VI–IX, and slightly marked on segments II–V (Fig. 5B).

Posterior margin of terga I–V with row of long, stout, hair-like setae; posterior margin of terga VI–IX with row of elongate (on tergum VI) and short (all other terga) stout setae with rounded apices (Fig. 5D); posterior margin of tergum X without stout setae (Fig. 5F). Mainly median area of terga with scattered short stout setae with divergent margins; most numerous on segments VI–X (Fig. 5G, H). Lateral areas of dorsal surfaces of terga III–VI with thin, hair-like setae and long, stout setae with serrated margins and apices. Narrow teeth present on posterior margin of submedian area of terga III–IV; the same teeth present on median and lateral areas of posterior margin of terga V–VI (they are not numerous at lateral areas) (Fig. 5D) and across entire posterior margin of terga VII–X (on tergum X not numerous); this kind of teeth absent on posterior margin of terga I–II. Sterna surface with a few scattered hair-like setae (Fig. 5B).

Gills on segments II–V (Fig. 6A, E–H); gill II with dorsal lamella operculate, oval and with entire margin, mainly basal half covered with scattered short stout setae (Fig. 6B); gills III–V with dorsal lamella incised medially.

Cerci length subequal to the body length, posterior margins of central segments with hair-like and forked stout setae; length of the stout setae less than length of corresponding segment (Fig. 5I). Paracercus absent.

Subimagos. Wings wholly grey, semitransparent in subimagos of both sexes.

Male imago. Body length: 5.6–6.5 mm; forewing length: 5.6–5.9 mm; cerci length: 11.0–13.3. General coloration brown; thorax dark brown. Turbinate eyes brick-colored (Fig. 7A, E).

Fore leg (Fig. 7E): coxa, trochanter, and femur brown; tibia whitish, its basal and distal ends distinctly marked with black; tarsus segment I blackish; tarsi segments II–V whitish, with slightly blackish distal ends; tarsal claws blackish. Middle and hind legs (Fig. 7A): coxa brown, all other parts yellowish; femora with narrow, intermittent longitudinal black line along outer margin; dorsal surface with several longitudinal indistinct smudges; lower protuberance of knee brown; distal end of tibia blackish. Both claws on fore leg blunt; inner claw at middle and hind legs hooked and pointed and outer claw blunt.

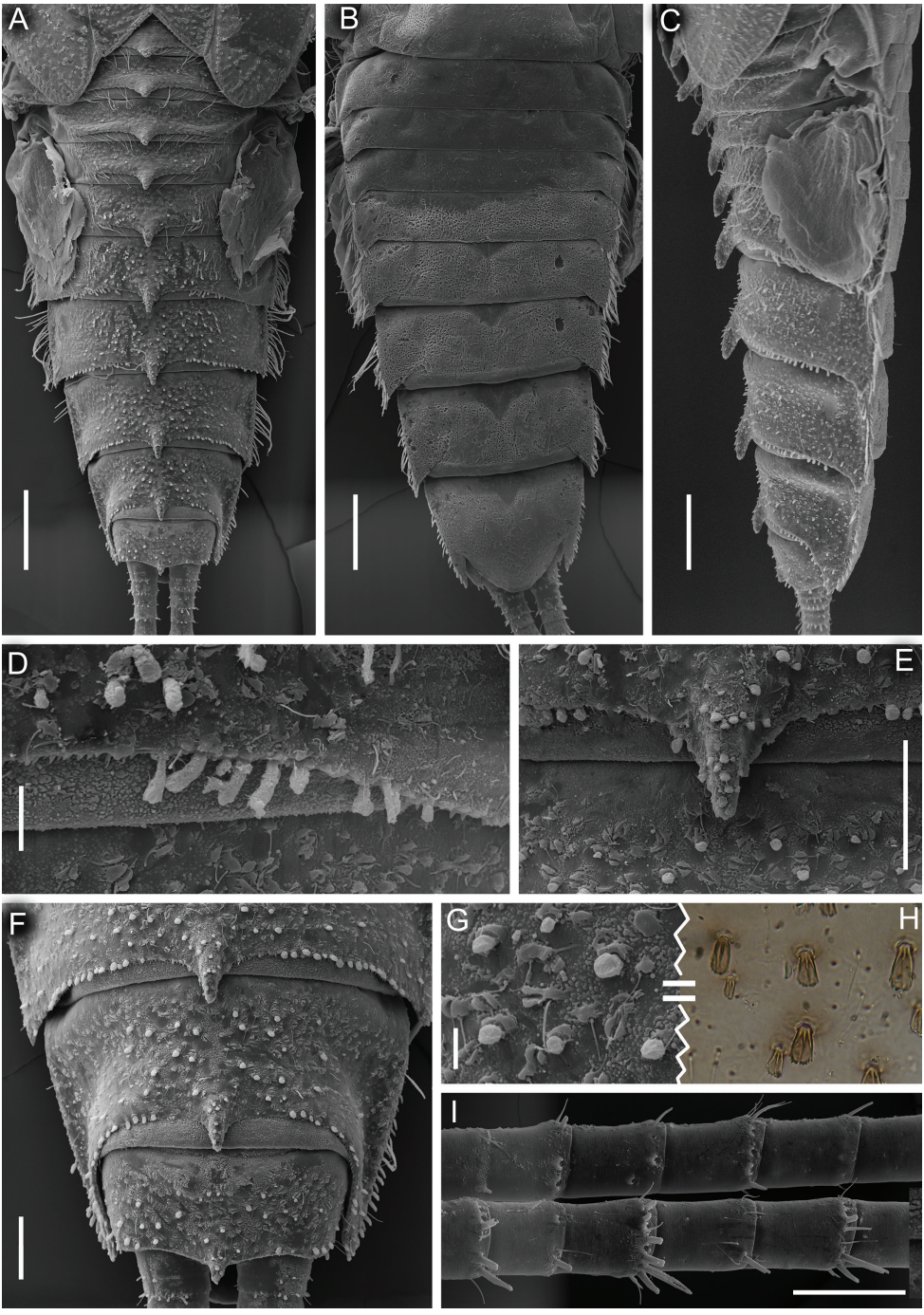

Figure 5. Larva of *Dudgeodes selvakumari* Martynov & Palatov, sp. nov., paratypes **A–C** abdomen, dorsal **A** ventral **B** and lateral **C** views **D** sublateral area of posterior margin of tergum VI **E** median tubercle of tergum VII **F** terga VIII–X, dorsal view **G, H** dorsal surface of tergum VIII, SEM microscopy **G** and light microscopy (**H**) **I** caudal filaments. Scale bars: 0.3 mm (**A–C**); 0.03 mm (**D, G**); 0.1 mm (**E, F, I**).

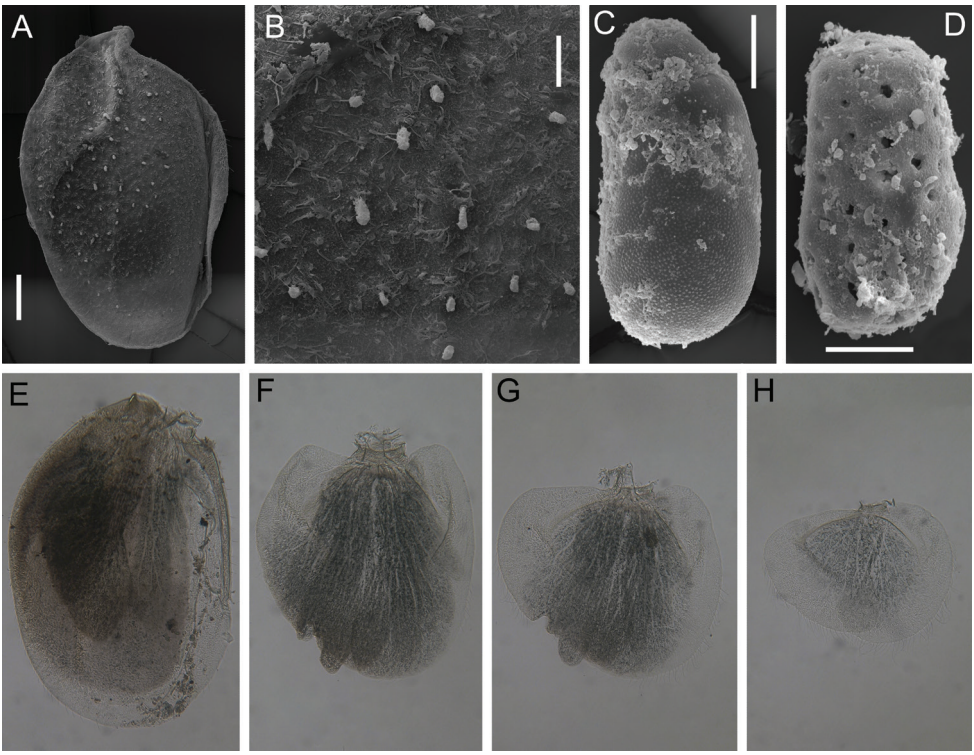

Figure 6. Larva of *Dudgeodes selvakumari* Martynov & Palatov, sp. nov., paratypes **A, E** gill II **B** dorsal surface of gill II **C, D** egg **F** gill III **G** gill IV **H** gill V. Scale bars: 0.1 mm (**A**); 0.03 mm (**B–D**).

Main area of fore wing transparent (Figs 7A, 8A); only basal area with a black marking, costal and subcostal fields translucent, milky. Pterostigmatic area with 8–10 cross-veins, several of them divided. Hind wing elongate, with large costal process. Three or four cross-veins between Sc and RA; two cross-veins between RA and IRA (Fig. 8B).

Abdominal terga IV–VIII with small pointed median tubercles, in some specimens these tubercles distances on terga IV–V only (Fig. 8C). Abdominal segments VI–IX with distinct rounded apically postero-lateral projections, largest on segments VIII and IX (Fig. 7B). Segments II–V with remnants of gill sockets (Fig. 7D). *Genitalia*: whitish; styliger plate straight to concave; forceps 3-segmented; segments I and II approximately same length; segment I subcylindrical; segment II slightly expanded at apex; segment III rounded apically, elongate, 1.8–1.9 times as long as wide. Penis lobes with rounded apices; lobes expanded closer to apices, maximum width on ca 0.7 of their length; fused for entire length except the apex; on ventral side a groove ends at the middle of the penis (Fig. 7B, C).

***Female imago*.** Body length: 6.0 mm; forewing length: 5.9 mm; cerci length: 12.8 mm. General coloration brown. Legs coloration as in male imago. Turbinate eyes brown.

On fore leg outer tarsal claw hooked and pointed and inner claw blunt. On middle and hind legs outer tarsal claw blunt and inner hooked and pointed. Wings venation

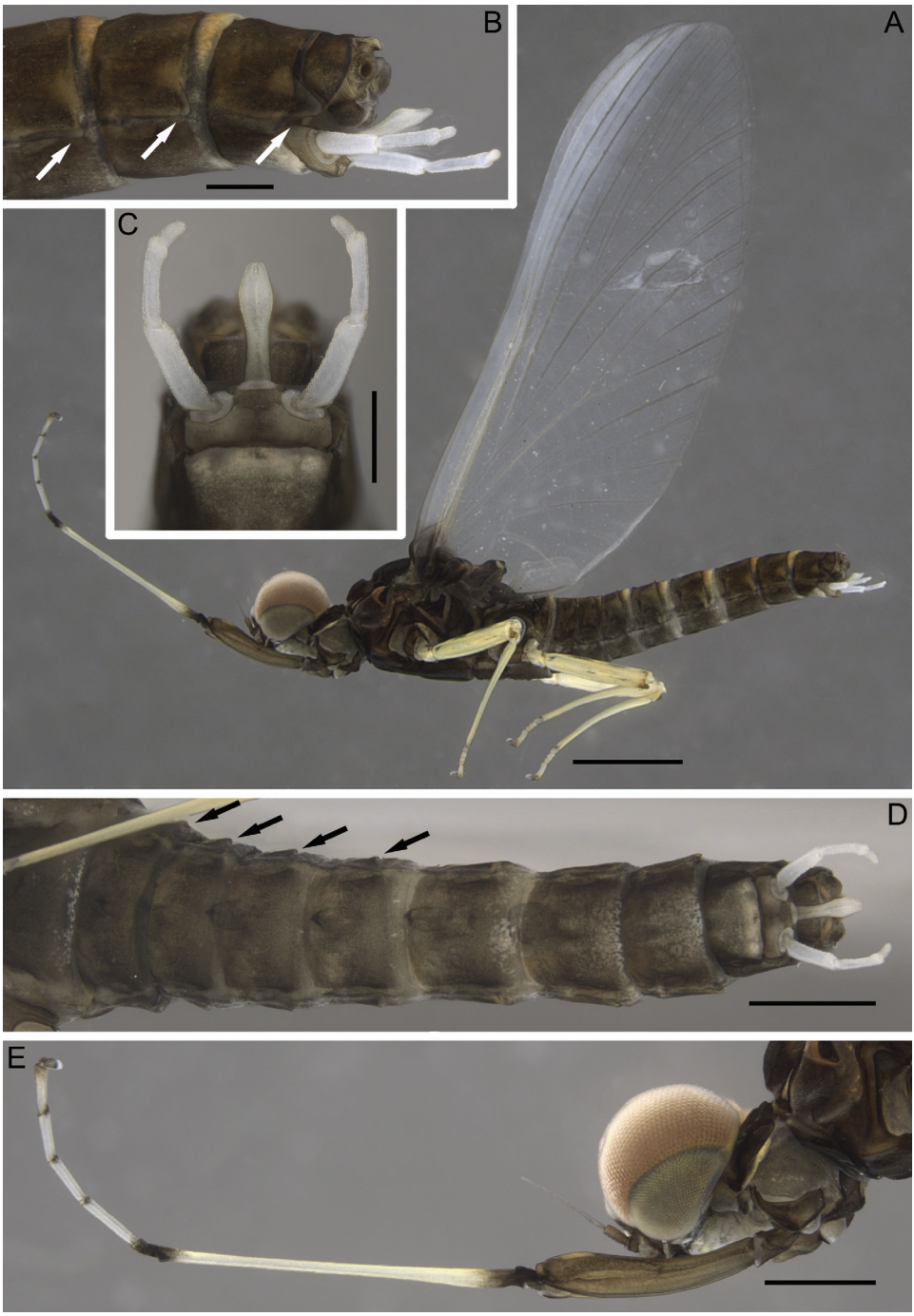

Figure 7. Imago male of *Dudgeodes selvakumari* Martynov & Palatov, sp. nov., holotype **A** total lateral view **B** abdominal segments VII–X, lateral view **C** genitalia, ventral view **D** abdomen, ventral view **E** head and fore leg, lateral view. Abbreviations: white arrows show postero-lateral projections of segments; black arrows show remnants of gill sockets. Scale bars: 1 mm (**A**); 0.2 mm (**B, C**); 0.5 mm (**D, E**).

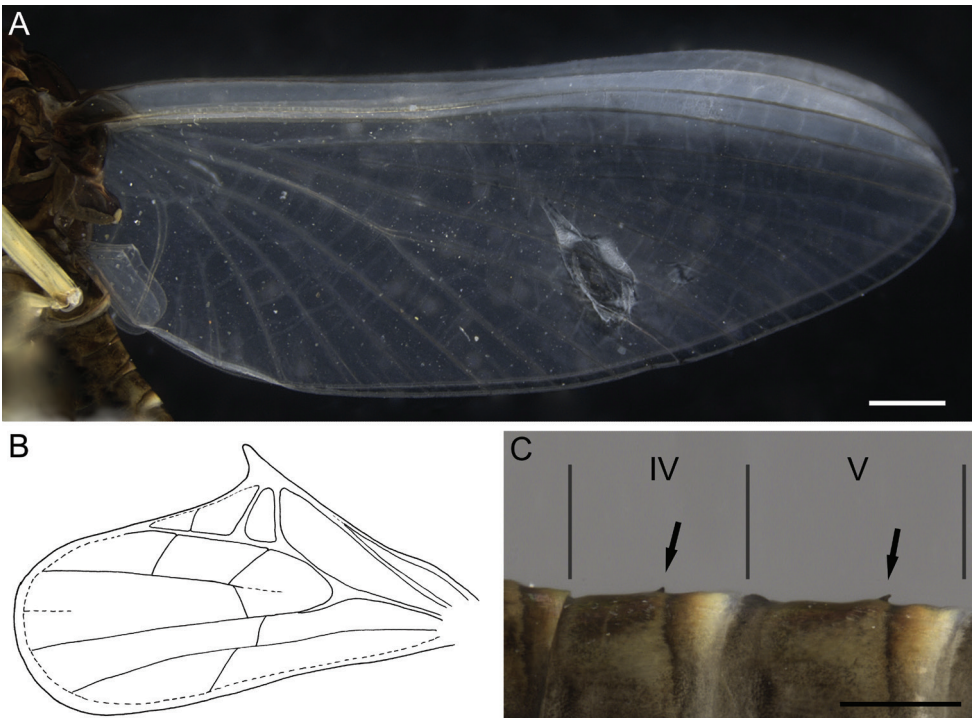

Figure 8. Imago male of *Dudgeodes selvakumari* Martynov & Palatov, sp. nov., holotype **A** wings **B** hind wing **C** abdominal segments IV and V, lateral view. Scale bars: 0.5 mm (**A**); 0.2 mm (**C**).

as in male imagos, but longitudinal veins browner. Only abdominal segments VII–IX with distinct rounded apically postero-lateral projections, largest on segments VIII and IX. Abdominal terga IV–VIII with small pointed median tubercles. Tergum X with longitudinal distinctly divergent median concavity that reach posterior margin. Segments II–V with remnants of gill sockets. Subgenital plate not elongate, with wide and shallow concavity. Subanal plate rounded.

Egg (dissected from mature larva). Shape (Fig. 6C) ovoid, with one polar cap; chorion lacking attachment structures; without geometrical marcorelief, only microgranules present. Another kind of observed eggs (Fig. 6D) we considered as unformed yet; lacking polar cap, microgranules on chorion indistinct; whole surface covered with numerous depressions and holes.

Distribution. Himalaya (Uttarakhand, India). All Indian representatives of *Dudgeodes*, excluding *D. selvakumari* sp. nov., are known from the Western Ghats only. *Dudgeodes selvakumari* sp. nov., which is distributed in the lower down part of Great Himalayan mountain range, is the most northern representative of the genus and family within India. This new species and *D. lugens* (Navás, 1933), which is known by single female subimago from Zhou Shan Island, in Zhejiang province, China (Sartori et al. 2008), are the most northern representatives of the family anywhere.

Habitats. Larvae of this species were collected in a mid-sized river (6–10 m wide) in a shallow woodland valley at an altitude of about 400 m a.s.l. in the southern foothills of the Great Himalaya Range (Nainital District, Uttarakhand state, India). The river was relatively warm (24–26 °C), had a current of moderate velocity (ca 0.3–0.7 m/s), and was with a mainly stony or rocky substrate. The river is located in the recreational zone of the Jim Corbett National park with a weak anthropogenic load. Larvae were collected from the riparian zone from stones or vegetation at local current velocity 0.05–0.2 m/s (Fig. 16A–D), along with different *Baetis* sp. (Baetidae), Heptageniidae, *Choroterpes* sp. (Leptophlebiidae), *Caenis* sp. (Caenidae), *Asiagomphus* sp. (Gomphidae), *Macromyia* sp. (Macromiidae), *Protohermes* sp. (Corydalidae), *Agapetus* sp. (Glossosomatidae), *Chimarra* sp. (Philopotamidae), *Marilia* sp. (Odontoceridae), and *Macrobrachium* sp. (Palaemonidae).

Diagnosis. The new species can be distinguished from other representatives of the genus by the following combination of characters. *Larva*: (i) dorsal part of male eyes brown; (ii) antennae length 1.15 times head width, flagellum with about 15 or more segments; (iii) labrum with transversal band of long, stout, hair-like setae; (iv) prothorax with three pairs of tubercles: SMs, SLs, and Ls; mesothorax with an MP, pair of SMMs and pair of LAs; (v) forefemur without transversal row of stout setae; (vi) outer margin of forefemur covered with a regular row of long, stout, hair-like setae, a few bunches, and single, thin, hair-like setae; (vii) submarginal row of setae of forefemur distinct, consisting of elongate and short, stout setae with slightly divided margins; (viii) tarsal claw of all legs with 4–6 medial denticles and without subapical denticles; (ix) terga I–X with moderately developed, narrowed (especially on terga V–X) median tubercles; the largest tubercles on terga V–VIII; tubercle of tergum X narrow and pointed; in lateral view, median tubercles of terga I–IX distinctly elongate; (x) posterolateral projections moderately developed on segments VI–IX, slightly marked on segments II–V. *Imago male*: (i) fore wing with numerous cross-veins; (ii) hind wing with 3–4 cross-veins between Sc and RA, and two cross-veins between RA and IRA; (iii) penis lobes maximum width on about 0.7 of their length; (iv) abdominal terga IV–VIII with small pointed median tubercles; in some specimens these tubercles distinct on terga IV–V only; (v) abdominal segments VI–IX with rounded apically postero-lateral projections. *Egg*: (i) without spines on pole opposite to polar cap; (ii) surface covered with microgranules.

The larva of *D. selvakumari* Martynov & Palatov, sp. nov. is easily distinguished from other Indian *Dudgeodes* species by: (i) absence of tubercles on head; (ii) number of tubercles on pro- and mesonotum; (iii) forefemur setation; (iv) shape of fore femur; (v) absence of subapical denticles on tarsal claws; (vi) shape of gill II; (vii) shape of median tubercles of abdominal terga.

***Dudgeodes molinerii* Sivaruban, Martynov, Srinivasan, Barathy & Isack, sp. nov.**
https://zoobank.org/060B341B-E366-4FC0-96B4-C81BE326FAF4
Figs 9–11

Material examined. *Holotype*: mature ♀ larva, India, Tamil Nadu, Theni district, Kurangani hills, Kottakudi River, 10.0809°N, 77.2552°E, 632 m a.s.l., 28.x.2020, Pan-

diarajan Srinivasan & Isack Rajasekaran leg., ZSI–SRC/I/E/654. ***Paratypes*****:** 5 larvae, ibid., 28.x.2020, Pandiarajan Srinivasan & Isack Rajasekaran leg., ZSI–SRC/I/E/655 (1 larva), AMC ZN 237 (4 larvae).

Etymology. The new species is named in honour of Dr Carlos Molineri of Argentina, who contributed significantly to the study of mayflies.

Description. ***Mature larva*****.** Body length 4.7–4.9 mm; cerci length subequal to body length. General coloration of the dorsal side of head dirty yellow, with dark brown to blackish maculations; thorax and abdomen dark brown to blackish, with dirty yellow maculations (Fig. 9A–D). Ventral side of body yellowish to light brown. Dorsal surface of femora with two blackish longitudinal stripes one medial along ridge and one along outer margin; also three (proximal, medial, and distal) black spots with indistinct borders along medial ridge; proximal and medial spots divided in two parts by brownish bands (Fig. 11A–C). Dorsal part of male eyes dark brown to black (Fig. 9D). Abdominal terga I–VIII with pair of submedian yellowish spots. Anterior part of tergum X yellowish (Fig. 9C).

Head with pair of occipital tubercles (Fig. 9D). Genae moderately developed. Lateral margin of head capsule from eye to labrum insertion with row of long, forked near the base, stout setae with pointed apices (Fig. 9E). Antennae length 1.25 times head width, flagellum with 11 segments. Head covered with scattered short hair-like setae and short stout setae with slightly divergent margins.

Mouthparts**.** Labrum compact, width/length ratio 2.51–2.53; with smooth anterior emargination; dorsal surface with transversal row of scattered, stout, hair-like setae (Fig. 10C, D); anterior area and margin of labrum densely covered with differently sized feathered setae. Mandibles slender with long, stout, hair-like seta in the middle of the outer margin (Fig. 10A, B). Number of teeth of both mandibular outer incisors cannot be determined precisely due to their wear in type specimens. Right mandible inner incisor with two teeth; prostheca reduced, with the appearance of a cluster of thin setae; small row of five long, stout, hair-like setae below mola and some short setae above mola. Left mandible inner incisor with two teeth inserted transversely, one smaller and rounded and other one larger and rounded; prostheca small; no setae below and above mola. Maxilla (Fig. 10F, G) slender, shape of canine impossible to determine (completely worn); two indented dentisetae and three long setae on inner apical part and cluster of long, simple setae at crown; inner margin at the base of lacinia, with two feathered, long setae; maxillary palp highly reduced to protuberance. Hypopharynx (Fig. 10E, H) with long, feathered setae on the rounded apexes of superlinguae and very short setae on lingua. Labial palp (Fig. 10I, J) three-segmented, slightly constricted towards apex; articulation between segments clearly visible; segment III elongate and rounded apically, length/width ratio at base 2.0–2.1. Surface and margins of segments I and II covered with scattered long, stout, hair-like setae; segment III bare. Submentum well developed laterally. Glossae and paraglossae short and broad, rounded apically, their apexes densely covered with differently sized, feathered, stout setae; outer margins of paraglossae covered with long feathered setae.

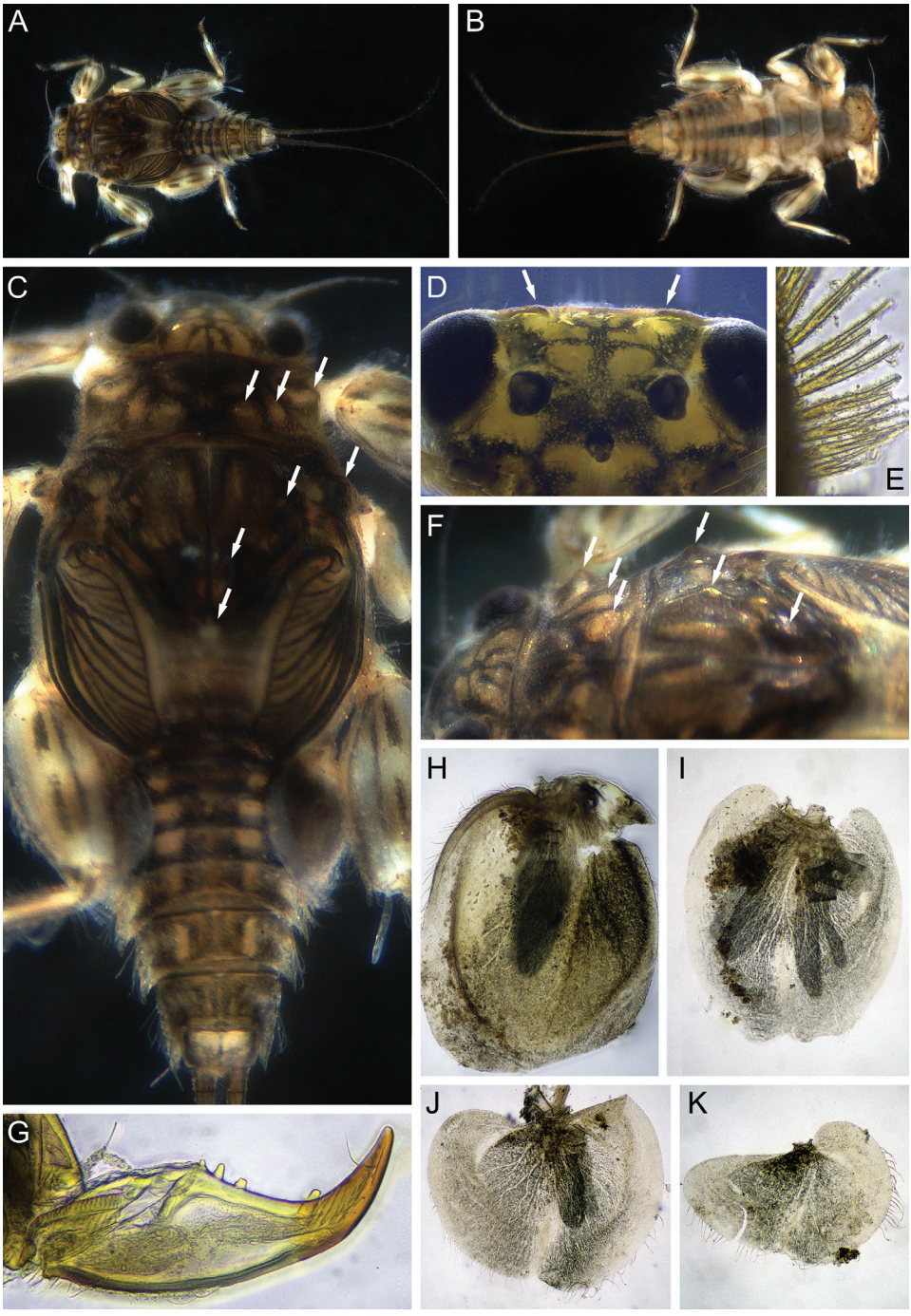

Figure 9. Larva of *Dudgeodes molinerii* Sivaruban, Martynov, Srinivasan, Barathy, Isack, sp. nov., paratypes **A** total dorsal view **B** total ventral view **C** head, thorax and abdomen, dorsal view **D** head, dorsal view **E** row of setae at outer margin of head **F** head and thorax, dorso-lateral view **G** tarsal claw **H** gill II **I** gill III **J** gill IV **K** gill V. Abbreviations: white arrows show tubercles.

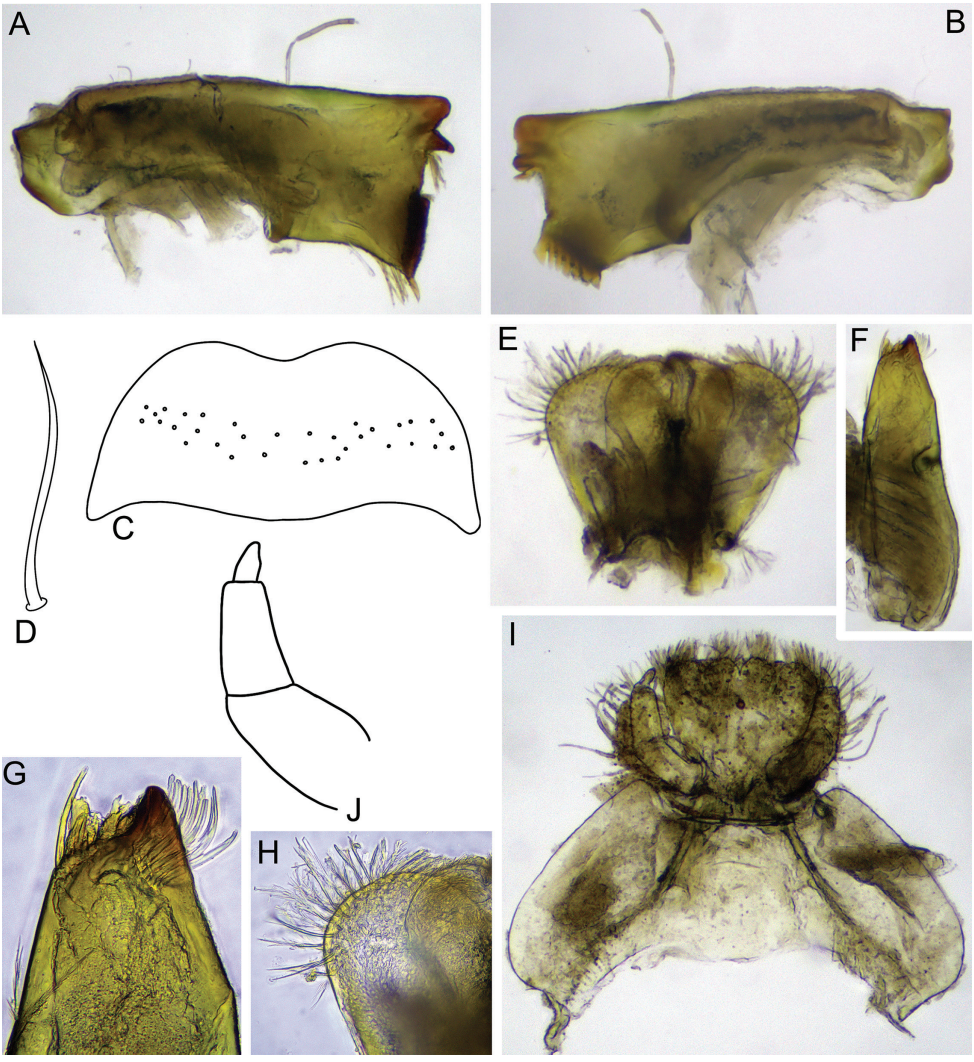

Figure 10. Larva of *Dudgeodes molinerii* Sivaruban, Martynov, Srinivasan, Barathy & Isack, sp. nov., paratypes **A, B** mandibles **C** labrum **D** stout setae of transversal row of labrum **E** hypopharynx **F** maxilla **G** apical part of maxilla **H** superlingua **I** labium **J** labial palp.

Thorax. Pronotum with three pairs of tubercles: SMs, SLs, and Ls; tubercles with a few short, rounded setae. Mesonotum with three pairs of tubercles: two pairs of SMMs, a pair of LAs, and unpaired MP (Fig. 9C, F).

Forefemur broad, ca 1.3 times longer than wide (Fig. 11A, D); outer margin covered with a row of long, stout, hair-like setae (Fig. 11G); submarginal row of setae composed of scattered, short, stout setae with rounded apices; basal half of inner margin with row of long, stout, hair-like setae; distal half almost without setae. Transverse row on the dorsal surface made of about 30 long, pointed apically stout setae

(Fig. 11E, F). Dorsal surface of fore femur covered with scattered, short, stout setae and thin, hair-like setae. Dorsal surface of fore tibia with solitary hair-like setae and oblique regular row of long, stout, hair-like setae; outer margins of tibia with regular row of long, stout, hair-like setae.

Middle and hind femora, in contrast to fore femur, more slender, ca 1.8–2 times longer than wide, with denser submarginal row of short, stout setae (Fig. 11B, C). Outer and inner margins covered with a regular row of long, stout, hair-like setae. Outer margin of middle and hind tibiae with a regular row of long, stout, hair-like setae. Setation of dorsal surface of middle and hind tibiae similar to those of fore leg.

Tarsal claw moderately hooked, bearing 3–6 medial denticles, 1–2 subapical denticles (if two subapical denticles present, they are situated each on opposite sides of claw) and a row of 3–4 subapical setae on dorsal and ventral sides (Fig. 9G).

Abdomen. All terga with median tubercles that bear short, stout setae with slightly divergent margins. Median tubercles moderately developed on terga IV–VIII, and slightly marked on terga I–III, IX, and X (Fig. 11H). Posterolateral projections moderately developed on segments VI–IX, and slightly marked on segments II–V. Submedian and sublateral areas of terga VI and VII with scattered stout setae with divided apices and a few small, rounded stout setae.

Gills on segments II–V (Fig. 9H–K); gill II with dorsal lamella operculate, oval and with entire margin; gills III–V with dorsal lamella incised medially.

Cerci length subequal to the body length; posterior margin of proximal half segments with elongate, stout setae with rounded apices; posterior margin of distal half segments with long, spine-like setae on the lateral margins; length of the stout setae less than length of corresponding segment. Paracercus absent.

Egg. Ovoid, ca 100–110 μm long, with numerous micropyles. Egg with one polar cap, on the opposite pole with a cluster of 18–20 spines (Fig. 11I–K).

Winged stages. Unknown.

Distribution. Western Ghats (Tamil Nadu, India).

Habitats. The larvae of *D. molinerii* sp. nov. inhabit cobble and pebble substrates of rivers with a strong current (Fig. 16E), where there is no significant anthropogenic stress. Water temperatures range between 20 and 22 °C and pH ranges between 7.1 and 7.4. This species was caught with other mayflies such as *Clypeocaenis malzacheri* Srinivasan, Sivaruban, Barathy & Isack, 2022 (Caenidae), *Nigrobaetis klugei* Sivaruban, Srinivasan, Barathy & Isack, 2022 (Baetidae), *Notophlebia* sp. (Leptophlebiidae), and *Tenuibaetis frequentus* (Müller-Liebenau & Hubbard, 1985) (Baetidae).

Diagnosis. *Dudgeodes molinerii* sp. nov. can be distinguished from other *Dudgeodes* species by the following combination of characters. *Larva*: (i) dorsal part of male eyes dark brown to black; (ii) head with pair of small occipital tubercles; (iii) antennae length 1.25 times head width, flagellum with 11 segments; (iv) labrum with transversal row of scattered, stout, hair-like setae; (v) forefemur with transverse row of about 30 long, apically pointed, stout setae; (vi) tarsal claw bearing 3–6 medial denticles, and 1–2 subapical denticles (if two, they are on opposite sides of claw), and 3–4 subapical setae on dorsal and ventral sides; (vii) pronotum bears three pairs of tubercles:

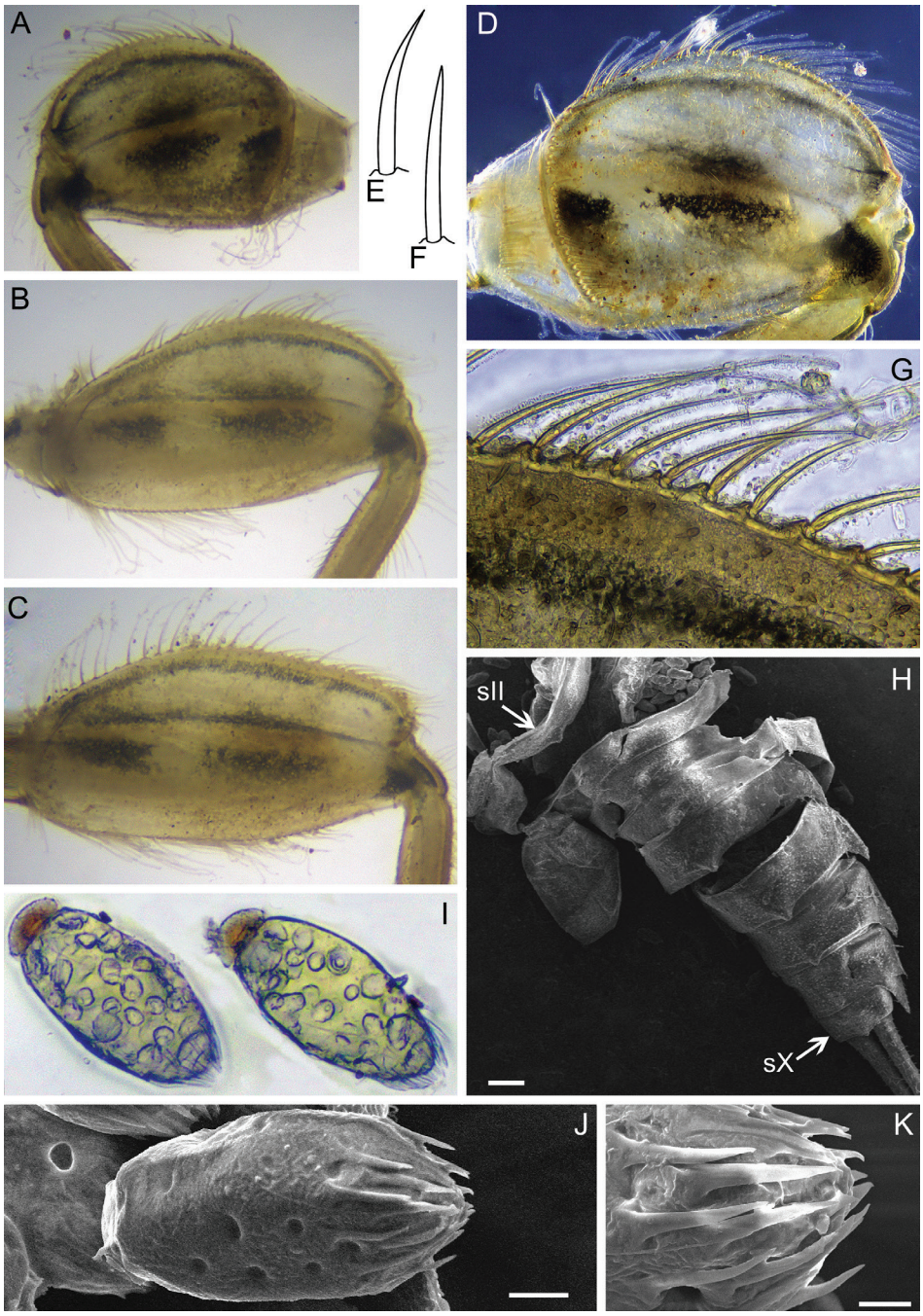

Figure 11. Larva of *Dudgeodes molinerii* Sivaruban, Martynov, Srinivasan, Barathy & Isack, sp. nov., paratypes **A, D** fore femur **B** middle femur **C** hind femur **E, F** stout setae of transversal row on forefemur **G** outer margin of fore femur **H** abdomen **I** eggs, light microscopy **J** egg, SEM microscopy **K** cluster of spines on pole of egg. Abbreviations: sII – abdominal segment II, sX – abdominal segment X. Scale bars: 0.2 mm (**H**); 0.02 mm (**J**); 0.01 mm (**K**).

SMs, SLs, and Ls; mesonotum bears three pairs of tubercles: two pairs of SMMs, a pair of LAs, and unpaired MP; (viii) median tubercles moderately developed on terga IV–VIII, and slightly marked on terga I–III, IX and X; (ix) posterolateral projections moderately developed on segments VI–IX, and slightly marked on segments II–V. *Egg*: (i) egg with cluster of 18–20 spines present on pole opposite to polar cap; (ii) surface without microgranules.

Larval stage of this new species can be easily distinguished from other Indian *Dudgeodes* by: (i) presence of tubercles on head; (ii) number of tubercles on pro- and mesonotum; (iii) shape of femora; (iv) setation of forefemur; (v) size and shape median tubercles on abdomen.

***Teloganodes barathyae* Sivaruban, Martynov, Srinivasan & Isack, sp. nov.**
https://zoobank.org/D430C0EB-5606-4AD4-9320-DBB8C546FF70
Figs 12–15

Material examined. ***Holotype*:** ♀ larva, India, Tamil Nadu, Theni District, Kurangani Hills, Kottakudi River, 10.0809°N, 77.2552°E, 632 m a.s.l., 28.x.2020, Pandiarajan Srinivasan & Isack Rajasekaran leg., ZSI–SRC/I/E/652. ***Paratypes*:** 2 larvae, ibid., 28.x.2020, Pandiarajan Srinivasan & Isack Rajasekaran leg., ZSI–SRC/I/E/653 (1 larva), AMC ZN 230 (1 larva).

Etymology. The new species is named in honour of Dr S. Barathy, an assistant professor in the Department of Zoology, Fatima College, Tamil Nadu, India, who contributed to the study aquatic insects of India.

Description. ***Mature larva*.** Body length up to 5.4–5.7 mm without cerci; cerci length subequal to body length. General colouration of dorsal side of head, thorax, and terga I–IX brownish to blackish; tergum X yellowish to whitish; ventral side of the head and thorax pale, sterna I–VIII with submedian black tinges; sternum IX pale (Fig. 12A–C, F); legs light brownish; femora light brownish with two distinct maculae (Fig. 14A–C); basal segment of cerci black; apical parts of cerci somewhat blacked out.

***Head*.** Lateral margins of head fringed with a row of long, stout setae, forked near base and with pointed apices, which run from posterior margin of eyes to labrum; anterior margin of clypeus with numerous stout setae of the same type (Fig. 12E). Antennae short, 0.8 times head width, flagellum with 13–14 segments. Dorsal part of male eyes reddish.

***Mouthparts*.** Labrum compact, ca 2.4 times wider than long, with smooth anterior emargination; dorsal surface with a transversal band of numerous feathered setae (Fig. 13C). Mandibles slender; middle of outer margin with one long, stout seta or without seta (when absent, probably broken). Right mandible (Fig. 13A) with inner incisor composed of two teeth; prostheca reduced, comprised of a cluster of thin setae; a small row of six long, stout, hair-like setae below mola and a bunch of short, thin setae above mola. Left mandible (Fig. 13B) inner incisor with two teeth inserted transversely, one smaller and pointed, other large and rectangular; prostheca small with three short and long setae;

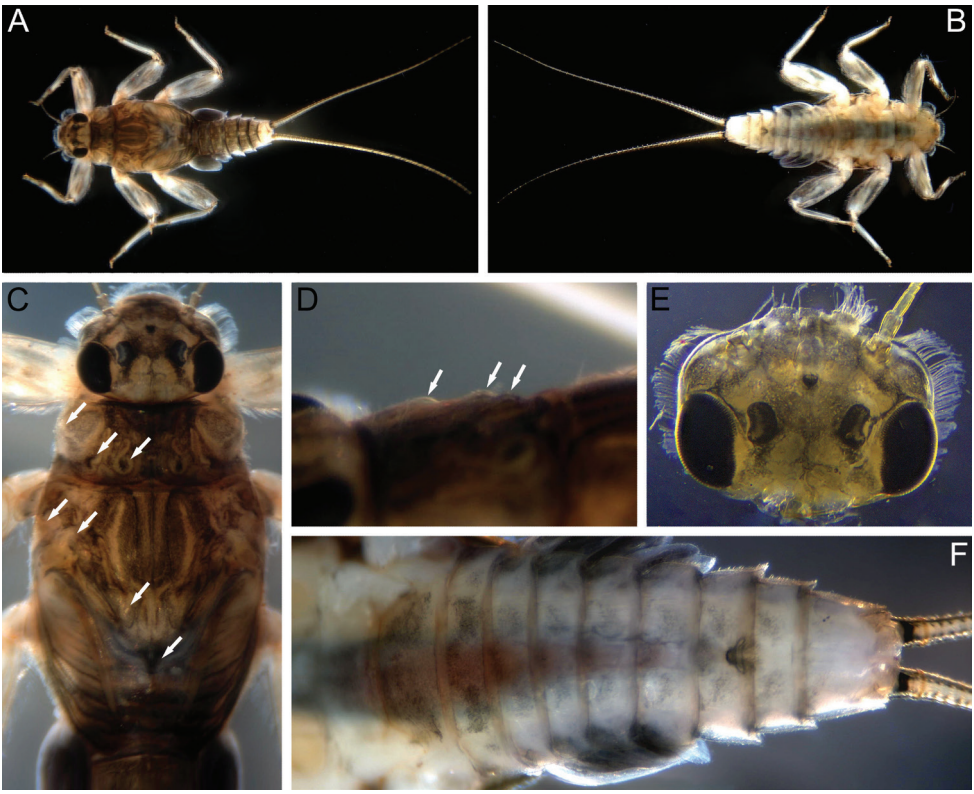

Figure 12. Larva of *Teloganodes barathyae* Sivaruban, Martynov, Srinivasan & Isack, sp. nov., paratypes **A** total view, dorsal view **B** total view, ventral view **C** head and thorax, dorsal view **D** pronotum, dorsolateral view **E** head, dorsal view **F** abdomen, ventral view. Abbreviations: white arrows show tubercles.

no setae below mola. Number of teeth of both mandibular outer incisors undetermined due to their wear in type specimens. Maxilla (Fig. 13F) slender, canine completely worn, its shape undetermined, two dentisetae serrated on the inner margin and three long setae on inner apical region, and cluster of long, simple setae at crown; inner margin at the base of lacinia, with a long, feathered seta dorsally and 4–5 setae of the same type ventrally; maxillary palp greatly reduced up to protuberance with seta. Superlinguae laterally angular, with a row of long, feathered setae at apex (Fig. 13D, I). Submentum well developed laterally; glossae and paraglossae partially fused; paraglossae larger than glossae; labial palp three-segmented, articulation between all three segments well visible; segments I and II subequal in length; segment III ca 1.8 times as long as wide (Fig. 13E, G, H).

Thorax. Pronotum with three pairs of rounded tubercles: SMs, SLs, and Ls. Mesonotum with three pairs of tubercles: two pairs of SMMs and LAs (lateral anterior tubercles), and an unpaired MP tubercle (Fig. 12C, D).

Forefemur (Fig. 14A) moderately broad, ca 2.4 times longer than wide; outer margin with a regular row of long, stout, hair-like setae. Dorsal surface with submarginal row of numerous short, stout setae with divergent margins (some of setae divided near apex

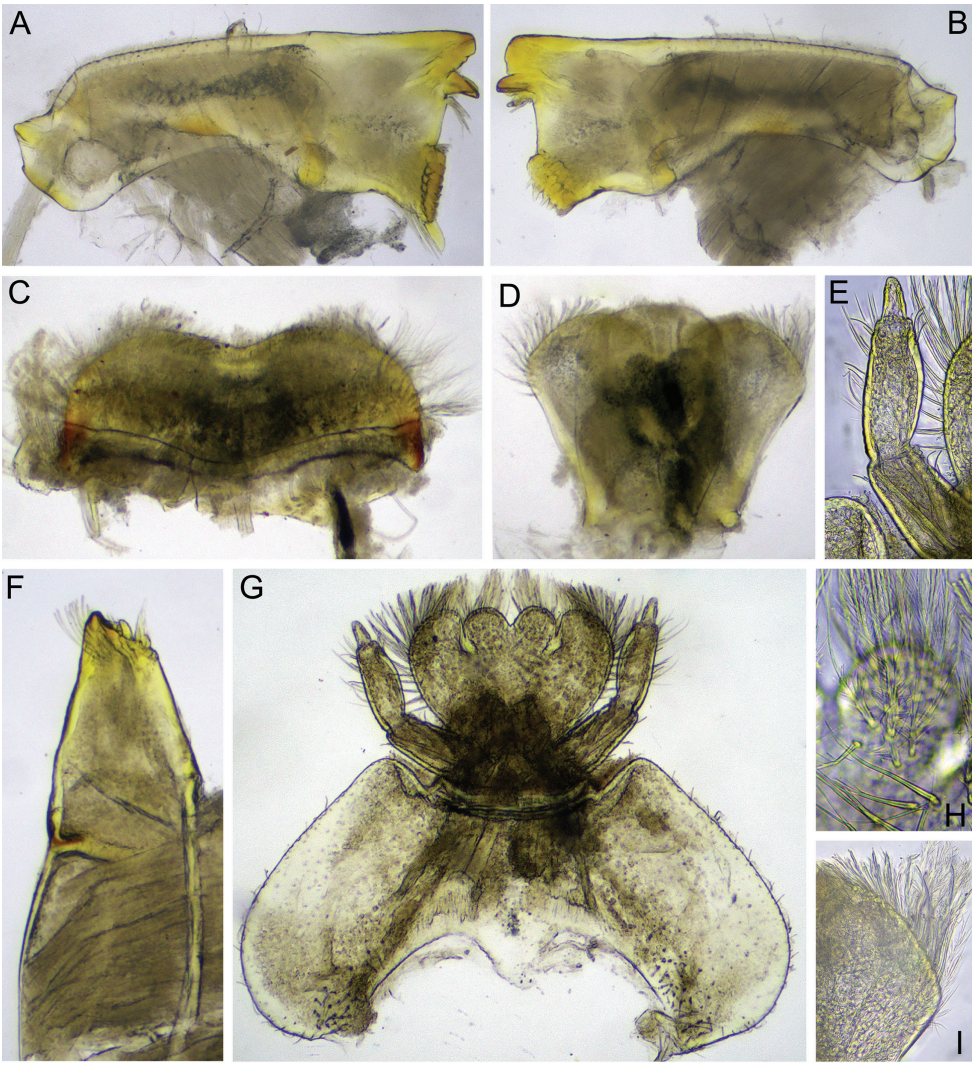

Figure 13. Larva of *Teloganodes barathyae* Sivaruban, Martynov, Srinivasan & Isack, sp. nov., paratypes. **A, B** mandibles **C** labrum **D** hypopharynx **E** labial palp **F** maxilla **G** labium **H** stout setae on glossa **I** superlingua.

into two rounded lobes); same stout setae scattered over whole dorsal surface; inner margin with a regular row of long, stout hair-like setae, this row continuing on dorsal surface to near articulation with trochanter; transverse row of stout setae absent. Dorsal surface of fore tibia with oblique regular row of long, stout, hair-like setae and solitary hair-like setae; outer margins of tibia with a regular row of long, stout, hair-like setae (Fig. 14E).

Middle and hind femora with ornamentation similar to foreleg (Fig. 14B–D). Middle and hind tibiae with a row of long and stout, hair-like setae on outer margin; dorsal surface with oblique row of long, stout, hair-like setae; also scattered short, stout

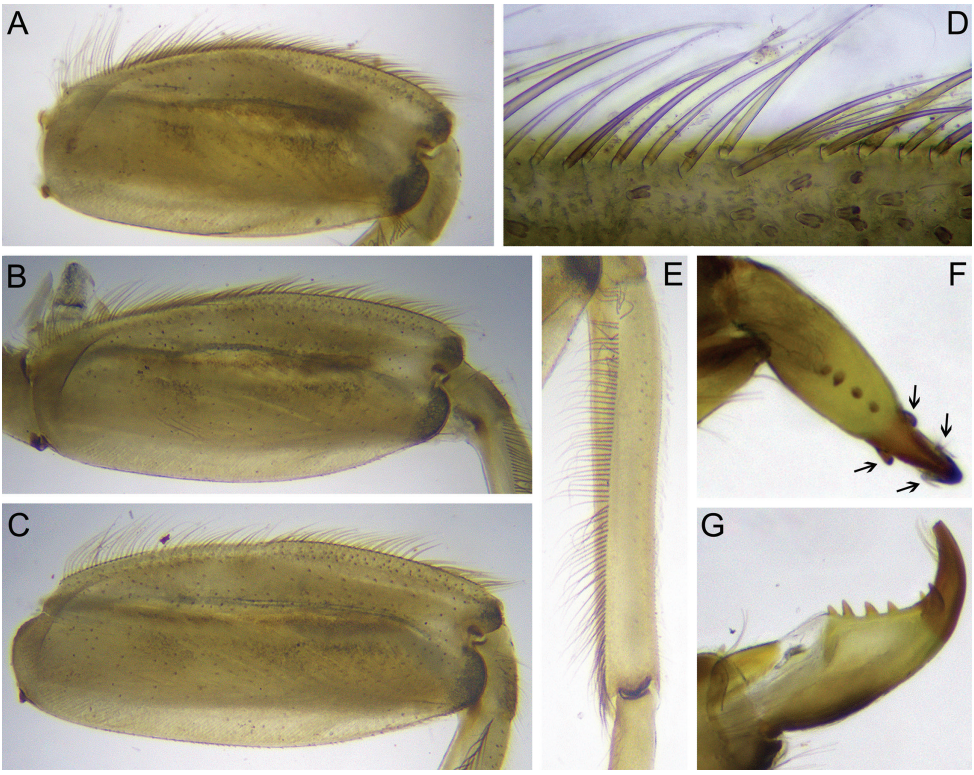

Figure 14. Larva of *Teloganodes barathyae* Sivaruban, Martynov, Srinivasan & Isack, sp. nov., paratypes **A** fore femur **B** middle femur **C** hind femur **D** outer margin of hind femur **E** fore tibia **F, G** tarsal claw, ventral **F** and lateral **G** view. Abbreviations: black arrows show subapical denticles and setae.

setae with divergent margins (some of the setae divided near apex into two rounded lobes) present on dorsal surface along outer margin.

Tarsal claw hooked, bearing four medial denticles and two subapical denticles on opposite sides of claw; dorsal and ventral surface of claw with a row of 3–5 subapical, hair-like setae (Fig. 14F, G).

Abdomen. Median tubercles on terga I–X present; on tergum I poorly developed; on terga II–IV moderately developed; on terga V–X most developed. In dorsal view tubercles I–IX broad and rounded apically, tubercle X distinctly slender and bluntly pointed (Fig. 15A, B). Median tubercles with short, stout setae (Fig. 15C). Posterolateral projections present on segments II–IX; slightly marked on segments I–VI; most distinct on segments VII–IX (Fig. 12F). Submedian and sublateral areas of terga VI and VII with differently sized (mainly medium-length and long) stout setae with slightly or moderately divided apices.

Gills present on abdominal segments II–VI. Gill II with dorsal lamella operculate and covering others, oval with margin entire; gills II–V with well-developed

Figure 15. Larva of *Teloganodes barathyae* Sivaruban, Martynov, Srinivasan & Isack, sp. nov., paratypes **A** abdomen, dorsal view **B** abdomen, lateral view **C** median tubercle of abdominal tergum VI **D** gill V **E** gill VI **F** setae of caudal filament.

flabelliform ventral lobe; gills III–V with dorsal lamella incised medially (Fig. 15D); gill VI with dorsal lamella entire (Fig. 15E).

Central portion of cerci with elongate stout setae with bluntly pointed apices and few long, hair-like setae; stout setae length less than half length of the corresponding segment (Fig. 15F).

Winged stages. Unknown.

Distribution. Western Ghats (Tamil Nadu, India).

Habitat. The same as for *D. molinerii* sp. nov.

Figure 16. Type habitats **A, B, D, E** of new species and cages (Martynov's construction) **C** used for *Dudgeodes selvakumari* Martynov & Palatov, sp. nov. winged stages rearing **A, B, D** type habitat of *Dudgeodes selvakumari* Martynov & Palatov, sp. nov. **C** Martynov-designed grow nets for mayfly winged stages rearing **E** type habitat of *Dudgeodes molinerii* Sivaruban, Martynov, Srinivasan, Barathy & Isack, sp. nov. and *Teloganodes barathyae* Sivaruban, Martynov, Srinivasan & Isack, sp. nov. Abbreviations: arrows show microhabitats with the highest density of a new species' larvae.

Diagnosis. Larva of *T. barathyae* sp. nov. can be distinguished from other species of *Teloganodes* by the following combination of characters: (i) dorsal surface of labrum with a transversal band of numerous feathered setae; (ii) inner incisor of the left man-

dible with two teeth inserted transversely, one smaller and pointed, the other large and rectangular; (iii) superlinguae angular laterally, with a row of long, feathered setae at apex; (iv) forefemur moderately broad, ca 2.4 times longer than wide; outer margin with regular row of long, stout, hair-like setae; without any combination of thin and stout setae in a row; (v) forefemur bears submarginal row of numerous short stout setae with divergent margins, (some of them divided near apex into two rounded lobes); same stout setae scattered over whole dorsal surface; (vi) fore femur without transverse row of stout setae; (vii) median tubercles on terga I–X, on tergum I poorly developed; on terga II–IV moderately developed; on terga V–X best developed; in dorsal view tubercles I–IX broad and rounded apically, tubercle X distinctly slender and bluntly pointed; (viii) posterolateral projections on segments II–IX, segments VII–IX well developed but not extremely.

Larvae of this new species can be distinguished for other Indian representatives of *Teloganodes* by: (i) shape of superlinguae; (ii) length of antennae; (iii) absence of transversal row of stout setae on forefemur; (iv) shape of forefemur; (v) shape of median tubercles of abdominal terga.

Teloganodes sp. IND1

Remark. This operational taxonomic unit is known by one specimen which distinctly differs from other representatives of the genus. We consider this material unacceptable for describing a new species now but provide a diagnosis.

Material examined. 1 larva, India, Tamil Nadu, Theni District, Kurangani Hills, Kottakudi River, 10.0809°N, 77.2552°E, 632 m a.s.l., 28.x.2020, Pandiarajan Srinivasan & Isack Rajasekaran leg., AMC ZN 243.

Diagnosis. This OTU can be distinguished from other representatives of *Teloganodes* by the following combination of characters: (i) superlinguae laterally angular; (ii) forefemur without transversal row of stout setae; (iii) outer margin of femora with a regular row of long, stout hair-like setae only; (iv) dorsal surface of femora with submarginal irregular row of short stout setae; (v) tarsal claw with four median denticles and 1–2 subapical denticles (if two, on opposite sides of claw); (vi) median tubercles on terga III–X, which are indistinct on tergum III; wide on terga IV–VI; largest and elongate on terga VII–IX; elongate and thin on terga X; (vii) sublateral areas of posterior margins of terga IV–VI with bunches of 3–4 extremely long, pointed, stout setae; (viii) surface of cerci covered with long, stout, hair-like setae; setae in posterior margin of cerci segments less than half length of corresponding segment.

Molecular results

In this study, we used all available COI sequences of *Dudgeodes* species. Notably, 10 *Dudgeodes* OTUs, which have not yet been described morphologically, have already been sequenced and their independent position is certain (Garces et al. 2020; GenBank data); these are included in our ML tree.

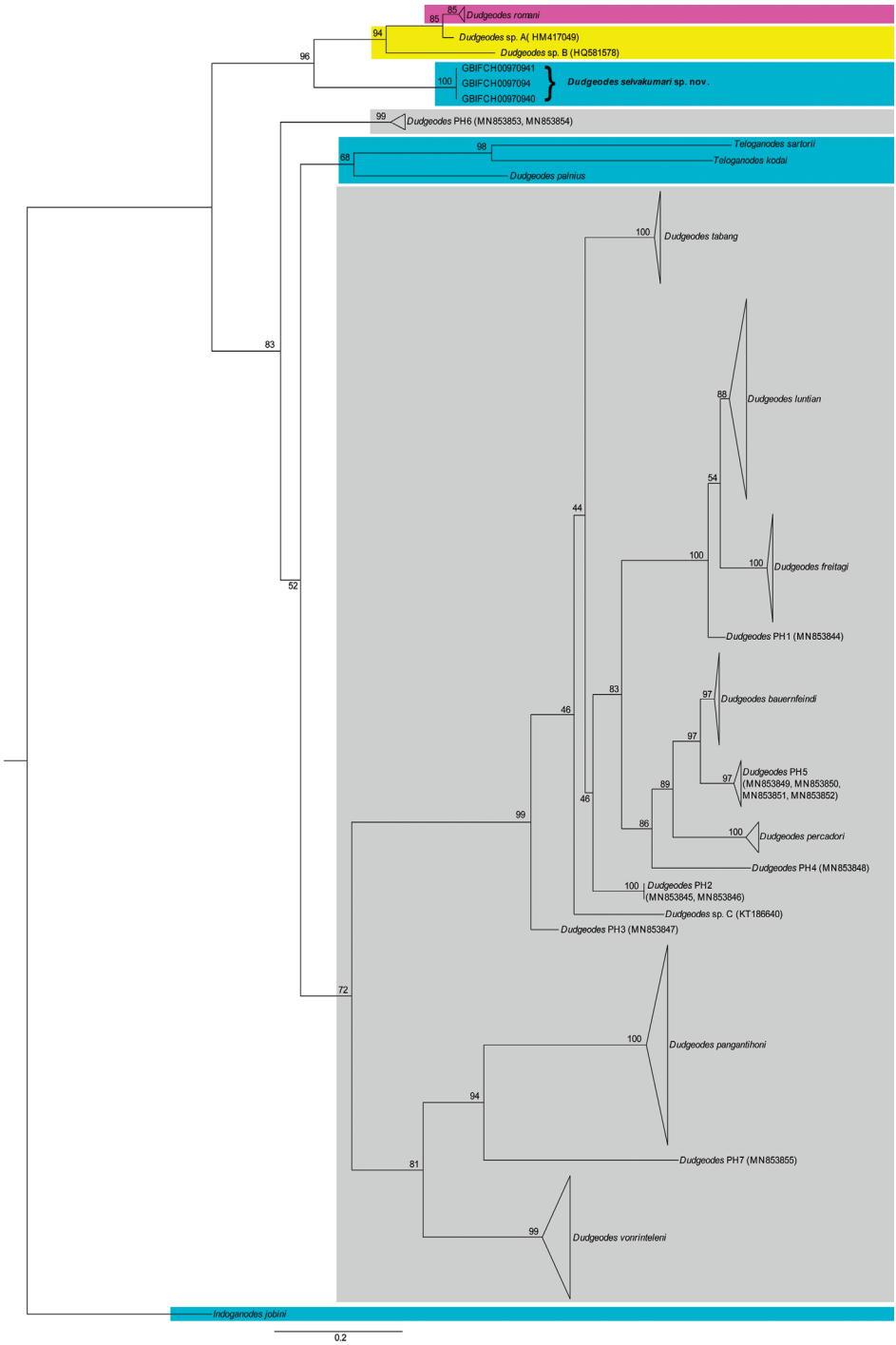

Figure 17. Maximum-likelihood tree including several representatives of the genus *Dudgeodes* and *Teloganodes*. Branches provided with bootstrap supports (BS). Abbreviations: pink –Cambodia, yellow – Thailand, blue – India, gray – Philippines.

Table 2. Genetic distances (COI) between sequenced *Dudgeodes* species of continental part of Southeast Asia, calculated using the Tamura-Nei (TN93) and Kimura 2-parameter (K2) models with a gamma distribution (G) (TN93+G/K2+G).

	Dudgeodes romani	***Dudgeodes* sp. B** (HQ581578)	***Dudgeodes* sp. A** (HM417049)	***Dudgeodes selvakumari* sp. nov.**
Dudgeodes romani	0.01/0.01			
Dudgeodes sp. B (HQ581578)	0.3226/0.3695	—		
Dudgeodes sp. A (HM417049)	0.0558/0.0545	0.3037/0.3585	—	
Dudgeodes selvakumari sp. nov.	0.4616/0.5456	0.4642/0.5376	0.4310/0.5140	0.00/0.00

All sequenced species of *Dudgeodes*, including undescribed OTUs, from continental Southeast Asia, excluding *D. palnius*, form a separate clade (Fig. 17). The phylogenetic reconstruction based of the COI gene supports *D. selvakumari* sp. nov. as a monophyletic clade with a bootstrap support of 100%. Genetic distances within the species is 0.00 (n = 3), which is partially due to all specimens having come from a single locality. Genetic distances between the new species and three other most related species according to ML tree (*D. romani*, *D.* sp. A, and *D.* sp. B) are large (0.43–0.46; Table 2). Notably that genetic distance, calculated using the Tamura-Nei with a gamma distribution, between *Dudgeodes palnius* and the clade of *D. selvakumari* sp. nov., *D. romani*, *D.* sp. A, and *D.* sp. B, that is not closely related to *D. palnius* according to the ML tree (genetic distance 0.70–0.84). There are also high genetic distances with these taxa using the Kimura 2-parameter model with a gamma distribution. These results cannot be explained and, in our opinion, mistakes in *D. palnius* sequencing cannot be excluded.

Acknowledgements

We are grateful to Andrii Khomenko (V.N. Karazin Kharkiv National University, Kharkiv, Ukraine) for his advice on molecular study, and to Céline Stoffel (Museum of Zoology, Lausanne, Switzerland) for her dedicated work with the genetic procedures. We are also grateful to the anonymous reviewers and editors, Robert Forsyth and Ben Price, who helped to improve the paper significantly.

References

Anbalagan S, Balachandran C, Kannan M, Dinakaran S, Krishnan M (2015) First record and a new species description of *Dudgeodes* (Ephemeroptera: Teloganodidae) from South India. Turkish Journal of Zoology 39(2): 308–313. https://doi.org/10.3906/zoo-1401-74

Auychinda Ch, Sartori M, Boonsoong B (2020) Review of *Notacanthella* Jacobus & McCafferty, 2008 (Ephemeroptera: Ephemerellidae) in Thailand, with the redescription of *Notacanthella commodema* (Allen, 1971). Zootaxa 4731(3): 414–424. https://doi.org/10.11646/zootaxa.4731.3.9

Chakrabarty P, Warren M, Page LM, Baldwin CC (2013) GenSeq: An updated nomenclature and ranking for genetic sequences from type and non-type sources. ZooKeys 346: 29–41. https://doi.org/10.3897/zookeys.346.5753

Folmer O, Black M, Hoeh W, Lutz R, Vrijenhoek R (1994) DNA primers for amplification of mitochondrial cytochrome c oxidase subunit I from diverse metazoan invertebrates. Molecular Marine Biology and Biotechnology 3(5): 294–299.

Garces JM, Sartori M, Freitag H (2020) Integrative taxonomy of the genus *Dudgeodes* Sartori, 2008 (Insecta, Ephemeroptera, Teloganodidae) from the Philippines with description of new species and supplementary descriptions of Southeast Asian species. ZooKeys 910: 93–129. https://doi.org/10.3897/zookeys.910.48659

Kimura M (1980) A simple method for estimating evolutionary rates of base substitutions through comparative studies of nucleotide sequences. Journal of Molecular Evolution 16: 111–120. https://doi.org/10.1007/BF01731581

Martynov AV, Palatov DM, Boonsoong B (2016) A new species of *Dudgeodes* Sartori, 2008 (Ephemeroptera: Teloganodidae) from Thailand. Zootaxa 4121(5): 545–554. https://doi.org/10.11646/zootaxa.4121.5.4

Martynov AV, Selvakumar C, Subramanian KA, Sivaramakrishnan KG, Chandra K, Palatov DM, Sinha B, Jacobus LM (2019) Review of the *Cincticostella insolta* (Allen, 1971) complex (Ephemeroptera: Ephemerellidae), with description of three new species from northern India and Nepal. Zootaxa 4551(2): 147–179. https://doi.org/10.11646/zootaxa.4551.2.2

Martynov AV, Selvakumar C, Palatov DM, Subramanian KA, Sivaramakrishnan KG, Vasanth M, Jacobus LM (2021a) Overview of Indian and Nepali representatives of the *Cincticostella nigra* (Uéno, 1928) complex (Ephemeroptera: Ephemerellidae), with discussion about *Cincticostella* Allen, 1971 species complexes. ZooKeys 1040: 123–166. https://doi.org/10.3897/zookeys.1040.64280

Martynov AV, Selvakumar C, Subramanian KA, Sivaramakrishnan KG, Varsanth M, Sinha B, Jacobus LM (2021b) Overview of Indian Hyrtanellini (Ephemeroptera: Ephemerellidae), with new species and records from related regions. Zootaxa 4975(3): 451–482. https://doi.org/10.11646/zootaxa.4975.3.2

Sartori M, Peters JG, Hubbard MD (2008) A revision of Oriental Teloganodidae (Insecta, Ephemeroptera, Ephemerelloidea). Zootaxa 1957(1): 1–51. https://doi.org/10.11646/zootaxa.1957.1.1

Selvakumar C, Sivaramakrishnan KG, Jacobus LM, Janarthyanan S, Arumugam M (2014) Two new genera and five new species of Teloganodidae (Ephemeroptera) from South India. Zootaxa 3846(1): 87–104. https://doi.org/10.11646/zootaxa.3846.1.4

Selvakumar C, Sivaramakrishnan KG, Janarthanan S (2016) DNA barcoding of mayflies (Insecta: Ephemeroptera) from South India. Mitochondrial DNA. Part B 1(1): 651–655. https://doi.org/10.1080/23802359.2016.1219623

Selvakumar C, Sivaramakrishnan KG, Kubendran T, Chandra K (2018a) Inventory of teloganodid mayflies (Ephemeroptera: Teloganodidae) from southern India with records of endemic taxa. Journal of Threatened Taxa 10(6): 11800–11805. https://doi.org/10.11609/jott.3834.10.6.11800-11805

Selvakumar C, Sinha B, Vasanth M, Subramanian KA, Sivaramakrishnan KG (2018b) A new record of monogeneric family Vietnamellidae (Insecta: Ephemeroptera) from India. Journal of Asia-Pacific Entomology 21(3): 994–998. https://doi.org/10.1016/j.aspen.2018.07.015

Sivaruban T, Srinivasan P, Barathy S, Rosi MB, Isack R (2021) A new species of *Sparsorythus* Sroka & Soldán, 2008 (Ephemeroptera: Tricorythidae) from Eastern Ghats of Southern India. Zootaxa 4915(2): 237–245. https://doi.org/10.11646/zootaxa.4915.2.3

Srinivasan P, Sivaruban T, Barathy S, Isack R (2021) A new species of *Dudgeodes* Sartori, 2008 (Ephemeroptera: Teloganodidae) from Megamalai hills of southern Western Ghats, India. Zootaxa 4990(3): 571–576. https://doi.org/10.11646/zootaxa.4990.3.8

Tamura K, Nei M (1993) Estimation of the number of nucleotide substitutions in the control region of mitochondrial DNA in humans and chimpanzees. Molecular Biology and Evolution 10(3): 512–526. https://doi.org/10.1093/oxfordjournals.molbev.a040023

Tamura K, Stecher G, Kumar S (2021) MEGA 11: Molecular Evolutionary Genetics Analysis Version 11. Molecular Biology and Evolution 38(7): 3022–3027. https://doi.org/10.1093/molbev/msab120

Vuataz L, Sartori M, Wagner A, Monaghan MT (2011) Toward a DNA taxonomy of Alpine *Rhithrogena* (Ephemeroptera, Heptageniidae) using a mixed Yule-coalescent analysis of mitochondrial and nuclear DNA. PLoS ONE 6(5): e19728. https://doi.org/10.1371/journal.pone.0019728

ZooKeys 1113: 199–227 (2022)
doi: 10.3897/zookeys.1113.85769
https://zookeys.pensoft.net

RESEARCH ARTICLE

A peer-reviewed open-access journal
ZooKeys
Launched to accelerate biodiversity research

A peculiar new species of *Dione* (*Agraulis*) Boisduval & Le Conte (Lepidoptera, Nymphalidae, Heliconiinae) associated with *Malesherbia* Ruiz & Pavón (Passifloraceae) in xeric western slopes of the Andes

Jackie Farfán[1,2], José Cerdeña[1,2], Héctor A. Vargas[3], Gislene L. Gonçalves[3,4], Gerardo Lamas[5], Gilson R. P. Moreira[6]

1 *PPG Biologia Animal, Departamento de Zoologia, Instituto de Biociências, Universidade Federal do Rio Grande do Sul, Av. Bento Gonçalves, 9500, Porto Alegre, RS 91501-970, Brazil* **2** *Museo de Historia Natural, Universidad Nacional de San Agustín de Arequipa, Av. Alcides Carrión s/n, Arequipa, Peru* **3** *Departamento de Recursos Ambientales, Facultad de Ciencias Agronómicas, Universidad de Tarapacá, Casilla 6-D, Arica, Chile* **4** *Departamento de Genética, Instituto de Biociências, Universidade Federal do Rio Grande do Sul, Av. Bento Gonçalves 9500, Porto Alegre RS, 91501-970, Brazil* **5** *Departamento de Entomología, Museo de Historia Natural, Universidad Nacional Mayor de San Marcos, Apartado 14-0434, Lima-14, Peru* **6** *Departamento de Zoologia, Instituto de Biociências, Universidade Federal do Rio Grande do Sul, Av. Bento Gonçalves 9500, Porto Alegre RS, 91501-970, Brazil*

Corresponding author: Jackie Farfán (jjackie4u@gmail.com)

Academic editor: Martin Wiemers | Received 26 April 2022 | Accepted 17 June 2022 | Published 18 July 2022

https://zoobank.org/C4EB0D82-D142-49EE-A95F-DA97BEBDEBB6

Citation: Farfan J, Cerdeña J, Vargas HA, Gonçalves GL, Lamas G, Moreira GRP (2022) A peculiar new species of *Dione* (*Agraulis*) Boisduval & Le Conte (Lepidoptera, Nymphalidae, Heliconiinae) associated with *Malesherbia* Ruiz & Pavón (Passifloraceae) in xeric western slopes of the Andes. ZooKeys 1113: 199–227. https://doi.org/10.3897/zookeys.1113.85769

Abstract

Butterflies associated with xerophytic environments of the Andes have been little studied, and they exhibit high levels of endemism. Herein *Dione* (*Agraulis*) *dodona* Lamas & Farfán, **sp. nov.** (Nymphalidae; Heliconiinae) is described, distributed on the western slopes of the Andes of Peru and northern Chile, between 800 and 3,000 m elevation. Adults of both sexes, and the immature stages, are described and illustrated based on light and scanning electron microscopy. The immature stages are associated with *Malesherbia tenuifolia* D. Don (Passifloraceae) found in xeric environments, representing a new record of this genus as a host plant for the subfamily Heliconiinae. Conspicuous morphological differences are presented for all stages at the generic level. Based on a phylogenetic analysis of the COI barcode mitochondrial gene

fragment, *D.* (*A.*) *dodona* Lamas & Farfán, **sp. nov.** is distinguished as an independent lineage within the *Agraulis* clade of *Dione*, with ca. 5% difference to congeneric species.

Keywords
Chile, Heliconiines, immature stages, Peru, taxonomy

Introduction

The Andes are a ~ 8000 km long mountain belt on western South America, forming one of the longest mountain ranges on Earth (Montgomery et al. 2001), and harboring a variety of ecosystems with different environmental characteristics (Myers et al. 2000; Veblen et al. 2007). The western slopes of the central Andes join the Peru-Chile Pacific and Atacama deserts from 10 °S in central Peru to 30 °S in northern Chile, where xerophytic shrub land vegetation is predominant between 1,500 and 3,000 m elevation (Gutiérrez et al. 1998; Montesinos et al. 2012), containing many endemic plants and animals (Zeballos-Patrón et al. 2001; Arakaki and Cano 2003; Gutiérrez et al. 2019; Farfán et al. 2020; Málaga et al. 2020). The butterfly fauna in this area is depauperate and poorly known, with very few species recorded among the Papilionidae, Hesperiidae, Pieridae, and Nymphalidae, including four species of passion-vine butterflies (Heliconiinae) previously ascribed to *Dione* Hübner, [1819] and *Agraulis* Boisduval & Le Conte, [1835] (Peña and Ugarte 2006; Benyamini et al. 2014; Farfán 2018).

Heliconiinae have been the subject of widespread study in various aspects of biology for the last 160 years, comprising more than 700 scientific publications (Bates 1862; Jiggins 2017), highlighting their importance as a model in the study of evolution (e.g., Mallet and Joron 1999), ecology (e.g., Gilbert 1991; Schluter 2000) and behavior (Deinert et al. 1994), among others. The phylogenetic relationships of the members of the Heliconiinae have been analyzed from a morphological (Penz 1999; Penz and Peggie 2003) and molecular (Brower and Egan 1997; Beltrán et al. 2002, 2007; Kozak et al. 2015) perspective, recognizing four tribes: Acraeini, Heliconiini, Argynnini and Vagrantini. The Heliconiini included until recently the genera *Philaethria* Billberg, 1820, *Podotricha* Michener, 1942, *Dryas* Hübner, [1807], *Dryadula* Michener, 1942, *Dione* Hübner, [1819], *Agraulis* Boisduval & Le Conte, [1835], *Eueides* Hübner, 1816, and *Heliconius* Kluk, 1780, of which the latter is the most diverse with ~ 45 species and 200 subspecies (Lamas 2004; Kozak et al. 2015; Zhang et al. 2019). All the heliconiine species have as host plants members of the Passifloraceae s. l. (Bremer et al. 2009), mainly *Passiflora* L. (de Castro et al. 2018). There is a large number of studies related to the coevolution between butterflies and host plants, using the *Passiflora*-heliconiine system as a model for the study of coevolution in insects (Ehrlich and Raven 1964; Gilbert 1972; Benson et al. 1975; de Castro et al. 2018).

Phylogenetic studies have proposed that *Agraulis* is among the oldest lineages within the Heliconiini (Brower and Egan 1997; Penz 1999; Beltrán et al. 2007). For a long time, it was considered as a monotypic genus, with eight subspecies, occupying the larg-

est distribution area within the tribe, ranging from the central west of the USA to the center of Argentina and Chile (Núñez et al. 2022). Recently, Zhang et al. (2019) through genome-scale phylogenetic analyses suggested that *Agraulis* is best treated as a subgenus of *Dione*. However, later on, Núñez et al. (2022) based on morphometric and molecular data maintained the two separate genera as valid. They also raised the eight subspecies of *Agraulis* to the species level including an undescribed species from the western slope of the Andes, previously listed as *Agraulis* n. sp. in the checklist of Neotropical butterflies (Lamas 2004). The proposal of Zhang et al. (2019) is followed in this study.

This undescribed species has been considered rare, with only seven museum specimens known until 2013. The first one was collected in northern Chile in 1951 at an altitude of 3,000 m, and erroneously identified as *A. vanillae* (Linnaeus, 1758), as illustrated in the book Butterflies of Chile (Peña and Ugarte 2006). The additional specimens are known from central and southern Peru, and northern Chile. During a recent exploration in the Department of Arequipa, southern Peru, adults of this undescribed species were observed flying, crossing the road in a sector of a desert hillside with very sparse vegetation, and laying eggs on the flowers of *Malesherbia tenuifolia* D. Don (Passifloracae). Thus, by finding the host plant, and then rearing the immatures, it was possible to obtain sufficient material to carry out a comparative study at the generic level, where we confirmed for all stages that it does not belong to any described species of *Dione* (*Agraulis*).

Thus, in the present paper, the new species is described and illustrated based on the morphology of adults and immature stages. We also present a phylogenetic analysis of mitochondrial (COI) DNA sequences including congeneric species.

Materials and methods

Immature stages were collected from plants of *Malesherbia tenuifolia* D. Don (Passifloraceae), near the village of Pacaychacra (15°50'57"S, 72°38'9"W), Condesuyos Province, 23–24 km SE from the town of Chuquibamba, Department of Arequipa, southern Peru, at 1,800 m elevation. They were brought to the laboratory of Área de Entomología, Museo de Historia Natural de la Universidad Nacional de San Agustin de Arequipa (**MUSA**), and maintained under natural conditions of temperature and humidity. The eggs were placed until larval hatching. Fresh larvae were transferred to small plastic containers and fed with *M. tenuifolia* leaves. Six larvae successfully completed development to adults, with four males and two females emerging that were deposited in the collection of the MUSA. Additional field-collected eggs, larvae and pupae were fixed in Dietrich´s fluid and preserved in 70% ethanol. Also, flying adults were eventually netted near the host plants. Studies of morphology of the immature stages were conducted at the Laboratório de Morfologia e Comportamento de Insetos (**LMCI**), Departamento de Zoologia, Universidade Federal do Rio Grande do Sul (**UFRGS**), Porto Alegre, RS, Brazil.

Adult specimens of related taxa were examined at Museo de Historia Natural, Universidad Nacional Mayor de San Marcos, Lima, Peru (**MUSM**), and at MUSA. Photographs of all relevant type specimens were examined at MUSM; such images are

also available in Warren et al. (2017). Images taken of male genitalia dissected from the new species are presented in Suppl. material 1.

Genitalia dissections were performed using standard techniques, where abdomens of adults were previously soaked in hot 10% KOH solution for 10 min, and dissected parts were stored in glycerol. To study the venation, wings were diaphanized by soaking them in 2% NaClO aqueous solution (bleach), and then dry-mounted.

Morphological observations were performed with the aid of a Zeiss Stemi 305 stereo microscope, and structures selected to be illustrated were previously photographed with a Nikon DS-Ri2 camera through a Nikon SMZ25 stereo microscope at the Laboratório de Sistemática Animal of Universidad Nacional San Agustin de Arequipa (**UNSA**). Images were assembled and edited in Nikon NIS-Elements and Photoshop version 21.2.0. The descriptive terminology of morphological structures follows da Silva et al. (2006), Beebe et al. (1960), Emsley (1963) and Klots (1970), for eggs, larvae, pupae, and adults, respectively.

For scanning electron microscope analyses, specimens were dehydrated in a Bal-Tec CPD 030 critical-point dryer, mounted with double-sided tape on metal stubs, and coated with gold in a Quorum Q150R plus sputter coater. They were then examined and photographed in a XL-30 Philips scanning electron microscope at the Laboratório Central de Microscopia e Microanálise (**LabCEMM**) of Pontifícia Universidade Católica do Rio Grande do Sul (**PUCRS**), Porto Alegre, RS, Brazil. Priority in this case was given to key diagnostic characters that were used to distinguish the new *Dione* species from congeners; additional scanning electron micrographs are presented for the immature stages in Suppl. material 2.

Genomic DNA was extracted from two specimens of the new *Dione* species (Table 1), collected in the type locality, following the procedures described in Huanca-Mamani et al. (2015). A fragment of 650 base pairs of the COI gene was amplified by polymerase chain reaction (PCR) with the primers LEP-F1 and LEP-R1 (Hebert et al. 2004). PCR amplicons were purified and sequenced by Macrogen (Republic of South Korea) using LEP-F1

Table 1. Specimens used for molecular analyses of *Dione* (*Agraulis*) *dodona* sp. nov. The collection sites (country/locality) and vouchers from which the sequences derived are presented, including the references. Genbank and BOLD identifiers link the record to the databases.

Species	Country/Locality	Voucher	Genbank/BOLD Accession code	Reference
Dione (*Agraulis*) *dodona* sp. nov.	Peru / Arequipa	J151	OM925454/BIGLE001-22	This study
Dione (*Agraulis*) *dodona* sp. nov.	Peru / Arequipa	459	OM925453 /BIGLE002-22	This study
Dione (*Agraulis*) *incarnata*	Costa Rica / Guanacaste	00-SRNP-16229	GU333737 / MHACG518-04	Núñez et al. 2022
Dione (*Agraulis*) *forbesi*	Peru	G3	MZ229712.1	Núñez et al. 2022
Dione (*Agraulis*) *insularis*	Dominican Republic	NW152-16	GQ864730	Núñez et al. 2022
Dione (*Agraulis*) *lucina*	Ecuador	LEP-58352	MZ229704.1	Núñez et al. 2022
Dione (*Agraulis*) *maculosa*	Argentina/ Entre Ríos	MACN-Bar-Lep-ct 01616	MF545390 / LEPAR178-11	Lavinia et al. 2017
Dione (*Agraulis*) *vanillae*	Ecuador	LEP-55200	MZ229702.1	Núñez et al. 2022
Dione (*Dione*) *glycera*	-	BMC17102	MN306819.1	Marín et al. 2021
Dione (*Dione*) *juno*	Peru/ San Martín	8727	KP074744.1	Kozak et al. 2015
Dione (*Dione*) *moneta*	Argentina/ Salta	MACN-Bar-Lep-ct 07589	MZ335918.1/LNOA484-16	NCBI deposit

primer. Sequences obtained in this study were deposited in GenBank and BOLD databases (Table 1). The phylogenetic status of the new *Dione* species was explored by combining our sequences with COI data of six congeners (*D.* (*A.*) *incarnata* Riley, 1926, *D.* (*A.*) *forbesi* Michener, 1942, *D.* (*A.*) *insularis* (Maynard, 1889), *D.* (*A.*) *lucina* (C. Felder & R. Felder, 1862), *D.* (*A.*) *maculosa* Stichel, [1908], and *D.* (*A.*) *vanillae* (Linnaeus, 1758)) obtained from Núñez et al. (2022). In addition, three species of *Dione* (*Dione*), *juno* (Cramer, 1779), *glycera* (C. Felder & R. Felder, 1861) and *moneta* Hübner, [1825] were included in the analysis (Table 1). The COI-tree was inferred by using the Maximum Likelihood (ML) method and General Time Reversible model (Nei and Kumar 2000), with heuristic search obtained automatically by applying Neighbor-Join and BioNJ algorithms to a matrix of pairwise distances, with 500 bootstrap replications. Analysis was conducted in MEGA X (Kumar et al. 2018). Genetic distances between species of subgenera *Agraulis* and *Dione* were quantified using the Kimura 2-parameter model in MEGA.

Abbreviations for the museum collections and institutions from which specimens were examined are:

LMCI Laboratório de Morfologia e Comportamento de Insetos, Universidade Federal do Rio Grande do Sul, Porto Alegre, Rio Grande do Sul, Brazil;
MHNS Museo Nacional de Historia Natural de Chile, Santiago de Chile, Chile;
IDEA Colección Entomológica de la Universidad de Tarapacá, Arica, Chile;
MUSA Museo de Historia Natural, Universidad Nacional de San Agustín de Arequipa, Arequipa, Peru;
MUSM Museo de Historia Natural, Universidad Nacional Mayor San Marcos, Lima, Peru.

Taxonomic account

***Dione* (*Agraulis*) *dodona* Lamas & Farfán, sp. nov.**
https://zoobank.org/687E38BC-19C6-48F0-9B93-EE7B9A7C40A5
Figs 1–10

Dione vanillae: Peña 1951: 262.
Agraulis vanillae: Ureta 1963: 114–115; Pérez-D'Angello 1970: 6; Etcheverry 1970: 95; Peña and Ugarte 2006: 313, figs; Benyamini et al. 2014: 18.
Agraulis vanillae forbesi: Herrera,1972: 73.
Agraulis [n. sp.]: Lamas 2004: 264.
Agraulis sp. n.: Farfán 2018: 367.
Agraulis sp.: Núñez et al. 2022: 152–178.

Type locality. Peru, Arequipa, Pacaychacra [15°54'S, 72°33'W], 1500 m.

Type material. ***Holotype*** ♂, Peru, Arequipa, Pacaychacra, 15°54'S, 72°33'W, 1500 m, reared from eggs collected on *Malesherbia tenuifolia* (Passifloraceae), 24.VII.2019, J. Farfán leg. deposited in MUSM. ***Paratypes*** (25♂, 17♀): Peru. **Lima**: 1♂, San

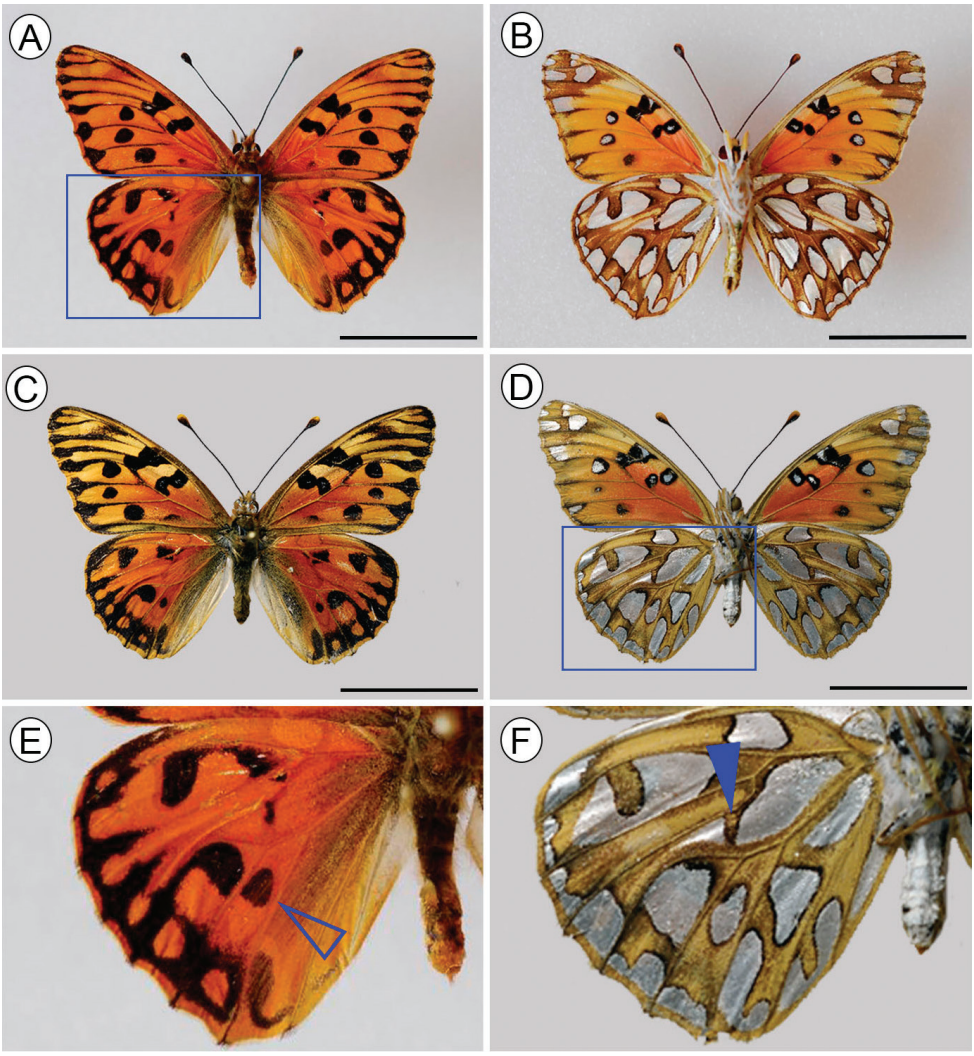

Figure 1. Adults of *Dione* (*Agraulis*) *dodona* sp. nov. **A, B** male, holotype **C, D** female paratype **E, F** details of hindwing pattern color (indicated by blue squares in **A** and **D** respectively), open arrow points black spot on Cu_1-Cu_2 cell, and close arrow on silver discal spot. Left: dorsal view; right: ventral view. Scale bars: 2 cm.

Bartolomé, 1600 m, [11°55'S, 76°31'W], 21.iii.[19]81, P. Hocking (MUSM); 1♀, Cocachacra, 1450 m, [11°55'S, 76°32'W], 6.x.[19]83, P. Hocking [MUSM-ENT 008630] (MUSM); 1♀, Río Rímac, Chaute, 2350 m, 11°56'S, 76°30'W, 12.v.2012, P. Hocking (MUSM). **Arequipa**: 2♀, 7 km E Cháparra, 1450m, [15°41'S, 73°49'W], 14.iv.[19]88, G. Lamas [MUSM-ENT 008631, 008632] (MUSM); 1♂, entre Majes y Chuquibamba, 15°55'S, 72°33'W, 1500 m, 24.iv.2017, G. Lamas (MUSM); 1♂ same data as holotype [LMCI 357–51] (LMCI); 1♂ same data as holotype (MUSA); 1♂, 2♀, same data as holotype but with date 15.XII.2020 (MUSA); 1♂ same data as holotype

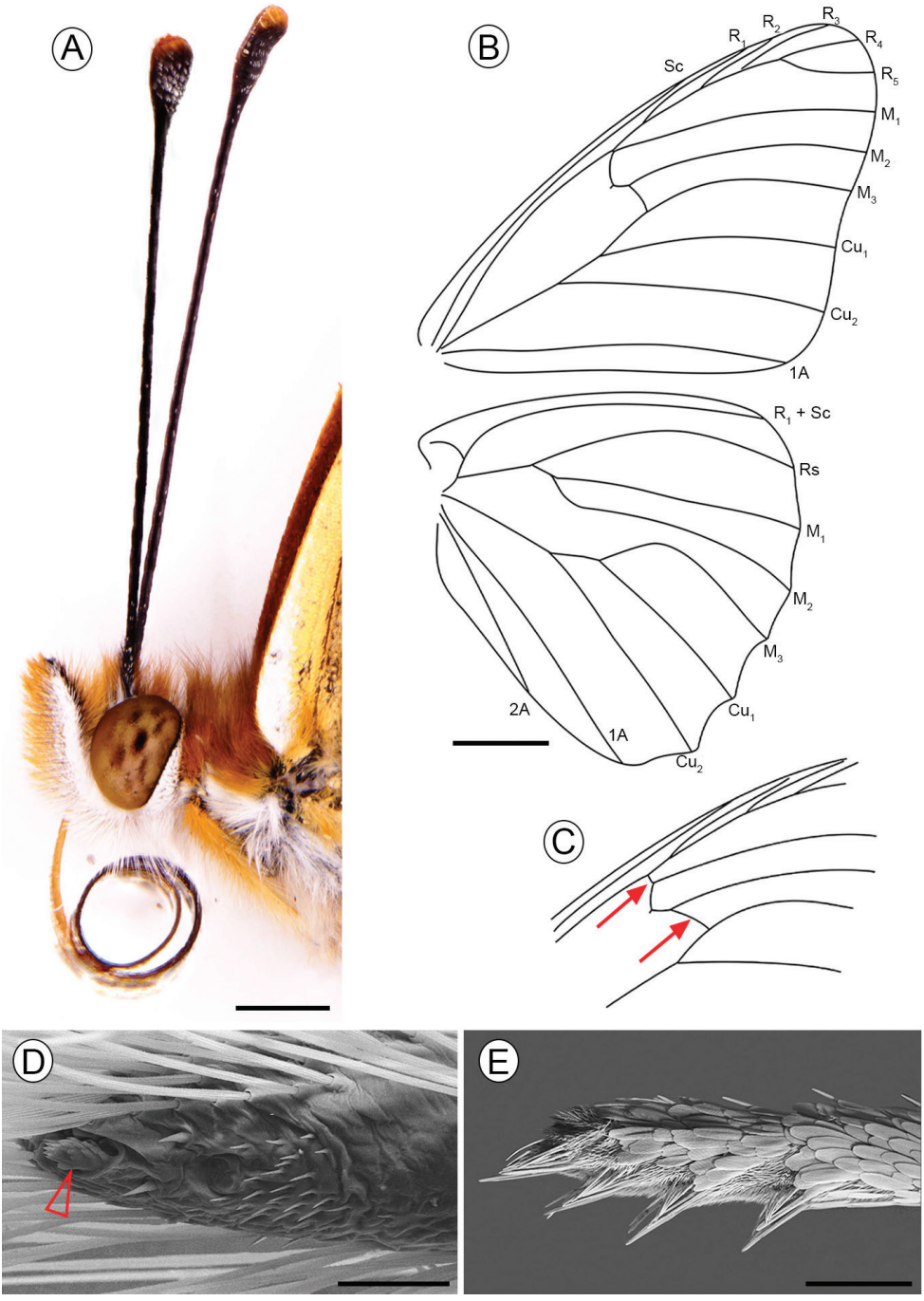

Figure 2. Adult morphology of *Dione* (*Agraulis*) *dodona* sp. nov. **A** head, male, lateral view **B** wing venation, male **C** detail of forewing venation, female (red setae points differences with male) **D, E** distal portion of prothoracic tarsi under scanning electron microscopy, male in ventral view **D** female in lateral view **E** distal tarsomere indicated by open arrow in E. Scale bars: 1 mm (**A**); 5 mm (**B**); 50 μm (**D**); 250 μm (**E**).

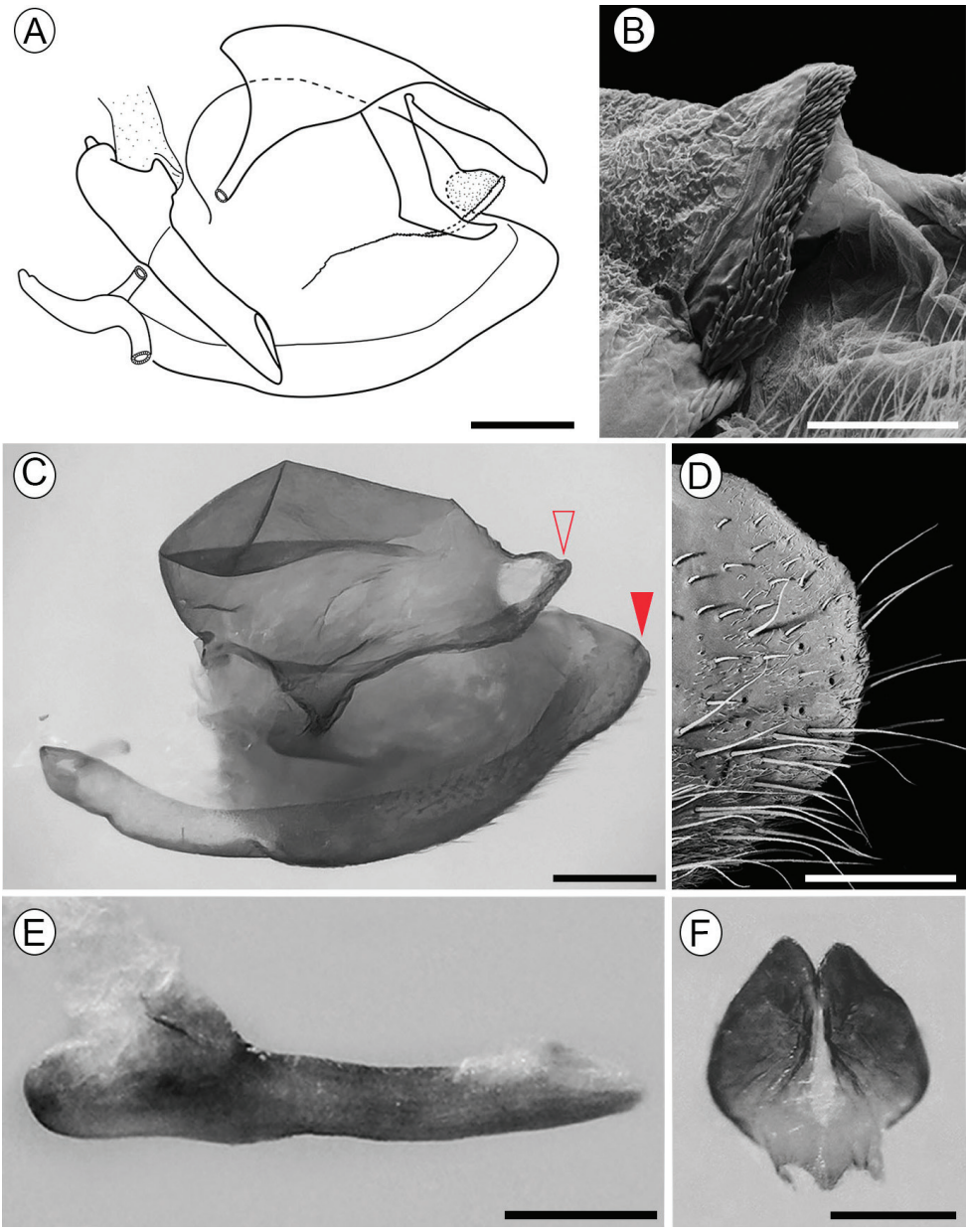

Figure 3. Male genitalia of *Dione* (*Agraulis*) *dodona* sp. nov. **A** general, mesal view **B** distal portion of valve crista under scanning electron microscopy (pointed with open arrow in **C**) **C** right valve **D** termen of valve under scanning electron microscopy (pointed with closed arrow in **C**) **E** aedeagus, lateral **F** juxta, posterior. Scale bars: 1mm (**A**); 250 μm (**B**); 500 μm (**C, E, F**); 200 μm (**D**).

but with date 24.vii.2021 (MUSA); 4♂ Aplao, Valle Majes, 15°53'46"S, 72°28'03"W, 800 m, 02.vi.2013, Leg. J. Cerdeña / M. Delgado (MUSA); 1♂, Condesuyos, Pacaychacra,15°54'59.2"S, 72°33'01.5"W, 1500 m, 02.IX.2020, Leg. Jose Cerdeña

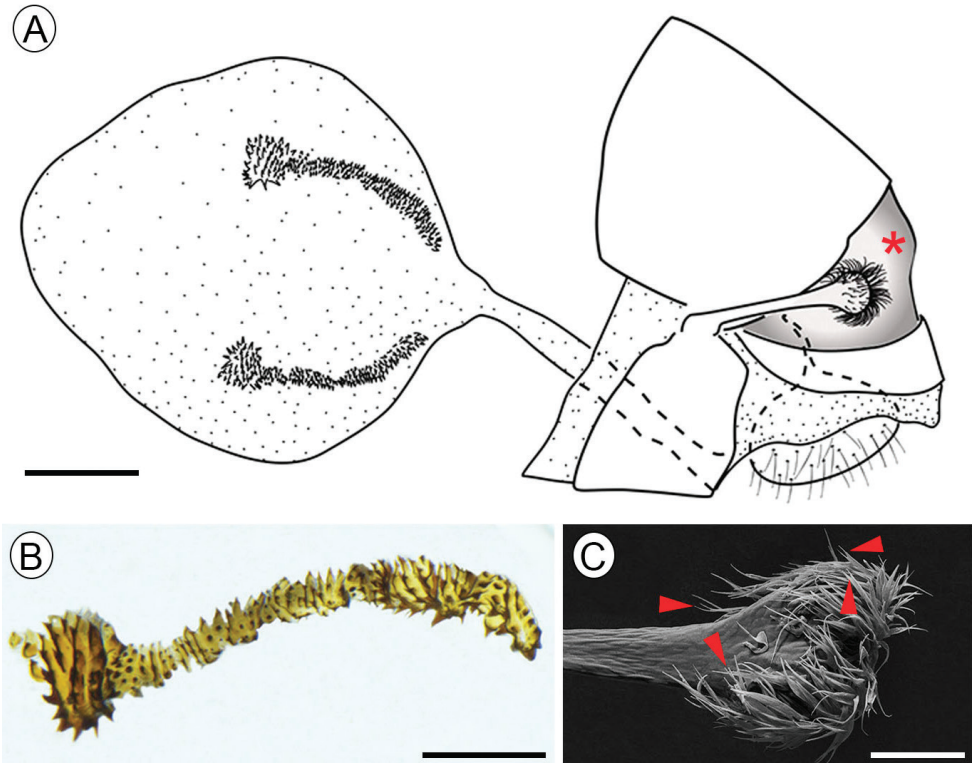

Figure 4. Female genitalia of *Dione* (*Agraulis*) *dodona* sp. nov. **A** external view, lateral **B** signum **C** stink club under scanning electron microscopy, specialized scales indicated by closed arrows. Asterisk indicated dorsal glands. Scale bars: 1 mm (**A**); 500 μm (**B**); 200 μm (**C**).

(MUSA); 1♂, same data, but 13.XII.2020 (MUSA); 1♀, same data, but 24.VII.2021, Jackie Farfán (MUSA); 1♀, same data, but 12.XI.2019, [LMCI 357–52] (LMCI); 3♂, Yura, 2 Km SW Yura viejo, 16°13'19"S, 71°42'23"W, 2600 m 21.IV.2022, Leg. Jackie Farfán (MUSA). **Moquegua**: 6♂, 1♀, Torata, 170630/705036 [17°06'30"S, 70°50'36"W], 2090m, 26.VII.2021, Leg. Jackie Farfán (MUSA); 1♂, 1♀, same data [LMCI 357–53, LMCI 357–54] (LMCI); 4♀, La Capilla, 13 Km S Puquina, 164450/711054 [16°44'50"S, 71°10'54"W], 1800 m, 28.XII.2013, Leg. J. Farfán / J. Cerdeña (MUSA); 1♀, Omate, 3 Km SW Omate, 16°41'15.27"S, 70°59'13.73"W, 2000 m, 27.X.2017, Leg. Robert Cornejo (MUSA). **Tacna**: 1♂, Chululuni, 17°22'02"S, 70°28'24"W, 1800 m, 18.XII.2020, Leg. Jackie Farfán (MUSA). CHILE. **Arica**: 1♂, Las Peñas, 18°33'08"S, 69°46'03"W, 1580 m, 02.XII.2020, H. A. Vargas leg. [IDEA-LEPI–2022–008] (IDEA); 1♀, same data, but 10.XI.2020; [IDEA-LEPI–2022–007] (IDEA). **Tarapacá**: 1♀, Iquique, Parca, 3000 m, [20°01'S, 69°01'W], ix/x.[19]51, L. E. Peña (MUSM); 1♂, Q[uebrada] de Guatacondo, "Cauquenisca" [= Cautenicsa], 2300 m, [20°56'S, 69°01'W], 26-X-1968, P. Millas (MHNS).

Immature stages preserved in 70% ethanol, with the same data as the holotype, collected on *Malesherbia tenuifolia* (Passifloraceae) with dates VI.2018, X.2019 and

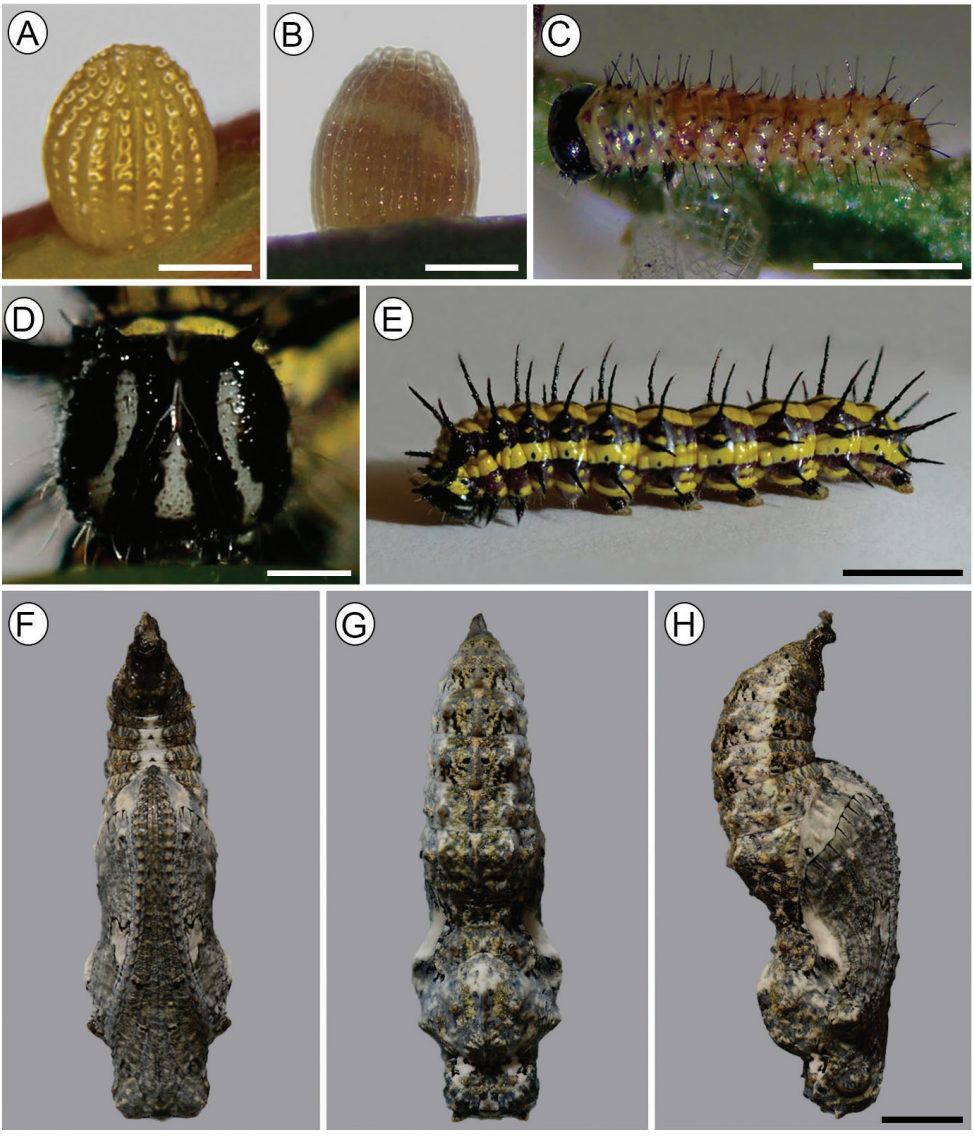

Figure 5. Immature stages of *Dione* (*Agraulis*) *dodona* sp. nov. **A** freshly-laid egg, lateral view **B** egg just prior to hatching, lateral **C** first instar, latero-dorsal **D, E** fifth instar, head in detail (anterior view) and general aspect (lateral), respectively **F, G, H** pupa in ventral, dorsal and lateral views, respectively. Scale bars: 400 µm (**A**); 1 mm (**C**); 5 mm (**E**); 4 mm (**H**).

IV.2021, were deposited in LMCI, under accession numbers 357–31 (14 eggs), 357–33, 357–40, 357–44 (20 larvae), 357–46, 357–47, 357–48, 357–49, 357–50 (5 pupae).

Diagnosis. *Dione* (*Agraulis*) *dodona* sp. nov. can be easily distinguished from its congeners by the wing pattern, presenting a black postdiscal spot between M_3-A_1 veins on the dorsal hindwing that is absent in all other species, and, also, by presenting a divided or partially divided silver spot in the discal cell on the ventral hindwing, always

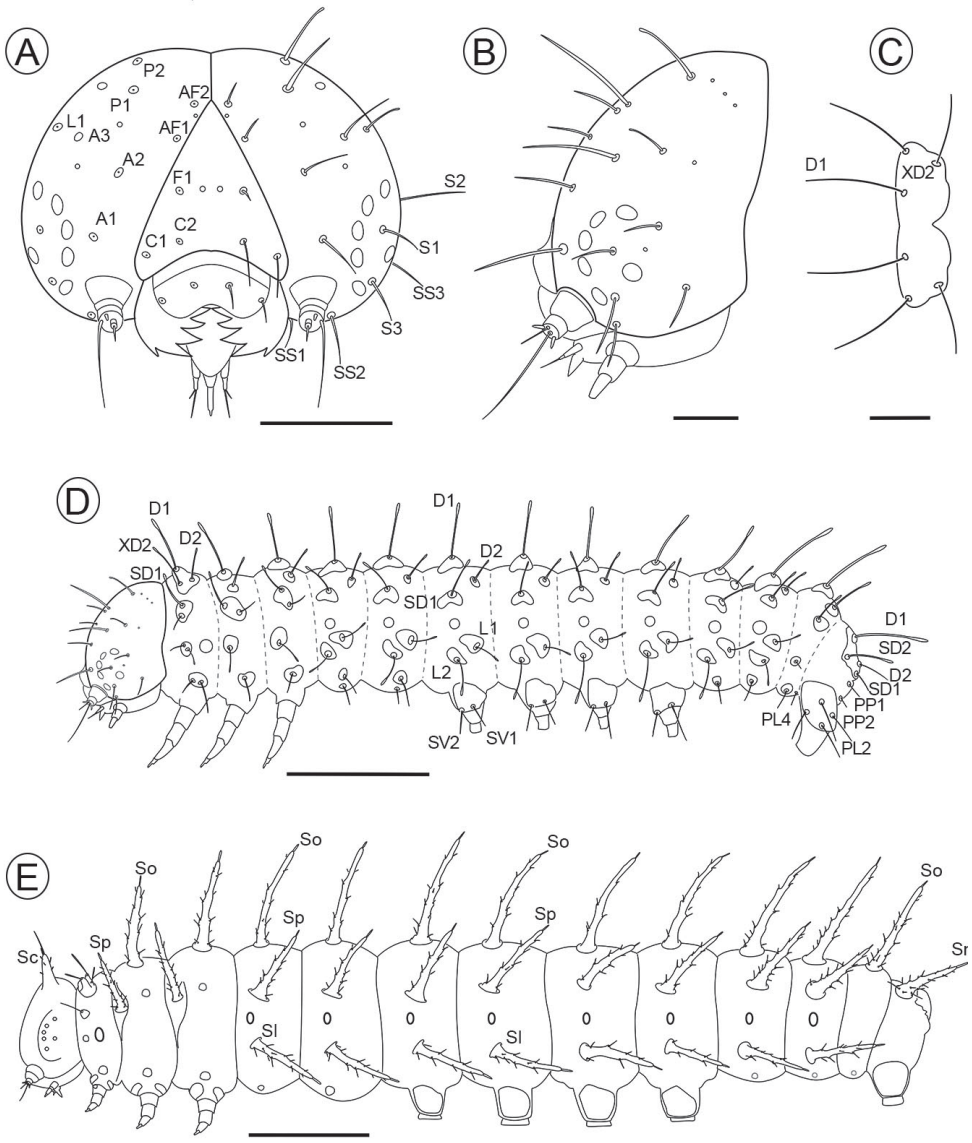

Figure 6. Larval chaetotaxy of *Dione* (*Agraulis*) *dodona* sp. nov. **A, B** head capsule, frontal and lateral view respectively **C** prothoracic dorsal shield, dorsal **D** first instar, lateral **E** fifth instar, lateral. A, anterior seta; AF, adfrontal seta; C, clypeal seta; D, dorsal seta; F, frontal seta; L, lateral seta; P, postero-dorsal seta; S, stemmatal seta; SS, sub-stemmatal seta; PL, seta of proleg cylindrical section of tenth abdominal segment; PP, paraproctal seta; Sc, cephalic scolus; SD, subdorsal seta; Sl, subspiracularscolus; Sn, anal scolus; So, dorsal scolus; Sp, supraspiracularscolus; SV, subventral seta; XD, prothoracic seta. Scale bars: 200 μm (**A**); 100 μm (**B, C**); 500 μm (**D**); 3 mm (**E**).

undivided in other species of *Dione* (*Agraulis*). In the male genitalia, the valvae have a rounded termen, without denticles, and the distal portion of the crista is narrow and straight. In other species, the termen is sub-triangular and shows denticles on the

Figure 7. Variation in coloration patterns among fifth-instar of *Dione* (*Agraulis*) *dodona* sp. nov., shown schematically for the head capsule and fourth abdominal segment, respectively, in frontal and lateral views **A** brownish **B** grayish **C** reddish.

margin, and the distal apex of the crista is transversally enlarged. Also, the juxta has its upper edge slightly split in *dodona*, which is widely open in other species. The aedeagus is straight in lateral view without cornuti in *dodona*, up-curved near distal end with cornuti in other species. The female genitalia possess evenly wide signa in the proximal portion, composed of robust spines, unlike other species that have smaller spines; the proximal apex of signa is narrower and progressively enlarges distally.

Furthermore, the immature stages of *Dione* (*Agraulis*) *dodona* sp. nov. show differences with the available data compared to other *Agraulis* species (Beebe et al. 1960; Brown 1981; da Silva et al. 2006). In the egg, the number of horizontal carinae almost doubles the number described for *Dione* (*Agraulis*) *maculosa* [cited as '*A. vanillae'*] (11–13 vs. 17–19), the egg being taller in *Dione* (*Agraulis*) *dodona* sp. nov. In relation to the larval stage, in the first instar, the main difference is the size of the D2 setae in the abdominal segments, being very small in *maculosa* and *insularis* (1/4 the length of D1) (Beebe et al. 1960; da Silva et al. 2006), but reaching more than half the length of D1 in *Dione* (*Agraulis*) *dodona* sp. nov. (Fig. 9B). In the fifth instar, the head scoli

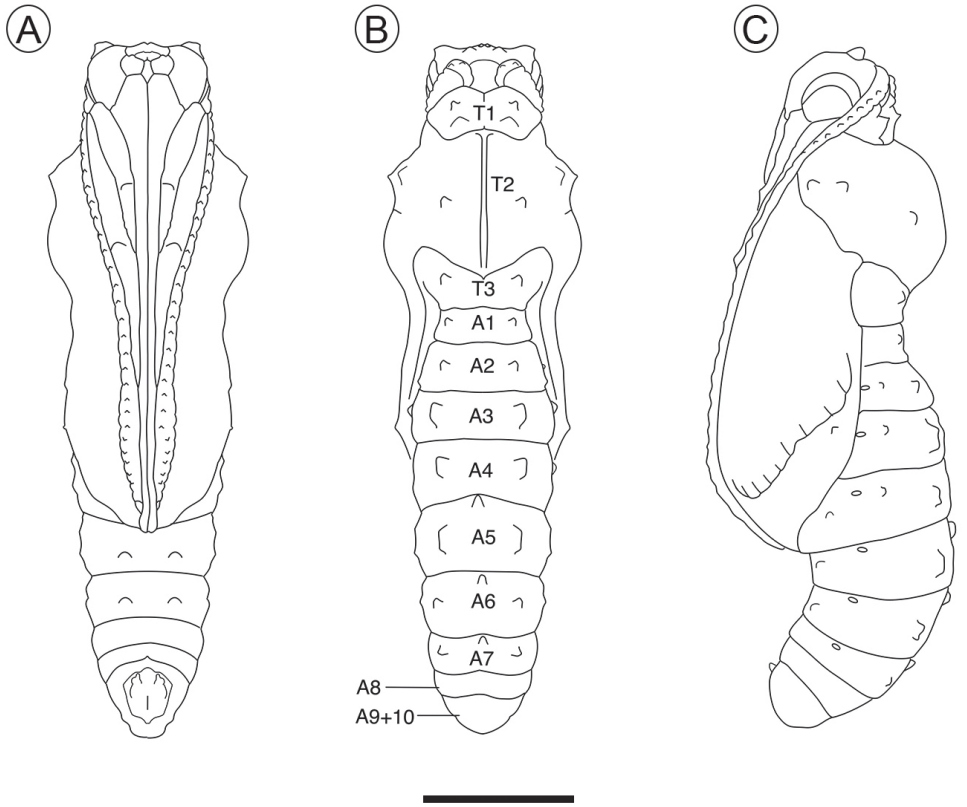

Figure 8. Pupa of *Dione* (*Agraulis*) *dodona* sp. nov. under **A** ventral **B** dorsal, and **C** lateral view, respectively. A, abdominal segment; T, thoracic segment. Scale bar: 4 mm.

in *maculosa* are well developed, whereas *Dione* (*Agraulis*) *dodona* sp. nov. bears short stout scoli (Figs 5D, 6E). Furthermore, the prothoracic dorsal plate in *Dione* (*Agraulis*) *dodona* sp. nov. has spine-like setae on top of enlarged conical projection (Fig. 9C), unlike *maculosa*, which has a simple seta bearing on a small projection (da Silva et al. 2006). In the pupa, the main differences are related to the head protuberances, which are small in *Dione* (*Agraulis*) *dodona* sp. nov. (Fig. 9D), more conspicuous, and as long as half the length of head in *maculosa*; also, the meso-dorsal crest is less pronounced in *Dione* (*Agraulis*) *dodona* sp. nov. (Fig. 9E), in *maculosa* the dorsal margins are more enlarged; protuberances on the abdominal segments do not occupy the entire length of the segment in *Dione* (*Agraulis*) *dodona* sp. nov. (Fig. 9F), in contrast to *maculosa* where protuberances fill all the length of the third abdominal segment.

Description. *Adult.* (Figs. 1–4). **Male:** Wingspan 44–52 mm (holotype 50 mm). *Head*: antennae approximately two thirds of the forewing in length, black with the tip of club orange (Fig. 2A), with 36 antennomers, 11 of which define the club. Palpus elongated, approximately twice the size of the head, with a dark brown dorsal color with light orange hairs, in ventral view white covered by white and orange hairs

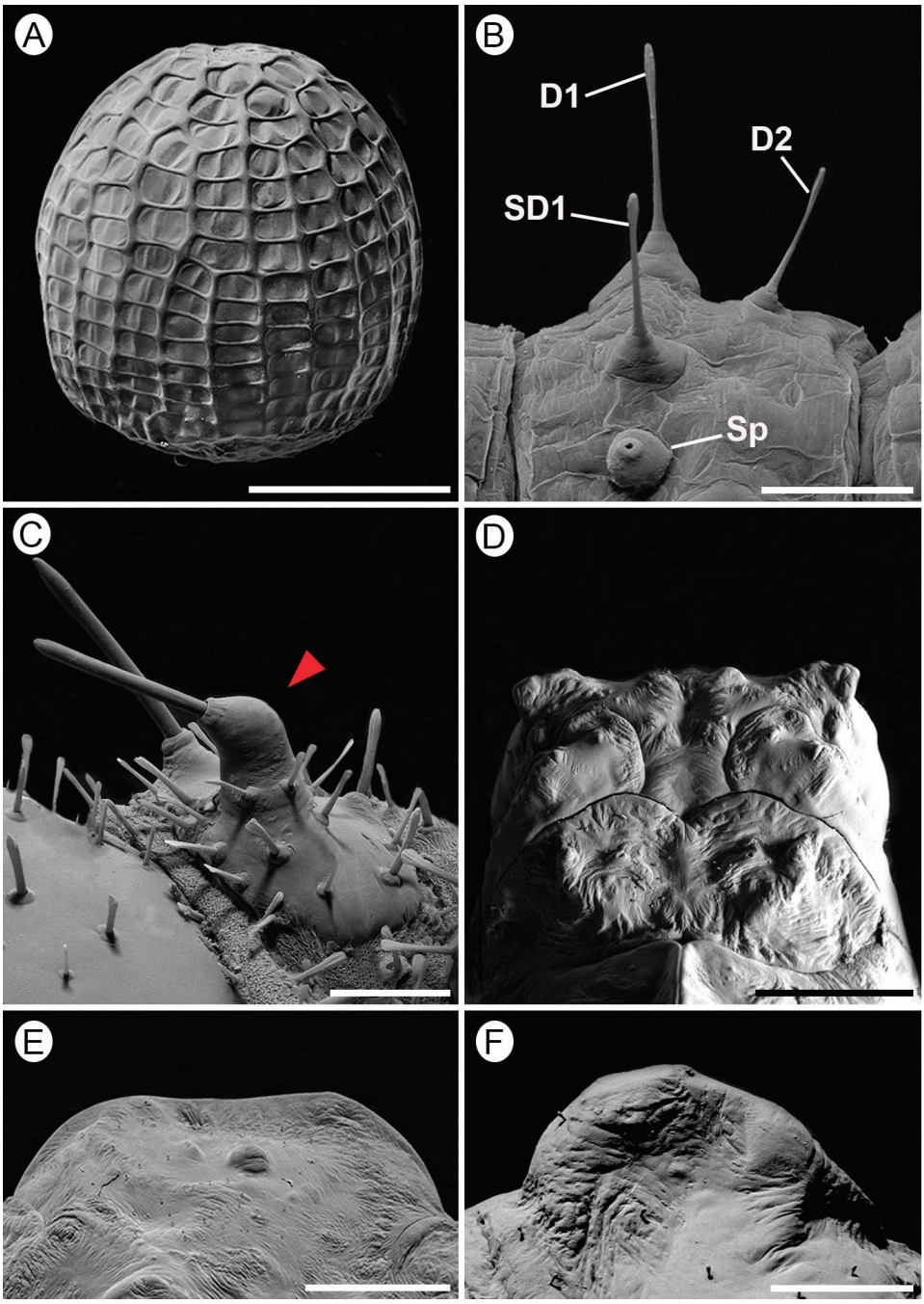

Figure 9. Immature stages of *Dione* (*Agraulis*) *dodona* sp. nov. under scanning electron microscopy **A** egg, lateral view **B** first instar, upper portion of fifth abdominal segment, lateral **C** fifth instar, prothoracic plate, postero-dorsal (protuberance pointed by close arrow) **D, E, F** pupal head (dorsal view), mesothoracic meso-dorsal crest (lateral), and latero-dorsal tubercle of third abdominal segment (lateral), respectively. Scale bars: 500 μm (**A, F**); 100 μm (**B**); 250 μm (**C**); 1.5 mm (**E, D**).

(Fig. 2A). *Thorax*: Generally brown. Body dorsally black with brown and orange hairs, ventrally covered by white and light orange scales, legs dorsally light orange with white and orange hairs at the base, ventrally white. Forewing length 25–28 mm (holotype: 27 mm), hindwing length 18–20 mm. Wing venation as described in Michener (1942) (Fig. 2B). Wing color pattern typical for the *Agraulis* clade except a black postdiscal spot between veins M_3-A_1 on dorsal hindwing and a silver spot located in the discal cell on ventral hindwing divided or partially divided (Fig. 1E, AF). *Abdomen*: dorsally brown with orange hairs, ventrally covered by white scales.

***Male genitalia*:** Rounded and subtriangular valvae occupying most of the genital capsule, being wide anteriorly and narrowest in the apex, with rounded pointed apex with hairs on ventral margin (Fig. 3D), costa with eversible pouch on its inner surface, bearing a median-ventral crista (Fig. 3C); crista narrow, turbinate-shaped, with apex protruded to dorsal margin of valve, and with little spines on surface (Fig. 3B), with wider prolongation on the proximal ventral surface connecting with saccus (Fig. 3A). Saccus short, with anterior process curved upwards and thinner apex. Tegumen long and wide, in dorsal view the basal portion of the uncus is wider, narrowing towards the tip, ending in a narrow apical process. Gnathos present, well developed, short tongue-shaped slightly up curved in lateral view (Fig. 3A), vinculum slim and proximally incurved with dorsal projection. Juxta wide in ventral view with a pointed anterior portion and a widened posterior portion as the shape of two slightly divided lobules (Fig. 3F). Aedeagus straight in lateral view, ~ 1/2 the length of the genital capsule, evenly wide, sclerotized, without cornuti (Fig. 3E).

Female: Wingspan 50–52 mm, forewing length 26–27 mm. Very similar to male, but paler, with the most prominent dorsal marks and spots mainly in the forewing apex, where it presents a faint stain between the veins R_1 to M_1, absent in males and with a paler background than the rest of the wing (Fig. 1C, D). Abdomen with stink-clubs attached to a lateral fold, dorsally on posterior margin of the eighth sternum, densely covered with elongated, either single or bifid, specialized scales (Fig. 3C).

***Female genitalia*:** Eighth segment narrow. Posterior apophysis ~ 1/2 the length of the papilla anales (Fig. 3A). Two signa slightly arched with the proximal tip near the ductus bursae, formed by four or five rows of wide spines (Fig. 3B).

Immature stages. *Egg* (Figs 5A, B, 9A, 2S)

Sub spherical, flat base slightly narrowed near apex. Yellow when recently laid (Fig. 5A), reddish brown with a whitish band subsequently, and showing larva by transparency close to hatching (Fig. 5B). Size (mean ± standard error): diameter -0.92 ± 0.03 mm; height -1.13 ± 0.02 mm (n = 10). The chorion is adorned with 19–20 vertical and 16 or 17 horizontal carinae of smooth surfaces, which when intersect delimit cells (Fig. 9A). In the lower part of the egg, the vertical carinae are generally twice as wide as the horizontal ones and some are interrupted at one or two cells before the micropylar region. In the upper third, they have similar widths. Aeropiles scattered in the intersection of carinae, and similar in shape to those of "*Agraulis vanillae*", as interpreted by da Silva et al. (2006). Micropylar region is surrounded by a rosette-like sculpture of the chorion.

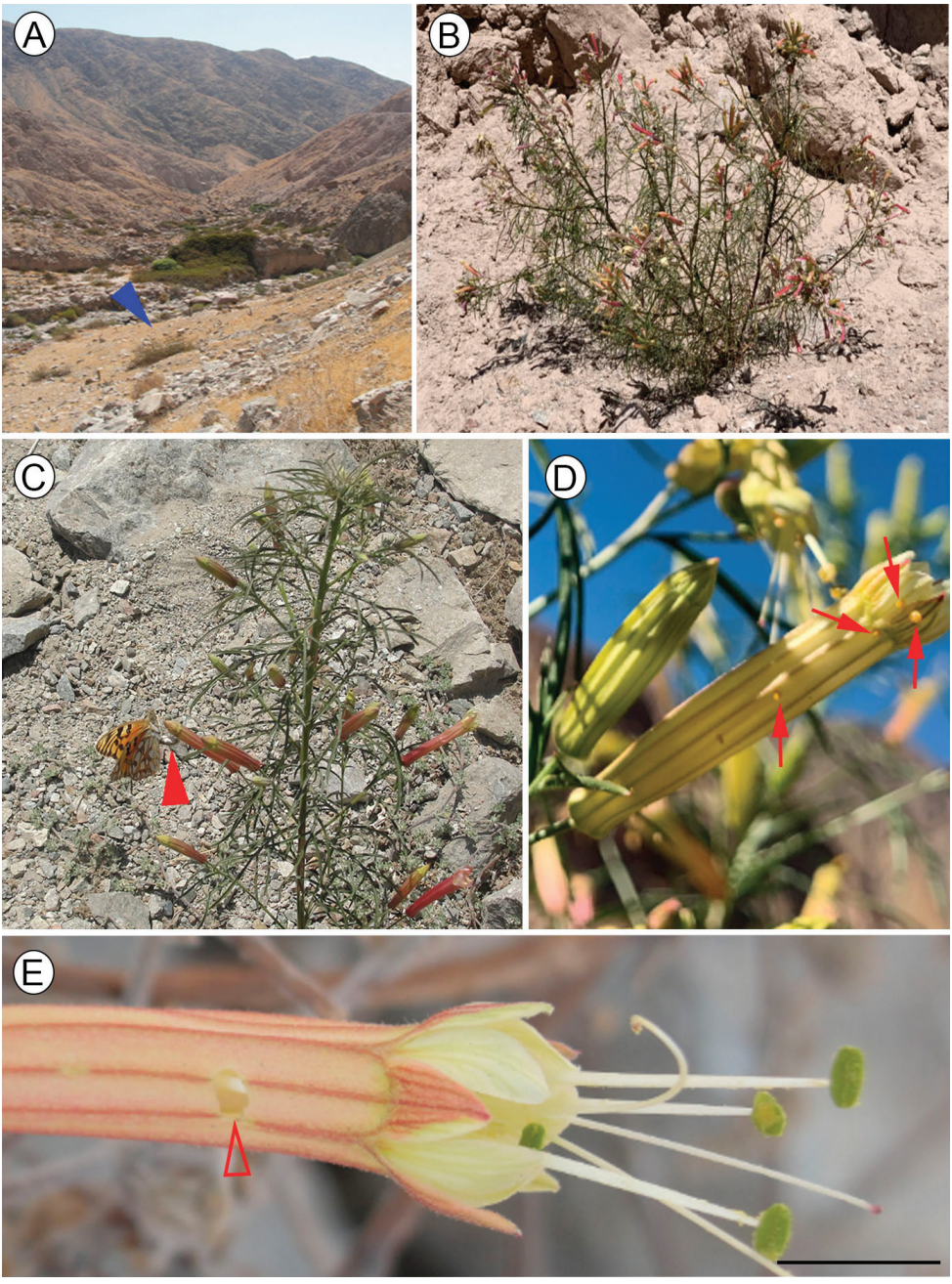

Figure 10. Life history of *Dione* (*Agraulis*) *dodona* sp. nov. **A** general view of type locality, Pacaychacra valley, Arequipa, Peru (blue close arrow points to larval hostplant) **B** host plant, *Malesherbia tenuifolia* Don **C** female laying eggs (close arrow point) on flowers of host plant **D** eggs (pointed by setae) on flower **E** detail of flower showing damage (entrance) by first instar larva (open arrow). Scale bar: 5 mm.

First instar. (Figs 5C, 6A–D, 9B, S2). Length (mean ± standard error; $n = 6$) = 3.56 ± 0.34 mm. Head, prothoracic dorsal shield, anal shield, pinnacles, legs and lateral plates of prolegs blackish; thorax and abdomen mostly creamy white, slightly translucent, reddish brown dorsally on A1–5 (Fig. 5C). Prothoracic dorsal shield trapezoidal with rounded angles, posterior margin with cleft at middle. Chaetotaxy as shown in Fig. 6A–D; SV group unisetose on T2–3; D2 ~ 1/2 the length of D1; and spiracles laterally on prothorax and A1–8, circular, with peritrema elevated (Fig. 9B).

Subsequent instars. From the second instar on, the head is black with thorax and abdomen yellow with two bands running along the subdorsal and subspiracular area. Three chromatic patterns were observed, mainly in the fifth instar, one of these patterns (brownish) is characterized by the head, legs and black scoli; thorax and abdomen yellow with brown band in the subdorsal and subspiracular area, with a thin dorsal brown line, the head has a pattern of white spots located on the frontoclypeous, and with the brown labrum, lateral plates of prolegs black (Fig. 7A); the second colored pattern (greyish) with head and black setae, thorax and abdomen with bands in the subdorsal and subspiracular area gray, the base of prolegs gray too, head with pattern of cream coloration with a larger area than the previous one and the gray labrum, with a triangular spot into the frontoclypeous, lateral plates of prolegs cream (Fig. 7B); the third pattern (reddish) is similar to second pattern but the color of the bands in abdomen, base of scoli and the head is more reddish (Fig. 7C). However, the predominant pattern observed in the field was the brownish one (Fig. 5D, E).

Fifth instar. (Figs 5C, D, 6E, S2) Length (mean ± standard error; $n = 5$) = 25.45 ± 1.78 mm. Head blackish, covered by a large number of hair-like setae and short chalaza-like setae, which vary in length, and bears two short stout scoli dorsally (Fig. 5D). The thorax has the integument covered by conical, striated microtrichia, prominent on coxa of legs and latero-ventral face of prothorax; abdomen with cuticular sculpturing composed of irregular ribs, except the last segment ventrally on posterior face of anal proleg with conspicuous microtrichia; prothoracic dorsal shield bears a number of short chalaza-like setae and two pairs of stout spine-like setae on dorsal conical projections; elliptical spiracles with pronounced peritrema laterally on prothorax and abdominal segments A1–8, those of prothorax and A8 slightly larger than the remaining ones; prolegs with lateral plates covered by several hair-like and chalaza-like setae, crochets in uniserial and multiordinal arrangement. Thirty pairs of thoracic and abdominal scoli, which are elongated conical, integumentary outgrowths, provided with some short chalaza-like setae on the surface, one of which, typically the longest one, is placed at the apex; 11 dorsal pairs (T2–3 and A1–9); ten supra-spiracular pairs (T2–3 and A1–8), with those of the meso- and metathorax anteriorly displaced; eight lateral pairs (A1–8), and one anal pair (A10). Twelve pairs of thoracic and abdominal verrucae; three pairs on prothorax, one between dorsal shield and spiracle, which is provided with a spine-like seta, another greatly reduced pair anterior to spiracle, and another pair between spiracle and coxa; two pairs on meso and metathorax, one posterior to supraspiracular scolus and another dorsal to coxa; one pair on A1–2 and A7–8, which is ventral to lateral scolus; and one pair on A9, on the latero-ventral face of the segment.

Instar identification. The successive instars can be accurately distinguished by the width of the head capsule, because they do not overlap (Table 2). The corresponding exponential growth equation was adjusted for the five instars: y = 0.328e^0.403x; n = 62; r^2 = 0.980; p < 0.05. Thus, the growth pattern of the head capsule follows the Brooks-Dyar´s rule (Daly 1985). The mean growth ratio among instars was 1.495, similar to ratios previously reported for other Neotropical heliconians (Antunes et al. 2002; Kaminski et al. 2002, 2008; Tavares et al. 2002; Paim et al. 2004; da Silva et al. 2006, 2008; Barão and Moreira 2010; Vargas et al. 2014; Barão et al. 2015).

Pupa (Figs 5F–H, 8, 9D–F) General shape elongated, ground color non-uniform, consisting of a mixture of shades of gray, light brown, and ocher (Fig. 5F–H), with variation between individuals in their intensity. Length (mean ± standard error; n = 5) = 19.98 ± 0.28 mm. Head with pair of short, angled cephalic projections (Figs 8, 9D); epicranial suture absent; eyes with sculptured region near antenna, bearing few short hair-like setae, and another smooth region near front; labrum as a slight, short longitudinal stripe between the mandibles; maxilla with well-developed galeae, along midline of ventral surface, anteriorly delimited by labrum and mandibles, slightly surpassing posterior margin of A4; antennae arising laterally on head, projected ventrally to apex of maxilla, with many smooth, round tubercles on surface. Thorax with the three segments exposed. Prothorax as a small hexagonal plate in dorsal view, with anterior and posterior margins broadly excavated, with two pair of lateral tubercles. Mesothorax broadly expanded laterally along anterior half with a meso-dorsal crest that is well developed, broadly rounded, bearing a pair of round lateral tubercles; two pairs of marginal and submarginal tubercles close to base of wings; one pair of submarginal tubercles each near apex of wing; mesothoracic spiracle opening laterally at anterior margin of segment. Metathorax as a narrow plate with anterior margin broadly excavated, with pair of lateral tubercles, hindwings as straight stripes between forewings and abdominal segments. Abdomen with segments A1–A4 partially hidden by wings; with pair of lateral tubercles on A1–A7 which are little developed on A1–A2, most developed on A3, and decreasing in size posteriorly; one meso-dorsal tubercle on A5–A7; one supraspiracular tubercle on A2–A4; one pair of subspiracular tubercle on A4, pair of ventral tubercles on A5–A6; spiracles of A1 and A2 hidden and partially hidden, respectively, by forewings, and spiracles of A3–A7 elliptical; anal segment with two prominent tubercles, ventrally. Cremaster quadrate, with truncate apex, and a large number of short, curved hooks.

Table 2. Mean and standard error (SE), interval of variation (IV), and growth rates (GR) of head capsule width in larval instars of *Dione* (*Agraulis*) *dodona* **sp. nov**. reared on *Malesherbia tenuifolia* D. Don.

Instar	N	Head capsule width (mm)		
		Mean ± SE	IV	GR
I	19	0.50 ± 0.01	0.46–0.56	-
II	12	0.72 ± 0.01	0.58–0.83	1.44
III	8	1.07 ± 0.03	0.95–1.17	1.48
IV	8	1.69 ± 0.04	1.56–1.87	1.52
V	5	2.50 ± 0.05	2.44–2.70	1.48

Etymology. The specific epithet is based on the locality of Dodona (Greece); it was a city-sanctuary in ancient Greece, where there was an oracle in which Dione was venerated as the (temporary) wife of Zeus, until she was replaced by Hera. Thus, the new species is named "dodona" to continue the classical Greek tradition.

Distribution. Adults of *Dione* (*Agraulis*) *dodona* sp. nov. are known from distinct populations, located in central and southern Peru, and northern Chile, on the western slopes of the Andes. In Peru, it has been found in the Departments of Lima (1,400–2,400 m elevation), Arequipa (between 800 and 2,600 m elevation), Moquegua (1,800–2,100 m elevation), and Tacna (1,800 m elevation). In Chile, two specimens were collected in 1951 and 1968 from two localities in the Tarapacá Region between 2,300 and 3,000 m elevation, and recently other two specimens were collected from Arica Region (1,580 m elevation).

Host plant. *Malesherbia tenuifolia* D. Don (Passifloraceae) is the only host plant known for the immature stages of *Dione* (*Agraulis*) *dodona* sp. nov. This species was described originally from northern Chile. It is distributed between 19–21 °S in Chile (Bull-Hereñu 2020), and was reported recently from southern Peru (Weigend et al. 2015; Beltrán et al. 2018), restricted to the western slopes of the Andes above 1,500 m. *M. tenuifolia* is a shrub with reddish or yellowish tubular flowers that grows to ca. 1 m in height (Fig. 10), associated with the dry beds and immediate surroundings of seasonal rivers in Chile (Bull-Hereñu 2020), and steep scree slopes along the road cuts in the type locality of *Dione* (*Agraulis*) *dodona* sp. nov. (Fig. 10A).

Life history. Adults of *Dione* (*Agraulis*) *dodona* sp. nov. were only observed on sunny days in the type locality, beginning to fly around 08:00 a.m., quickly disappearing when weather conditions became cloudy. They usually fly close to the ground, up to 1–2 m high. Females were seen alighting on the host plant. Territorial behavior, courtship and mating behavior were not observed. Adults were seen feeding on flowers of other plants growing around *Malesherbia* hosts. The species is multivoltine in the population of the type locality, flying all year round. From three to seven individuals were usually observed in a typical sunny day (4–5 h of observation), most of which were males. This species is sympatric with *Dione* (*Agraulis*) *forbesi*, but they do not fly in the same habitat; *forbesi* was observed in areas with higher humidity and vegetation, compared to *dodona*, which was found only in xerophytic areas associated with the host plant (Fig. 10A, B). Females were observed laying eggs particularly on flowers (Fig. 10D). Oviposition occurred with the female sitting on top of the flower and curling the abdomen around the flower edge so that eggs were deposited underneath (Fig. 10C). During visits made at different months of the year in the type locality, freshly laid eggs were always collected, both on flowers and leaves. Between one and eight eggs were found in the same plant, in different flowers or leaves, but sometimes several eggs were obtained from the same flower (Fig. 10D). The eggs are laid isolated from each other. Newly hatched larvae first consumed the chorion, and afterwards began to feed inside of flower, leaving a hole through which they enter the flower (Fig. 10E). Subsequent instars feed externally on leaves. Larvae were consistently solitary in all instars, regarding all activities, such as feeding or resting. Pupae were found

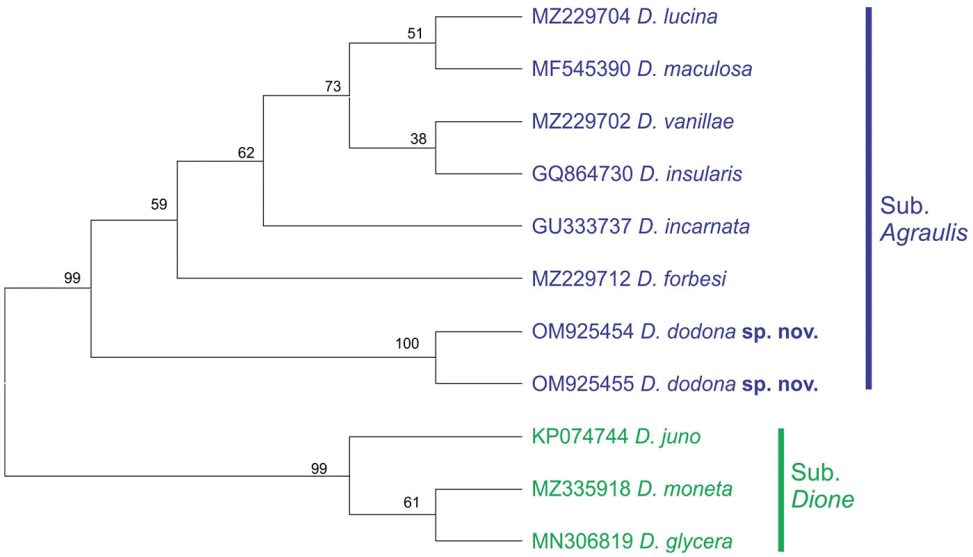

Figure 11. Phylogenetic status of *Dione* (*Agraulis*) *dodona* sp. nov. based on 650 bp-sequences of the Cytochrome oxidase subunit I gene. The consensus tree was inferred with the Maximum Likelihood method and General Time Reversible model, with 500 bootstrap replicates. The branch support (bootstrap) is shown next to the nodes.

Table 3. Genetic distance (%) between *Dione* (*Agraulis*) *dodona* sp. nov. and its congeners. Analysis used 650 base pairs sequences of the Cytochrome oxidase subunit I gene under the Kimura 2-parameter model. Specimens included in the analysis are presented in Table 1.

Taxa	1.	2.	3.	4.	5.	6.	7.	8.
1. *Dione* (*Agraulis*) *dodona* sp. nov.	-							
2. *Dione* (*Agraulis*) *forbesi*	5.8	-						
3. *Dione* (*Agraulis*) *lucina*	4.6	3.9	-					
4. *Dione* (*Agraulis*) *vanillae*	5.3	4.4	2.2	-				
5. *Dione* (*Agraulis*) *incarnata*	5.1	4.6	3.4	3.4	-			
6. *Dione* (*Agraulis*) *insularis*	4.6	3.9	1.9	1.9	3.2	-		
7. *Dione* (*Agraulis*) *maculosa*	4.4	3.4	1.1	1.7	2.7	1.1	-	
8. *Dione* (*Dione*) spp.	9.5	8.9	8.6	8.6	9.3	9.4	8.8	-

predominantly off the host plant, clinging to rocks near the host plant, and sometimes on branches of the host plant close to the ground.

Molecular data. *Dione* (*Agraulis*) *dodona* sp. nov. was recovered as an independent lineage within the *Agraulis* clade of the COI-tree (Fig. 11), diverging in ca. 5% to the group formed by its other species, and 9.5% to the *Dione* clade (Table 3).

Discussion

The identification key to adults of *Agraulis* provided by Núñez et al. (2022) based on external morphology, indicated only one character of the wing pattern color to separate *Dione* (*Agraulis*) *dodona* sp. nov. (listed as *Agraulis* sp.), an extra black spot on the upper hindwing cell Cu_1-Cu_2 (Fig. 1E). As already mentioned, we propose in addition the divided silver discal spot on the hindwing underside (Fig. 1F); this last trait is not found in other species of the *Agraulis* clade, but is shared with other species of *Dione*. Núñez et al. (2022) found that *Dione* (*Agraulis*) *galapagensis* W. Holland, 1890 and *Dione* (*Agraulis*) *dodona* sp. nov. have similar size (forewing length 27 mm or less) but are smaller in relation to other species of the *Agraulis* clade. These findings are supported by the specimens studied by us, where the longest wings of *Dione* (*Agraulis*) *dodona* sp. nov. were from a male and a female, reaching up to 28 and 27 mm, respectively; however, this should not be a morphological attribute to be used to separate species. Regarding the male and female genitalia, *Dione* (*Agraulis*) *dodona* sp. nov. are very distinct from those of other members of the *Agraulis* clade, the most notable differences being in the valval termen without denticles, the narrow crista projection and the shape of yuxta in males (see Suppl. material 1), as well as the shape of the signum in females. According to Emsley (1963), these characters have an important value to differentiate among species within Heliconiinae. Thus, morphological characters of adults described for *Dione* (*Agraulis*) *dodona* sp. nov. allow its clear differentiation from other species. Similarly, phylogenetic relationships inferred from DNA sequence data support *Dione* (*Agraulis*) *dodona* sp. nov. as a distinct taxon, placed as external to the group formed by its congeners, considered the earliest diverging (ca. 8 Mya) lineage within the *Agraulis* clade (Núñez et al. 2022). Although sharing morphological traits with the *Dione* clade, the genetic distance of nearly 10% is quite high, which together with previous inferences using several molecular markers (Kozak et al. 2015; Massardo et al. 2015), supports the recognition of two evolutionary lineages that shared a common ancestor around 14 million years ago (Núñez et al. 2022). Following Zhang et al. (2019), we consider that the phylogenetically most informative hypothesis is to treat *Dione* and *Agraulis* as equivalent subgenera. In summary, as previously accepted by Núñez et al. (2022), *Dione* (*Agraulis*) *dodona* sp. nov. is evidenced as a valid species based on morphological and molecular evidence.

Thus, results presented herein show clearly that *Dione* (*Agraulis*) *dodona* sp. nov. is distinct from its congeneric species at all development levels. On the other hand, particularly in the larval stage, our study also showed that it shares some characters with species of the *Dione* clade; in the first instar, the D2 setae are well developed accordingly in the latter; in subsequent instars, the cephalic scoli are reduced similar with *Dione moneta*, and the prothoracic plate with enlarged conical protuberances bears setae. In fact, such traits had been used up to now to separate genera of heliconiines at the larval stage (Fleming 1960; Tavares et al. 2002; Kaminski et al. 2008). Also, *Dione* (*Agraulis*) *dodona* sp. nov. exhibits some unique characters in the fifth instar that were not observed in other species in the genus *Dione* s. l. Among them, it is worth highlighting the spiracles with pronounced peritrema, the predominance of short chalaza-like setae covering abdominal segments including scoli, and the linear

distance between stemmata I and II larger than distance between stemmata II and III in head (see Suppl. material 2). Since the phylogenetic relationships between the *Agraulis* and *Dione* clades and their taxonomic consequences have been controversial, we suggest to explore the evolutionary history of these genera taking into account morphological characters herein found for *Dione* (*Agraulis*) *dodona* sp. nov. within a cladistic approach.

Females of *Dione* (*Agraulis*) *dodona* sp. nov. lay eggs predominantly on flowers, where first instar feed on the internal parts. There is no documentation of another species of Heliconiinae that oviposits preferentially on flowers or larvae feeding on them (de Castro et al. 2018). The host plant of *Dione* (*Agraulis*) *dodona* sp. nov., *Malesherbia tenuifolia*, represents the first record of the genus as a host plant in Heliconiinae (Beccaloni et al. 2008). This genus represents one of the oldest lineages of the Passifloraceae s.l. (Tokuoka 2012), considered until a few years ago as a separate family (Malesherbiaceae) (Gengler-Nowak 2003), but recent phylogenetic studies proposed to include it in Passilforaceae s. l. (Soltis et al. 2007; Bremer et al. 2009). *Malesherbia* are a little-known group of xerophytic plants endemic to a variety of arid habitats in the Pacific coastal desert and adjacent Andes of Peru, Chile, and neighboring Argentina (Gengler-Nowak 2002; Bull-Hereñu 2020). The subgeneric classification of *Malesherbia* comprises five sections (Gengler-Nowak 2003), *M. tenuifolia* belongs to the *Malesherbia* section Gengler-Nowak (2003: 343) along with other species that are distributed at the northern limit of the genus, from central Peru to northern Chile (Gengler-Nowak 2003; Beltrán et al. 2018; Bull-Hereñu 2020). Coincidentally, the known populations of *Dione* (*Agraulis*) *dodona* sp. nov. follow the geographical distribution of this section of *Malesherbia*, and this could imply that *Dione* (*Agraulis*) *dodona* sp. nov. uses other *Malesherbia* species as hostplants, considering that in the Department of Lima (central Peru) where *Dione* (*Agraulis*) *dodona* sp. nov. was collected, four *Malesherbia* species have been reported, but not *M. tenuifolia* (Beltrán et al. 2018).

Finally, it is important to mention that, historically, *Dione* (*Agraulis*) *dodona* sp. nov. was erroneously cited for decades as "*Agraulis vanillae*" in Chile, based on two specimens collected between 1950 and 1970 in the Tarapacá region, northern Chile. Peña (1951) reported it for the first time in Chile based on a male specimen collected in the locality of Parca, and afterwards Pérez-D'Angello (1970) reported a second specimen from Guatacondo, in the collection of Pedro Millas. Subsequently, all Chilean butterfly checklists published cited "*A. vanillae*" as a species distributed in northern Chile (Ureta 1963; Etcheverry 1970; Herrera 1972; Peña and Ugarte 2006; Benyamini et al. 2014). By examining both specimens that are currently at MUSM (the second one on loan from MHNS), we confirm their identity as *Dione* (*Agraulis*) *dodona* sp. nov. Probably, the host plant used by this population from northern Chile is *M. tenuifolia*, reported in these localities of Tarapacá region (Bull-Hereñu 2020).

Acknowledgements

We are grateful to Leandro Menezes Baum from Laboratório Central de Microscopia e Microanálise (LabCEMM) of Pontifícia Universidade Católica do Rio Grande do Sul (PUCRS), Porto Alegre, RS, Brazil, for helping with scanning electron microscopy analyses. Thanks also to Dr. Evaristo López (Museo de Historia Natural, Universidad Nacional San Agustín, Arequipa, Perú [MUSA]) for access to the Laboratorio de Sistemática Animal of Universidad Nacional San Agustin de Arequipa (UNSA). The first version of the manuscript benefitted from valuable suggestions provided by André Freitas (UNICAMP). JF was supported by a CAPES scholarship. GLG and GRPM were assisted by FAPERGS and CNPq grants, respectively. This study was supported in part by a project of the Universidad Nacional de San Agustin de Arequipa (UNSA) with Contract IBAB-001-2019-UNSA.

References

Antunes FF, Menezes Jr AO, Tavares M, Moreira GRP (2002) Morfologia dos estágios imaturos de heliconíneos neotropicais: I. *Eueides isabella dianasa* (Hübner, 1806). Revista Brasileira de Entomologia 46(4): 601–610. https://doi.org/10.1590/S0085-56262002000400016

Arakaki M, Cano A (2003) Composición florística de la cuenca del río Ilo-Moquegua y lomas de Ilo, Moquegua. Revista Peruana de Biología 10(1): 5–15. https://doi.org/10.15381/rpb.v10i1.2472

Barão KR, Moreira GRP (2010) External morphology of the immature stages of Neotropical heliconians: VIII. *Philaethria wernickei* (Röber) (Lepidoptera, Nymphalidae, Heliconiinae). Revista Brasileira de Entomologia 54(3): 406–418. https://doi.org/10.1590/S0085-56262010000300008

Barão KR, da Silva DS, Moreira GRP (2015) External morphology of the immature stages of Neotropical heliconians: X. *Heliconius sara apseudes* (Lepidoptera, Nymphalidae, Heliconiinae). Iheringia (Zoologia) 105(4): 523–533. https://doi.org/10.1590/1678-476620151054523533

Bates HW (1862) Contributions to an insect fauna of the Amazon valley. Lepidoptera: Heliconidae. Transactions of the Linnean Society of London 23(3): 495–566. https://doi.org/10.1111/j.1096-3642.1860.tb00146.x

Beccaloni GW, Hall SK, Viloria AL, Robinson GS (2008) Catalogue of the hostplants of the Neotropical butterflies / Catálogo de las plantas huésped de las mariposas Neotropicales. Sociedad Entomológica Aragonesa, Zaragoza. (Monografías Del Tercer Milenio, Vol. 8) 536 pp.

Beebe W, Crane J, Fleming H (1960) A comparison of eggs, larvae and pupae in fourteen species of Heliconiine butterflies from Trinidad, W.I. Zoologica (New York) 45(3): 111–154. https://doi.org/10.5962/p.203357

Beltrán M, Jiggins CD, Bull V, Linares M, Mallet JLB, McMillan WO, Bermingham EP (2002) Phylogenetic discordance at the species boundary: Comparative gene genealogies among rapidly radiating *Heliconius* butterflies. Molecular Biology and Evolution 19(12): 2176–2190. https://doi.org/10.1093/oxfordjournals.molbev.a004042

Beltrán M, Jiggins CD, Brower AVZ, Bermingham EP, Mallet JLB (2007) Do pollen feeding, pupal-mating and larval gregariousness have a single origin in *Heliconius* butterflies? Inferences from multilocus DNA sequence data. Biological Journal of the Linnean Society 92(2): 221–239. https://doi.org/10.1111/j.1095-8312.2007.00830.x

Beltrán H, Roque J, Cáceres C (2018) A synopsis of the genus *Malesherbia* (Passifloraceae) in Peru. Revista Peruana de Biología 25(3): 229–240. https://doi.org/10.15381/rpb.v25i3.13408

Benson WW, Brown Jr KS, Gilbert LE (1975) Coevolution of plants and herbivores: Passion flower butterflies. Evolution 29(4): 659–680. https://doi.org/10.1111/j.1558-5646.1975.tb00861.x

Benyamini D, Ugarte A, Shapiro AM, Mielke OHH, Pyrcz T, Bálint Z (2014) An updated list of the butterflies of Chile (Lepidoptera, Papilionoidea and Hesperioidea) including distribution, flight period and conservation status. Part I, comprising the families: Papilionidae, Pieridae, Nymphalidae (in part) and Hesperiidae describing a new species of *Hypsochila* (Pieridae) and new subspecies of *Yramea modesta* (Nymphalidae). Boletín del Museo Nacional de Historia Natural (Santiago de Chile) 63: 9–31.

Bremer B, Bremer K, Chase MW, Fay MF, Reveal JL, Soltis DE, Soltis PS, Stevens PF, Anderberg AA, Moore MJ, Olmstead RG, Rudall PJ, Sytsma KJ, Tank DC, Wurdack K, Xiang JQY, Zmarzty S (2009) An update of the angiosperm phylogeny group classification for the orders and families of flowering plants: APG III. Botanical Journal of the Linnean Society 161(2): 105–121. https://doi.org/10.1111/j.1095-8339.2009.00996.x

Brower AVZ, Egan MG (1997) Cladistic analysis of *Heliconius* butterflies and relatives (Nymphalidae: Heliconiiti): a revised phylogenetic position for *Eueides* based on sequences from mtDNA and a molecular gene. Proceedings. Biological Sciences 264(1384): 969–977. https://doi.org/10.1098/rspb.1997.0134

Brown Jr KS (1981) The biology of *Heliconius* and related genera. Annual Review of Entomology 26(1): 427–456. https://doi.org/10.1146/annurev.en.26.010181.002235

Bull-Hereñu K (2020) The genus *Malesherbia* Ruiz & Pav. (Passifloraceae) in Chile. Phytotaxa 468(1): 1–44. https://doi.org/10.11646/phytotaxa.468.1.1

Daly HW (1985) Insect morphometrics. Annual Review of Entomology 30:415–438. https://doi.org/10.1080/11250003.2012.685766

da Silva DS, Dell'Erba R, Kaminski LA, Moreira GRP (2006) Morfologia externa dos estágios imaturos de heliconíneos neotropicais: V. *Agraulis vanillae maculosa* (Lepidoptera, Nymphalidae, Heliconiinae). Iheringia (Zoologia) 96(2): 219–228. https://doi.org/10.1590/S0073-47212006000200013

da Silva DS, Kaminski LA, Dell'Erba R, Moreira GRP (2008) Morfologia externa dos estágios imaturos de heliconíneos neotropicais: VII. *Dryadula phaetusa* (Linnaeus) (Lepidoptera, Nymphalidae, Heliconiinae). Revista Brasileira de Entomologia 52(4): 500–509. https://doi.org/10.1590/S0085-56262008000400003

de Castro ECP, Zagrobelny M, Cardoso MZ, Bak S (2018) The arms race between heliconiine butterflies and *Passiflora* plants – new insights on an ancient subject. Biological Reviews 93(1): 555–573. https://doi.org/10.1111/brv.12357

Deinert EI, Longino JT, Gilbert LE (1994) Mate competition in butterflies. Nature 370(6484): 23–24. https://doi.org/10.1038/370023a0

Ehrlich PR, Raven PH (1964) Butterflies and plants – a study in coevolution. Evolution 18(4): 586–608. https://doi.org/10.1111/j.1558-5646.1964.tb01674.x

Emsley MG (1963) A morphological study of imagine Heliconiinae (Lep.: Nymphalidae) with a consideration of the evolutionary relationships within the group. Zoologica (New York) 48(3): 85–130. https://doi.org/10.5962/p.203312

Etcheverry M (1970) Syrphidae (Diptera) y Rhopalocera (Lepidoptera) colectados en la Provincia de Tarapacá (Chile). Revista Peruana de Entomología 13(1): 94–96.

Farfán J (2018) Mariposas (Lepidoptera: Papilionoidea) de Arequipa, Perú: lista preliminar con dos nuevos registros para Perú. Revista Peruana de Biología 25(4): 357–370. https://doi.org/10.15381/rpb.v25i4.15536

Farfán J, Lamas G, Cerdeña J (2020) A new species of *Mathania* Oberthür, 1890 from Peru (Lepidoptera, Pieridae). Zootaxa 4758(3): 589–595. https://doi.org/10.11646/zootaxa.4758.3.11

Fleming H (1960) The first instar larvae of the Heliconiinae (butterflies) of Trinidad. W.I. Zoologica (New York) 45(3): 91–110. https://doi.org/10.5962/p.203356

Gengler-Nowak KM (2002) Reconstruction of the biogeographical history of Malesherbiaceae. Botanical Review 68(1): 171–188. https://doi.org/10.1663/0006-8101(2002)068[0171:ROTBHO]2.0.CO;2

Gengler-Nowak KM (2003) Molecular phylogeny and taxonomy of Malesherbiaceae. Systematic Botany 28(2): 333–344. https://www.jstor.org/stable/3094002

Gilbert LE (1972) Pollen feeding and reproductive biology of *Heliconius* butterflies. Proceedings of the National Academy of Sciences of the United States of America 69(6): 1403–1407. https://doi.org/10.1073/pnas.69.6.1403

Gilbert LE (1991) Biodiversity of a Central American *Heliconius* community: pattern, process, and problems. In: Price P, Lewinsohn T, Fernandes T, Benson W (Eds) Plant-animal interactions: evolutionary ecology in tropical and temperate regions John Wiley & Sons, New York, 403–427.

Gutiérrez JR, López-Cortés F, Marquet PA (1998) Vegetation in an altitudinal gradient along the Rıo Loa in the Atacama Desert of Northern Chile. Journal of Arid Environments 40(4): 383–399. https://doi.org/10.1006/jare.1998.0462

Gutiérrez H, Castañeda R, Quipuscoa V, Peterson PM (2019) *Aristida surperuanensis* (Poaceae, Aristidoideae), a new species from a desert valley in southern Peru. Phytotaxa 419(2): 182–188. https://doi.org/10.11646/phytotaxa.419.2.4

Hebert PDN, Penton EH, Burns JM, Janzen DH, Hallwachs WD (2004) Ten species in one: DNA barcoding reveals cryptic species in the neotropical skipper butterfly *Astraptes fulgerator*. Proceedings of the National Academy of Sciences of the United States of America 101(41): 14812–14817. https://doi.org/10.1073/pnas.0406166101

Herrera J (1972) Mariposas comunes a Chile y Perú (Lepidoptera, Rhopalocera). Revista Peruana de Entomología 15(1): 72–74.

Huanca-Mamani W, Rivera-Cabello D, Maita-Maita J (2015) A simple, fast, and inexpensive CTAB-PVP-Silica based method for genomic DNA isolation from single, small in-

sect larvae and pupae. Genetics and Molecular Research 14(3): 8001–8007. https://doi.org/10.4238/2015.July.17.8

Jiggins CD (2017) The ecology and evolution of *Heliconius* butterflies. Oxford University Press, New York, [ix +] 277 pp. https://doi.org/10.1093/acprof:oso/9780199566570.001.0001

Kaminski LA, Tavares M, Ferro VG, Moreira GRP (2002) Morfologia externa dos estágios imaturos dos heliconíneos neotropicais. III. *Heliconius erato phyllis* (Fabricius) (Lepidoptera, Nymphalidae, Heliconiinae). Revista Brasileira de Zoologia 19(4): 977–993. https://doi.org/10.1590/S0101-81752002000400003

Kaminski LA, Dell'Erba R, Moreira GRP (2008) Morfologia externa dos estágios imaturos de heliconíneos neotropicais: VI. *Dione moneta moneta* Hübner (Lepidoptera, Nymphalidae, Heliconiinae). Revista Brasileira de Entomologia 52(1): 13–23. https://doi.org/10.1590/S0085-56262008000100003

Klots AB (1970) Lepidoptera. In: Tuxen SL (Ed.) Taxonomist's Glossary of Genitalia in Insects. (Ed. 2). Munksgaard, Copenhagen, 115–130.

Kozak KM, Wahlberg N, Neild AFE, Dasmahapatra KK, Mallet J, Jiggins CD (2015) Multilocus species trees show the recent adaptive radiation of the Mimetic *Heliconius* butterflies. Systematic Biology 64(3): 505–524. https://doi.org/10.1093/sysbio/syv007

Kumar S, Stecher G, Li M, Knyaz C, Tamura K (2018) MEGA X: Molecular Evolutionary Genetics Analysis across Computing Platforms. Molecular Biology and Evolution 35(6): 1547–1549. https://doi.org/10.1093/molbev/msy096

Lamas G (2004) Checklist: Part 4A. Hesperioidea - Papilionoidea. Atlas of Neotropical Lepidoptera. Volume 5A (Ed. by J.B. Heppner). Gainesville: Association for Tropical Lepidoptera; Scientific Publishers.

Lavinia PD, Núñez Bustos EO, Kopuchian C, Lijtmaer DA, García NC, Hebert PDN, Tubaro PL (2017) Barcoding the butterflies of southern South America: Species delimitation efficacy, cryptic diversity and geographic patterns of divergence. PLoS ONE 12(10): e0186845. https://doi.org/10.1371/journal.pone.0186845

Málaga B, Díaz RD, Arias S, Medina CE (2020) Una especie nueva de *Lasiurus* (Chiroptera: Vespertilionidae) del suroeste de Perú. Revista Mexicana de Biodiversidad 91(0, e913096): 1–14. https://doi.org/10.22201/ib.20078706e.2020.91.3096

Mallet J, Joron M (1999) Evolution of diversity in warning color and mimicry: Polymorphisms, shifting balance, and speciation. Annual Review of Ecology and Systematics 30(1): 201–233. https://doi.org/10.1146/annurev.ecolsys.30.1.201

Marín MA, López-Rubio A, Clavijo A, Pyrcz TW, Freitas AVL, Uribe SI, Álvarez CF (2021) Use of species delimitation approaches to tackle the cryptic diversity of an assemblage of high Andean butterflies (Lepidoptera: Papilionoidea). Genome 64(10): 937–949. https://doi.org/10.1139/gen-2020-0100

Massardo D, Fornel R, Kronforst M, Lopes-Goncalves G, Pires-Moreira GR (2015) Diversification of the silverspot butterflies (Nymphalidae) in the Neotropics inferred from multilocus DNA sequences. Molecular Phylogenetics and Evolution 82(A): 156–165. https://doi.org/10.1016/j.ympev.2014.09.018

Michener CD (1942) A review of the subspecies of *Agraulis vanillae* (Linnaeus) (Lepidoptera: Nymphalidae). American Museum Novitates 1215: 1–7.

Montesinos D, Cleef A, Sýkora K (2012) Andean shrublands of Moquegua, South Peru: Prepuna plant communities. Phytocoenologia 42(1–2): 29–55. https://doi.org/10.1127/0340-269X/2012/0042-0516

Montgomery DR, Balco G, Willett SD (2001) Climate, tectonics, and the morphology of the Andes. Geology 29(7): 579–582. https://doi.org/10.1130/0091-7613(2001)029<0579:CTATMO>2.0.CO;2

Myers N, Mittermeier RA, Mittermeier CG, da Fonseca GAB, Kent J (2000) Biodiversity hotspots for conservation priorities. Nature 403(6772): 853–858. https://doi.org/10.1038/35002501

Nei M, Kumar S (2000) Molecular Evolution and Phylogenetics. Oxford University Press, New York.

Núñez R, Willmott KR, Álvarez Y, Genaro JA, Pérez-Asso AR, Quejereta M, Turner T, Miller JY, Brévignon C, Lamas G, Hausmann A (2022) Integrative taxonomy clarifies species limits in the hitherto monotypic passion-vine butterfly genera *Agraulis* and *Dryas* (Lepidoptera, Nymphalidae, Heliconiinae). Systematic Entomology 47(1): 152–178. https://doi.org/10.1111/syen.12523

Paim AC, Kaminski LA, Moreira GRP (2004) Morfologia externa dos estágios imaturos de heliconíneos neotropicais. IV. *Dryas iulia alcionea* (Lepidoptera: Nymphalidae: Heliconiinae). Iheringia (Zoologia) 94(1): 25–35. https://doi.org/10.1590/S0073-47212004000100005

Peña LE (1951) Algunos lepidópteros ropalóceros de Tarapacá (9-X-1951). Revista Chilena de Entomologia 1: 262.

Peña LE, Ugarte AJ (2006) Las Mariposas de Chile / Butterflies of Chile. Editorial Universitaria, Santiago de Chile, 359 pp.

Penz CM (1999) Higher level phylogeny for the passion-vine butterflies (Nymphalidae, Heliconiinae) based on early stage and adult morphology. Zoological Journal of the Linnean Society 127(3): 277–344. https://doi.org/10.1111/j.1096-3642.1999.tb00680.x

Penz CM, Peggie D (2003) Phylogenetic relationships among Heliconiinae genera based on morphology (Lepidoptera: Nymphalidae). Systematic Entomology 28(4): 451–479. https://doi.org/10.1046/j.1365-3113.2003.00221.x

Pérez-D'Angello V (1970) Nota sobre *Agraulis vanillae* (Linnaeus, 1758). Noticiario mensual. Museo Nacional de Historia natural (Santiago de Chile) 14(167): 5.

Schluter D (2000) The ecology of adaptive radiation. Oxford University Press, Oxford.

Soltis DE, Gitzendanner MA, Soltis PS (2007) A 567-taxon data set for Angiosperms: The challenges posed by Bayesian analyses of large data sets. International Journal of Plant Sciences 168(2): 137–157. https://doi.org/10.1086/509788

Tavares M, Kaminski LA, Moreira GRP (2002) Morfologia externa dos estágios imaturos de heliconíneos neotropicais: II. *Dione juno juno* (Cramer) (Lepidoptera: Nymphalidae: Heliconiinae). Revista Brasileira de Zoologia 19(4): 961–976. https://doi.org/10.1590/S0101-81752002000400002

Tokuoka T (2012) Molecular phylogenetic analysis of Passifloraceae sensu lato (Malpighiales) based on plastid and nuclear DNA sequences. Journal of Plant Research 125(4): 489–497. https://doi.org/10.1007/s10265-011-0472-4

Ureta E (1963) Catálogo de lepidópteros de Chile. Boletín del Museo Nacional de Historia Natural (Santiago de Chile) 28(2): 53–149.

Vargas HA, Barão KR, Massardo D, Moreira GRP (2014) External morphology of the immature stages of Neotropical heliconians: IX. *Dione glycera* (C. Felder & R. Felder) (Lepidoptera, Nymphalidae, Heliconiinae). Revista Brasileira de Entomologia 58(2): 129–141. https://doi.org/10.1590/S0085-56262014000200004

Veblen TT, Young KR, Orme AR (2007) The physical geography of South America. Oxford University Press, Inc., Oxford. https://doi.org/10.1093/oso/9780195313413.001.0001

Warren AD, Davis KJ, Stangeland EM, Pelham JP, Willmott KR, Grishin NV (2017) Illustrated lists of American butterflies (North and South America). [Available at:] https://www.butterfliesofamerica.com/L/Neotropical.htm [last accessed on 15 April 2022]

Weigend M, Jossberger T, Beltrán H (2015) Notes on *Malesherbia* (Passifloraceae) in Peru: A new species from southern Peru, a new record and a first report on interspecific hybridization in *Malesherbia*. Phytotaxa 202(4): 250–258. https://doi.org/10.11646/phytotaxa.202.4.2

Zeballos-Patrón H, Pacheco V, Baraybar L (2001) Diversidad y conservación de los mamíferos de Arequipa, Perú. Revista Peruana de Biología 8(2): 94–104. https://doi.org/10.15381/rpb.v8i2.6564

Zhang J, Cong Q, Shen J, Opler PA, Grishin NV (2019) Changes to North American butterfly names. The Taxonomic Report of the International Lepidoptera Survey 8(2): 1–11.

Supplementary material 1

Figure S1

Authors: Jackie Farfán

Data type: Image.

Explanation note: Male genitalia of *Dione* (*Agraulis*) species congeners to *Dione* (*Agraulis*) *dodona* sp. nov. (A) *D.* (*A*) *galapagensis*; (B) *D.* (*A.*) *lucina*; (C) *D.* (*A.*) *maculosa*; (D) *D.* (*A.*) *vanillae*; (E) *D.* (*A.*) *forbesi*; (F) *D.* (*A.*) *insularis*; (G) *D.* (*A.*) *incarnata incarnata*; (H) *D.* (*A.*) *incarnata nigrior*. From right to left column: General, mesal view, aedeagus removed; termen of valve, mesal; juxta, ventral; aedeagus, lateral. Scale bars: 1mm, 0.25mm, 0.25mm, 0.5mm, respectively.

Link: https://doi.org/10.3897/zookeys.1113.85769.suppl1

Supplementary material 2

Figure S2

Authors: Jackie Farfán

Data type: Image.

Explanation note: Scanning electron micrographs of Dione (Agraulis) dodona sp. nov. immature stages: (A-C) Egg; (D-J) First instar; (K-P) Fifth instar. (A) micropylar region; (B) aeropyle; (C) upper cells; (D) stemmatal region, lateral; (E) antenna, antero-lateral; (F) spinneret, lateral; (G) metathoracic leg; (H) apex of setae of abdominal segment, lateral; (I) proleg with exposed crochets; (J) last abdominal segment, posterior; (K) stemmatal region, dorso-frontal; (L) short chalaza-like setae; (M) proleg of six abdominal segments; (N) seventh abdominal segment, latero-dorsal; (O) spiracle; (P) corresponding spiracle in detail. Mp, micropyles; Ac, aeropyle; Uc, upper cell. Scale bars: 50 μm (A, E, F, I, L, Q); 10 μm (B); 150 μm (C, P); 100 μm (D, G, J); 25 μm (H, M); 250 μm (K); 0,5 mm (N); 1mm (O).

Link: https://doi.org/10.3897/zookeys.1113.85769.suppl2